

Electronic Thesis and Dissertation Repository

---

12-9-2015 12:00 AM

## Intracellular Trafficking Governs the Processing of the Amyloid Precursor Protein and the Secretion of Beta-Amyloid

Joshua Hoi Ki Tam  
*The University of Western Ontario*

Supervisor  
Dr. Stephen Pasternak  
*The University of Western Ontario*

Graduate Program in Physiology and Pharmacology  
A thesis submitted in partial fulfillment of the requirements for the degree in Doctor of Philosophy  
© Joshua Hoi Ki Tam 2015

Follow this and additional works at: <https://ir.lib.uwo.ca/etd>



Part of the [Medical Cell Biology Commons](#), [Medical Molecular Biology Commons](#), and the [Nervous System Diseases Commons](#)

---

### Recommended Citation

Tam, Joshua Hoi Ki, "Intracellular Trafficking Governs the Processing of the Amyloid Precursor Protein and the Secretion of Beta-Amyloid" (2015). *Electronic Thesis and Dissertation Repository*. 3462.  
<https://ir.lib.uwo.ca/etd/3462>

This Dissertation/Thesis is brought to you for free and open access by Scholarship@Western. It has been accepted for inclusion in Electronic Thesis and Dissertation Repository by an authorized administrator of Scholarship@Western. For more information, please contact [wlsadmin@uwo.ca](mailto:wlsadmin@uwo.ca).

INTRACELLULAR TRAFFICKING GOVERNS THE PROCESSING OF THE  
AMYLOID PRECURSOR PROTEIN AND THE SECRETION OF BETA-AMYLOID.

(Thesis format: Integrated Article)

by

Joshua Hoi Ki Tam

Graduate Program in Physiology

A thesis submitted in partial fulfillment  
of the requirements for the degree of  
Doctor of Philosophy

The School of Graduate and Postdoctoral Studies  
The University of Western Ontario  
London, Ontario, Canada

© Joshua H.K. Tam 2016

## Abstract

One of the hallmarks of Alzheimer's disease (AD) is the pathological accumulation of  $\beta$ -amyloid ( $A\beta$ ) in the brains of AD patients. Oligomeric and fibrillar aggregates of  $A\beta$  have been shown to be neurotoxic to neurons and hippocampal slices. Therefore, limiting  $A\beta$  production is an important area of research in order to delay or stop AD progression.  $A\beta$  is produced by amyloidogenic cleavage of amyloid precursor protein (APP). Amyloidogenic cleavage requires ectodomain removal by  $\beta$ -secretase and intramembrane  $\gamma$ -cleavage by  $\gamma$ -secretase to release  $A\beta$  products ranging from 38-43 residues. Work from our lab has shown that APP and  $\gamma$ -secretase are resident proteins of the lysosome. Furthermore, the acidic environment of lysosomes that promotes the aggregation of  $A\beta$ . While many lines of evidence demonstrate that APP internalization is important to the  $A\beta$  production, the intracellular itinerary of APP, from production to cleavage, is unclear.

In order to follow the intracellular trafficking of APP and  $A\beta$ , we have applied various microscopy techniques, in combination with fluorescently-tagged proteins. Using a photoactivatable mutant of GFP (paGFP), we accurately photoactivated nascent APP and followed its trafficking to lysosomes. To our surprise, we found that APP was delivered to lysosomes, where it is cleaved by  $\gamma$ -secretase, through an entirely intracellular pathway. This intracellular pathway was dependent upon an interaction between APP and adaptor protein 3. We found that the interaction between APP and AP-3 is dependent on the <sup>709</sup>YTSI<sup>712</sup> tyrosine motif. Furthermore, phosphorylation of the serine within this motif, by PKC $\epsilon$ , can disrupt this interaction. By decreasing APP trafficking to lysosomes, through disrupting the APP/AP-3 interaction we decreased the production of  $A\beta$ . While lysosomes have traditionally been thought to be responsible for cellular waste disposal, they also have a secretory role in a number of cell types; including neurons. We demonstrate that lysosomes are not only responsible for the production of  $A\beta$ , but may also be responsible for the secretion of lysosomal  $A\beta$  into the extracellular space. This research may provide new therapeutic targets to limit the production and release of  $A\beta$ .

## Keywords

Alzheimer's disease, amyloid precursor protein, beta-amyloid, beta-amyloid secretion, beta-amyloid production, lysosomes, intracellular trafficking, lysosomal secretion, adapter protein 3, Rab27b, protein kinase C.

## Co-Authorship Statement

### Chapter 1: **Introduction and Literature Review**

I wrote and edited the entire manuscript. My supervisor, Dr. Stephen Pasternak, had significant input into the final manuscript and also edited the manuscript. I would also like to thank Dr. John DiGugliemo for his input into this part of my thesis. I also created all the images in this section of the thesis.

Parts of this section of the thesis will be included in a review article that will be submitted in 2016.

### Chapter 2: **The Amyloid Precursor Protein is rapidly transported from the Golgi apparatus to the lysosome and where it is processed into beta-amyloid.**

This chapter has been published in its entirety in the journal Molecular Brain. I performed many of the experiments and wrote the manuscript. While I performed many of the experiments, Claudia Seah performed the neuron dissection and performed some of the immunostaining in neurons. My supervisor, Dr. Stephen Pasternak, conceived and helped design many of the experiments, and assisted with the final drafting of the manuscript.

Note: Molecular Brain is an Open Access journal and does not require a request for copyright permission to use material published in a thesis.

### Chapter 3: **Tyrosine binding protein sites regulate the intracellular trafficking and processing of Amyloid Precursor Protein through a novel lysosome-directed pathway.**

This chapter has been submitted to the journal, PLOS One. I performed many of the manuscripts and wrote the manuscript. I had help from Rebecca Cobb, who performed some of the internalization experiments. Claudia Seah helped with the maintenance of cells throughout the project. My supervisor, Dr. Stephen Pasternak, helped with experimental design and with the final draft of the manuscript.

### Chapter 4: **The secretion of beta-amyloid from neuronal lysosomes.**

For this chapter, I performed many of the experiments and wrote the manuscript. My supervisor, Dr. Stephen Pasternak, conceived and helped design the experiments. He also helped with the final draft of the manuscript. Claudia Seah performed the experiments in which LAMP1 was stained on the surface of neurons after ionomycin treatment. The neurons were dissected by Fabiana Caetano and Claudia Seah from mice provided by Dr. Stephen Ferguson.

## Acknowledgments

I'd like to thank my supervisor Dr. Stephen Pasternak for his support and guidance throughout the last seven years of my training. I am grateful for the time and effort you have spent to hone my skills as a scientist. Without your optimism and encouragement, the completion of these projects would not have been possible. Thank you for helping me reach my goals.

I would also like to thank the members of my advisory committee, Drs. Jane Rylett, Marco Prado, and John DiGuglielmo for your time and guidance throughout my training. A special thank you to Dr. DiGuglielmo for reading and editing this manuscript. This could not have been accomplished without your efforts.

To the past and present members of the Pasternak Lab, thank you for making this experience the best it could be. Thanks to Wei, Jon, Rebecca, Mai and Justin for your friendship and company as I made this journey. Thank you Claudia and your family for your friendship, generosity, and advice. I could not ask for a better person to have worked with the past few years. All the best to you in the future. Also a special thank you to the Ferguson, Rylett, Cregan, and Prado labs for sharing your resources throughout the years.

I would also like to thank the Canadian Institute of Health Research, Ontario Graduate Scholarship, and the Queen Elizabeth II Graduate Scholarship in Science and Technology for their financial support through my training.

I'd also like to thank my friends in London and Mississauga for giving me well-needed distractions from the lab. This would not have been possible without your friendship and companionship through the years.

Also a special thank you to Ciric To and Ashbeel Roy for encouraging me to continue my training even when I absolutely did not want to continue. Thank you for your friendship and advice. Best of luck on your post doctoral fellowships and in the future.

I'd also like to thank my family, especially my parents for helping me every step of the way so that I could achieve my goals.

# Table of Contents

Abstract.....	ii
Co-Authorship Statement.....	iv
Acknowledgments.....	vi
Table of Contents.....	vii
List of Figures.....	xii
List of Appendices.....	xiv
List of Abbreviations.....	xv
Chapter 1.....	1
1 Introduction and Literature Review.....	1
1.1 Amyloid Precursor Protein.....	4
1.1.1 Non-amyloidogenic or amyloidogenic cleavage.....	4
1.1.2 Amyloid Cascade Hypothesis.....	9
1.1.3 A $\beta$ Oligomers.....	12
1.1.4 Structure of the Amyloid Precursor Protein Carboxyl-Terminal Tail.....	14
1.1.5 Amyloid Precursor Protein Phosphorylation by Protein Kinase C.....	15
1.1.6 Amyloid Precursor Protein Adaptors.....	17
1.2 Lysosomal Trafficking.....	20
1.2.1 Adaptor Proteins in lysosomal protein trafficking.....	21
1.2.2 GGA Adaptors.....	24
1.2.3 Trafficking of Lysosomal Hydrolases.....	25
1.2.4 Sorting of Lysosomal Membrane proteins.....	30
1.3 Trafficking of the Amyloid Precursor Protein.....	37
1.4 Lysosomal Pathology in Alzheimer's Disease.....	41
1.5 Lysosomal Secretion.....	44



1.6 Rationale and Hypothesis .....	47
1.7 Objectives .....	48
1.8 References.....	49
Chapter 2.....	98
2 The Amyloid Precursor Protein is rapidly transported from the Golgi apparatus to the lysosome and where it is processed into beta-amyloid. ....	98
2.1 Introduction.....	98
2.2 Materials and Methods.....	101
2.2.1 Antibodies .....	101
2.2.2 Cell Culture and Transfection.....	101
2.2.3 DNA Constructs.....	102
2.2.4 Confocal Microscopy.....	102
2.2.5 Live Cell Imaging .....	103
2.2.6 Colocalization Analysis .....	103
2.2.7 Immunostaining .....	104
2.2.8 Proximity Ligation Assay (PLA).....	104
2.2.9 Cell Lysis and Western Blots.....	105
2.3 Results.....	106
2.3.1 APP-paGFP can be followed as it traffics from the Golgi apparatus to LAMP1-labeled compartments.....	106
2.3.2 APP-paGFP traffics preferentially to lysosomes from the Golgi apparatus .....	120
2.3.3 APP-paGFP is cleaved in a LAMP1 positive compartment .....	123
2.3.4 The Swedish mutation dramatically increases APP clearance from the lysosome, but not the Golgi apparatus.....	134
2.3.5 APP interacts with adaptor protein AP-3.....	138
2.3.6 AP-3 Knockdown Disrupts Trafficking of APP to Lysosomes .....	143
2.4 Discussion.....	149

2.5	References.....	153
Chapter 3.....		
3	Tyrosine Binding Protein sites regulate the intracellular trafficking and processing of Amyloid Precursor Protein through a novel lysosome-directed pathway.....	165
3.1	Introduction.....	165
3.2	Materials and Methods.....	167
3.2.1	Antibodies and Chemicals .....	167
3.2.2	Cell Culture.....	167
3.2.3	Plasmid Constructs.....	167
3.2.4	Confocal Microscopy.....	167
3.2.5	Live-Cell Imaging.....	168
3.2.6	Colocalization Analysis .....	168
3.2.7	Proximity Ligation Assay .....	169
3.2.8	Internalization Assay .....	169
3.2.9	A $\beta$ 40 and A $\beta$ 42 ELISA.....	170
3.3	Results.....	171
3.3.1	Tyrosine Motifs and the Intracellular trafficking of APP.....	171
3.3.2	Amyloid Precursor Protein Internalization .....	176
3.3.3	Amyloid Precursor Protein and AP-3 Interaction.....	181
3.3.4	Pseudo-phosphorylation of Serine 711 .....	184
3.3.5	PKC Activation Controls Intracellular Trafficking of APP.....	185
3.4	Discussion.....	196
3.5	References.....	199
Chapter 4.....		
4	Lysosomal secretion of beta-amyloid in neuronal cells.....	205
4.1	Introduction.....	205

4.2	Materials and Methods.....	207
4.2.1	Antibodies and Chemicals .....	207
4.2.2	Cell Culture.....	207
4.2.3	Plasmid Constructs.....	207
4.2.4	Confocal Microscopy.....	207
4.2.5	Total internal reflection fluorescence microscopy (TIR-FM) .....	208
4.2.6	Counting vesicles at the cell surface.....	209
4.2.7	Detecting Exocytosis .....	210
4.2.8	Neuronal Culture.....	210
4.2.9	Colocalization Analysis .....	211
4.2.10	APP internalization into lysosomes .....	211
4.2.11	Staining of LAMP1 at the Cell Surface .....	211
4.2.12	A $\beta$ 40 and A $\beta$ 42 ELISA.....	211
4.2.13	Statistical Analysis.....	212
4.3	Results.....	212
4.3.1	Lysosomes at the cell surface .....	212
4.3.2	Rab27b Mutants Reduce Number of Lysosomes at Cell Surface.....	216
4.3.3	Rab27b Mutants Interefere with Lysosomal Exocytosis .....	219
4.3.4	Live-cell Video tracking of Lysosomal Secretion .....	219
4.3.5	Intracellular Accumulation of A $\beta$ .....	229
4.3.6	Rab27b Mutants Decrease A $\beta$ Secreted into Culture Media .....	232
4.4	Discussion.....	235
4.5	References.....	238
	Chapter 5.....	246
5	Discussion .....	246
5.1	Summary of Novel Observations.....	246

5.2 APP intracellular trafficking .....	247
5.3 Manipulating the Intracellular Trafficking of APP.....	249
5.4 Lysosomal secretion of A $\beta$ .....	252
5.5 Conclusion .....	253
5.6 References.....	257
Appendices.....	265
Curriculum Vitae .....	270

## List of Figures

<b>Figure 1.1:</b> Non-Amyloidogenic and Amyloidogenic Cleavage .....	7
<b>Figure 1.2:</b> Trafficking of Lysosomal Hydrolases .....	27
<b>Figure 1.3:</b> Trafficking of Lysosomal Membrane Proteins .....	31
<b>Figure 1.4:</b> The trafficking of Amyloid Precursor Protein .....	38
<b>Figure 2.1:</b> Schematic of constructs .....	107
<b>Figure 2.2:</b> Cleavage of $\beta$ APP-paGFP .....	109
<b>Figure 2.3:</b> Colocalization of HA-tag and $\beta$ APP-CFP .....	111
<b>Figure 2.4:</b> APP is rapidly trafficked from the Golgi apparatus to LAMP1-labeled compartment. ....	116
<b>Figure 2.5:</b> Enlarged images of APP trafficking .....	118
<b>Figure 2.6:</b> APP is primarily transported to a LAMP1 compartment .....	121
<b>Figure 2.7:</b> APP is processed in the lysosome by a $\gamma$ -secretase like activity .....	126
<b>Figure 2.8:</b> The Swedish mutation causes rapid clearance of APP from lysosomes. ....	136
<b>Figure 2.9:</b> Knockdown of AP3 and AP1 by siRNA .....	139
<b>Figure 2.10:</b> AP-3 $\delta$ and APP colocalize and interact. ....	141
<b>Figure 2.11:</b> AP-3 mediates direct trafficking of APP to lysosomes .....	145
<b>Figure 2.12:</b> AP-3 mediates processing to A $\beta$ . ....	147
<b>Figure 3.1:</b> Tyrosine mutations modulate the intracellular trafficking of APP. ....	174
<b>Figure 3.2:</b> Tyrosine disrupts internalization into early endosomes .....	177

<b>Figure 3.3:</b> Y743A disrupts internalization into lysosomes. ....	179
<b>Figure 3.4:</b> Tyrosine motif mutations affect on APP/AP-3 interaction. ....	182
<b>Figure 3.5:</b> S711E disrupts trafficking to lysosomes. ....	186
<b>Figure 3.6:</b> PMA treatment alters the intracellular trafficking of APP. ....	188
<b>Figure 3.7:</b> Staurosporine but not Gö6976 treatment restores trafficking of APP to lysosomes. ....	192
<b>Figure 3.8:</b> DCP-LA treatment of SN56 cells diverts APP into early endosome compartments. ....	194
<b>Figure 4.1:</b> Neuronal lysosomes are found at the plasma membrane. ....	214
<b>Figure 4.2:</b> Neuronal lysosomes can undergo stimulated exocytosis. ....	217
<b>Figure 4.3:</b> Kiss-and-run exocytosis and Full exocytosis. ....	221
<b>Figure 4.4:</b> Detection of Lysosomal Secretion with pHluorin. ....	223
<b>Figure 4.5:</b> Localization of mApple-LAMP1-pHluorin. ....	227
<b>Figure 4.6:</b> A $\beta$ accumulates in lysosomes. ....	230
<b>Figure 4.7:</b> Rab27b inhibits A $\beta$ releases in SN56 cells. ....	233
<b>Figure 5.1:</b> APP trafficking and A $\beta$ production and secretion. ....	255

## List of Appendices

Appendix A: Figure Legends to Chapter 2 Videos.....	265
Appendix B: Figure Legends to Chapter 3 Videos.....	267
Appendix C: Figure Legends to Chapter 4 Videos.....	269

## List of Abbreviations

Amyloid precursor protein	APP
Beta amyloid	A $\beta$
Kunitz-type protease inhibitor	KPI
Alzheimer's disease	AD
Familial Alzheimer's disease	FAD
Presenilin	PS
Lysosome associated membrane protein	LAMP1
A disintegrin and metalloproteinase	ADAM
Green fluorescent protein	GFP
Photoactivatable green fluorescent protein	paGFP
Cyan fluorescent protein	CFP
Red fluorescent protein	RFP
Cherry fluorescent protein	ChFP
Tetanus-insensitive vesicle associated membrane protein	TIVAMP
Neurofibrillary tangles	NFTs
Paired helical filaments	PHFs
Adaptor protein	AP
$\gamma$ -ear containing, Golgi-localized, Arf-binding protein	GGA
Lysosomal membrane protein	LMP



Mannose-6-phosphate	M6P
Mannose-6-phosphate receptor	M6PR
Cation independent Mannose-6-phosphate receptor	CI-M6PR
Cation dependent Mannose-6-phosphate receptor	CD-M6PR
Clathrin-mediated endocytosis	CME
Niemman-Picks disease	NPD
Niemman-Picks disease type C	NPC
Lysosomal storage disease	LSD
Cathepsin D	CatD
Hexosaminidase	Hex
Protein kinase C	PKC
Total internal reflection microscopy	TIR-FM

## Chapter 1

### 1 Introduction and Literature Review

Alzheimer's disease (AD) is the most common form of dementia. The major risk factor for AD is age. Between age 65-90 the risk for AD doubles every 5 years [1]. In 2010, AD cost the American economy \$179 billion to care for AD patients. These numbers are closely mirrored in Canada. Because there is no cure for AD, the cost is expected to rise above \$1 trillion by 2050

[2]. It is estimated that there are 500 000 AD patients in Canada, with the number expected to rise to more than 1 million by 2038 [3]. The cost of caring for these patients is estimated to be \$15 billion/year and is expected to increase ten-fold by 2038 [3]. Without intervention, AD presents a pressing public health issue to Western economies. In AD, long-term memory is typically preserved, but short-term episodic memory is lost. Short-term episodic memory is typically one of the earliest clinical signs of AD. The clinical symptoms are indicative of the underlying neuronal damage. The two main pathological hallmarks found in AD are the neurofibrillary tangles (NFTs) and amyloid plaques.

NFTs are intracellular aggregates, which accompanies the neuronal loss [4,5]. Electron microscopy studies of NFTs revealed that they were composed of smaller units known as paired helical filaments [6]. However, it was over two decades before hyperphosphorylated tau was uncovered as the major constituent of PHFs and NFTs [7]. While tau has important roles in maintaining microtubule stability [8], these properties of tau are lost with hyperphosphorylated tau [9-13].

Perhaps because of the close relationship between NFTs and neuronal survival, NFTs afflict brain areas that correspond with neurological deficits that appear in AD patients [14]. For example, AD typically begins with the loss of memory. The transentorhinal and entorhinal cortex, which serve as critical relay stations to the hippocampus, are the first areas to be afflicted with abnormal accumulation of neurofibrillary tangles (NFTs) [14]. Over the course of AD, tau pathology spreads from the medial limbic region to other areas of the neocortex; including the prefrontal, parietal, and temporal cortices [14]. Neuronal damage in these areas is associated with

deficits in areas of cognition; including language, visuospatial function, frontal executive function, and praxis. At the end-stage of the disease, the patient succumbs to AD or a related comorbidity. AD prognosis from diagnosis until death is approximately 5-8 years [15].

Despite the strong association between the clinical presentation of AD and tau pathology, NFTs and tau do not fully explain AD pathology. A transgenic mouse model over-expressing human tau can recapitulate NFTs found in AD. However, this process requires 22-months and only correlates to pathology found quite early in AD [16]. In addition, NFTs on their own are not sufficient to disrupt neuronal networks in mice [17,18]. Furthermore, tau mutations in humans, which cause NFT pathology, cannot recapitulate amyloid deposition found in AD. Rather, these mutations lead to diseases with different phenotypes, such as Frontotemporal Dementia (FTD) and Amyotrophic Lateral Sclerosis (ALS). Consequently, tau pathology does not sufficiently account for all aspects of AD pathology.

Perhaps, the aetiology of AD lies with the amyloid plaques, which are the other prominent feature found in AD. The main constituent of these plaques was found to be aggregates of  $\beta$ -amyloid ( $A\beta$ ) [19].  $A\beta$  is produced by amyloidogenic cleavage of the amyloid precursor protein (APP). APP is first cleaved by  $\beta$ -secretase to release the large ectodomain into the luminal compartment. The subsequent cleavage, of the remaining carboxyl terminal fragment, by  $\gamma$ -secretase complex produces  $A\beta$  species ranging from 38-43 residues. The  $A\beta_{42}$  has a higher propensity to aggregate and is the major constituent of amyloid plaques [20,21] (Figure 1.1). Insoluble fibrillar aggregates have been shown to be neurotoxic to cells in culture and hippocampal slices [22-26]. There is evidence suggesting that  $A\beta$  pathology is upstream of tau pathology. For example, rat hippocampal neurons treated with fibrillar aggregates of  $A\beta$  cause the generation of phosphorylated tau [27]. Furthermore, transgenic mouse models of AD lacking tau were protected from cognitive decline [28]. Therefore,  $A\beta$  aggregation and accumulation may play a central role in AD pathology.

While fibrillar aggregates of  $A\beta$  were shown to be neurotoxic in cell culture and hippocampal slices [22-26], the progression of  $A\beta$  deposition does not follow the clinical signs of AD. According to the Braak staging of AD, amyloid deposits are initially found in the prefrontal,

parietal, and temporal cortices [14]. However, recent work has shown that when total A $\beta$  (aggregated and soluble) is accounted for, A $\beta$  levels in the brain correlate well with disease progression. As patients progress from cognitively normal to early AD there is a 6-7 fold increase in A $\beta$  in the entorhinal cortex [29]. In support of these findings, other work has shown that soluble oligomeric A $\beta$  is neurotoxic and synaptotoxic to cells and hippocampal slices [30-34].

Because of its central role in AD pathology, it has been suggested that pathological accumulation of A $\beta$  in the brain can lead to AD [35,36]. Known as the amyloid cascade hypothesis, this hypothesis has been the main motivation for much of the research in AD. Despite the success of A $\beta$  reducing therapies in mouse models, this initial success has not translated into viable therapeutics for human AD patients, suggesting further research is required to further our understanding of the underlying disease processes [37,38].

One area in need of further research is to determine the exact subcellular organelle responsible for APP cleavage and the mechanism regulating trafficking to and away from this compartment. Several lines of evidence suggest that the specific intracellular locale of APP can influence the production of A $\beta$ . For example, the carbon length of phospholipid membranes of different organelles may determine the processivity of the  $\gamma$ -secretase complex [39]. Furthermore, deacidification of intracellular organelles lowers A $\beta$  production. Work from our lab has identified that PS1, the catalytic component of the  $\gamma$ -secretase complex, has an acidic optimal pH [40]. Moreover, our lab has shown that APP and members of the  $\gamma$ -secretase complex have been identified as resident proteins of the lysosomes [40,41]. Although many subcellular compartments have been implicated in AD, work from our lab implicates the lysosome in A $\beta$  production.

The subcellular sorting of APP is important in controlling the levels of A $\beta$  produced. Synaptic activity can increase the production of A $\beta$ , in an endocytosis dependent manner [42,43]. Pharmacological and genetic disruption of APP internalization to endosomes and lysosomes can also decrease the production of A $\beta$  [42,44]. Moreover, retrograde trafficking of APP from

endosomes and lysosomes to the Golgi limit the production of A $\beta$ , and has been implicated in AD pathology [45-47].

In this thesis, we will review the specifics of amyloid production and the amyloid cascade hypothesis. Then we will review the trafficking of APP and other proteins towards and away from the endosomal/lysosomal system; including adaptors and other protein machinery required to facilitate this trafficking. Then we will present data describing a new pathway for APP trafficking to the lysosome and subsequent cleavage. Furthermore, we will present data demonstrating that lysosomes are critical for the secretion of A $\beta$ .

## 1.1 Amyloid Precursor Protein

### 1.1.1 Non-amyloidogenic or amyloidogenic cleavage

APP can be processed by the amyloidogenic or non-amyloidogenic pathway. Amyloidogenic cleavage of APP produces the neurotoxic A $\beta$  species ranging from 38-43 residues. Conversely, cleavage of APP in the non-amyloidogenic pathway decreases the production of A $\beta$  by cleaving APP within the A $\beta$  region. It has been suggested there is competition between the amyloidogenic and non-amyloidogenic pathways for limited APP substrate [48,49] (Figure 1.1). Cleavage in both pathways depends on removal of the large N-terminal ectodomain. In the non-amyloidogenic pathway, removal of the large, luminal ectodomain is mediated by  $\alpha$ -secretase cleavage, which produces a soluble APP ectodomain (APPs $\alpha$ ) product and an 83-residue carboxyl-terminal fragment (CTF). The candidates for  $\alpha$ -secretase have been suggested as members of the ADAM (a disintegrin and metalloprotease) family. Of the 21 members of the ADAM family, ADAM10 and ADAM17 are the likely  $\alpha$ -secretases [50-52]. ADAM10 is responsible for constitutive  $\alpha$ -cleavage of APP, while cleavage by ADAM17 is up-regulated by PKC activation [48,51,53,54]. However, there is at least one report of ADAM17 facilitating constitutive shedding of the APP ectodomain in HEK cells [55]. ADAM10, BACE, and APP mRNA are all expressed within the same neuronal population [49], which suggests that ADAM10 may be the relevant secretase *in vivo*. In addition, over-expression of ADAM10 in mice expressing APP<sub>Lon</sub> increased non-amyloidogenic cleavage of APP, decreased plaque load, and improved cognition [56].

The delicate balance between non-amyloidogenic and amyloidogenic cleavage is critical in managing the levels of A $\beta$ . Recent studies in a Finnish population has revealed that elderly individuals bearing the A673T mutation in APP are protected from cognitive decline [57]. The A673 residues is immediately carboxyl terminal to the  $\beta$ -cleavage site in APP. **Membrane anchored aspartic proteinase of the pepsin family-2 (Memapsin-2, also known as  $\beta$ -site APP-cleaving enzyme 1, BACE1)** was identified as the enzyme responsible for catalyzing the first step in amyloidogenic cleavage of APP [58,59]. While proteolytically active ADAM10 is localized to the cell surface [51,60], active BACE1 appears to be localized to early endosomes. BACE1 has an optimal pH of 4.5, and is not active at the cell surface; suggesting involvement of the endosomal/lysosomal system [58]. Furthermore, BACE1 has been localized to early endosomes by fluorescence resonance energy transfer (FRET) [61]. In healthy neurons, the intracellular levels of BACE1 are controlled by lysosomal degradation. However, depletion of the adaptor GGA3 (discussed later) in AD decreases lysosomal degradation of BACE1, and promotes amyloidogenic cleavage of APP [62-65].

BACE cleavage of APP produces a 99-CTF, which is processed by  $\gamma$ -secretase. The 99-CTF and 83-CTF produce monomeric A $\beta$  and p3, respectively, after cleavage by  $\gamma$ -secretase. While the  $\gamma$ -secretase can cleave many substrates (including Notch, E-cadherin, and LRP) [66],  $\gamma$ -secretase is of interest, because of its role in A $\beta$  production. A functional  $\gamma$ -secretase complex is composed of at least Aph-1 (anterior pharynx-defective 1), Pen-2 (presenilin enhancer 2), nicastrin, and Presenilin 1 (PS1). The CTF stub produced, after  $\alpha$ - or  $\beta$ - secretase cleavage, is recognized by nicastrin, which serves as a 'gatekeeper' to the  $\gamma$ -secretase complex [67]. PS1 is a large protein with 9-10 transmembrane domains, and serves as the catalytic component of  $\gamma$ -secretase. In order to form a functional  $\gamma$ -secretase complex, it is believed that Aph-1 and nicastrin form a sub-complex, which binds to PS1 and Pen-2 sequentially. Alternatively, the Aph-1/nicastrin sub-complex may bind directly as a PS1-Pen-2 sub-complex to generate mature, active presenilin [68].

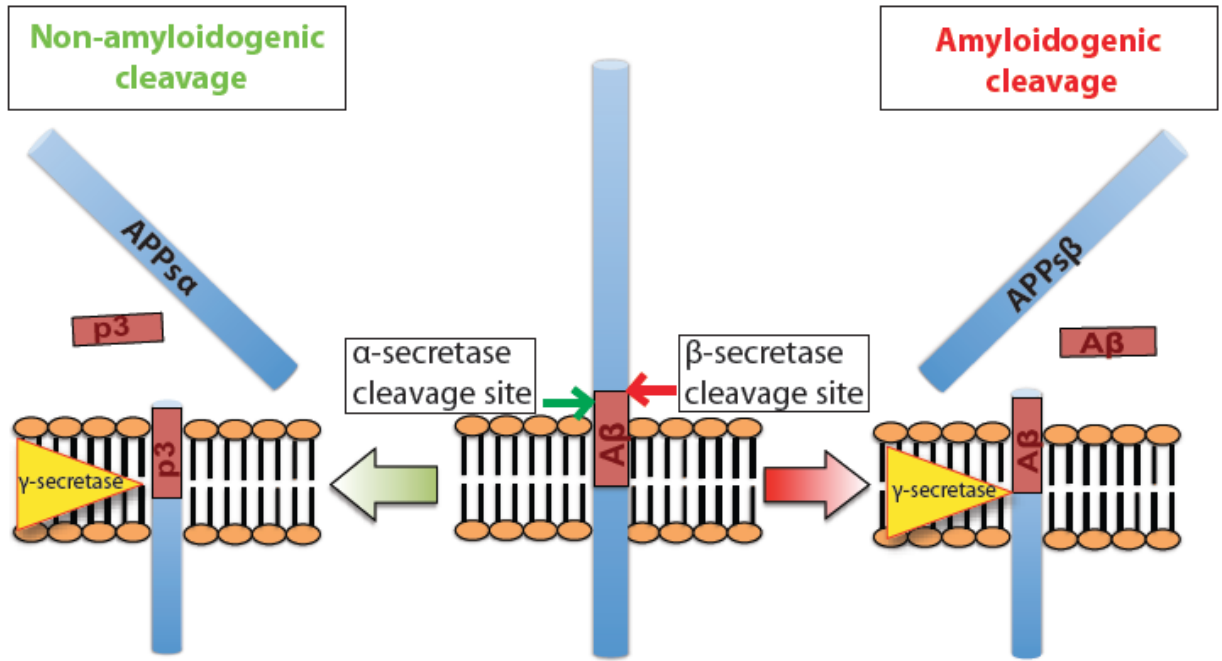
The importance of PS1 to AD pathology is illustrated by over 160 mutations known to cause familial early-onset AD. Although the effects of these mutations are not completely understood,

it is generally accepted that many FAD PS1 mutations increase the relative levels of A $\beta$ 42 with respect to A $\beta$ 40 [69]. A $\beta$ 42 is the primary constituent of amyloid plaques and is more likely to aggregate in solution [20,21]. A $\beta$  species range from 38-43 residues, and the wide variation is due to the imprecise  $\gamma$ -cleavage of APP by  $\gamma$ -secretase. Cleavage of the APP-CTF begins with cleavage at the  $\epsilon$  site by  $\gamma$ -secretase, which is approximately 48-49 residues distal to the  $\beta$ -cleavage site. After  $\epsilon$ -cleavage, the carboxyl end of the remaining transmembrane stub is cleaved 3-4 peptides at a time to yield A $\beta$  species of varying lengths [70]. The processivity of PS1 depends upon its intracellular milieu. Slight changes to the length and fatty acid chain isomer have profound effects on the activity of  $\gamma$ -secretase and the A $\beta$ 42/40 ratio [39]. Furthermore, studies from our lab have shown that  $\gamma$ -secretase has an optimal pH of  $\sim$ 4.5 [40]. In fact, PS1 and nicastrin have been localized to lysosomes, suggesting they likely resident lysosomal membrane proteins [40,41]. These results have been corroborated by Nixon and colleagues, which showed  $\gamma$ -secretase activity in lysosomal and autophagic compartments [71]. Furthermore, deacidification of lysosomes pharmacologically or genetically, severely hampers cleavage of APP CTFs [72,73].

**Figure 1.1: Non-Amyloidogenic and Amyloidogenic Cleavage**

Amyloid precursor protein (APP) can be cleaved via either an amyloidogenic or non-amyloidogenic manner. Non-amyloidogenic pathway precludes the formation of A $\beta$  by cleavage of APP by  $\alpha$ -secretase.  $\alpha$ -cleavage results in the release of the APPs $\alpha$  luminal domain and an 83 residue carboxyl-terminal fragment (CTF). The CTF is cleaved by  $\gamma$ -secretase to release p3 into the lumen and an APP intracellular domain (AICD) to the lysosome. Conversely, cleavage of APP by  $\beta$ -secretase removes the APPs $\beta$  luminal domain, but preserves the A $\beta$  domain in the membrane attached 99-residue CTF. A $\beta$  is produced by  $\gamma$ -cleavage of CTF99.





### 1.1.2 Amyloid Cascade Hypothesis

One of the hallmarks of AD is the accumulation of the 4kDa fragment known as A $\beta$ . It was identified as the dominant protein in neuritic plaques in AD and Down syndrome patients [19]. As first postulated by John Hardy, the amyloid cascade hypothesis states that A $\beta$  accumulation is central to AD pathology, and leads to neurofibrillary tangles, cell loss, vascular damage, and dementia [35]. More recently, this hypothesis has been revised to include the latest discovery of neurotoxic A $\beta$  oligomers [36]. Despite its role in AD pathology, A $\beta$  is normally, constitutively produced in all cells, and tissues including human and rat cortical cultures [74-76], suggesting a possible physiological role [77].

An important step in our understanding of amyloid plaques occurred when A $\beta$  was identified as the major constituent of plaques and its protein sequence from plaques in the brains of AD patients and from Down's syndrome (DS) patients [19,78]. Invariably, patients with DS have amyloid plaques and the characteristic pathology of AD and most show clinical signs of AD [79,80]. In DS, chromosome 21 fails to separate during meiosis, which results in trisomy 21. Therefore, amyloid precursor protein (APP), which is encoded on chromosome 21, is over expressed in these individuals [81]. While AD pathology may be caused by any number of genes on chromosome 21, familial AD has been found in families with only the gene for APP duplicated [82]. This suggests that there is a gene-dosage effect of APP. Transgenic mice over-expressing APP also show cognitive deficits and A $\beta$  deposition [83].

In a small percentage of AD cases, there is early-onset of AD and are thus named early-onset familial AD (FAD). Of these mutations, 10-15% are mapped to APP [84], which further implicates APP in AD pathology. In agreement with the findings from DS patients, some of these FAD mutations lead to a pathological increase in APP expression. FAD mutations have been identified in the promoter for APP, which causes a two-fold increase in promoter activity [82]. Other FAD mutations can cause duplication of the APP gene, which also leads to APP overexpression [85,86]. Alternatively, other mutations have been identified on exon 16 and 17, which encode the A $\beta$  region in APP. These mutations affect the processivity of  $\alpha$ -,  $\beta$ -, and  $\gamma$ -

secretase. For example, the Swedish mutation ( $APP_{Swe}$ ), is located at the  $\beta$ -cleavage site and promotes  $\beta$ -cleavage of APP by 10-fold [87]. Consequently, there is a dramatic increase in  $A\beta$  production [88-90]. Recently, a mutation carboxyl to the  $\beta$ -cleavage site that reduced the amyloidogenic cleavage of APP and protected against AD [57].

Mutations can also affect the  $\gamma$ -cleavage of APP and lead to AD. For example the London mutation ( $APP_{Lon}$ ), which causes a relative increase in  $A\beta_{42}$  production, by changing specificity of the  $\gamma$ -cleavage site (residue 717 by APP 751 numbering) [91-93]. In addition, the French and German FAD mutations were found two residues upstream at valine 715, which both caused a relative increase in the amount of  $A\beta_{42}$  species produced as compared to  $A\beta_{40}$  [94,95]. A similar increase in the  $A\beta_{42}/A\beta_{40}$  ratio is also seen in patients with the Florida FAD mutation [95]. Interestingly, the French mutation decreases the total level of  $A\beta$  produced, but preferentially decreases  $A\beta_{40}$  production. Furthermore, the French mutation also increases  $\alpha$ -cleavage of APP [95]. These findings suggest that while increasing the total  $A\beta$  produced is important, the relative increase in  $A\beta_{42}$  may also be critical for AD pathology.

In addition to the secretase cleavage sites, FAD mutations have also been identified in the  $A\beta$  region itself. The Dutch (E693Q), Flemish (A692G), Osaka (E693 $\Delta$ ), and Arctic (E693G) mutations lead to presenile dementia, parenchymal amyloid deposition, and cerebral amyloid angiopathy [96-101]. The Flemish, Dutch, Osaka, and Arctic mutations make  $A\beta$  resistant to cleavage by neprilysin [102], which is one of the main proteases for  $A\beta$  [103]. Moreover,  $A\beta$  bearing either the Dutch or the Arctic mutation have a higher propensity to form protofibrils and fibrils, despite a lower  $A\beta_{42}/40$  ratio, as compared to wild-type APP [100,104,105].

Interestingly, the Osaka mutation did not enhance fibrillization, but enhanced formation of oligomeric species. These oligomeric species inhibited hippocampal long-term potentiation more potently than the wild-type peptide ( $A\beta$  oligomers are discussed in further detail below)[106]. Furthermore, the Flemish mutation causes a conformational change in APP, which facilitates  $\gamma$ -secretase cleavage of APP [107,108]. Therefore, FAD mutations in APP can cause AD pathology by changing secretase cleavage and promoting fibrilization or oligomerization of  $A\beta$ .

Early-onset FAD mutations were also mapped to chromosomes 14, which encodes presenilin 1 (PS1), and chromosome 1 which encodes its homologue presenilin 2 PS2 [109]. PS1 contains catalytic component of the heterotetrameric  $\gamma$ -secretase complex, and contains an aspartic acid residue at its active site that cleaves various membrane-bound carboxyl-terminal fragments. Plasma and fibroblasts from patients with FAD mutations in PS1 and PS2 have increased A $\beta$ 42 levels relative to A $\beta$ 40 [110]. When PS1 and PS2 FAD mutations are over-expressed in cell lines, a relative increase of A $\beta$ 42 was also observed [69,110,111]. Mutations in PS1 and PS2 are not localized to a specific region of the protein, which suggests there are multiple mechanisms for regulating A $\beta$  production. It is unclear if these mutations result in a gain-of-function (increase in A $\beta$ 42 production) or loss-of-function (decrease in A $\beta$ 40 production [69]. However, it is clear that there is an increase in the A $\beta$ 42/40 ratio, which leads to the pathology seen in AD.

Despite the evidence implicating A $\beta$  in FAD pathology, FAD only accounts for 1% of all AD cases. The majority of AD cases are late-onset AD (LOAD), and the aetiology of these cases is unclear. AD prevalence studies in twins show that 80% of the risk for developing AD is heritable [112]. Through a number of genome wide association studies (GWAS), the locus for apolipoprotein E has been repeatedly implicated in AD. There are three alleles for *APOE* ( $\epsilon$ 2,  $\epsilon$ 3, and  $\epsilon$ 4). The  $\epsilon$ 3 allele is the most common followed by  $\epsilon$ 4 and finally  $\epsilon$ 2. The  $\epsilon$ 2 allele is known to have a protective effect in AD, while the  $\epsilon$ 4 allele exacerbates AD [113]. Individuals heterozygous for the  $\epsilon$ 4 allele have a 2-3 fold increased risk for AD, and homozygous individuals have a 12-fold increased risk [114].

Homozygosity for the  $\epsilon$ 4 allele increases A $\beta$  deposition in the middle frontal gyrus, superior temporal gyrus, and inferior parietal lobule of human AD patients [115]. Concomitantly, patients bearing the  $\epsilon$ 4 allele have lower levels of A $\beta$  42 in their CSF, which is indicative of A $\beta$  deposition in the brain [116]. However, the mechanism by which ApoE increases brain deposition of A $\beta$  is unclear. Some studies suggest that ApoE is critical for A $\beta$  fibrillogenesis. Transgenic AD mice with ApoE KO have lower levels of A $\beta$  deposition, which can be increased by expression of human ApoE. If the  $\epsilon$ 4 variant is introduced into these mice, A $\beta$  deposition is even further increased [117]. During *in vitro* studies, the presence of ApoE

accelerates A $\beta$  fibrillization, and is further increased by the presence of the  $\epsilon$ 4 isoform [118,119]. ApoE may also be involved in clearance of A $\beta$  from the brain parenchyma. In transgenic AD mice expressing the different isoforms of ApoE, the  $\epsilon$ 4 allele decreases the clearance of A $\beta$  from the CSF [116]. ApoE also promotes the proteolytic clearance of A $\beta$  by microglia, in a lysosome-dependent manner [120]. The evidence from the ApoE studies demonstrates that A $\beta$  is also an important component of late-onset AD (LOAD) pathology.

The deposition of A $\beta$  appears to be an age dependent process [121], in agreement with the age-dependent increase in AD risk. Furthermore, DS patients also initially present with diffuse plaques, which gradually aggregates into dense core plaques, like the ones seen in AD [122]. Initially, plaques are enriched in the A $\beta$ 42 species, and mature plaques incorporate A $\beta$  40 [123,124]. The presence of plaques in the brains of AD patients suggests that the aggregation of A $\beta$  is critical for its neurotoxicity. In agreement, early experiments showed that insoluble, fibrillar aggregates of A $\beta$  neurotoxic and were likely responsible for AD pathology [23,125]. The toxicity and ability to aggregate is dependent on the hydrophobic C-terminal of the A $\beta$  peptide. The hydrophobic tail promotes A $\beta$  aggregation and is crucial for A $\beta$  toxicity [126]. Treatment of hippocampal cultures with fibrillar aggregates, but not amorphous aggregates of A $\beta$  1-40, decreased neuronal viability and synaptic density [127-129]. Inhibition of A $\beta$  fibrillation was capable of rescuing cell viability [25,26,127], and prevents A $\beta$  accumulation in a transgenic mouse model [130]. However, more recent work suggests that soluble A $\beta$  oligomers may be the pathologically relevant A $\beta$  species (see below for discussion).

### 1.1.3 A $\beta$ Oligomers

For the first 2 decades after the sequencing of A $\beta$ , the field of AD was dominated by the idea that insoluble fibrillar A $\beta$  was the main neurotoxic species. However, the pattern of A $\beta$  deposition does not correlate with the appearance of clinical signs of AD [131-133]. A $\beta$  deposition first occurs in the prefrontal cortex before afflicting the memory centres in the medial temporal lobe [14,134]. Recently, soluble oligomers of A $\beta$  have come to the forefront as the toxic species in AD [135]. When soluble forms of A $\beta$  are measured, there is a 6-7 fold increase in the levels of A $\beta$  in the entorhinal cortex before increasing in the neocortex [29]. The pattern of increased A $\beta$

matches the pattern of NFT pathology observed by Braak and Braak [14]. Furthermore soluble A $\beta$  species can be detected in the brains of AD and DS patients, but not in cognitively normal controls [30,136,137]. The A $\beta$  oligomers (A $\beta$ Os) were neurotoxic to hippocampal slices and cultured cells [30,31,138,139].

The identity of the A $\beta$ O receptor still remains to be elucidated and may be important for the development of the next generation of therapeutics. Laurén et al. [140] identified the A $\beta$ O receptor as the prion protein PrP<sup>c</sup>. Knockout of PrP<sup>c</sup> abrogated the long-term potentiation impairment after treatment with A $\beta$ Os [31,139-142]. PrP<sup>c</sup> was also shown to mediate cell death after treatment with A $\beta$ Os [139]. However, the role of the prion protein in AD pathology was challenged when other investigators found that PrP<sup>c</sup> expressing and PrP<sup>c</sup>-null neurons were equally vulnerable to treatment with A $\beta$ Os [143]. Furthermore, removal of all PrP<sup>c</sup> from the cell surface did not abolish A $\beta$ Os binding to the cell surface. Synaptosomes treated with trypsin could not bind A $\beta$ Os, which suggests a membrane protein receptor [144]. Furthermore, A $\beta$ Os treatment appeared to directly increase the clustering of metabotropic glutamate receptor 5 (mGluR5); suggesting mGluR5 as the receptor for A $\beta$ Os [145]. Supporting this idea, mGluR5 knockout animals crossed with mice expressing APP and PS1 with FAD mutations had lower levels of plaque deposition and were protected from cognitive deficits [146].

A possible solution to this ambiguity is that there may be multiple proteins involved in A $\beta$ O signal transduction. As PrP<sup>c</sup> is a glycosylphosphatidylinositol (GPI) anchored protein, it necessitates a transmembrane receptor to transduce the signal from the extracellular to the intracellular space. PrP<sup>c</sup> is a promiscuous protein and can interact with various proteins to form cell-surface signalling platforms [147]. PrP<sup>c</sup> was shown to co-immunoprecipitate with mGluR5 and knock out of either protein was sufficient to abrogate the synaptic dysfunction in response to A $\beta$ Os [148]. Therefore, PrP<sup>c</sup> and mGluR5 may act as co-receptors to mediate cellular and synaptic toxicity characteristic of AD.

A $\beta$ Os also cause a pathological increase of intracellular calcium, because of an increase in NMDA receptors (NMDAR) at the cell surface [145,148]. A pathological activation of extrasynaptic NR2b can cause cell death [149,150]. Furthermore, kainite-induced excitotoxicity

in the mouse hippocampus leads to the activation of compensatory mechanisms seen in AD, and can be prevented by tau knockout [151]. Activation of the PrP<sup>c</sup>/mGluR5 co-receptor by A $\beta$ Os can activate the Src kinase, Fyn, which can phosphorylate the NR2b receptor at Y1472. Phosphorylation of NR2b increases the level of NR2b containing NMDARs at the cell surface [148,152]. The phosphorylation of NMDAR depends on Fyn translocation to the dendritic spine. Fyn translocation to dendritic spines depends on its interaction with tau [153]. PHF associated phosphorylation of tau can promote the delivery of tau to the dendritic spine [154]. Therefore, the synaptic receptor scaffold, consisting of tau, Fyn, PrP<sup>c</sup>, and mGluR5, may be responsible for the toxic effects of A $\beta$ Os.

#### 1.1.4 Structure of the Amyloid Precursor Protein Carboxyl-Terminal Tail

A $\beta$  was identified as the major constituent of senile plaques and the amino acid composition and N-terminal sequence was identified [19,78]. From the N-terminal sequence, a cDNA expressing the amyloid precursor protein (APP), containing the A $\beta$  sequence, was identified and mapped to chromosomes 21 [155-157]. The APP gene spans over 170kbp and contains 19 exons [158]. There are 8 isoforms of APP, which are produced by alternatively splicing. The three main isoforms of APP contain 695, 751, or 770 residues [159,160].

While the extracellular domain of APP has interesting biology, this thesis will focus on the C-terminal tail and the motifs found therein. Nuclear magnetic resonance (NMR) studies of the APP cytoplasmic tail (last 49 residues) have revealed that this region does not adopt a stable folded structure. Rather, it is a dynamic region, which is capable of adopting transient structural features [161,162]. The N-terminal end of the APP C-terminal (residues 649-670) adopts a predominately random-coil structure, while the carboxyl end (residues 670-695) adopts a predominately  $\alpha$ -helical structure [162].

Of note, there are two type 1 reverse turn conformations at <sup>668</sup>TPEE<sup>671</sup> and <sup>684</sup>NPTY<sup>687</sup> [161,162]. In relation to APP physiology, the TPEE and NPTY motifs are essential for the interaction of APP and various adaptor proteins that modulate APP processing and signalling [163-168]. The NPXY (where X is any amino acid) is an internalization motif found on the

cytoplasmic domains of many putative cell-surface receptors [169-172]. In addition to serving as an internalization motif (the role of NPXY motifs in internalization will be discussed more thoroughly in another section), the NPXY motifs are binding sites for phosphotyrosine-binding (PTB) domains [173-176]. The  $\beta$ -sheet structure of the NPTY motif nestles in the pleckstrin homology (PH)-fold formed by anti-parallel sheets in the PTB domains of adaptor proteins such as Mint1 and Fe65 [177,178].

Apart from the NPTY motif, residues preceding and following the motif also play a critical role in APP binding to the PTB motifs of Mint and Fe65. Residues N680 to T686 participate in hydrogen bonding with  $\beta$ -strands in the Mint1 PTB [178]. The hydrophobic region, C-terminal to the NPTY motif, also participates in hydrophobic interactions with Mint1 and Fe65 PTB domains [177,178]. Binding of APP is also influenced by the distant TPEE motif, which forms an N-terminal helix cap. The N-terminal helix cap maintains an  $\alpha$ -helix that is critical in the interaction with Fe65 PTB2. Phosphorylation of Thr668 can disrupt the cap and reduce APP interaction with Fe65 [177,179].

Thr668 is followed immediately by a proline, which can adopt either a cis or a trans isomer. Phosphorylation of Thr668 promotes the adoption of the cis isomer, which disrupts interaction with adaptors that can influence APP signalling, trafficking, and processing [177,180,181]. The relative abundance of cis and trans isomers is under the control of Peptidyl-prolyl cis-trans isomerase NIMA-interacting 1 (Pin1). Pin1 catalyzes the transition from cis to trans isomer [181]. Pin1 knockdown also increases the interaction of APP with Fe65, by promoting cis conformation [180]. Pin1 knockout increases amyloidogenic processing of APP, by increasing the levels of the cis isomer [181].

### 1.1.5 Amyloid Precursor Protein Phosphorylation by Protein Kinase C

The phosphorylation of APP on residue T668 appears to be involved in the control of the cell cycle [182]. As such, residue T668 has been shown to be phosphorylated by cell cycle control proteins, such as cyclin D kinase 5, GSK3 $\beta$ , and cell division cycle protein 2 [182-184]. In addition to T668, there are eight possible phosphorylation sites [185]. Y653, S655, T668, S675,



Y682, T686, and Y687 have been shown to be phosphorylated in the brains of AD patients [185]. APP can be phosphorylated at these residues by a variety of kinases; including protein kinase C (PKC), calmodulin-dependent protein kinase II (CaMKII), Abl kinase, and the cell cycle kinases mentioned above [186-189].

Perhaps the most interesting candidate is the PKC family. Activation of PKC promotes the non-amyloidogenic cleavage of APP [190-194]. PKC can be activated by M1 and M3 muscarinic acetylcholine receptors and up-regulates the non-amyloidogenic cleavage of APP [195,196]. The activation of nicotinic receptors can also stimulate the activation of PKC [197]. The ability to stimulate non-amyloidogenic cleavage of APP may lend itself to the effectiveness of cholinergic treatments in AD. Our most effective pharmacological interventions in AD (such as Donepezil, Rivastigmine, and Galantamine) are based on the finding that cholinergic neurons are preferentially lost in AD [Kasa:1997ht]. Despite these AChE inhibitors, they are not capable of stopping or reversing the disease, but only delay the progression of AD [198-200].

G protein-coupled receptors, such as M1 and M3 acetylcholine receptors (AChR) can activate PKCs through activation of phospholipase C [201-203]. M1 and M3 AChR are Gq/G11 protein coupled and ligand binding activates PLC [202-206]. PLC activation leads to the formation of inositol trisphosphate (IP<sub>3</sub>) and diacylglycerol (DAG) [205]. IP<sub>3</sub> binds to IP<sub>3</sub> receptors to induce the release of calcium from the ER. Calcium and DAG are potent signalling molecules, which can lead to the activation of PKC. PKCs are sorted into three families in accordance with their response to IP<sub>3</sub> and DAG signals [207]. Conventional PKCs (cPKCs) comprise PKC $\alpha$ , PKC $\beta$ , and PKC $\gamma$ , and are activated by a combination of DAG (or lipid) and calcium binding. Conversely, novel PKCs (nPKCs) ( $\delta$ ,  $\epsilon$ ,  $\theta$ , and  $\eta$ ) are activated in response to DAG or lipids. Finally, atypical PKCs (aPKCs) ( $\iota$  and  $\zeta$ ) are not responsive to either calcium or DAG [208]. Rather, aPKCs are activated via an interaction with the partitioning defective 6 (PAR6)- CDC42 complex [209].

Phosphorylation of the APP C-terminal tail by PKC may influence the intracellular trafficking of APP and modulate its metabolism. Indeed, PKC activation appears to favour non-amyloidogenic cleavage of APP at the expense of amyloidogenic cleavage [48]. Perhaps the most poignant

example is the phosphorylation of S655 in the APP tail [186,210,211]. Phosphorylation of S655 diverts APP away from the cell surface and endosomes and increases APP localization to the Golgi apparatus [210,211] (Figure 1.4, Step 4). In addition to influencing the trafficking of APP, PKC activation also appears to up-regulate the function of  $\alpha$ -secretases. PKC activation increased the levels of mature, enzymatically active ADAM10 and ADAM17 (putative  $\alpha$ -secretases) [212]. Furthermore, PKC activation also decreased the cellular levels of  $\beta$ -secretase, which resulted in reduced A $\beta$  production [212]. Therefore, PKC activation likely plays an important role in controlling APP metabolism. The presence or absence of phosphorylation may also influence the binding of APP adaptor proteins, which can influence APP metabolism and cellular signaling.

### 1.1.6 Amyloid Precursor Protein Adaptors

Mint, Fe65 and other adaptor proteins that interact with the NPXY motif can modify APP processing and intracellular trafficking. Furthermore, some of these adaptors can act as signalling platforms and modulate cell activity. The Mint family of proteins appear to be involved in regulating the trafficking of APP. Mint 2 and 3 (also known as X11  $\beta$  and  $\gamma$ ) are localized to the Golgi apparatus [167,213,214]. Mint 3 has been shown to be recruited to Golgi vesicles in the presence of APP and modulates the egress of APP from the Golgi apparatus to lysosomes [167,214] (Figure 1.4, Step 1). Mint 1 and 2 have also been suggested to be important for APP internalization [166,215]. Knock-out of all Mint proteins decreases APP internalization, but this can be rescued by expression of phosphorylated Mint 2 [166]. Mint 1 expression appears to be crucial for activity induced APP internalization and subsequent production of A $\beta$  [42,43,215]. *Mint 1* KO neurons produce lower levels of A $\beta$ , which can be rescued by expression of Mint 1-GFP [215]. However, precise role of Mint in regulating A $\beta$  production is unclear. At least one set of experiments demonstrate that over expression of Mint 1 can also decrease A $\beta$  secretion [163]. More study into the role of Mint in APP trafficking and processing must be completed to fully understand the role of the Mint proteins.

Fe65 can also regulate the production of A $\beta$  [179,216,217]. Initial experiments with Marine-Darby canine kidney cells demonstrated that Fe65 and APP co-localize in the perinuclear area,

and over expression of Fe65 increased APP expression at the cell-surface. The increased cell-surface levels of APP is correlated with increased release of the soluble APP ectodomain (APPs) and A $\beta$  [216]. In agreement with these studies, primary cortical neurons from Fe65 knockout animals have lowered production of A $\beta$  [217]. The Fe65-regulated processing of APP may be a cellular response to extracellular signals. N-methyl-D-aspartate (NMDA) treatment increases intracellular levels of APP CTF and decreases A $\beta$  production [217]. With NMDA receptor activation, there is a phosphorylation of APP at Thr668, which, as described earlier, reduces APP interaction with Fe65 [177,179,217]. Signalling through APP-mediated mechanisms may depend upon the formation of a tripartite complex formed between APP, Fe65, and low-density lipoprotein (LDL) receptor-related protein (LRP) [218,219]. LRP-deficient mouse fibroblasts had increased cell-surface APP levels and reduced the production of A $\beta$ , which is similar to the phenotype in Fe65 knockout cells [219].

Fe65 may also link APP to proteins that regulate the actin cytoskeleton [220-222]. Fe65 forms a tripartite complex with Fe65, APP, and Mena. Mena binds to the WW motif of Fe65 and can organize the actin cytoskeleton [223]. In accordance with this role, APP, Fe65, and Mena are localized to the leading edge of migrating cells and localized to focal adhesions [220]. Extending these results into neurons, Fe65 and APP are both localized to the highly motile growth cone [221].

The role of APP at growth cones at the leading edge can also be facilitated by interactions with disabled 1 (Dab1). The disabled family of genes is evolutionarily conserved and regulates the correct positioning of neurons in the brain [224-226]. Dab1 interacts with APP family members through an interaction between the Dab1 PTB domain and the NPTY motif [227,228]. Dab1 and APP colocalize in growth cones of cultured hippocampal neurons [227]. Dab1 and APP knockdown neurons do not migrate successfully from the subventricular zone to the cortical plate [229]. The abnormally placed neurons may relate to an extracellular matrix protein known as reelin. Reelin is the defective protein in reeler mice that have malformations of the cerebral cortex [230]. Mutations in reelin disrupt the positioning of neurons in the cerebral cortex, and

this phenotype is also seen in mice with mutations in Dab1 [224-226]. In agreement, with these findings, APP can bind to reelin, and this interaction promotes neurite outgrowth [231].

Therefore, the interaction between APP and Dab1 may serve as a signalling platform for reelin and control growth cone motility. Reelin promotes the interaction between Dab1 and APP, which increased APP ectodomain release and APP CTF production, and decreased A $\beta$  production [232]. Dab1 also recruits the Src family kinase, Fyn, to the APP/Dab1 complex [233]. This may serve to modulate the strength of interaction between Dab1 and APP. Fyn recruitment results in the phosphorylation of APP at Tyr682 and tyrosines on Dab1 [233]. APP and Dab1 phosphorylation have divergent effects. APP phosphorylation at Y682 increases the affinity of APP for Dab1. While phosphorylation of Dab1, decreases the affinity of Dab1 for APP [233]. Tyrosine phosphorylated APP and Dab1 preferentially sort to signalling platforms known as lipid rafts through an increased affinity of tyrosine phosphorylated APP for Dab1 [234-236]. APP sequestered into lipid rafts by Dab1, also loses the ability to interact with other adaptors such as Fe65 and Mint [232,234].

The Dab family of proteins may also direct the internalization of APP and other cargo. The NPXY motifs of several transmembrane receptor proteins, including APP, LDLR and related receptors, and others, interact with the PTB domain of Dab [175,227,237]. Dab2 has been localized to clathrin coated pits (CCPs) [237]. At the CCPs, Dab regulates the formation of the clathrin lattice [238]. Consistent with these findings, Dab2 has been shown to mediate the loading of LRP6 into CCPs and away from the caveolin endocytosis pathway [239]. Dab2 can also interact with another AP-2, a heterotetrameric adaptor protein involved in clathrin endocytosis [237,240] (Figure 1.4, Step 2a). Therefore, Dab2 may aid in sorting cargo to CCPs through its interaction with cellular machinery for clathrin-mediated endocytosis.

The NPTY motif in APP is also responsible for interactions with JNK-interacting proteins (JIPs) [165,241]. The JIP family proteins serve as a scaffolding protein for the mitogen-activated protein kinase (MAPK) and c-Jun NH<sub>2</sub>-terminal protein kinases (JNKs) [242,243]. JNKs have important roles in regulating apoptosis, stress-response, neuronal migration, and microtubule stability [244]. Co-expression of JIP, JNK, and APP increases phosphorylation of APP at Thr668

[165,245-247]. Inhibition of JNK with an inhibitory peptide can shift APP processing towards non-amyloidogenic processing [245]. In the TgCRND8 mouse model of AD, the same inhibitory peptide lowered the levels of A $\beta$  oligomers in the brain, reversed LTP deficits, lowered plaque area, and improved performance on memory tasks [246]. In addition to its role in regulating APP metabolism, JIPs also connect APP to kinesin light chain (KLC), thus APP serves as a vesicle tether [165,248]. Neurons depend on anterograde transport (kinesin dependent) to move newly synthesized components from the cell body to axon terminals. Retrograde transport (dynein dependent) is equally important in transporting neurotrophic signals and endosomes from the axon terminals to the cell body. Disruption of the JNK signalling pathway results in the aberrant accumulation of synaptic proteins in the axon [249]. In agreement with these findings, APP-eGFP vesicles undergo more retrograde excursions at the expense of anterograde trafficking in JIP-1 deficient neurons [248].

## 1.2 Lysosomal Trafficking

Lysosomes are membrane bound organelles that are present in all nucleated eukaryotic cells. Morphologically, lysosomes typically range from 0.1 $\mu$ m-2 $\mu$ m in diameter, and appear as electron dense vesicles by electron microscopy. Lysosomes have an intraluminal pH of approximately 4.5, which is maintained by an ATP-dependent proton pump (vacuolar ATPases).

The acidity in lysosomes promotes the activity of the resident acidic hydrolases present within the lysosomal lumen. The hydrolases perform the primary cellular function of the lysosomes, which is to degrade and recycle macromolecules. Within lysosomes, there are approximately 50 different hydrolases [250]. The diversity of hydrolases allows lysosomes to digest a multitude of macromolecules, including proteins, nucleic acids, carbohydrates, and lipids.

Lysosomes also have integral membrane proteins and membrane associated membrane proteins. Proteomic studies have identified 215 integral membrane proteins and 55-membrane associated proteins. These proteins perform numerous functions including vesicular trafficking, metabolism, molecular transport, membrane structure, immunity, and other functions [251]. Two of the major integral membrane proteins are LAMP1 and LAMP2. Due to the heavy glycosylation of LAMP1

and LAMP2 they were originally thought to protect the lysosomal membrane from luminal hydrolases and maintain membrane integrity [252-254]. More recent work has now revealed that LAMP2 may have multiple roles, including autophagosome maturation and uptake of cytosolic proteins for chaperone-mediated autophagy [254].

### 1.2.1 Adaptor Proteins in lysosomal protein trafficking

One of the major pathways to the lysosome is through internalization at the cell surface. The best characterized mechanism is through clathrin coated vesicles [255]. Clathrin is recruited to cargo destined for internalization and forms a polygonal lattice on the cytoplasmic side of the membrane [256,257]. The membrane invaginates and detaches from the membrane before delivery to intracellular targets [258]. The signals responsible for internalization typically lie within 30Å from the membrane [259], but the clathrin lattice is 100Å from the membrane [260]. Therefore, endocytosis of cargo necessitates an adaptor to connect the cargo to the clathrin lattice. Electron microscopy of coated vesicles reveal a ‘fuzzy’ coat between the cargo and clathrin lattice [261]. These adaptor proteins were later identified as members of the heterotetrameric complex, AP-2. AP-2 is localized to the cell surface and is important in clathrin-mediated internalization. AP-2, and other members of this adaptor protein family, is composed of two large ( $\alpha$  and  $\beta$ 2, ~100kDa), one medium ( $\mu$ 2, 50kDa), and one small subunit ( $\sigma$ 2, 17kDa). The large subunits are composed of three regions; a trunk domain, an ear domain, and a hinge domain. The trunk domains of the large subunits,  $\sigma$ 2, and  $\mu$ 2 form the core of the AP-2 complex. The hinge domains connect the core to the ear domains [262]. The  $\beta$ 2 subunit hinge domain has a clathrin-binding sequence and interacts with the clathrin heavy chain and promotes lattice formation [263,264]. AP-2 binding to clathrin can be abrogated by serine phosphorylation within the hinge region [265]. The  $\alpha$  subunit has also been suggested to interact and promote the assembly of the clathrin lattice [266]. The  $\mu$ 2 subunit interacts with tyrosine internalization motifs (discussed later) and with phosphatidylinositol 4,5-bisphosphate (PI4,5P) [267]. PI4,5P is enriched at the plasma membrane, therefore the  $\mu$ 2 domain may help localize AP-2 to the cell surface, where it is critical for clathrin mediated internalization of cell surface proteins.

As in the AP-2 complex, the other members of this family are heterotetrameric complexes, which are composed of two large subunits, one medium subunit, and one small subunit [268]. The two large subunits of AP-1 are  $\gamma 1$  and  $\beta 1$ . The medium and small subunit are  $\mu 1$  and  $\sigma 1$ , respectively [269]. AP-1 is localized to endosomes and the trans-Golgi network (TGN), and has important roles in TGN export to lysosomes and endosomes, recycling at the plasma membrane, and retromer function [270-278]. As with the  $\beta 2$  subunit of AP-2, the  $\beta 1$  subunit interacts with clathrin and can promote clathrin lattice formation [263]. This interaction is also negatively regulated by serine phosphorylation within the hinge region [265]. There are two different isoforms of AP-1 and are distinguished by their different  $\mu 1$ -adaptin, A and B. The  $\mu 1A$  and  $\mu 1B$  adaptin are differentially localized in the cell, and associate with different cargo [274].  $\mu 1A$  sorts cargo from the TGN to endosome [279], and is preferentially localized to the TGN.  $\mu 1A$  deficient mice have drastic misrouting of lysosomal hydrolases [280]. Conversely, the  $\mu 1B$  adaptin preferentially colocalizes to sorting endosomes [273,274,276], and directs cargo to the basolateral membrane at the sorting endosome [274,276,277,281]. In the absence of  $\mu 1B$ ,  $\mu 1A$  containing complexes can also sort cargo to the basolateral membrane, albeit less efficiently than  $\mu 1B$ -containing complexes [276]. However,  $\mu 1B$  cannot adequately substitute for  $\mu 1A$ , as  $\mu 1A$ -KD is embryonically lethal in mice [280].  $\mu 1A$  deficient mice also have drastic misrouting of lysosomal hydrolases [280].

The third member of the adaptor protein family is AP-3. AP-3 has two large  $>100\text{kDa}$  ( $\beta$  and  $\delta$ ) subunits, one medium  $\sim 50\text{kDa}$  subunit ( $\mu 3$ ), and small  $\sim 25\text{kDa}$  subunit ( $\sigma 3$ ) [282-284]. The  $\beta 3$ ,  $\mu 3$ , and  $\sigma 3$  subunits are represented in A and B isoforms. The A isoform of AP-3 is ubiquitously expressed, but the B isoform is mainly expressed in neuronal tissue [282,283,285,286]. The role of AP-3 was first elucidated in yeast, where deletions of any of the AP-3 subunits disrupted delivery of alkaline phosphatase to the vacuole [287-289]. Disruption of the heterotetrameric AP-3 complex led to the retention of alkaline phosphatase (ALP) within the yeast Golgi [287]. These results were echoed in drosophila bearing the *garnet* or *ruby* mutation, which present with abnormal eye pigmentation due to mutations in the  $\delta$  and  $\beta 3A$  subunits, respectively [283,290]. Electron microscopy of retinal cells from drosophila revealed a dramatic decrease in the numbers of pigment granules, suggesting a deficit in pigment granule biogenesis [291]. Mice with

mutations in the  $\beta 3A$  or  $\delta$  subunit also had fewer pigment granules in the retinal epithelium and fewer platelet dense granules [292-294]. In humans, a mutation in the  $\beta 3A$  subunit was seen in a subtype of patients with Hermansky-Pudlak syndrome. These patients presented with oculocutaneous albinism, immunodeficiency and bleeding diathesis [295-297]. The melanosomes, cytolytic granules and platelet dense granules, which mediate skin pigmentation, immune function, and blood clotting, contain lysosomal proteins and are known as lysosome-related organelles (LROs) [298,299]. Therefore, AP-3 may have a role in lysosome and LRO biogenesis.

The AP-3 complex is localized to the tubulovesicular structures near the TGN and endosomes [282,284,300]. AP-3 is proposed to select cargo at the TGN or endosomal membrane for delivery to the lysosome. Human and mouse fibroblasts deficient in AP-3 misrouted LMPs (LAMP-1, CD63) to the cell surface [301,302]. Furthermore, cytosol depleted of  $\delta 3$  subunit was unable facilitate formation of melanosome protein and LAMP1 positive vesicles from donor Golgi membrane. Interestingly, loss of the  $\delta 3$  subunit had no effect on mannose-6-phosphate receptor (M6PR) vesicle formation [303]. Therefore, the function of AP-3 likely sequesters cargo into vesicles at the TGN or endosome for delivery to lysosomes. However, it remains to be determined if these vesicles are clathrin-coated. Initial studies could not identify AP-3 in clathrin-coated vesicles (CCV) fractions or by electron microscopy [282,286]. However, a later study identified a clathrin-binding motif on the trunk domain of  $\beta 3$  and localized AP-3 to clathrin at the TGN and endosomes [304].

The most recently discovered AP complexes are AP-4 and AP-5 [305,306]. AP-4 was first discovered by a BLAST sequence search for expressed sequences tags (EST) with similarity to subunits in AP 1-3. The search revealed a heterotetrameric complex with two large subunits ( $\beta 4$  and  $\epsilon$ ), one medium ( $\mu 4$ ), and one small ( $\sigma 4$ ) subunits. Unlike AP-1 and AP-3, only one isoform of AP-4 is known [305,306]. The new subunits localized strongly to the TGN and sequestered cargo into non-clathrin coated vesicles [305-307]. Initial studies on its function revealed it was responsible for sorting cargo to the basolateral membrane [307]. However, a more recent study by Burgos and colleagues [308] revealed a role for TGN to endosome trafficking.  $\mu 4$  KD



increased retention of APP in the TGN and increased A $\beta$  production [308]. Interestingly, AP-1 and AP-4 both sort cargo to the basolateral membrane from the TGN. With AP-1 being the more abundant isoform, AP-4 may serve as a specialized cargo adaptor [309]. However, when the cellular machinery for forming AP-1 clathrin coated vesicles was disrupted, there was a significant increase in the formation of AP-4 coated vesicles [310,311]. While the current evidence is unclear, it appears that AP-4 is responsible for sorting cargo to endosomes or the basolateral membrane from the TGN.

The newest member of the AP family is AP-5. Like the other members of the family, it contains two large subunits ( $\beta 5$  and  $\zeta$ ), one medium subunit ( $\mu 5$ ), and one small subunit ( $\sigma 5$ ). AP-5 strongly colocalizes with LAMP1 positive vesicles. Although the AP-5 cargo and functions remains to be fully revealed, early findings suggest a role for AP-5 in endosome and lysosome trafficking [312].

### 1.2.2 GGA Adaptors

Another family of proteins was discovered based on their homology to  $\gamma$ -adapting [313-315]. These monomeric proteins colocalized mainly to the TGN [313-317]. Localization to the TGN was abrogated in the presence of the Arf-GEF inhibitor, Brefeldin A [313,318]. The protein family was named  $\gamma$ -ear containing, Golgi-localized, Arf-binding protein (GGA).

The GGA family consists of three related proteins. Each protein contains a conserved VHS (Vps27, Hrs, Stam) domain, GAT (GGA and Tom1) domain, and a  $\gamma$ -adapting ear (GAE) domain. The VHS domain is responsible for cargo interaction [319]. The GAT domain is sufficient for TGN localization, and is recruited by GTP bound Arf proteins [314,320]. GGAs were found on the TGN or in nearby tubulovesicular structures, and were frequently associated with clathrin-coated buds [313,318]. Expression of a dominant negative mutant of GGA1 in HeLa cells resulted in impaired TGN-endosome trafficking, and resulted in mannose-6-phosphate receptor (M6PR) retention at the TGN [318].

GGA contains a clathrin-binding domain in the hinge region between the GAT and GAE domain [318]. The GAE domain interacts with accessory proteins that may participate in membrane

trafficking [321,322]. These findings suggest that GGA, like AP-1, may have a role in nucleating CCV formation at the TGN. However, GGA could not be detected in the clathrin-coated vesicle (CCV) fraction [313]. There are two possibilities that may resolve this paradox. GGA may facilitate the formation of vesicles distinct from AP-1 vesicles or GGA and AP-1 may work cooperatively to nucleate vesicle formation at the TGN. More recent studies are in support of the latter theory. Doray and colleagues [323] found that the GGA hinge domain interacts directly with the  $\gamma$ -ear of AP-1. Furthermore, casein kinase 2 (CK2) associates with AP-1 and can phosphorylate GGA1 [279,323]. CK2 phosphorylates GGA1 and GGA3 at a serine preceding an internal DXXLL (where X is any amino acid) motif. Serine phosphorylation increases the affinity of this motif for the DXXLL binding site on the VHS domain of GGA [323]. The phosphorylated internal motif outcompetes the DXXLL motif on the cargo for the binding site on the VHS domain. The auto-inhibition, by the internal DXXLL motif, decreases GGA's affinity for cargo and could facilitate the transfer of cargo from GGA adaptors to AP-1 adaptors.

While the majority of GGA localization is with the TGN, there is also colocalization between GGA and endosomes [313-317,320,324,325]. In live-cell imaging experiments, GGA1 is visualized leaving an endosome for the TGN-area [324], which suggests a possible role for GGA in retrograde trafficking.

GGA2 in yeast and GGA3 in mammalian cells can also interact with ubiquitin tagged cargo through their GAT domains [325-327]. Yeast with a GGA2 knockdown failed to deliver ubiquitinated cargo to the vacuole and misrouted ubiquitinated cargo to the cell surface [326]. Similarly, knockdown of GGA3 in mammalian cells leads to accumulation ubiquitinated EGF receptor and ubiquitinated BACE (memapsin 2) in early endosomes, which leads to a failure of BACE and EGFR degradation [325,327].

### 1.2.3 Trafficking of Lysosomal Hydrolases

The initial steps of lysosomal hydrolase synthesis are shared with other secretory proteins. The proteins are inserted into the endoplasmic reticulum lumen, and subsequent cleavage of the signal sequence. They are then glycosylated on selected asparagine residues by preformed

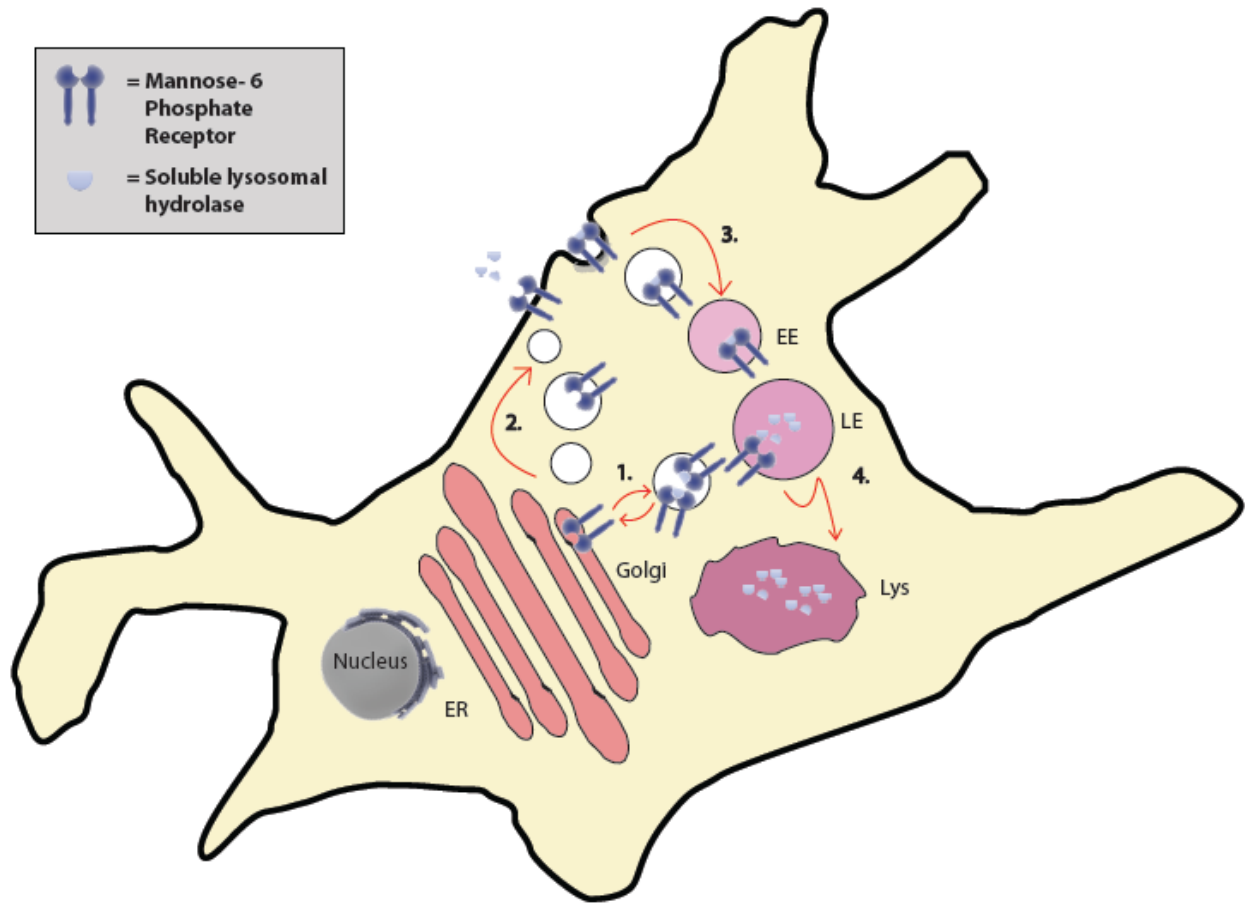
oligosaccharides. Recognition and transport of lysosomal hydrolases depends on the M6P marker. After glycosylation, the mannose residues are phosphorylated as the protein transits through the ER and Golgi [328]. The importance of mannose-6 phosphorylation is evident in patients with forms of mucopolidosis (I-Cell disease, Pseudo-Hurler polydystrophy). Cells from patients with mucopolidosis fail to phosphorylate M6P, and acidic hydrolases are secreted instead of properly sorted into lysosomes [329,330].

M6P is recognized by 2 distinct M6P receptors (M6PR). There is a cation-independent (CI) M6PR with a molecular mass of 300kDa and a cation-dependent (CD) M6PR with a mass of 46kDa. The CI M6PR contains 15 contiguous repeats, with each repeat being approximately 147 residues [328]. Each CI M6PR is capable of binding one completely phosphorylated hydrolase [331]. The CD M6PR is 159 residues and has 14-28% homology to each of the repeats in CI M6PR [328]. It exists as a dimer, and each dimer binds one hydrolase [331-333].

At the TGN, the M6PR are sorted into CCVs at the TGN, which then fuse with endosomes [334-336] (Figure 1.2, Step 1). Efficient sorting of M6PR to endosomes depends on dileucine motifs (LLHV and HLLPM) within the carboxyl terminals of CI M6PR and CD M6PR [320,337,338]. Mutagenesis of both motifs results in CatD secretion to the extracellular space [338]. The dileucine motifs found in the tail of M6PR, and other cytoplasmic tails, can interact VHS domain of GGA [319,324,339-341].

**Figure 1.2: Trafficking of Lysosomal Hydrolases**

Soluble lysosomal hydrolases are transported to the lysosome via the mannose-6-phosphate receptor (M6PR). The M6PR recognizes M6P moieties on the lysosomal hydrolase. **1)** It is believed that GGA1 and AP-1 may work cooperatively recruit and transport M6PR to the endosome. **2)** A small proportion (3-10) of M6PR, both cation dependent (CD) and cation independent (CI), can also be transported to the cell surface. **3)** At the cell surface, CI M6PR can internalize lysosomal hydrolases into endosomes. **4)** At the late endosome, M6PRs are recycled back to the Golgi, while the hydrolases continue on to the lysosome.



In addition to interacting with GGA proteins, M6PRs can also interact with a hetero-tetrameric adaptor protein (AP) family [342-345]. There are two binding sites for AP-1 within the CD M6PR tail (amino acids 28-42 and 49-67) [342]. As discussed earlier, there is evidence suggesting that GGAs and AP-1 work cooperatively to package M6PRs into CCVs at the TGN [323]. Active GGAs are purported to retain M6PRs in non-clathrin coated regions of the TGN [346]. The hinge region of GGA1 can interact with AP-1 and may be crucial in transferring M6PR into AP-1 positive CCVs [323]. Deletion of the hinge region results in AP-1 binding deficient GGA1 and traps M6PR in the TGN [320,323,347].

Beyond cargo sorting, GGAs and AP-1 also aid in CCV trafficking and fusion with early endosomes. While clathrin is released from vesicles relatively quickly after vesicle formation [348-352], AP-1 remains associated for an extended period. The  $\beta$ -subunit of AP-1 interacts with kinesin 13A, which could transport the M6PR towards intracellular targets [353]. Furthermore, the GAE domain of GGA and the  $\gamma$  subunit of AP-1 can interact with rabaptin5 [347]. Rabpatin5 interacts with Rab5 and likely aids in fusion of the vesicle with early endosomes [354-357].

Eventually, the lysosomal hydrolases are delivered into lysosomes through fusions between endosomes and lysosomes. However, the M6PR that deliver the hydrolases are recycled and do not appear in the lysosomes [358] (Figure 1.2, Step 4). On the C-terminal of M6PR there is a phenylalanine-tryptophan (FW) endosome retention motif recognized by TIP47 [359]. TIP47 also interacts with GTP bound Rab9 and this complex recycles M6PR from late endosomes; preventing M6PR from entering lysosomes [359-361]. Alternatively, M6PRs can be returned to the TGN via the actions of the Phosphofurin acidic cluster sorting protein 1 (PACS-1). PACS-1 directly interacts with AP-1 and M6PR at early endosomal membrane and mediates recycling from early endosomes [362,363] (Figure 1.2, Step 1).

While the majority of lysosomal hydrolases traffic directly to endosomes, a small proportion of both M6PRs (3-10% of total cellular M6PR) are present at the cell surface (Figure 1.2, Step 3). However, only CI-M6PR is responsible for endocytosis of M6P-containing ligands [336,364]. Rapid internalization of CI M6PR from the cell surface is dependent on the YSKV motif in the

cytosolic tail [365-367]. AP-2 can bind tyrosine and dileucine motifs and are crucial in the internalization of M6PR from the cell surface [368].

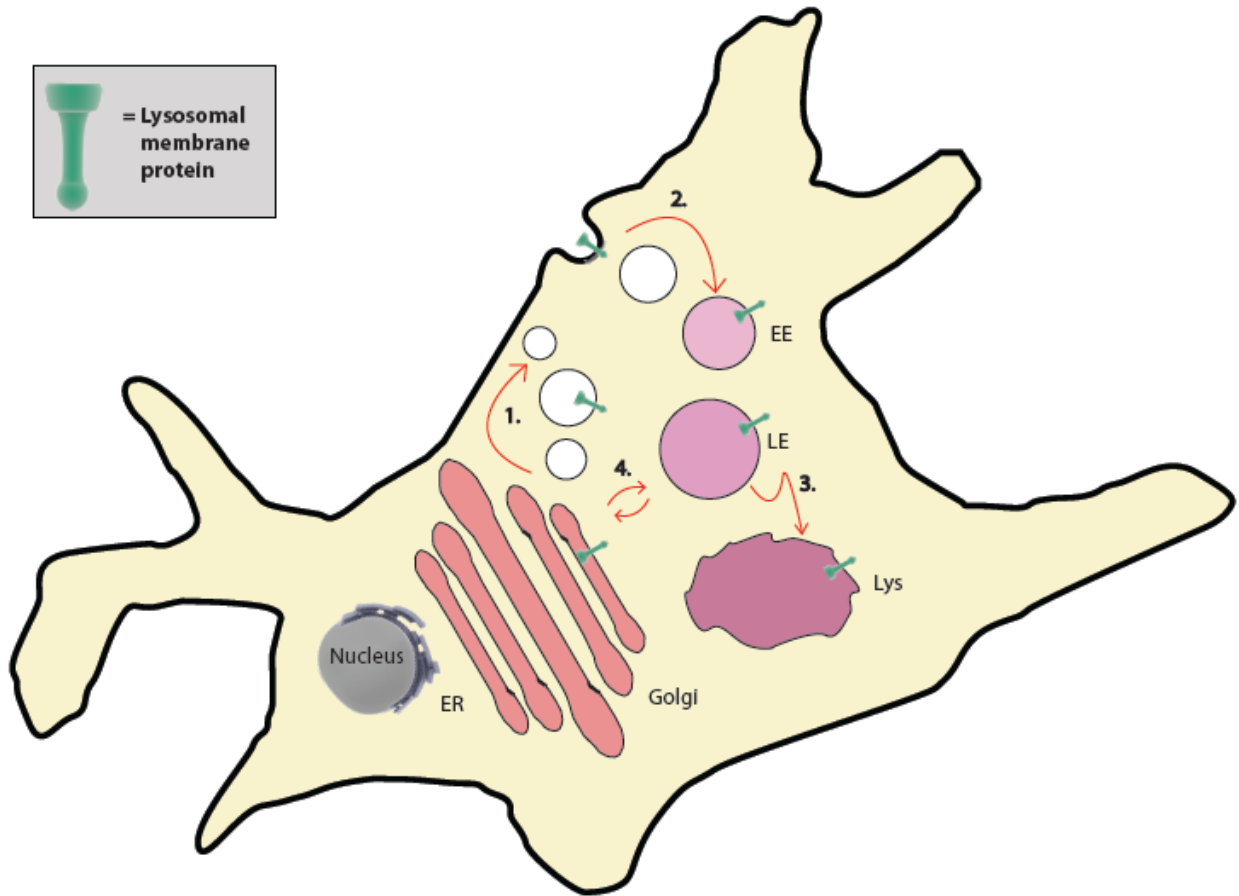
#### 1.2.4 Sorting of Lysosomal Membrane proteins

While soluble lysosomal hydrolases are responsible for the digestive role of lysosomes, membrane proteins (LMPs) are responsible for a number of important functions; including maintaining the acidity of the lysosomal lumen, formation of a protective glycocalyx [369], translocation of macronutrients to the cytosol from the lysosomal lumen, and lysosomal homotypic and heterotypic fusion. Lysosomal biogenesis is dependent on cooperation between the endocytic and biosynthetic systems of the cell. There are two pathways for LMPs to reach lysosomes. The first is directly from the TGN to the endosomal system. Other LMPs are delivered indirectly, by transiting through the cell surface before reaching the endosomal system (Figure 1.3). Sorting of LMPs by these pathways is dependent upon sequences within the cytosolic tail of LMPs. These motifs are degenerate sequences, of 4-7 residues and dependent on critical residues for their function. The main motifs can be separated into two main classes, named for their critical residuals; namely tyrosine- and dileucine-based motifs. These sorting motifs are saturatable, which suggests a dependence upon adaptor proteins.

**Figure 1.3:** Trafficking of Lysosomal Membrane Proteins

**1)** Membrane proteins destined for the lysosome can first be presented at the cell surface, and **2)** subsequently internalized by clathrin-mediated endocytosis. **3)** The proteins are eventually delivered to the lysosomal membrane. **4)** Lysosomal membrane proteins can also traffic directly to the late endosome and lysosomes via an intracellular pathway, which does not pass through the cell surface.





#### 1.2.4.1 NPXY Motifs

The importance of tyrosine motifs was seen in patients with familial hypercholesterolemia. Mutant alleles of the LDL receptor (LDLR) produced protein lacking the cytoplasmic domain were internalization defective [169]. This suggested an important motif within the cytoplasmic domain of LDLR. A mutation found in patient J.D. recapitulated the internalization defect, with a tyrosine to cysteine mutation in the cytoplasmic domain [170]. The critical tyrosine was later discovered to be within the NPVY motif of the LDLR. Mutation of any residues in the NPVY motif to alanine also diminished internalization of the LDL [370]. A minimal consensus NPXY motif was found in a subset of type 1 integral membrane proteins, and is responsible for rapid internalization of these proteins (where X represents a non-conserved residue). These proteins include family members of integrins, amyloid precursor protein, and LDL receptor. The  $\mu 2$  (~50kDa) and  $\delta 2$  (~17kDa) subunits form the core of AP-2 and recognize tyrosine-based motifs, including NPXY motifs. AP-2 interacts with the FDNPVY motif of LDLR through the  $\mu 2$  - adaptin subunit [259].

While the NPXY portion is the minimal motif shared among these proteins, there are other factors that influence the trafficking of these proteins. For example, mutation of a phenylalanine two residues preceding the asparagine also disrupts LDLR internalization [170]. Furthermore, replacing the transferrin receptor internalization motif with the minimal NPVY motif from LDLR does not promote rapid internalization of the transferrin receptor. However, transplantation of the entire motif, including the phenylalanine residue (FDNPVY), recapitulates rapid endocytosis in the transferrin receptor [171]. In contrast, internalization of APP is dependent on the longer GYENPTY motif [89,371]. The GYENPTY motif contains a tyrosine at position occupied by phenylalanine in the LDL receptor.

In some cases, the NPXY motif may also tolerate a phenylalanine at the critical tyrosine [372].  $\beta 1$  integrins contain two NPXY motifs in its cytoplasmic tail. However, tyrosine to phenylalanine mutations to both motifs does not interfere with protein internalization. In fact, mutated integrins are delivered more efficiently to lysosomes. However,  $\beta 1$ -integrin dependent

viral infection is hampered in Spinner-adapted murine L929 cells [172]. Tyrosine, but not phenylalanine, can be phosphorylated, which suggests that phosphorylation of the NPXY motif can regulate intracellular trafficking.

#### 1.2.4.2 YXXØ Motifs

AP-2 also interacts with another tyrosine motif of the form YXXØ (where X is any amino acid and Ø is any bulky amino acid) [259,373-376]. The  $\mu$ 2-adaptin domain of AP-2 recognizes the YXXØ motif, albeit at different residues from the NPXY motifs. Unlike the NPXY motif, the critical tyrosine residue cannot be substituted with phenylalanine. Recognition of the YXXØ motif absolutely requires the presence of tyrosine and bulky amino acid [373,375,377]. The crystal structure of  $\mu$ 2-adaptin bound to YXXØ peptides from EGFR and TGN38 has been resolved and revealed hydrophobic pockets that facilitate the binding of tyrosine and the bulky amino acid [378].

Deviations from the YXXØ motif can occur. The P2X4 receptor contains two YXXØ motifs (canonical: YKVL and non-canonical: YEQGL). Mutation of the canonical, but not the non-canonical motif interferes with P2X4 internalization [379]. While the distance between the critical tyrosine residue and the hydrophobic residue is highly conserved in the YXXØ motif, the presence of the glycine in the non-canonical YEQGL motif does not interfere with AP-2 interaction. The tyrosine and leucine occupy the same hydrophobic pockets as the canonical motif, as the glycine affords sufficient flexibility to the main chain [380].

In addition to the required tyrosine and hydrophobic amino acid, AP-2 also has a third hydrophobic pocket. P-selectin has a leucine residue, 3 residues preceding (L-3) the critical tyrosine that can interact with the third hydrophobic pocket. In P-selectin, mutagenesis the YGVF motif to AGVF or YGVA, unexpectedly, had little effect on internalization [381], which suggests the participation of other residues. Crystallography revealed the presence of binding pocket for a L-3 [382]. The cytoplasmic tail of the GABAAR  $\gamma$ 2 subunit also has a hydrophobic residue upstream of the YXXØ motif that binds to the same hydrophobic pocket [383].

Therefore, some motifs may depend on a 'third-prong' to interact with the  $\mu$ 2 subunit of AP-2.

As in NPXY motifs, there is evidence that tyrosines within the YXXØ motif can be phosphorylated. Tyrosine residues in the YGYECL are phosphorylated within the  $\gamma 2$  subunit of the GABA<sub>A</sub> receptor. Phosphorylation of these residues abrogates  $\mu 2$ -adaptin interaction with YGYECL motif *in vivo* [383]. Mice expressing the  $\gamma$  subunit with a phenylalanine mutation at these tyrosines increases the post-synaptic level of GABA<sub>A</sub> receptor and increases the frequency of miniature inhibitory post-synaptic potentials [384]. These results are substantiated by the failure of the phosphorylated TGN38 YXXØ motif to interact with  $\mu 2$ -adaptin [374,375].

In addition to phosphorylation of the tyrosine motif, the interaction between cargo and the AP-2 domain can also be regulated by phosphorylation of adaptin subunits in AP-2. The kinase interacts with the  $\alpha$  adaptin subunit and phosphorylates residue 156 of  $\mu 2$ -adaptin. This phosphorylation increases affinity of  $\mu 2$ -adaptin for YXXØ [385,386]. AP-2 can also be phosphorylated within the hinge region of large  $\alpha$  and  $\beta$  subunits and disrupts clathrin coat-assembly. Therefore, there is exquisite balance of phosphorylation and dephosphorylation of the AP-2 complex that regulates CCV formation.

While the tyrosine and hydrophobic residues in the YXXØ motif are critical, the internal X residues also dictate binding specificity. The  $\mu 2$  domain has the broadest binding specificity and highest affinity for YXXØ motifs. The  $\mu 2$  domain will tolerate a wide range of residues at the Y+1 and Y+2 positions [374,375,387]. The  $\mu 2$  domain prefers basic amino acids at Y+1 and Y+2, with a particularly strong preference for arginine at Y+2 [375,387]. Interestingly, internalization signals, but few lysosomal targeting signals have basic residues between the Y and Ø residues [366,367]. This agrees with the findings that AP-2 is responsible for internalization at the plasma membrane. Conversely,  $\mu 3a$  and  $\mu 3b$ , from AP-3, have a preference for glutamic acid at Y+1, which is characteristic of many lysosomal targeting YXXØ motifs. In addition  $\mu 3a$  is also the only domain that prefers glycine at position Y-1, which is a residue also found in many lysosomal targeting signals [387]. This suggests a role for AP-3 in lysosomal targeting. The  $\mu 1$  domain has a preference for aspartic acid and leucine at Y-1, but the functional consequences of  $\mu 1$  amino acid preference remain unclear [387].

### 1.2.4.3 Dileucine Motifs

Dileucine motifs, like tyrosine motifs, can signal protein internalization and delivery to endosomes and lysosomes. Dileucine motifs are present on lysosomal proteins (LIMP-II, NPC1), LRO proteins (TRP-1, Pmel17, and QNR-17). The dileucine motif was first discovered by Letourneur and Klausner who studied the rapidly internalizing CD3- $\gamma$  chain of the T-cell antigen receptor [388]. Despite deletion of the YQPL motif in the CD3- $\gamma$  chain tail, the protein was still rapidly internalized into endosomes and degraded in lysosomes. However, the combination of YQPL deletion and mutation of leucines, in the DKQTLL sequence, to alanine abrogated protein internalization and degradation [388]. The role of dileucine motif in internalization and lysosomal targeting was later confirmed in CD4 down-regulation by Nef, the HIV protein [389]. The motif was also found to be crucial for basolateral sorting in NPP1, CD44, FcRII  $\beta$ 2 receptor [390-392].

In addition to the critical leucines, an acidic cluster 3-4 residues preceding the initial leucine were also important for protein internalization [393]. Mutation of the acidic cluster (typically aspartic acid or glutamic acid) to the basic amino acid, arginine, results in misrouting of protein to the cell surface [394]. The spacing of the acidic cluster from the initial leucine is also crucial. Increasing the spacing of the acidic cluster from the leucines also disrupts protein trafficking [394]. The entire dileucine motif takes the form of [DE]XXXL[LI] or DXXLL.

The adaptor protein family can interact with dileucine motifs. Despite sharing an adaptor with the tyrosine motifs, there is no competition [395]. However, the nature of the dileucine binding site has not been confirmed. The  $\beta$  adaptins and  $\mu$  adaptins have been suggested as possible binding sites for dileucine motifs [396,397]. More recent evidence has suggested that the hemicomplexes formed by  $\sigma$  1/ $\gamma$ 1,  $\sigma$  2/ $\alpha$ 2, or  $\sigma$ 3a and b/ $\delta$ 3 can interact with dileucine motifs [398-402]. The  $\sigma$ 2 subunit provides a hydrophobic patch that facilitates the binding of the dileucine residues. A basic patch on the  $\sigma$  subunit interacts with the acidic cluster preceding the leucine residues [402]. These binding domains can also be found on hemicomplexes from AP-1 and AP-3 [400].

The non-conserved residues in dileucine motifs may offer some specificity to adaptor protein binding as well. A proline is preferred at one residue preceding the first leucine, because it allows for a protein conformation that facilitates binding [401]. The proline is not absolutely required by AP-2, which reflects the flexibility of AP-2 in substrate binding. However, the absence of proline appears to negatively affect AP-1 binding, but has a milder effect on AP-3 interaction [401]. This suggests that slight modifications to the X residues in dileucine motifs can influence adaptor binding [401]. A prime example is lysosome integral membrane protein II (LIMP2), which can bind AP-3, but not AP-1 or AP-2 [403].

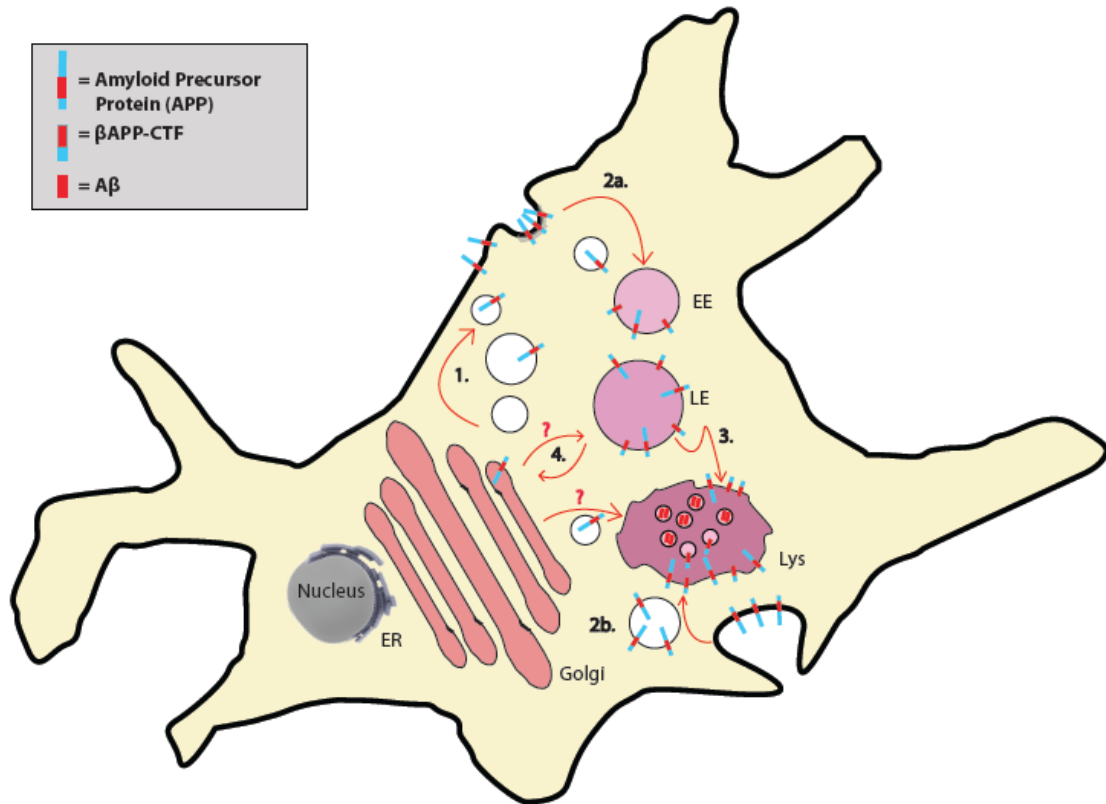
GGA proteins also interact with dileucine motifs via its VHS domain. Crystallography has revealed that the VHS domain of GGA forms a super-helix of eight helices. Helices 6 and 8 form a binding pocket that allows for hydrogen bonding between the helices and the acidic residues on the dileucine motifs (aspartic or glutamic acid). There is also a hydrophobic pocket that buries the leucines within the VHS domain [319]. Mutation of the acidic residues or the leucines to alanine disrupts internalization and lysosomal delivery of cargo.

### 1.3 Trafficking of the Amyloid Precursor Protein

In addition to serving as a binding site for PTB proteins, the NPTY motif is also involved in internalization of APP [44,371]. As discussed earlier, the NPTY motif is part of a family of NPXY internalization motifs [404]. In the cytoplasmic terminus of APP, the NPTY motif is part of a larger motif (GYENPTY), which contain residues that contribute to APP internalization [44,371]. AP-2 binds to NPXY motifs via its  $\mu 2$  subunit, and facilitates internalization [259,370]. AP-2 serves as a connector between the cytoplasmic tail of cargo to clathrin and other protein machinery involved in clathrin-mediated endocytosis (CME) [405]. AP-2 can immunoprecipitated with APP, and AP-2 knockdown decreases the internalization of APP [406,407]. After AP-2 recruitment, the membrane deforms and is coated with clathrin, and the vesicle is released from the membrane by dynamin scission [405]. Knockdown of dynamin and clathrin reduced APP internalization and reduced A $\beta$  production [42,408,409] (Figure 1.4, Step 2a).

**Figure 1.4:** The trafficking of Amyloid Precursor Protein

The known trafficking pathways for APP. After synthesis in the endoplasmic reticulum and glycosylation in the Golgi, **1)** it is generally accepted that APP is delivered in secretory vesicles to the cell surface. **2a)** Subsequently, APP is internalized by clathrin-mediated endocytosis (clathrin depicted as gray shading) into early endosomes. **3)** APP is eventually delivered to lysosomes and processed to form A $\beta$ . **2b)** Alternatively, recent work from our lab has demonstrated that APP can be internalized rapidly via macropinocytosis into lysosomes. **4)** APP can also be recycled to the Golgi from the endosome, by an interaction with the retromer.





Lipoprotein receptor-related protein 1 (LRP1) can also interact with APP and regulate its internalization [218,219,410]. The cytoplasmic tail of LRP contains two NPXY motifs, which participate in AP-2 mediated internalization [170,259,370]. The  $\alpha$  isoform of LRP1 promotes internalization, and increases A $\beta$  production, while the  $\beta$  isoform decreases internalization and promotes non-amyloidogenic processing of APP [411].

APP also interacts with other members of the heterotetrameric adaptor protein family (AP-1b and AP-4) [281,308]. AP-1b and AP-4 are involved in basolateral cargo sorting in polarized epithelial cells [281,307,412]. Neurons are also polarized cells and are divided into an axonal compartment and a somatodendritic compartment [413]. APP is delivered first to the axonal compartment [414,415], before being endocytosed from the axonal plasma membrane and delivered to dendrites [414]. The AP-1 complex in *C. elegans* is responsible for targeting of multiple proteins to the dendritic compartment [416]. In a similar way, disruption of the AP-4 complex in mouse neurons results in the misrouting of AMPA receptors to axonal autophagosomes [417,418]. Although the exact roles of AP-1 and AP-4 in neuronal cells remains to be elucidated, they may serve to regulate the polarized sorting of APP, and thereby control the amount of A $\beta$  produced (Figure 1.4, Step 1).

Recent work from our lab suggests that APP may also be internalized rapidly (within 15 minutes after appearance at the cell surface) into lysosomes [419]. This rapid internalization appears to be Arf6-dependent [420] (Figure 1.4, Step 2b). Electron microscopy revealed that APP is internalized into structures reminiscent of macropinosomes [421,422]. Furthermore, previous work has demonstrated that macropinosomes are capable of rapidly internalizing cargo to lysosomes within 15-minutes [422]. We have also demonstrated that rapid APP internalization depends on antibody cross-linking [420], which suggests that this pathway is dependent on the transduction of extracellular signals. Fe65, an APP interacting protein (described in detail above), has been shown to interact with Arf6 [222]. Therefore, it is tempting to suggest a signaling complex between APP, Fe65, and Arf6. The activation of Arf6 in this complex may activate downstream effectors of Arf6 (Rac1, phospholipase D1, PIP5K) to regulate cell shape

and APP macropinocytosis [423]. However, further evidence will be required to confirm the presence of this proposed signaling pathway. Indeed, recent work from the Annaert lab [424] suggests it is BACE1, and not APP that is internalized in an Arf6-dependent manner in non-neuronal cells. Therefore, further work will be required to elucidate the role of Arf6 in APP trafficking.

## 1.4 Lysosomal Pathology in Alzheimer's Disease

Lysosomes also appear to have a critical, yet not fully understood role, in AD pathology [425-427]. Perhaps the first evidence of lysosomal involvement in AD aetiology was the presence of active lysosomal enzymes (i.e. Cathepsin D,  $\beta$ -hexosaminidase) as a major constituent of senile plaques [428-430]. The enzymes were associated with membrane-delimited lipofuscin granules, which contain the lipid and protein remains of failed lysosomal degradation [428]. Enlarged early endosomes and lysosomes are among the earliest abnormalities observed in AD, and appear before the appearance of neurofibrillary pathology or extracellular amyloid-plaques [431-434]. Strikingly, these enlarged endosomes are found in layers of the cortical mantle that are afflicted in the early stages of AD suggesting that endosomal/lysosomal pathology may precede the more traditional markers (neurofibrillary tangles and amyloid plaques) of AD [14,431,434]. Fibroblasts of Down syndrome patients, who invariably develop AD pathology by age 30, also have enlarged early endosomes and abnormal endocytosis [435]. Furthermore, these fibroblasts redistribute CatD from lysosomes to early endosomes. CD-MPR expression is increased in AD and over expression of CatD in murine fibroblasts increases CatD localization to early endosomes [434,436]. CD-MPR over expression in cultured cells can recapitulate the mis-localization of CatD and increase the secretion of A $\beta$ 40 and A $\beta$ 42 [436]. CatD expression is abnormally increased in AD, and follows the laminar pattern seen with NFT and enlarged endosomes [428,430,437-440].

The abnormal increase of CatD expression, and other lysosomal hydrolases, is recapitulated in various mouse models of AD [441,442]. In TgCRND8, a mouse model of AD, there is an increase in the number of enlarged CatD-positive lysosomes. These vesicles also stained for ubiquitin and LC3, which suggests an accumulation of undigested proteins in autolysosomes

[442]. Restoring CatD activity reduced the number of abnormal lysosomes and autophagosomes, decreased amyloid plaque load, and improved cognition [442]. Up-regulation of lysosomal activity can increase the clearance of intracellular A $\beta$  [443]. In animals bearing FAD mutants of PS1 and APP, there was a significant increase in autophagic bodies in the cell bodies and neurites of neurons [444]. The increased number and size of autophagic vacuoles can also be found in the brains of AD patients [444,445]. These autophagic vacuoles are enriched in dystrophic neurites, which are found surrounding the core of the amyloid plaque [445,446]. A $\beta$  can be immunolocalized to autophagic vacuoles and lysosomes, and A $\beta$  production can be potentiated by activation of autophagy [444]. Treatment of neurons with fibrillar aggregates of A $\beta$  can increase neurite dystrophy [447]. There appears to be a deficiency in lysosomal proteolysis in AD.

Lysosomes serve as an optimal intracellular milieu to nucleate A $\beta$ . Indeed, Hu et al. [448] demonstrated that A $\beta$  accumulated in lysosomes can seed the formation of A $\beta$  fibrils *in vitro*. The lysosomes offer an acidic environment, which is optimal for A $\beta$  aggregation [449]. The acidic environment also promotes the insertion of A $\beta$  into the lipid membranes, which protects A $\beta$  from degradation [450]. Interestingly, A $\beta$  can interact with ganglioside clusters to form a complex, which encourages A $\beta$  fibrilization [451,452]. Transgenic AD mice treated with an antibody against the ganglioside/A $\beta$  complex reduced plaque deposition [453]. Therefore, the acidic milieu and the lipid composition of the lysosomal membrane can promote lysosomal aggregation of A $\beta$ .

The deficiency of lysosomal enzyme activity can cause the accumulation of lipids and gangliosides in the lumen. These enzyme deficiencies cause lysosomal storage diseases and result in the accumulation of A $\beta$  in the neurons of mouse models and human patients. For example, in *HEXB* KO mice (Sandhoff disease mouse model), there was an accumulation of ganglioside/A $\beta$  complexes in endosomes and lysosomes [454]. Pharmacologically-induced accumulation of GM1 recapitulates the endosomal fibrilization of A $\beta$  on ganglioside clusters [455]. The secondary accumulation of A $\beta$  can also be seen in animal models of Niemann Picks Disease (NPD), which accumulate cholesterol in the lysosomal lumen. In rabbits fed a high

cholesterol diet, there were perturbed lysosomal protease activity, enlarged endosomes and lysosomes, and increased the intracellular accumulation of A $\beta$  in the brain [432]. Furthermore, addition of excess cholesterol in the cell culture media of cultured rat neurons also resulted in lysosomal pathology and an increase in A $\beta$  production [456]. The cholesterol-induced enlargement of endosomes and lysosomes are also seen in NPD type C [457]. Therefore, the accumulation of lipids, reminiscent of lysosomal storage diseases, can promote the secondary accumulation of A $\beta$ .

The aberrant accumulation of cholesterol may also affect the activity of secretases participating in APP metabolism. The accumulation of cholesterol can influence the function of secretases involved in the processing of APP. High concentrations of cholesterol can decrease the membrane fluidity and decrease the interaction of  $\alpha$ -secretase and APP [458]. The decreased  $\alpha$ -secretase cleavage of APP can result in the increased amyloidogenic cleavage [48]. The accumulation of cholesterol in NPD type C can also modulate the localization and activity of  $\beta$ -secretase [459]. CHO cells with a NPC knockout have an increased production of  $\beta$ -CTF, which suggests increased  $\beta$ -secretase cleavage; despite no change in enzyme activity. [460]. It was later revealed that in CHO NPC KO cells,  $\beta$ -secretase (BACE) is localized to early endosomes, and the trafficking defect can be rescued by correcting cholesterol accumulation [461]. Furthermore, cerebrospinal fluid from NPD type C patients revealed a relative increase in the amount of neurotoxic A $\beta$ 42, which suggests the modulation of  $\gamma$ -secretase cleavage [462].

Conversely, the accumulation of intracellular A $\beta$  may inhibit the activity of lysosomal proteases. While the most obvious aggregates of amyloid in AD are extracellular, there is accumulating evidence of intracellular lysosomal amyloid aggregates; well before the appearance of extracellular plaques [463]. Perhaps the first observation of intracellular amyloid was seen in human foreskin fibroblasts, which accumulated exogenous A $\beta$  intracellularly [464]. Shortly after, there were observations of endogenous A $\beta$  accumulating intracellularly in neuronal cell lines and human primary neuronal cultures [52,141,465,466]. Interestingly, these intracellular aggregates appear to be resistant to degradation [52,464], and accumulate in the endosomal/lysosomal system [463,467,468] [432,439,456,469].

In addition FAD mutations in PS1 may also play a role in regulating lysosomal enzyme activity through maintaining lysosomal pH. PS1 is the catalytic component of the  $\gamma$ -secretase complex, but may have other roles; including regulate lysosomal pH and ER-calcium storage [470,471]. Lysosomes in PS1<sup>-/-</sup> neurons have increased pH, which leads to the accumulation of autophagic vacuoles [471,472]. However, it should be noted that these results are controversial, as these findings were not replicated by other laboratories [473-475]. The effects of PS1<sup>-/-</sup> are independent of PS's catalytic activity, because inhibition of  $\gamma$ -secretase does not result in the accumulation of autophagic bodies [472]. Introducing PS1 FAD mutants to PS1<sup>-/-</sup> fibroblasts does not re-acidify lysosomes and cannot rescue lysosomal proteolysis [471]. However, the effect of PS1 FAD mutants on lysosomal activity remains to be elucidated, as a conflicting study found that reintroduction of PS1 FAD mutants can clear cells of autophagic bodies [472]. More recently, fibroblasts from patients expressing the PS1 FAD mutation, A246E, also have a decrease in lysosomal pH and decreased maturation of CatD [476]. This suggests that PS1 may have an important role in maintaining lysosomal pH.

The intracellular accumulation may have several deleterious consequences to neurons. Luminal aggregates of A $\beta$  make the lysosomal membrane more labile, which leads to the leaking of lysosomal proteases into the cytosol [450]. Indeed, the release of lysosomal hydrolases into the cytosol can precede apoptotic cell death [477-479]. In some cases, the intracellular A $\beta$  may lead to cell rupture. The immunohistochemical examination of entorhinal and hippocampal cortex from AD patients revealed the presence of ruptured cells, which more numerous surrounding amyloid plaques [480]. Alternatively, it has also been suggested that the intracellular aggregates of A $\beta$  can be released into the extracellular space by exosomes and seed the fibrilization of A $\beta$  (intraluminal vesicles in endosomes and lysosomes) [481]. The trans-cellular spread of intracellular aggregates is not restricted to amyloid, but can also be observed in Parkinson's disease in the exosomal release of  $\alpha$ -synuclein [482,483].

## 1.5 Lysosomal Secretion

Lysosomes are commonly viewed as the disposal system of the cell, but are recognized to have a secretory function in many cell types [484]. Lysosomes are secreted to the cell surface for

membrane repair [485,486]. Furthermore, in neurons lysosomes potentially provide the membrane required for neurite outgrowth [487]. They are involved in the secretion of thyroid hormone, pulmonary surfactant, albumin, and cytotoxic molecules from cytotoxic T lymphocytes (CTLs) [485,488,489]. Vesicles carrying these cargo belong to a family of lysosome-related organelles (LROs) [490]. LROs share some hydrolases and membrane proteins with lysosomes, but are unique in the cargo they carry to perform specialized roles.

The mechanism underlying LRO and conventional lysosome secretion is complex and requires the cooperation of many proteins. Before successful degranulation, each secretory granule must be delivered to the cell surface, tethered, docked, and stimulated to release by increased intracellular calcium [491]. Genetic disruption of steps in LRO release can lead to familial hemophagocytic lymphohistiocytosis (FHL) or Griscelli syndrome (GS).

Griscelli syndrome is an autosomal recessive disease that is characterized by partial albinism and immunodeficiency [492]. There are three types of GS and they affect genes expressing a group of three interacting proteins (myosin Va, Rab27a, and melanophilin). Type 2 GS is caused by a mutation in Rab27a [493]. In GS, melanocytes accumulate pigment in melanosomes and natural killer (NK) cells have decreased cytotoxic activity [494]. Expression of dominant negative mutants of Rab27b (a brain expressed isoform) [495] in PC12 cells decreases ACTH secretion from dense core granules [496]. These deficits are likely due to disrupted LRO trafficking and plasma membrane docking. Rab27a deficient melanocytes mis-sort melanosomes to the perinuclear region [497]. Expression of dominant negative mutants of Rab27a in a melanocyte cell line phenocopies the melanosome distribution [498]. In addition to vesicle delivery to the subplasmalemmal region, Rab27 likely also participates in vesicle docking. Lytic granules in CTLs from *ashen* mice (Rab27a KO mice) can polarize towards the target cell, but do not dock at the plasma membrane [499]. Furthermore, knockdown of Rab27a or Rab27b leads to increased mobility of lysosomes at the cell surface, which suggests that Rab27 may participate in lysosomes and LRO docking [500]. Therefore, Rab27 has an important role governing the transport and docking of LROs, and likely lysosomes.

The function of Rab27 depends on the function of its many effectors. Rab27 effectors have an amino terminal Rab interacting domain and, typically, two carboxyl terminal C2 domains. The C2 domains are not present in all interacting proteins [501]. These effectors facilitate the docking and transport functions of Rab27 by facilitating interaction with microtubules, actin filaments, and SNARE complexes [501,502].

Melanophilin (Mlph) is a Rab27 interacting protein and mutations that impair its interaction with Rab27 result in GS type 3 [503]. In addition to Rab27, Mlph also interacts with the actin motor, Myosin Va (MyoVa), which results in a tripartite complex [504]. Mutation of any of these three proteins results in GS [505]. Indeed, expression of the Rab27 binding domain of Mlph acts as a dominant-negative, likely by sequestering active Rab27, causing melanosomes to accumulate in the perinuclear area [504]. Interestingly, Mlph also tracks the plus end of microtubules, through an interaction with the microtubule associated end binding protein 1 (EB1). This suggests that it may participate in melanosome delivery to cell periphery [506]. MyoVa also tracks the microtubule plus end in a Mlph dependent manner [506]. However, in the absence of MyoVa, bidirectional microtubule transport of melanosomes is normal [507]. However, in the absence of MyoVa, melanosomes are not captured in the actin-rich periphery and become concentrated in the perinuclear region [508,509]. Therefore, the Rab27a, Mlph, and MyoVa complex is involved in vesicle trafficking to the cell periphery and efficiently dock them at the cell membrane.

Another Rab27 effector, Exophilin 7 in neutrophils, is involved in the organization of actin filaments. Exophilin 7 interacts with the RhoA-GTPase-activating protein (GAP), Gem-interacting protein (GMIP), and participates in actin filament depolymerization [510]. Cortical actin serves as a physical barrier between vesicles and the cell membrane [511,512]. At the cell periphery, azurophilic granules, from human neutrophils, can traverse cortical actin barrier by depolymerizing actin. However, preventing actin depolymerisation, by loss of GMIP-mediated RhoA inactivation, decreases granule attachment to the membrane [510].

In addition to trafficking and docking to the cell periphery, there is also cellular machinery to facilitate the fusion of lysosomes and LROs with the cell surface. The mechanism responsible is the SNARE machinery, which was first identified in studies of synaptic vesicle exocytosis. In

synaptic vesicle exocytosis, the formation of the SNARE complex is thought to provide the energy needed for membrane fusion. Target SNARE (t-SNARE) proteins on the plasma membrane (SNAP-23, synaptobrevin 2) interact with vesicular SNARE (v-SNARE) proteins to form a four-helix bundle [513].

The exact SNARE machinery for LRO and lysosome exocytosis is likely dependent on the cell-type in question. In cells of the hemopoietic lineage, syntaxin 11 is required for the formation of the SNARE complex with vesicle associated membrane protein 8 (VAMP8) and SNAP-23 [514]. Mutations in syntaxin 11 leads to the development of familial hemophagocytic lymphohistiocytosis (FHL) 4 [515]. Platelets and CTLs from FHL 4 patients have a deficit in LRO degranulation [514,516].

FHL can also be caused by mutations in Munc13-4 and Munc 18, which cause FHL 3 and FHL 5, respectively [517]. Munc 13-4 complexes with Rab27 and is critical for docking secretory lysosomes to the cell surface after stimulation. Mutation of critical residues that participate in Rab27 binding abrogates vesicle tethering to the cell surface and decreases lysosome secretion [517]. Munc 18-2 likely catalyzes membrane fusion between lysosomes and the cell surface. In synaptic vesicles, Munc 18 proteins are absolutely required for the fusion of synaptic vesicles with the presynaptic membrane [513]. In agreement, natural killer cells properly polarize cytotoxic granules to the immunological synapse, but do not degranulate and result in decreased cell killing [518,519].

## 1.6 Rationale and Hypothesis

According to the amyloid cascade hypothesis, the pathological production and accumulation of A $\beta$  is thought to be the initiating factor in AD pathology [35]. Work from our lab and others have implicated the endosomal/lysosomal system in A $\beta$  production [40,42,44,419]. Recent work has revealed that endosomes and lysosomes accumulate intraluminal A $\beta$  [439,463,464,467]. These intracellular A $\beta$  aggregates are resistant to degradation and can seed the formation of A $\beta$  fibrils *in vitro* [52,464].



In AD, the production and accumulation of A $\beta$  appears to be a critical part of the disease process. Despite the importance of APP trafficking to lysosomes in production of A $\beta$ , the process is not fully understood. The intracellular trafficking of nascent APP to the endosomal/lysosomal system is relatively understudied, due to the difficulty in tagging nascent proteins for microscopy. APP also contains three tyrosine motifs, which have been shown to be involved in endocytosis and basolateral sorting [44,281]. However, the role of these motifs, if any, in the sorting of nascent APP from the Golgi apparatus is unknown. While it is thought that A $\beta$  is produced intracellularly in lysosomes, the mechanism, which allows these intracellular stores to access the extracellular space has yet to be elucidated. *It is hypothesized that APP can traffic intracellularly to lysosomes to produce A $\beta$ , which can be secreted via lysosome exocytosis.*

## 1.7 Objectives

To test this hypothesis, the following objectives were studied. 1) Using a photoactivatable version of GFP attached to the C-terminal end of APP, we will demonstrate the intracellular trafficking of APP from the Golgi to lysosomes, without first transiting the cell surface. 2) We will to modulate the intracellular trafficking of APP by genetically and pharmacologically manipulating the C-terminal sorting signals of APP. 3) Finally, we will determine the eventual fate of A $\beta$  produced in the lysosome.

## 1.8 References

1. Corrada MM, Brookmeyer R, Paganini-Hill A, Berlau D, Kawas CH. Dementia incidence continues to increase with age in the oldest old: the 90+ study. *Ann Neurol*. 2010;67: 114–121. doi:10.1002/ana.21915
2. Alzheimer's Association. Changing the Trajectory of Alzheimer's Disease: How a Treatment by 2025 Saves Lives and Dollars. *Alzheimers Dement*. 2015;10: e47–92.
3. Smetanin P, Smetanin P, Kobak P, Briante C, Stiff D, Sherman G, et al. Rising Tide: The Impact of Dementia in Canada 2008 to 2038. 2009.
4. Goedert M, Wischik CM, Crowther RA, Walker JE, Klug A. Cloning and sequencing of the cDNA encoding a core protein of the paired helical filament of Alzheimer disease: identification as the microtubule-associated protein tau. *Proc Natl Acad Sci USA*. 1988;85: 4051–4055.
5. Ball MJ. Neuronal loss, neurofibrillary tangles and granulovacuolar degeneration in the hippocampus with ageing and dementia. A quantitative study. *Acta Neuropathol*. 1977;37: 111–118. doi:10.1007/BF00692056
6. Kidd M. Paired helical filaments in electron microscopy of Alzheimer's disease. *Nature*. 1963;197: 192–193. doi:10.1038/197192b0
7. Wischik CM, Novak M, Thøgersen HC, Edwards PC, Runswick MJ, Jakes R, et al. Isolation of a fragment of tau derived from the core of the paired helical filament of Alzheimer disease. *Proc Natl Acad Sci USA*. 1988;85: 4506–4510.
8. Weingarten MD, Lockwood AH, Hwo SY, Kirschner MW. A protein factor essential for microtubule assembly. *Proc Natl Acad Sci USA*. 1975;72: 1858–1862.
9. Biernat J, Gustke N, Drewes G, Mandelkow EM, Mandelkow E. Phosphorylation of Ser262 strongly reduces binding of tau to microtubules: distinction between PHF-like immunoreactivity and microtubule binding. *Neuron*. 1993;11: 153–163.
10. Lindwall G, Cole RD. Phosphorylation affects the ability of tau protein to promote microtubule assembly. *Journal of Biological Chemistry*. 1984;259: 5301–5305.
11. Mandelkow EM, Drewes G, Biernat J, Gustke N, Van Lint J, Vandenhede JR, et al. Glycogen synthase kinase-3 and the Alzheimer-like state of microtubule-associated protein tau. *FEBS Letters*. 1992;314: 315–321.
12. Utton MA, Vandecandelaere A, Wagner U, Reynolds CH, Gibb GM, Miller CC, et al. Phosphorylation of tau by glycogen synthase kinase 3beta affects the ability of

- tau to promote microtubule self-assembly. *Biochem J.* 1997;323 ( Pt 3): 741–747.
13. Zaidi T, Grundke-Iqbal I, Iqbal K. Role of abnormally phosphorylated tau in the breakdown of microtubules in Alzheimer disease. *Proc Natl Acad Sci USA.* 1994;91: 5562–5566.
  14. Braak H, Braak E. Neuropathological staging of Alzheimer-related changes. *Acta Neuropathol.* 1991;82: 239–259.
  15. Förstl H, Kurz A. Clinical features of Alzheimer's disease. *Eur Arch Psychiatry Clin Neurosci.* 1999;249: 288–290. doi:10.1038/nm.2785
  16. Liu L, Drouet V, Wu JW, Witter MP, Small SA, Clelland C, et al. Trans-synaptic spread of tau pathology in vivo. Ikezu T, editor. *PLoS ONE.* 2012;7: e31302. doi:10.1371/journal.pone.0031302
  17. Kuchibhotla KV, Wegmann S, Kopeikina KJ, Hawkes J, Rudinskiy N, Andermann ML, et al. Neurofibrillary tangle-bearing neurons are functionally integrated in cortical circuits in vivo. *Proceedings of the National Academy of Sciences.* 2014;111: 510–514. doi:10.1073/pnas.1318807111
  18. Rudinskiy N, Hawkes JM, Wegmann S, Kuchibhotla KV, Muzikansky A, Betensky RA, et al. Tau pathology does not affect experience-driven single-neuron and network-wide Arc/Arg3.1 responses. *Acta Neuropathol Commun.* 2014;2: 63. doi:10.1186/2051-5960-2-63
  19. Masters CL, Simms G, Weinman NA, Multhaup G, McDonald BL, Beyreuther K. Amyloid plaque core protein in Alzheimer disease and Down syndrome. *Proc Natl Acad Sci USA.* 1985;82: 4245–4249.
  20. Snyder SW, Lador US, Wade WS, Wang GT, Barrett LW, Matayoshi ED, et al. Amyloid-beta aggregation: selective inhibition of aggregation in mixtures of amyloid with different chain lengths. *Biophysical Journal.* Elsevier; 1994;67: 1216–1228. doi:10.1016/S0006-3495(94)80591-0
  21. Halverson K, Fraser PE, Kirschner DA, Lansbury PT. Molecular determinants of amyloid deposition in Alzheimer's disease: conformational studies of synthetic beta-protein fragments. *Biochemistry.* 1990;29: 2639–2644.
  22. Yankner BA, Lorenzo A, Yuan M, Zhang Z, Paganetti PA, Sturchler-Pierrat C, et al. Amyloid beta interacts with the amyloid precursor protein: a potential toxic mechanism in Alzheimer's disease. *Nature Neuroscience.* 2000;3: 460–464. doi:10.1038/74833
  23. Li YP, Bushnell AF, Lee CM, Perlmutter LS, Wong SK. Beta-amyloid induces apoptosis in human-derived neurotypic SH-SY5Y cells. *Brain Research.* 1996;738:

196–204.

24. Lorenzo A, Yankner BA. Amyloid fibril toxicity in Alzheimer's disease and diabetes. *Annals of the New York Academy of Sciences*. 1996;777: 89–95. doi:10.1111/j.1749-6632.1996.tb34406.x
25. Monji A, Yoshida I, Tashiro K, Hayashi Y, Matsuda K, Tashiro N. Inhibition of A beta fibril formation and A beta-induced cytotoxicity by senile plaque-associated proteins. *Neuroscience Letters*. 2000;278: 81–84. doi:10.1016/S0304-3940(99)00899-X
26. Soto C, Sigurdsson EM, Morelli L, Kumar RA, Castaño EM, Frangione B. Beta-sheet breaker peptides inhibit fibrillogenesis in a rat brain model of amyloidosis: implications for Alzheimer's therapy. *Nat Med*. 1998;4: 822–826. doi:10.1038/nm0798-822
27. Busciglio J, Lorenzo A, Yeh J, Yankner BA. beta-amyloid fibrils induce tau phosphorylation and loss of microtubule binding. *Neuron*. 1995;14: 879–888.
28. Roberson ED, Scarce-Levie K, Palop JJ, Yan F. Reducing Endogenous Tau Ameliorates Amyloid  $\beta$ -Induced Deficits in an Alzheimer's Disease Mouse Model. *Science*. American Association for the Advancement of Science; 2007;316: 750–754. doi:10.1126/science.1141736
29. Naslund J, Haroutunian V, Mohs R, Davis KL, Davies P, Greengard P, et al. Correlation between elevated levels of amyloid beta-peptide in the brain and cognitive decline. *JAMA*. 2000;283: 1571–1577.
30. Kaye R, Head E, Thompson JL, McIntire TM, Milton SC, Cotman CW, et al. Common structure of soluble amyloid oligomers implies common mechanism of pathogenesis. *Science*. 2003;300: 486–489. doi:10.1126/science.1079469
31. Lambert MP, Barlow AK, Chromy BA, Edwards C, Freed R, Liosatos M, et al. Diffusible, nonfibrillar ligands derived from Abeta1-42 are potent central nervous system neurotoxins. *Proc Natl Acad Sci USA*. 1998;95: 6448–6453.
32. Lacor PN, Buniel MC, Furlow PW, Clemente AS, Velasco PT, Wood M, et al. Abeta oligomer-induced aberrations in synapse composition, shape, and density provide a molecular basis for loss of connectivity in Alzheimer's disease. *Journal of Neuroscience*. 2007;27: 796–807. doi:10.1523/JNEUROSCI.3501-06.2007
33. Park J, Jang M, Chang S. Deleterious effects of soluble amyloid- $\beta$  oligomers on multiple steps of synaptic vesicle trafficking. *Neurobiology of Disease*. 2013;55: 129–139. doi:10.1016/j.nbd.2013.03.004
34. Zempel H, Luedtke J, Kumar Y, Biernat J, Dawson H, Mandelkow E, et al.

- Amyloid- $\beta$  oligomers induce synaptic damage via Tau-dependent microtubule severing by TLL6 and spastin. *The EMBO Journal*. 2013;32: 2920–2937. doi:10.1038/emboj.2013.207
35. Hardy JA, Higgins GA. Alzheimer's disease: the amyloid cascade hypothesis. *Science*. 1992;256: 184–185.
  36. Hardy J. Alzheimer's disease: the amyloid cascade hypothesis: an update and reappraisal. *J Alzheimers Dis*. 2006;9: 151–153.
  37. De Strooper B, Chávez Gutiérrez L. Learning by Failing: Ideas and Concepts to Tackle  $\gamma$ -Secretases in Alzheimer Disease and Beyond. *Annu Rev Pharmacol Toxicol*. 2014;55: 141204113359009. doi:10.1146/annurev-pharmtox-010814-124309
  38. De Strooper B. Lessons from a Failed  $\gamma$ -Secretase Alzheimer Trial. *Cell*. 2014;159: 721–726. doi:10.1016/j.cell.2014.10.016
  39. Holmes O, Paturi S, Ye W, Wolfe MS, Selkoe DJ. Effects of Membrane Lipids on the Activity and Processivity of Purified  $\gamma$ -Secretase. *Biochemistry*. 2012;51: 3565–3575. doi:10.1021/bi300303g
  40. Pasternak SH, Bagshaw RD, Guiral M, Zhang S, Ackerley CA, Pak BJ, et al. Presenilin-1, nicastrin, amyloid precursor protein, and gamma-secretase activity are co-localized in the lysosomal membrane. *J Biol Chem*. 2003;278: 26687–26694. doi:10.1074/jbc.M212192200
  41. Bagshaw RD, Pasternak SH, Mahuran DJ, Callahan JW. Nicastrin is a resident lysosomal membrane protein. *Biochemical and Biophysical Research Communications*. 2003;300: 615–618.
  42. Cirrito JR, Kang J-E, Lee J, Stewart FR, Verges DK, Silverio LM, et al. Endocytosis Is Required for Synaptic Activity-Dependent Release of Amyloid- $\beta$  In Vivo. *Neuron*. 2008;58: 42–51. doi:10.1016/j.neuron.2008.02.003
  43. Cirrito JR, Yamada KA, Finn MB, Sloviter RS, Bales KR, May PC, et al. Synaptic Activity Regulates Interstitial Fluid Amyloid- $\beta$  Levels In Vivo. *Neuron*. 2005;48: 913–922. doi:10.1016/j.neuron.2005.10.028
  44. Perez RG, Soriano S, Hayes JD, Ostaszewski B, Xia W, Selkoe DJ, et al. Mutagenesis identifies new signals for beta-amyloid precursor protein endocytosis, turnover, and the generation of secreted fragments, including Abeta42. *J Biol Chem*. 1999;274: 18851–18856.
  45. Fjorback AW, Seaman M, Gustafsen C, Mehmedbasic A, Gokool S, Wu C, et al. Retromer binds the FANSHY sorting motif in SorLA to regulate amyloid precursor

- protein sorting and processing. *Journal of Neuroscience*. 2012;32: 1467–1480. doi:10.1523/JNEUROSCI.2272-11.2012
46. Vieira SI, Rebelo S, Esselmann H, Wiltfang J, Lah J, Lane R, et al. Retrieval of the Alzheimer's amyloid precursor protein from the endosome to the TGN is S655 phosphorylation state-dependent and retromer-mediated. *Molecular Neurodegeneration*. 2010;5: 40. doi:10.1186/1750-1326-5-40
  47. Retromer in Alzheimer disease, Parkinson disease and other neurological disorders. 2015;16: 126–132. doi:10.1038/nrn3896
  48. Skovronsky DM, Moore DB, Milla ME, Doms RW, Lee VM. Protein kinase C-dependent alpha-secretase competes with beta-secretase for cleavage of amyloid-beta precursor protein in the trans-golgi network. *Journal of Biological Chemistry*. 2000;275: 2568–2575. doi:10.1074/jbc.275.4.2568
  49. Marcinkiewicz M, Marcinkiewicz M, Seidah NG, Seidah NG. Coordinated expression of beta-amyloid precursor protein and the putative beta-secretase BACE and alpha-secretase ADAM10 in mouse and human brain. *Journal of Neurochemistry*. 2000;75: 2133–2143.
  50. Endres K, Fahrenholz F. Regulation of  $\alpha$ -secretase ADAM10 expression and activity. *Exp Brain Res*. 2012;217: 343–352. doi:10.1007/s00221-011-2885-7
  51. Lammich S, Kojro E, Postina R, Gilbert S, Pfeiffer R, Jasionowski M, et al. Constitutive and regulated alpha-secretase cleavage of Alzheimer's amyloid precursor protein by a disintegrin metalloprotease. *Proc Natl Acad Sci USA*. 1999;96: 3922–3927.
  52. Skovronsky DM, Doms RW, Lee VM. Detection of a novel intraneuronal pool of insoluble amyloid beta protein that accumulates with time in culture. *Journal of Cell Biology*. The Rockefeller University Press; 1998;141: 1031–1039.
  53. Lemjabbar-Alaoui H, Sidhu SS, Mengistab A, Gallup M, Basbaum C. TACE/ADAM-17 Phosphorylation by PKC-Epsilon Mediates Premalignant Changes in Tobacco Smoke-Exposed Lung Cells. Rich B, editor. *PLoS ONE*. 2011;6: e17489. doi:10.1371/journal.pone.0017489.g008
  54. Buxbaum JD, Liu KN, Luo Y, Slack JL, Stocking KL, Peschon JJ, et al. Evidence that tumor necrosis factor alpha converting enzyme is involved in regulated alpha-secretase cleavage of the Alzheimer amyloid protein precursor. *J Biol Chem*. 1998;273: 27765–27767.
  55. Slack BE, B S, Ma LK, L MA, C S, Seah CC. Constitutive shedding of the amyloid precursor protein ectodomain is up-regulated by tumour necrosis factor-alpha

- converting enzyme. *Biochem J.* 2001;357: 787–794.
56. Postina R, Schroeder A, Dewachter I, Bohl J, Schmitt U, Kojro E, et al. A disintegrin-metalloproteinase prevents amyloid plaque formation and hippocampal defects in an Alzheimer disease mouse model. *Journal of Clinical Investigation.* 2004;113: 1456–1464. doi:10.1172/JCI20864
  57. Jonsson T, Atwal JK, Steinberg S, Snaedal J, Jonsson PV, Bjornsson S, et al. A mutation in APP protects against Alzheimer's disease and age-related cognitive decline. *Nature.* 2012;488: 96–99. doi:10.1038/nature11283
  58. Vassar R, Bennett BD, Babu-Khan S, Kahn S, Mendiaz EA, Denis P, et al. Beta-secretase cleavage of Alzheimer's amyloid precursor protein by the transmembrane aspartic protease BACE. *Science.* 1999;286: 735–741.
  59. Lin X, Koelsch G, Wu S, Downs D, Dashti A, Tang J. Human aspartic protease memapsin 2 cleaves the beta-secretase site of beta-amyloid precursor protein. *Proc Natl Acad Sci USA.* 2000;97: 1456–1460.
  60. Saraceno C, Marcello E, Di Marino D, Borroni B, Claeysen S, Perroy J, et al. SAP97-mediated ADAM10 trafficking from Golgi outposts depends on PKC phosphorylation. *Cell Death Dis.* 2014;5: e1547. doi:10.1038/cddis.2014.492
  61. Kinoshita A. Demonstration by FRET of BACE interaction with the amyloid precursor protein at the cell surface and in early endosomes. *Journal of Cell Science.* 2003;116: 3339–3346. doi:10.1242/jcs.00643
  62. Tesco G, Koh YH, Kang EL, Cameron AN, Das S, Sena-Esteves M, et al. Depletion of GGA3 Stabilizes BACE and Enhances  $\beta$ -Secretase Activity. *Neuron.* 2007;54: 721–737. doi:10.1016/j.neuron.2007.05.012
  63. Kang EL, Cameron AN, Piazza F, Walker KR, Tesco G. Ubiquitin Regulates GGA3-mediated Degradation of BACE1. *Journal of Biological Chemistry.* 2010;285: 24108–24119. doi:10.1074/jbc.M109.092742
  64. Walker KR, Kang EL, Whalen MJ, Shen Y, Tesco G. Depletion of GGA1 and GGA3 Mediates Postinjury Elevation of BACE1. *Journal of Neuroscience.* 2012;32: 10423–10437. doi:10.1523/JNEUROSCI.5491-11.2012
  65. Arnim von CAF, Tangredi MM, Peltan ID, Lee BM, Irizarry MC, Kinoshita A, et al. Demonstration of BACE (beta-secretase) phosphorylation and its interaction with GGA1 in cells by fluorescence-lifetime imaging microscopy. *Journal of Cell Science.* 2004;117: 5437–5445. doi:10.1242/jcs.01422
  66. Haapasalo A, Kovacs DM. The many substrates of presenilin/ $\gamma$ -secretase. *J Alzheimers Dis.* IOS Press; 2011;25: 3–28. doi:10.3233/JAD-2011-101065

67. Shah S, Lee S-F, Tabuchi K, Hao Y-H, Yu C, LaPlant Q, et al. Nicastrin functions as a gamma-secretase-substrate receptor. *Cell*. 2005;122: 435–447. doi:10.1016/j.cell.2005.05.022
68. St George-Hyslop P, Fraser PE. Assembly of the presenilin  $\gamma$ - $\epsilon$ -secretase complex. *Journal of Neurochemistry*. 2011;120: 84–88. doi:10.1111/j.1471-4159.2011.07505.x
69. Bentahir M, Nyabi O, Verhamme J, Tolia A, Horre K, Wiltfang J, et al. Presenilin clinical mutations can affect gamma-secretase activity by different mechanisms. *Journal of Neurochemistry*. 2006;96: 732–742. doi:10.1111/j.1471-4159.2005.03578.x
70. Takami M, Nagashima Y, Sano Y, Ishihara S, Morishima-Kawashima M, Funamoto S, et al. gamma-Secretase: successive tripeptide and tetrapeptide release from the transmembrane domain of beta-carboxyl terminal fragment. *Journal of Neuroscience*. 2009;29: 13042–13052. doi:10.1523/JNEUROSCI.2362-09.2009
71. Yu WH, Kumar A, Peterhoff C, Shapiro Kulnane L, Uchiyama Y, Lamb BT, et al. Autophagic vacuoles are enriched in amyloid precursor protein-secretase activities: implications for beta-amyloid peptide over-production and localization in Alzheimer's disease. *Int J Biochem Cell Biol*. 2004;36: 2531–2540. doi:10.1016/j.biocel.2004.05.010
72. Golabek AA, Kida E, Walus M, Kaczmarek W, Michalewski M, Wisniewski KE. CLN3 protein regulates lysosomal pH and alters intracellular processing of Alzheimer's amyloid-beta protein precursor and cathepsin D in human cells. *Molecular Genetics and Metabolism*. 2000;70: 203–213. doi:10.1006/mgme.2000.3006
73. Schrader-Fischer G, Paganetti PA. Effect of alkalizing agents on the processing of the beta-amyloid precursor protein. *Brain Research*. 1996;716: 91–100. doi:10.1016/0006-8993(96)00002-9
74. Haass C, Schlossmacher MG, Hung AY, Vigo-Pelfrey C, Mellon A, Ostaszewski BL, et al. Amyloid beta-peptide is produced by cultured cells during normal metabolism. *Nature*. 1992;359: 322–325. doi:10.1038/359322a0
75. Seubert P, Oltersdorf T, Lee MG, Barbour R, Blomquist C, Davis DL, et al. Secretion of beta-amyloid precursor protein cleaved at the amino terminus of the beta-amyloid peptide. *Nature*. 1993;361: 260–263. doi:10.1038/361260a0
76. Moghekar A, Rao S, Li M, Ruben D, Mammen A, Tang X, et al. Large quantities of Abeta peptide are constitutively released during amyloid precursor protein metabolism in vivo and in vitro. *Journal of Biological Chemistry*. 2011;286: 15989–



15997. doi:10.1074/jbc.M110.191262
77. Pearson HA, Peers C. Physiological roles for amyloid beta peptides. *The Journal of Physiology*. 2006;575: 5–10. doi:10.1113/jphysiol.2006.111203
  78. Glenner GG, Wong CW. Alzheimer's disease: initial report of the purification and characterization of a novel cerebrovascular amyloid protein. *Biochemical and Biophysical Research Communications*. 1984;120: 885–890.
  79. Mann DM, YATES PO, MARCYNIUK B. Alzheimer's presenile dementia, senile dementia of Alzheimer type and Down's syndrome in middle age form an age related continuum of pathological changes. *Neuropathol Appl Neurobiol*. 1984;10: 185–207. doi:10.1111/j.1365-2990.1984.tb00351.x
  80. Wisniewski KE, Wisniewski HM, Wen GY. Occurrence of neuropathological changes and dementia of Alzheimer's disease in Down's syndrome. *Ann Neurol*. 1985;17: 278–282. doi:10.1002/ana.410170310
  81. Podlisny MB, Lee G, Selkoe DJ. Gene dosage of the amyloid beta precursor protein in Alzheimer's disease. *Science*. 1987;238: 669–671.
  82. Theuns J, Brouwers N, Engelborghs S, Sleegers K, Bogaerts V, Corsmit E, et al. Promoter mutations that increase amyloid precursor-protein expression are associated with Alzheimer disease. *The American Journal of Human Genetics*. 2006;78: 936–946. doi:10.1086/504044
  83. Moechars D, Dewachter I, Lorent K, Reversé D, Baekelandt V, Naidu A, et al. Early phenotypic changes in transgenic mice that overexpress different mutants of amyloid precursor protein in brain. *J Biol Chem*. 1999;274: 6483–6492.
  84. Pagon RA, Adam MP, Dolan CR, Fong C-T, Smith RJ, Stephens K, et al. *Early-Onset Familial Alzheimer Disease*. Seattle (WA): University of Washington, Seattle; 1993.
  85. Sleegers K, Brouwers N, Gijssels I, Theuns J, Goossens D, Wauters J, et al. APP duplication is sufficient to cause early onset Alzheimer's dementia with cerebral amyloid angiopathy. *Brain*. 2006;129: 2977–2983. doi:10.1093/brain/awl203
  86. Cabrejo L, Guyant-Maréchal L, Laquerrière A, Vercelletto M, la Fournière De F, Thomas-Antérion C, et al. Phenotype associated with APP duplication in five families. *Brain*. 2006;129: 2966–2976. doi:10.1093/brain/awl237
  87. Mullan M, Crawford F, Axelman K, Houlden H, Lilius L, Winblad B, et al. A pathogenic mutation for probable Alzheimer's disease in the APP gene at the N-terminus of beta-amyloid. *Nat Genet*. 1992;1: 345–347. doi:10.1038/ng0892-345

88. Thinakaran G, Teplow DB, Siman R, Greenberg B, Sisodia SS. Metabolism of the "Swedish" amyloid precursor protein variant in neuro2a (N2a) cells. Evidence that cleavage at the "beta-secretase" site occurs in the golgi apparatus. *J Biol Chem.* 1996;271: 9390–9397.
89. Perez RG, Squazzo SL, Koo EH. Enhanced release of amyloid beta-protein from codon 670/671 "Swedish" mutant beta-amyloid precursor protein occurs in both secretory and endocytic pathways. *J Biol Chem.* 1996;271: 9100–9107.
90. Citron M, Vigo-Pelfrey C, Teplow DB, Miller C, Schenk D, Johnston J, et al. Excessive production of amyloid beta-protein by peripheral cells of symptomatic and presymptomatic patients carrying the Swedish familial Alzheimer disease mutation. *Proc Natl Acad Sci USA.* 1994;91: 11993–11997.
91. Maruyama K, Tomita T, Shinozaki K, Kume H, Asada H, Saido TC, et al. Familial Alzheimer's disease-linked mutations at Val717 of amyloid precursor protein are specific for the increased secretion of A beta 42(43). *Biochemical and Biophysical Research Communications.* 1996;227: 730–735. doi:10.1006/bbrc.1996.1577
92. Suzuki N, Cheung TT, Cai XD, Odaka A, Otvos L, Eckman C, et al. An increased percentage of long amyloid beta protein secreted by familial amyloid beta protein precursor (beta APP717) mutants. *Science.* 1994;264: 1336–1340.
93. Goate A, Chartier-Harlin MC, Mullan M, Brown J, Crawford F, Fidani L, et al. Segregation of a missense mutation in the amyloid precursor protein gene with familial Alzheimer's disease. *Nature.* 1991;349: 704–706. doi:10.1038/349704a0
94. Cruts M, Dermaut B, Rademakers R, Van den Broeck M, Stögbauer F, Van Broeckhoven C. Novel APP mutation V715A associated with presenile Alzheimer's disease in a German family. *J Neurol.* Steinkopff-Verlag; 2003;250: 1374–1375. doi:10.1007/s00415-003-0182-5
95. Ancolio K, Dumanchin C, Barelli H, Warter JM, Brice A, Campion D, et al. Unusual phenotypic alteration of beta amyloid precursor protein (betaAPP) maturation by a new Val-715 --> Met betaAPP-770 mutation responsible for probable early-onset Alzheimer's disease. *Proc Natl Acad Sci USA. National Academy of Sciences;* 1999;96: 4119–4124.
96. Levy E, Carman MD, Fernandez-Madrid IJ, Power MD, Lieberburg I, van Duinen SG, et al. Mutation of the Alzheimer's disease amyloid gene in hereditary cerebral hemorrhage, Dutch type. *Science.* 1990;248: 1124–1126.
97. van Broeckhoven C, Haan J, Bakker E, Hardy JA, Van Hul W, Wehnert A, et al. Amyloid beta protein precursor gene and hereditary cerebral hemorrhage with amyloidosis (Dutch). *Science.* 1990;248: 1120–1122.

98. Fernandez-Madrid I, Levy E, Marder K, Frangione B. Codon 618 variant of Alzheimer amyloid gene associated with inherited cerebral hemorrhage. *Ann Neurol.* 1991;30: 730–733. doi:10.1002/ana.410300516
99. Kamino K, Orr HT, Payami H, Wijsman EM, Alonso ME, Pulst SM, et al. Linkage and mutational analysis of familial Alzheimer disease kindreds for the APP gene region. *The American Journal of Human Genetics.* Elsevier; 1992;51: 998–1014. doi:10.1002/ana.21321
100. Nilsberth C, Westlind-Danielsson A, Eckman CB, Condron MM, Axelman K, Forsell C, et al. The 'Arctic' APP mutation (E693G) causes Alzheimer's disease by enhanced A $\beta$  protofibril formation. *Nature Neuroscience.* Nature Publishing Group; 2001;4: 887–893. doi:10.1038/nn0901-887
101. Hendriks L, van Duijn CM, Cras P, Cruts M, Van Hul W, van Harskamp F, et al. Presenile dementia and cerebral haemorrhage linked to a mutation at codon 692 of the beta-amyloid precursor protein gene. *Nat Genet.* Nature Publishing Group; 1992;1: 218–221. doi:10.1038/ng0692-218
102. Tsubuki S, Takaki Y, Saido TC. Dutch, Flemish, Italian, and Arctic mutations of APP and resistance of A $\beta$  to physiologically relevant proteolytic degradation. *Lancet.* 2003;361: 1957–1958.
103. Iwata N, Tsubuki S, Takaki Y, Shirotani K, Lu B, Gerard NP, et al. Metabolic regulation of brain A $\beta$  by neprilysin. *Science.* 2001;292: 1550–1552. doi:10.1126/science.1059946
104. Walsh DM, Hartley DM, Condron MM, Selkoe DJ, Teplow DB. In vitro studies of amyloid beta-protein fibril assembly and toxicity provide clues to the aetiology of Flemish variant (Ala692-->Gly) Alzheimer's disease. *Biochem J.* 2001;355: 869–877. doi:10.1046/j.1471-4159.2000.0742209.x/full
105. Cheng IH, Palop JJ, Esposito LA, Bien-Ly N, Yan F, Mucke L. Aggressive amyloidosis in mice expressing human amyloid peptides with the Arctic mutation. *Nat Med.* 2004;10: 1190–1192. doi:10.1038/nm1123
106. Tomiyama T, Nagata T, Shimada H, Teraoka R, Fukushima A, Kanemitsu H, et al. A new amyloid beta variant favoring oligomerization in Alzheimer's-type dementia. *Ann Neurol.* 2008;63: 377–387. doi:10.1002/ana.21321
107. Tian Y, Bassit B, Chau D, Li Y-M. An APP inhibitory domain containing the Flemish mutation residue modulates  $\gamma$ -secretase activity for A $\beta$  production. *Nature Structural & Molecular Biology.* Nature Publishing Group; 2010;17: 151–158. doi:10.1038/nsmb.1743

108. Tang T-C, Hu Y, Kienlen-Campard P, Haylani El L, Decock M, Van Hees J, et al. Conformational changes induced by the A21G Flemish mutation in the amyloid precursor protein lead to increased A $\beta$  production. *Structure*. 2014;22: 387–396. doi:10.1016/j.str.2013.12.012
109. Sherrington R, Rogaev EI, Liang Y, Rogaeva EA, Levesque G, Ikeda M, et al. Cloning of a gene bearing missense mutations in early-onset familial Alzheimer's disease. *Nature*. 1995;375: 754–760. doi:10.1038/375754a0
110. Scheuner D, Eckman C, Jensen M, Song X, Citron M, Suzuki N, et al. Secreted amyloid beta-protein similar to that in the senile plaques of Alzheimer's disease is increased in vivo by the presenilin 1 and 2 and APP mutations linked to familial Alzheimer's disease. *Nat Med*. 1996;2: 864–870.
111. Borchelt DR, Thinakaran G, Eckman CB, Lee MK, Davenport F, Ratovitsky T, et al. Familial Alzheimer's Disease–Linked Presenilin 1 Variants Elevate A $\beta$ 1–42/1–40 Ratio In Vitro and In Vivo. *Neuron*. Elsevier; 1996;17: 1005–1013. doi:10.1016/S0896-6273(00)80230-5
112. Gatz M, Reynolds CA, Fratiglioni L, Johansson B, Mortimer JA, Berg S, et al. Role of genes and environments for explaining Alzheimer disease. *Arch Gen Psychiatry*. 2006;63: 168–174. doi:10.1001/archpsyc.63.2.168
113. Karch CM, Cruchaga C, Goate AM. Alzheimer's Disease Genetics: From the Bench to the Clinic. *Neuron*. 2014;83: 11–26. doi:10.1016/j.neuron.2014.05.041
114. Kim J, Castellano JM, Jiang H, Basak JM, Parsadanian M, Pham V, et al. Overexpression of Low-Density Lipoprotein Receptor in the Brain Markedly Inhibits Amyloid Deposition and Increases Extracellular A $\beta$ ; Clearance. *Neuron*. Elsevier Ltd; 2009;64: 632–644. doi:10.1016/j.neuron.2009.11.013
115. Schmechel DE, Saunders AM, Strittmatter WJ, Crain BJ, Hulette CM, Joo SH, et al. Increased amyloid beta-peptide deposition in cerebral cortex as a consequence of apolipoprotein E genotype in late-onset Alzheimer disease. *Proc Natl Acad Sci USA*. 1993;90: 9649–9653.
116. Castellano JM, Kim J, Stewart FR, Jiang H, DeMattos RB, Patterson BW, et al. Human apoE isoforms differentially regulate brain amyloid- $\beta$  peptide clearance. *Sci Transl Med*. 2011;3: 89ra57. doi:10.1126/scitranslmed.3002156
117. Holtzman DM, Bales KR, Tenkova T, Fagan AM, Parsadanian M, Sartorius LJ, et al. Apolipoprotein E isoform-dependent amyloid deposition and neuritic degeneration in a mouse model of Alzheimer's disease. *Proc Natl Acad Sci USA*. 2000;97: 2892–2897. doi:10.1073/pnas.050004797

118. Ma J, Yee A, Brewer HB, Das S, Potter H. Amyloid-associated proteins alpha 1-antichymotrypsin and apolipoprotein E promote assembly of Alzheimer beta-protein into filaments. *Nature*. 1994;372: 92–94. doi:10.1038/372092a0
119. Wisniewski T, Castaño EM, Golabek A, Vogel T, Frangione B. Acceleration of Alzheimer's fibril formation by apolipoprotein E in vitro. *Am J Pathol*. 1994;145: 1030–1035.
120. Jiang Q, Lee CYD, Mandrekar S, Wilkinson B, Cramer P, Zelcer N, et al. ApoE promotes the proteolytic degradation of Abeta. *Neuron*. 2008;58: 681–693. doi:10.1016/j.neuron.2008.04.010
121. Selkoe DJ. Altered structural proteins in plaques and tangles: what do they tell us about the biology of Alzheimer's disease? *NBA*. Elsevier; 1986;7: 425–432.
122. Mann D, Esiri MM. The pattern of acquisition of plaques and tangles in the brains of patients under 50 years of age with Down's syndrome. *J Neurol Sci*. Elsevier; 1989;89: 169–179. doi:10.1016/0022-510X(89)90019-1
123. Iwatsubo T, Mann DM, Odaka A, Suzuki N, Ihara Y. Amyloid beta protein (A beta) deposition: A beta 42(43) precedes A beta 40 in Down syndrome. *Ann Neurol*. 1995;37: 294–299. doi:10.1002/ana.410370305
124. Iwatsubo T, Odaka A, Suzuki N, Mizusawa H, Nukina N, Ihara Y. Visualization of A beta 42(43) and A beta 40 in senile plaques with end-specific A beta monoclonals: evidence that an initially deposited species is A beta 42(43). *Neuron*. 1994;13: 45–53.
125. Yankner BA, Duffy LK, Kirschner DA. Neurotrophic and neurotoxic effects of amyloid beta protein: reversal by tachykinin neuropeptides. *Science*. 1990;250: 279–282.
126. Lovestone S, McLoughlin DM. Protein aggregates and dementia: is there a common toxicity? *J Neurol Neurosurg Psychiatr*. 2002;72: 152–161. doi:10.1136/jnnp.72.2.152
127. Lorenzo A, Yankner BA. Beta-amyloid neurotoxicity requires fibril formation and is inhibited by congo red. *Proc Natl Acad Sci USA*. 1994;91: 12243–12247.
128. Takadera T, Sakura N, Mohri T, Hashimoto T. Toxic effect of a beta-amyloid peptide (beta 22-35) on the hippocampal neuron and its prevention. *Neuroscience Letters*. 1993;161: 41–44.
129. Harrigan MR, Kunkel DD, Nguyen LB, Malouf AT. Beta amyloid is neurotoxic in hippocampal slice cultures. *NBA*. 1995;16: 779–789.

130. Chacón MA, Barría MI, Soto C, Inestrosa NC. Beta-sheet breaker peptide prevents Abeta-induced spatial memory impairments with partial reduction of amyloid deposits. *Mol Psychiatry*. 2004;9: 953–961. doi:10.1038/sj.mp.4001516
131. Dickson DW, Yen SH. Beta-amyloid deposition and paired helical filament formation: which histopathological feature is more significant in Alzheimer's disease? *NBA*. 1989;10: 402–4— discussion 412–4.
132. Terry RD, Masliah E, Salmon DP, Butters N, DeTeresa R, Hill R, et al. Physical basis of cognitive alterations in Alzheimer's disease: synapse loss is the major correlate of cognitive impairment. *Ann Neurol*. 1991;30: 572–580. doi:10.1002/ana.410300410
133. Katzman R, Terry R, DeTeresa R, Brown T, Davies P, Fuld P, et al. Clinical, pathological, and neurochemical changes in dementia: a subgroup with preserved mental status and numerous neocortical plaques. *Ann Neurol*. 1988;23: 138–144. doi:10.1002/ana.410230206
134. Thal DR, Rüb U, Schultz C, Sassin I, Ghebremedhin E, Del Tredici K, et al. Sequence of Abeta-protein deposition in the human medial temporal lobe. *J Neuropathol Exp Neurol*. 2000;59: 733–748.
135. Klein WL. Abeta toxicity in Alzheimer's disease: globular oligomers (ADDLs) as new vaccine and drug targets. *Neurochemistry International*. 2002;41: 345–352.
136. Kuo Y-M, Emmerling MR, Vigo-Pelfrey C, Kasunic TC, Kirkpatrick JB, Murdoch GH, et al. Water-soluble A (N-40, N-42) oligomers in normal and Alzheimer disease brains. *J Biol Chem. ASBMB*; 1996;271: 4077–4081.
137. Teller JK, Russo C, Debusk LM, Angelini G, Zaccheo D, Dagna-Bricarelli F, et al. Presence of soluble amyloid beta-peptide precedes amyloid plaque formation in Down's syndrome. *Nat Med*. 1996;2: 93–95. doi:10.1038/nm0196-93
138. Kim H-J, Chae S-C, Lee D-K, Chromy B, Lee SC, Park Y-C, et al. Selective neuronal degeneration induced by soluble oligomeric amyloid beta protein. *The FASEB Journal*. 2003;17: 118–120. doi:10.1096/fj.01-0987fje
139. Ostapchenko VG, Beraldo FH, Mohammad AH, Xie Y-F, Hirata PHF, Magalhaes AC, et al. The prion protein ligand, stress-inducible phosphoprotein 1, regulates amyloid- $\beta$  oligomer toxicity. *Journal of Neuroscience. Society for Neuroscience*; 2013;33: 16552–16564. doi:10.1523/JNEUROSCI.3214-13.2013
140. Laurén J, Gimbel DA, Nygaard HB, Gilbert JW, Strittmatter SM. Cellular prion protein mediates impairment of synaptic plasticity by amyloid- $\beta$  oligomers. *Nature. Nature Publishing Group*; 2009;457: 1128–1132. doi:10.1038/nature07761

141. Walsh DM, Tseng BP, Rydel RE, Podlisny MB, Selkoe DJ. The oligomerization of amyloid beta-protein begins intracellularly in cells derived from human brain. *Biochemistry*. 2000;39: 10831–10839. doi:10.1021/bi001048s
142. Wang H-W, Pasternak JF, Kuo H, Ristic H, Lambert MP, Chromy B, et al. Soluble oligomers of beta amyloid (1-42) inhibit long-term potentiation but not long-term depression in rat dentate gyrus. *Brain Research*. 2002;924: 133–140. doi:10.1016/S0006-8993(01)03058-X
143. Balducci C, Beeg M, Stravalaci M, Bastone A, Sclip A, Biasini E, et al. Synthetic amyloid- oligomers impair long-term memory independently of cellular prion protein. *Proceedings of the National Academy of Sciences*. 2010;107: 2295–2300. doi:10.1073/pnas.0911829107
144. Wilcox KC, Marunde MR, Das A, Velasco PT, Kuhns BD, Marty MT, et al. Nanoscale Synaptic Membrane Mimetic Allows Unbiased High Throughput Screen That Targets Binding Sites for Alzheimer's-Associated A $\beta$  Oligomers. Ventura S, editor. *PLoS ONE*. 2015;10: e0125263. doi:10.1371/journal.pone.0125263
145. Renner M, Lacor PN, Velasco PT, Xu J, Contractor A, Klein WL, et al. Deleterious effects of amyloid beta oligomers acting as an extracellular scaffold for mGluR5. *Neuron*. 2010;66: 739–754. doi:10.1016/j.neuron.2010.04.029
146. Hamilton A, Esseltine JL, DeVries RA, Cregan SP, Ferguson SSG. Metabotropic glutamate receptor 5 knockout reduces cognitive impairment and pathogenesis in a mouse model of Alzheimer's disease. *Mol Brain*. 2014;7: 40. doi:10.1186/1756-6606-7-40
147. Linden R, Martins VR, Prado MAM, Cammarota M, Izquierdo I, Brentani RR. Physiology of the Prion Protein. *Physiological Reviews*. 2008;88: 673–728. doi:10.1152/physrev.00007.2007
148. Um JW, Kaufman AC, Kostylev M, Heiss JK, Stagi M, Takahashi H, et al. Metabotropic glutamate receptor 5 is a coreceptor for Alzheimer a $\beta$  oligomer bound to cellular prion protein. *Neuron*. 2013;79: 887–902. doi:10.1016/j.neuron.2013.06.036
149. Hardingham GE, Fukunaga Y, Bading H. Extrasynaptic NMDARs oppose synaptic NMDARs by triggering CREB shut-off and cell death pathways. *Nature Neuroscience*. 2002;5: 405–414. doi:10.1038/nn835
150. Amadoro G, Ciotti MT, Costanzi M, Cestari V, Calissano P, Canu N. NMDA receptor mediates tau-induced neurotoxicity by calpain and ERK/MAPK activation. *Proc Natl Acad Sci USA*. 2006;103: 2892–2897. doi:10.1073/pnas.0511065103

151. Palop JJ, Chin J, Roberson ED, Wang J, Thwin MT, Bien-Ly N, et al. Aberrant excitatory neuronal activity and compensatory remodeling of inhibitory hippocampal circuits in mouse models of Alzheimer's disease. *Neuron*. 2007;55: 697–711. doi:10.1016/j.neuron.2007.07.025
152. Larson M, Sherman MA, Amar F, Nuvolone M, Schneider JA, Bennett DA, et al. The Complex PrPc-Fyn Couples Human Oligomeric A $\beta$  with Pathological Tau Changes in Alzheimer's Disease. *Journal of Neuroscience*. 2012;32: 16857–16871. doi:10.1523/JNEUROSCI.1858-12.2012
153. Ittner LM, Ke YD, Delerue F, Bi M, Gladbach A, van Eersel J, et al. Dendritic function of tau mediates amyloid-beta toxicity in Alzheimer's disease mouse models. *Cell*. Elsevier Ltd; 2010;142: 387–397. doi:10.1016/j.cell.2010.06.036
154. Xia D, Li C, Götz J. Pseudophosphorylation of Tau at distinct epitopes or the presence of the P301L mutation targets the microtubule-associated protein Tau to dendritic spines. *Biochim Biophys Acta*. 2015;1852: 913–924. doi:10.1016/j.bbadis.2014.12.017
155. Robakis NK, Ramakrishna N, Wolfe G, Wisniewski HM. Molecular cloning and characterization of a cDNA encoding the cerebrovascular and the neuritic plaque amyloid peptides. *Proc Natl Acad Sci USA*. 1987;84: 4190–4194.
156. Kang J, Lemaire HG, Unterbeck A, Salbaum JM, Masters CL, Grzeschik KH, et al. The precursor of Alzheimer's disease amyloid A $\beta$  protein resembles a cell-surface receptor. *Nature*. 1987;325: 733–736. doi:10.1038/325733a0
157. Tanzi R, Gusella J, Watkins P, Bruns G, St George-Hyslop P, Van Keuren M, et al. Amyloid beta protein gene: cDNA, mRNA distribution, and genetic linkage near the Alzheimer locus. *Science*. 1987;235: 880–884. doi:10.1126/science.2949367
158. Yoshikai S, Yoshikai S, Sasaki H, Sasaki H, Doh-ura K, Doh-ura K, et al. Genomic organization of the human amyloid beta-protein precursor gene. *Gene*. 1990;87: 257–263.
159. Weidemann A, König G, Bunke D, Fischer P, Salbaum JM, Masters CL, et al. Identification, biogenesis, and localization of precursors of Alzheimer's disease A $\beta$  amyloid protein. *Cell*. 1989;57: 115–126.
160. Rohan de Silva HA, Jen A, Wickenden C, Jen LS, Wilkinson SL, Patel AJ. Cell-specific expression of beta-amyloid precursor protein isoform mRNAs and proteins in neurons and astrocytes. *Brain Res Mol Brain Res*. 1997;47: 147–156.
161. Ramelot TA, Nicholson LK. Phosphorylation-induced structural changes in the amyloid precursor protein cytoplasmic tail detected by NMR. *J Mol Biol*. 2001;307:



- 871–884. doi:10.1006/jmbi.2001.4535
162. Kroenke CD, Ziemnicka-Kotula D, Xu J, Kotula L, Palmer AG. Solution conformations of a peptide containing the cytoplasmic domain sequence of the beta amyloid precursor protein. *Biochemistry*. 1997;36: 8145–8152. doi:10.1021/bi9705669
163. Mueller HT, Borg JP, Margolis B, Turner RS. Modulation of amyloid precursor protein metabolism by X11alpha /Mint-1. A deletion analysis of protein-protein interaction domains. *Journal of Biological Chemistry*. 2000;275: 39302–39306. doi:10.1074/jbc.M008453200
164. Cao X, Sudhof TC. A transcriptionally [correction of transcriptively] active complex of APP with Fe65 and histone acetyltransferase Tip60. *Science*. 2001;293: 115–120. doi:10.1126/science.1058783
165. Taru H, Kirino Y, Suzuki T. Differential roles of JIP scaffold proteins in the modulation of amyloid precursor protein metabolism. *J Biol Chem*. 2002;277: 27567–27574. doi:10.1074/jbc.M203713200
166. Chaufty J, Sullivan SE, Ho A. Intracellular Amyloid Precursor Protein Sorting and Amyloid- Secretion Are Regulated by Src-Mediated Phosphorylation of Mint2. *Journal of Neuroscience*. 2012;32: 9613–9625. doi:10.1523/JNEUROSCI.0602-12.2012
167. Caster AH, Sztul E, Kahn RA. A role for cargo in Arf-dependent adaptor recruitment. *J Biol Chem*. 2013;288: 14788–14804. doi:10.1074/jbc.M113.453621
168. Borg JP, Ooi J, Levy E, Margolis B. The phosphotyrosine interaction domains of X11 and FE65 bind to distinct sites on the YENPTY motif of amyloid precursor protein. *Molecular and Cellular Biology*. 1996;16: 6229–6241.
169. Lehrman MA, Goldstein JL, Brown MS, Russell DW, Schneider WJ. Internalization-defective LDL receptors produced by genes with nonsense and frameshift mutations that truncate the cytoplasmic domain. *Cell*. 1985;41: 735–743. doi:10.1016/S0092-8674(85)80054-4
170. Davis CG, Lehrman MA, Russell DW, Anderson RG, Brown MS, Goldstein JL. The J.D. mutation in familial hypercholesterolemia: amino acid substitution in cytoplasmic domain impedes internalization of LDL receptors. *Cell*. 1986;45: 15–24.
171. Collawn JF, Kuhn LA, Liu LF, Tainer JA, Trowbridge IS. Transplanted LDL and mannose-6-phosphate receptor internalization signals promote high-efficiency endocytosis of the transferrin receptor. *The EMBO Journal*. 1991;10: 3247–3253.

172. Maginnis MS, Mainou BA, Derdowski A, Johnson EM, Zent R, Dermody TS. NPXY motifs in the beta1 integrin cytoplasmic tail are required for functional reovirus entry. *Journal of Virology*. 2008;82: 3181–3191. doi:10.1128/JVI.01612-07
173. Songyang Z, Margolis B, Chaudhuri M, Shoelson SE, Cantley LC. The phosphotyrosine interaction domain of SHC recognizes tyrosine-phosphorylated NPXY motif. *J Biol Chem*. 1995;270: 14863–14866. doi:10.1074/jbc.270.25.14843
174. Dilworth SM, Brewster CE, Jones MD, Lanfrancone L, Pelicci G, Pelicci PG. Transformation by polyoma virus middle T-antigen involves the binding and tyrosine phosphorylation of Shc. *Nature*. 1994;367: 87–90. doi:10.1038/367087a0
175. Campbell KS, Ogris E, Burke B, Su W, Auger KR, Druker BJ, et al. Polyoma middle tumor antigen interacts with SHC protein via the NPTY (Asn-Pro-Thr-Tyr) motif in middle tumor antigen. *Proc Natl Acad Sci USA*. 1994;91: 6344–6348.
176. Mathew S, Lu Z, Palamuttam RJ, Mernaugh G, Hadziselimovic A, Chen J, et al.  $\beta$ 1 integrin NPXY motifs regulate kidney collecting-duct development and maintenance by induced-fit interactions with cytosolic proteins. *Molecular and Cellular Biology*. 2012;32: 4080–4091. doi:10.1128/MCB.00568-12
177. Radzimanowski J, Simon B, Sattler M, Beyreuther K, Sinning I, Wild K. Structure of the intracellular domain of the amyloid precursor protein in complex with Fe65-PTB2. *EMBO Rep*. 2008;9: 1134–1140. doi:10.1038/embor.2008.188
178. Zhang Z, Lee CH, Mandiyan V, Borg JP, Margolis B, Schlessinger J, et al. Sequence-specific recognition of the internalization motif of the Alzheimer's amyloid precursor protein by the X11 PTB domain. *The EMBO Journal*. 1997;16: 6141–6150. doi:10.1093/emboj/16.20.6141
179. Ando K, Iijima KI, Elliott JI, Kirino Y, Suzuki T. Phosphorylation-dependent regulation of the interaction of amyloid precursor protein with Fe65 affects the production of beta-amyloid. *J Biol Chem*. 2001;276: 40353–40361. doi:10.1074/jbc.M104059200
180. Pastorino L, Ma SL, Balastik M, Huang P, Pandya D, Nicholson L, et al. Alzheimer's disease-related loss of Pin1 function influences the intracellular localization and the processing of A $\beta$ PP. *J Alzheimers Dis*. 2012;30: 277–297. doi:10.3233/JAD-2012-111259
181. Pastorino L, Sun A, Lu P-J, Zhou XZ, Balastik M, Finn G, et al. The prolyl isomerase Pin1 regulates amyloid precursor protein processing and amyloid- $\beta$  production. *Nature*. 2006;440: 528–534. doi:10.1038/nature04543
182. Judge M, Hornbeck L, Potter H, Padmanabhan J. Mitosis-specific phosphorylation

- of amyloid precursor protein at threonine 668 leads to its altered processing and association with centrosomes. *Molecular Neurodegeneration*. 2011;6: 80. doi:10.1186/1750-1326-6-80
183. Chang K-A, Kim H-S, Ha T-Y, Ha J-W, Shin KY, Jeong YH, et al. Phosphorylation of amyloid precursor protein (APP) at Thr668 regulates the nuclear translocation of the APP intracellular domain and induces neurodegeneration. *Molecular and Cellular Biology*. 2006;26: 4327–4338. doi:10.1128/MCB.02393-05
184. Liu F, Su Y, Li B, Zhou Y, Ryder J, Gonzalez-DeWhitt P, et al. Regulation of amyloid precursor protein (APP) phosphorylation and processing by p35/Cdk5 and p25/Cdk5. *FEBS Letters*. 2003;547: 193–196. doi:10.1016/S0014-5793(03)00714-2
185. Lee M-S, Kao S-C, Lemere CA, Xia W, Tseng H-C, Zhou Y, et al. APP processing is regulated by cytoplasmic phosphorylation. *Journal of Cell Biology*. 2003;163: 83–95. doi:10.1083/jcb.200301115
186. Suzuki T, Nairn AC, Gandy SE, Greengard P. Phosphorylation of Alzheimer amyloid precursor protein by protein kinase C. *NSC*. 1992;48: 755–761. doi:10.1016/0306-4522(92)90264-3
187. Gandy S, Czernik AJ, Greengard P. Phosphorylation of Alzheimer disease amyloid precursor peptide by protein kinase C and Ca<sup>2+</sup>/calmodulin-dependent protein kinase II. *Proc Natl Acad Sci USA*. 1988;85: 6218–6221.
188. Slack BE, Breu J, Petryniak MA, Srivastava K, Wurtman RJ. Tyrosine phosphorylation-dependent stimulation of amyloid precursor protein secretion by the m3 muscarinic acetylcholine receptor. *J Biol Chem*. 1995;270: 8337–8344.
189. Zambrano N, Bruni P, Minopoli G, Mosca R, Molino D, Russo C, et al. The beta-amyloid precursor protein APP is tyrosine-phosphorylated in cells expressing a constitutively active form of the Abl protooncogene. *Journal of Biological Chemistry*. American Society for Biochemistry and Molecular Biology; 2001;276: 19787–19792. doi:10.1074/jbc.M100792200
190. Benussi L, Govoni S, Gasparini L, Binetti G, Trabucchi M, Bianchetti A, et al. Specific role for protein kinase C alpha in the constitutive and regulated secretion of amyloid precursor protein in human skin fibroblasts. *Neuroscience Letters*. 1998;240: 97–101.
191. Kinouchi T, Sorimachi H, Maruyama K, Mizuno K, Ohno S, Ishiura S, et al. Conventional protein kinase C (PKC)-alpha and novel PKC epsilon, but not -delta, increase the secretion of an N-terminal fragment of Alzheimer's disease amyloid precursor protein from PKC cDNA transfected 3Y1 fibroblasts. *FEBS Letters*. 1995;364: 203–206.

192. Nelson PT, Braak H, Markesbery WR. Neuropathology and cognitive impairment in Alzheimer disease: a complex but coherent relationship. *J Neuropathol Exp Neurol*. 2009;68: 1–14. doi:10.1097/NEN.0b013e3181919a48
193. Yeon SW, Jung MW, Ha MJ, Kim SU, Huh K, Savage MJ, et al. Blockade of PKC $\epsilon$  Activation Attenuates Phorbol Ester-Induced Increase of  $\alpha$ -Secretase-Derived Secreted Form of Amyloid Precursor Protein. *Biochemical and Biophysical Research Communications*. 2001;280: 782–787. doi:10.1006/bbrc.2000.4181
194. Gabuzda D, Busciglio J, Yankner BA. Inhibition of beta-amyloid production by activation of protein kinase C. *Journal of Neurochemistry*. 1993;61: 2326–2329. doi:10.1111/j.1471-4159.1993.tb07479.x
195. Nitsch R, Slack B, Wurtman R, Growdon J. Release of Alzheimer amyloid precursor derivatives stimulated by activation of muscarinic acetylcholine receptors. *Science*. 1992;258: 304–307. doi:10.1126/science.1411529
196. Cisse M, Braun U, Leitges M, Fisher A, Pages G, Checler F, et al. ERK1-independent  $\alpha$ -secretase cut of  $\beta$ -amyloid precursor protein via M1 muscarinic receptors and PKC $\alpha/\epsilon$ . *Molecular and Cellular Neuroscience*. Elsevier Inc. Elsevier Inc; 2011;47: 223–232. doi:10.1016/j.mcn.2011.04.008
197. Messing RO, Stevens AM, Kiyasu E, Sneade AB. Nicotinic and muscarinic agonists stimulate rapid protein kinase C translocation in PC12 cells. *J Neurosci*. 1989;9: 507–512.
198. Möbius HJ. Memantine in treatment of AD. In: Richter RW, Richter BZ, editors. *Alzheimer's Disease*. Totowa, New Jersey: Humana Press; 2004. pp. 203–209.
199. Farlow MR. Rivastigmine for Treatment of AD. In: Richter RW, Richter BZ, editors. *Alzheimer's Disease*. Totowa, New Jersey: Humana Press; 2004. pp. 187–192.
200. Hsiung G-YR, Feldman H. Donepezil in Treatment of AD. In: Richter RW, Richter BZ, editors. *Alzheimer's Disease*. Totowa, New Jersey: Humana Press; 2004. pp. 179–185.
201. Fisher A. M1 muscarinic agonists target major hallmarks of Alzheimer's disease--the pivotal role of brain M1 receptors. *Neurodegenerative Dis*. 2008;5: 237–240. doi:10.1159/000113712
202. Biddlecome GH, Berstein G, Ross EM. Regulation of phospholipase C-beta1 by Gq and m1 muscarinic cholinergic receptor. Steady-state balance of receptor-mediated activation and GTPase-activating protein-promoted deactivation. *Journal of Biological Chemistry*. 1996;271: 7999–8007.

203. Kim D, Jun KS, Lee SB, Kang NG, Min DS, Kim YH, et al. Phospholipase C isozymes selectively couple to specific neurotransmitter receptors. *Nature*. 1997;389: 290–293. doi:10.1038/38508
204. Smrcka AV, Hepler JR, Brown KO, Sternweis PC. Regulation of polyphosphoinositide-specific phospholipase C activity by purified Gq. *Science*. 1991;251: 804–807. doi:10.1126/science.1846707
205. Rhee SG. Regulation of phosphoinositide-specific phospholipase C. *Annu Rev Biochem*. 2001;70: 281–312. doi:10.1146/annurev.biochem.70.1.281
206. Oldham WM, Hamm HE. Heterotrimeric G protein activation by G-protein-coupled receptors. *Nat Rev Mol Cell Biol*. Nature Publishing Group; 2008;9: 60–71. doi:10.1038/nrm2299
207. Rosse C, Linch M, Kermorgant S, Cameron AJM, Boeckeler K, Parker PJ. PKC and the control of localized signal dynamics. *Nat Rev Mol Cell Biol*. 2010;11: 103–112. doi:10.1038/nrm2847
208. Nishizuka Y. Protein kinase C and lipid signaling for sustained cellular responses. *FASEB J*. 1995;9: 484–496.
209. Nishimura T, Yamaguchi T, Kato K, Yoshizawa M, Nabeshima Y-I, Ohno S, et al. PAR-6–PAR-3 mediates Cdc42-induced Rac activation through the Rac GEFs STEF/Tiam1. *Nature Cell Biology*. 2005;7: 270–277. doi:10.1038/ncb1227
210. Vieira SI, Rebelo S, Esselmann H, Wiltfang J, Lah J, Lane R, et al. Retrieval of the Alzheimer's amyloid precursor protein from the endosome to the TGN is S655 phosphorylation state-dependent and retromer-mediated. *Molecular Neurodegeneration*. 2010;5: 40. doi:10.1186/1750-1326-5-40
211. Vieira SI, Rebelo S, Domingues SC, Cruz e Silva EF, Cruz e Silva OAB. S655 phosphorylation enhances APP secretory traffic. *Mol Cell Biochem*. 2009;328: 145–154. doi:10.1007/s11010-009-0084-7
212. Yang H-Q, Pan J, Ba M-W, Sun Z-K, Ma G-Z, Lu G-Q, et al. New protein kinase C activator regulates amyloid precursor protein processing in vitro by increasing alpha-secretase activity. *Eur J Neurosci*. 2007;26: 381–391. doi:10.1111/j.1460-9568.2007.05648.x
213. Hill K, Hill K, Li Y, Li Y, Bennett M, Bennett M, et al. Munc18 interacting proteins: ADP-ribosylation factor-dependent coat proteins that regulate the traffic of beta-Alzheimer's precursor protein. *Journal of Biological Chemistry*. 2003;278: 36032–36040. doi:10.1074/jbc.M301632200
214. Shrivastava-Ranjan P, Faundez V, Fang G, Rees H, Lah JJ, Levey AI, et al.

- Mint3/X11 Is an ADP-Ribosylation Factor-dependent Adaptor that Regulates the Traffic of the Alzheimer's Precursor Protein from the Trans-Golgi Network. *Mol Biol Cell*. 2008;19: 51–64. doi:10.1091/mbc.E07-05-0465
215. Sullivan SE, Dillon GM, Sullivan JM, Ho A. Mint proteins are required for synaptic activity-dependent amyloid precursor protein (APP) trafficking and amyloid  $\beta$  generation. *J Biol Chem*. 2014;289: 15374–15383. doi:10.1074/jbc.M113.541003
216. Sabo SL, Lanier LM, Ikin AF, Khorkova O, Sahasrabudhe S, Greengard P, et al. Regulation of beta-amyloid secretion by FE65, an amyloid protein precursor-binding protein. *Journal of Biological Chemistry*. 1999;274: 7952–7957.
217. Suh J, Lyckman A, Wang L, Eckman EA, Guénette SY. FE65 proteins regulate NMDA receptor activation-induced amyloid precursor protein processing. *Journal of Neurochemistry*. Blackwell Publishing Ltd; 2011;119: 377–388. doi:10.1111/j.1471-4159.2011.07419.x
218. Pietrzik CU, Yoon I-S, Jaeger S, Busse T, Weggen S, Koo EH. FE65 constitutes the functional link between the low-density lipoprotein receptor-related protein and the amyloid precursor protein. *Journal of Neuroscience*. 2004;24: 4259–4265. doi:10.1523/JNEUROSCI.5451-03.2004
219. Pietrzik CU, Busse T, Merriam DE, Weggen S, Koo EH. The cytoplasmic domain of the LDL receptor-related protein regulates multiple steps in APP processing. *The EMBO Journal*. 2002;21: 5691–5700.
220. Sabo SL, Ikin AF, Buxbaum JD, Greengard P. The Alzheimer amyloid precursor protein (APP) and FE65, an APP-binding protein, regulate cell movement. *Journal of Cell Biology*. 2001;153: 1403–1414.
221. Sabo SL, Ikin AF, Buxbaum JD, Greengard P. The amyloid precursor protein and its regulatory protein, FE65, in growth cones and synapses in vitro and in vivo. *Journal of Neuroscience*. 2003;23: 5407–5415.
222. Cheung HNM, Dunbar C, Mórotz GM, Cheng WH, Chan HYE, Miller CCJ, et al. FE65 interacts with ADP-ribosylation factor 6 to promote neurite outgrowth. *The FASEB Journal*. 2014;28: 337–349. doi:10.1096/fj.13-232694
223. Ermekova KS, Zambrano N, Linn H, Minopoli G, Gertler F, Russo T, et al. The WW domain of neural protein FE65 interacts with proline-rich motifs in Mena, the mammalian homolog of *Drosophila* enabled. *Journal of Biological Chemistry*. 1997;272: 32869–32877.
224. Howell BW, Hawkes R, Soriano P, Cooper JA. Neuronal position in the developing brain is regulated by mouse disabled-1. *Nature*. 1997;389: 733–737.

doi:10.1038/39607

225. Ware ML, Fox JW, González JL, Davis NM, Lambert de Rouvroit C, Russo CJ, et al. Aberrant splicing of a mouse disabled homolog, mdab1, in the scrambler mouse. *Neuron*. 1997;19: 239–249.
226. Sheldon M, Rice DS, D'Arcangelo G, Yoneshima H, Nakajima K, Mikoshiba K, et al. Scrambler and yotari disrupt the disabled gene and produce a reeler-like phenotype in mice. *Nature*. 1997;389: 730–733. doi:10.1038/39601
227. Howell BW, Lanier LM, Frank R, Gertler FB, Cooper JA. The disabled 1 phosphotyrosine-binding domain binds to the internalization signals of transmembrane glycoproteins and to phospholipids. *Molecular and Cellular Biology*. 1999;19: 5179–5188.
228. Homayouni R, Rice DS, Sheldon M, Curran T. Disabled-1 binds to the cytoplasmic domain of amyloid precursor-like protein 1. *Journal of Neuroscience*. 1999;19: 7507–7515.
229. Young-Pearse TL, Young-Pearse TL, Bai J, Bai J, Chang R, Chang R, et al. A critical function for beta-amyloid precursor protein in neuronal migration revealed by in utero RNA interference. *Journal of Neuroscience*. 2007;27: 14459–14469. doi:10.1523/JNEUROSCI.4701-07.2007
230. D'Arcangelo G, Miao GG, Chen SC, Soares HD, Morgan JI, Curran T. A protein related to extracellular matrix proteins deleted in the mouse mutant reeler. *Nature*. 1995;374: 719–723. doi:10.1038/374719a0
231. Hoe H-S, Lee KJ, Carney RSE, Lee J, Markova A, Lee J-Y, et al. Interaction of reelin with amyloid precursor protein promotes neurite outgrowth. *Journal of Neuroscience*. 2009;29: 7459–7473. doi:10.1523/JNEUROSCI.4872-08.2009
232. Hoe H-S, Tran TS, Matsuoka Y, Howell BW, Rebeck GW. DAB1 and Reelin effects on amyloid precursor protein and ApoE receptor 2 trafficking and processing. *Journal of Biological Chemistry. American Society for Biochemistry and Molecular Biology*; 2006;281: 35176–35185. doi:10.1074/jbc.M602162200
233. Hoe H-S, Minami SS, Makarova A, Lee J, Hyman BT, Matsuoka Y, et al. Fyn modulation of Dab1 effects on amyloid precursor protein and ApoE receptor 2 processing. *Journal of Biological Chemistry. American Society for Biochemistry and Molecular Biology*; 2008;283: 6288–6299. doi:10.1074/jbc.M704140200
234. Minami SS, Hoe H-S, Rebeck GW. Fyn kinase regulates the association between amyloid precursor protein and Dab1 by promoting their localization to detergent-resistant membranes. *Journal of Neurochemistry*. 2011;118: 879–890.

doi:10.1111/j.1471-4159.2011.07296.x

235. Simons K, Gruenberg J. Jamming the endosomal system: lipid rafts and lysosomal storage diseases. *Trends in Cell Biology*. 2000;10: 459–462.
236. Fessler MB, Parks JS. Intracellular Lipid Flux and Membrane Microdomains as Organizing Principles in Inflammatory Cell Signaling. *The Journal of Immunology*. 2011;187: 1529–1535. doi:10.4049/jimmunol.1100253
237. Morris SM, Cooper JA. Disabled-2 colocalizes with the LDLR in clathrin-coated pits and interacts with AP-2. *Traffic*. 2001;2: 111–123. doi:10.1034/j.1600-0854.2001.020206.x
238. Chetrit D, Ziv N, Ehrlich M. Dab2 regulates clathrin assembly and cell spreading. *Biochem J*. 2009;418: 701–715. doi:10.1042/BJ20081288
239. Jiang Y, He X, Howe PH. Disabled-2 (Dab2) inhibits Wnt/ $\beta$ -catenin signalling by binding LRP6 and promoting its internalization through clathrin. *The EMBO Journal*. 2012;31: 2336–2349. doi:10.1038/emboj.2012.83
240. Maurer ME, Cooper JA. The adaptor protein Dab2 sorts LDL receptors into coated pits independently of AP-2 and ARH. *Journal of Cell Science*. 2006;119: 4235–4246. doi:10.1242/jcs.03217
241. Matsuda S, Yasukawa T, Homma Y, Ito Y, Niikura T, Hiraki T, et al. c-Jun N-terminal kinase (JNK)-interacting protein-1b/islet-brain-1 scaffolds Alzheimer's amyloid precursor protein with JNK. *Journal of Neuroscience*. 2001;21: 6597–6607.
242. Whitmarsh AJ, Cavanagh J, Tournier C, Yasuda J, Davis RJ. A mammalian scaffold complex that selectively mediates MAP kinase activation. *Science*. 1998;281: 1671–1674.
243. Yasuda J, Whitmarsh AJ, Cavanagh J, Sharma M, Davis RJ. The JIP group of mitogen-activated protein kinase scaffold proteins. *Molecular and Cellular Biology*. 1999;19: 7245–7254.
244. Yamasaki T, Yamasaki T, Yamasaki T, Kawasaki H, Kawasaki H, Kawasaki H, et al. Diverse Roles of JNK and MKK Pathways in the Brain. *J Signal Transduct*. Hindawi Publishing Corporation; 2012;2012: 459265–9. doi:10.1155/2012/459265
245. Colombo A, Bastone A, Ploia C, Scip A, Salmona M, Forloni G, et al. JNK regulates APP cleavage and degradation in a model of Alzheimer's disease. *Neurobiology of Disease*. 2009;33: 518–525. doi:10.1016/j.nbd.2008.12.014
246. Scip A, Antoniou X, Colombo A, Camici GG, Pozzi L, Cardinetti D, et al. c-Jun N-terminal kinase regulates soluble A $\beta$  oligomers and cognitive impairment in AD



- mouse model. *J Biol Chem*. 2011;286: 43871–43880. doi:10.1074/jbc.M111.297515
247. Inomata H, Nakamura Y, Hayakawa A, Takata H, Suzuki T, Miyazawa K, et al. A scaffold protein JIP-1b enhances amyloid precursor protein phosphorylation by JNK and its association with kinesin light chain 1. *Journal of Biological Chemistry*. 2003;278: 22946–22955. doi:10.1074/jbc.M212160200
248. Chiba K, Araseki M, Nozawa K, Furukori K, Araki Y, Matsushima T, et al. Quantitative analysis of APP axonal transport in neurons: role of JIP1 in enhanced APP anterograde transport. *Mol Biol Cell*. 2014;25: 3569–3580. doi:10.1091/mbc.E14-06-1111
249. Horiuchi D, Collins CA, Bhat P, Barkus RV, Diantonio A, Saxton WM. Control of a kinesin-cargo linkage mechanism by JNK pathway kinases. *Curr Biol*. 2007;17: 1313–1317. doi:10.1016/j.cub.2007.06.062
250. Journet A, Chapel A, Kieffer S, Roux F, Garin J. Proteomic analysis of human lysosomes: application to monocytic and breast cancer cells. *Proteomics*. 2002;2: 1026–1040. doi:10.1002/1615-9861(200208)2:8<1026::AID-PROT1026>3.0.CO;2-I
251. Bagshaw RD, Mahuran DJ, Callahan JW. A proteomic analysis of lysosomal integral membrane proteins reveals the diverse composition of the organelle. *Mol Cell Proteomics*. 2005;4: 133–143. doi:10.1074/mcp.M400128-MCP200
252. Fukuda M. Lysosomal membrane glycoproteins. Structure, biosynthesis, and intracellular trafficking. *J Biol Chem*. 1991;266: 21327–21330.
253. Eskelinen E-L, Tanaka Y, Saftig P. At the acidic edge: emerging functions for lysosomal membrane proteins. *Trends in Cell Biology*. 2003;13: 137–145. doi:10.1016/S0962-8924(03)00005-9
254. Saftig P, Beertsen W, Eskelinen E-L. LAMP-2: A control step for phagosome and autophagosome maturation. *Autophagy*. 2014;4: 510–512. doi:10.4161/auto.5724
255. Conner SD, Schmid SL. Differential requirements for AP-2 in clathrin-mediated endocytosis. *The Journal of Cell Biology*. 2003.
256. Heuser J. Three-dimensional visualization of coated vesicle formation in fibroblasts. *Journal of Cell Biology*. 1980;84: 560–583.
257. Smith CJ, Grigorieff N, Pearse BM. Clathrin coats at 21 Å resolution: a cellular assembly designed to recycle multiple membrane receptors. *The EMBO Journal*. 1998;17: 4943–4953. doi:10.1093/emboj/17.17.4943
258. Perry MM, Gilbert AB. Yolk transport in the ovarian follicle of the hen (*Gallus*

- domesticus): lipoprotein-like particles at the periphery of the oocyte in the rapid growth phase. *Journal of Cell Science*. 1979;39: 257–272.
259. Boll W, Rapoport I, Brunner C, Modis Y, Prehn S, Kirchhausen T. The  $\mu$ 2 Subunit of the Clathrin Adaptor AP-2 Binds to FDNPVY and YppO Sorting Signals at Distinct Sites. *Traffic*. 2002;3: 590–600. doi:10.1034/j.1600-0854.2002.30808.x
260. Musacchio A, Smith CJ, Roseman AM, Harrison SC, Kirchhausen T, Pearse BM. Functional organization of clathrin in coats: combining electron cryomicroscopy and X-ray crystallography. *Molecular Cell*. Elsevier; 1999;3: 761–770. doi:10.1093/emboj/17.17.4943
261. Vigers GP, Crowther RA, Pearse BM. Location of the 100 kd-50 kd accessory proteins in clathrin coats. *The EMBO Journal*. 1986;5: 2079–2085.
262. Owen DJ, Collins BM, Evans PR. Adaptors for clathrin coats: structure and function. *Annu Rev Cell Dev Biol*. 2004;20: 153–191. doi:10.1146/annurev.cellbio.20.010403.104543
263. Gallusser A, Kirchhausen T. The beta 1 and beta 2 subunits of the AP complexes are the clathrin coat assembly components. *The EMBO Journal*. 1993;12: 5237–5244.
264. Shih W, Gallusser A, Kirchhausen T. A clathrin-binding site in the hinge of the beta 2 chain of mammalian AP-2 complexes. *J Biol Chem*. 1995;270: 31083–31090.
265. Wilde A, Brodsky FM. In vivo phosphorylation of adaptors regulates their interaction with clathrin. *Journal of Cell Biology*. 1996;135: 635–645.
266. Goodman OB, Keen JH. The alpha chain of the AP-2 adaptor is a clathrin binding subunit. *J Biol Chem*. 1995;270: 23768–23773.
267. Rohde G. A phosphatidylinositol (4,5)-bisphosphate binding site within micro2-adaptin regulates clathrin-mediated endocytosis. *The Journal of Cell Biology*. 2002;158: 209–214. doi:10.1083/jcb.200203103
268. Schröder S, Ungewickell E. Subunit interaction and function of clathrin-coated vesicle adaptors from the Golgi and the plasma membrane. *J Biol Chem*. 1991;266: 7910–7918.
269. Kirchhausen T. Adaptors for clathrin-mediated traffic. *Annu Rev Cell Dev Biol*. 1999;15: 705–732. doi:10.1146/annurev.cellbio.15.1.705
270. Robinson MS, Pearse BM. Immunofluorescent localization of 100K coated vesicle proteins. *Journal of Cell Biology*. 1986;102: 48–54.
271. Ahle S, Mann A, Eichelsbacher U, Ungewickell E. Structural relationships between

- clathrin assembly proteins from the Golgi and the plasma membrane. *The EMBO Journal*. 1988;7: 919–929.
272. Traub LM, Kornfeld S, Ungewickell E. Different domains of the AP-1 adaptor complex are required for Golgi membrane binding and clathrin recruitment. *J Biol Chem*. 1995;270: 4933–4942.
273. Folsch H, Pypaert M, Schu P, Mellman I. Distribution and function of AP-1 clathrin adaptor complexes in polarized epithelial cells. *The Journal of Cell Biology*. 2001;152: 595–606.
274. Folsch H. The AP-1A and AP-1B clathrin adaptor complexes define biochemically and functionally distinct membrane domains. *The Journal of Cell Biology*. 2003;163: 351–362. doi:10.1083/jcb.200309020
275. Gravotta D, Deora A, Perret E, Oyanadel C, Soza A, Schreiner R, et al. AP1B sorts basolateral proteins in recycling and biosynthetic routes of MDCK cells. *Proc Natl Acad Sci USA*. 2007;104: 1564–1569. doi:10.1073/pnas.0610700104
276. Gravotta D, Carvajal-Gonzalez JM, Mattera R, Deborde S, Banfelder JR, Bonifacino JS, et al. The clathrin adaptor AP-1A mediates basolateral polarity. *Developmental Cell*. 2012;22: 811–823. doi:10.1016/j.devcel.2012.02.004
277. Gan Y, McGraw TE, Rodriguez-Boulan E. The epithelial-specific adaptor AP1B mediates post-endocytic recycling to the basolateral membrane. *Nature Cell Biology*. 2002;4: 605–609. doi:10.1038/ncb827
278. Lefkir Y, Malbouyres M, Gotthardt D, Ozinsky A, Cornillon S, Bruckert F, et al. Involvement of the AP-1 adaptor complex in early steps of phagocytosis and macropinocytosis. *Mol Biol Cell*. 2004;15: 861–869. doi:10.1091/mbc.E03-06-0365
279. Doray B, Bruns K, Ghosh P, Kornfeld SA. Autoinhibition of the ligand-binding site of GGA1/3 VHS domains by an internal acidic cluster-dileucine motif. *Proc Natl Acad Sci USA*. 2002;99: 8072–8077. doi:10.1073/pnas.082235699
280. Meyer C, Zizioli D, Lausmann S, Eskelinen EL, Hamann J, Saftig P, et al. mu1A-adaptin-deficient mice: lethality, loss of AP-1 binding and rerouting of mannose 6-phosphate receptors. *The EMBO Journal*. 2000;19: 2193–2203. doi:10.1093/emboj/19.10.2193
281. Icking A, Amaddii M, Ruonala M, Höning S, Tikkanen R. Polarized Transport of Alzheimer Amyloid Precursor Protein Is Mediated by Adaptor Protein Complex AP1-1B. *Traffic*. 2006;8: 285–296. doi:10.1111/j.1600-0854.2006.00526.x
282. Simpson F, Bright NA, West MA, Newman LS, Darnell RB, Robinson MS. A novel adaptor-related protein complex. *The Journal of Cell Biology*. 1996;133: 749–760.

283. Ooi CE, Moreira JE, Dell'Angelica EC, Poy G, Wassarman DA, Bonifacino JS. Altered expression of a novel adaptin leads to defective pigment granule biogenesis in the *Drosophila* eye color mutant garnet. *The EMBO Journal*. 1997;16: 4508–4518. doi:10.1093/emboj/16.15.4508
284. Dell'Angelica EC, Ohno H, Ooi CE, Rabinovich E, Roche KW, Bonifacino JS. AP-3: an adaptor-like protein complex with ubiquitous expression. *The EMBO Journal*. 1997;16: 917–928. doi:10.1093/emboj/16.5.917
285. Pevsner J, Volkandt W, Wong BR, Scheller RH. Two rat homologs of clathrin-associated adaptor proteins. *Gene*. 1994;146: 279–283. doi:10.1016/0378-1119(94)90306-9
286. Newman LS, McKeever MO, Okano HJ, Darnell RB. Beta-NAP, a cerebellar degeneration antigen, is a neuron-specific vesicle coat protein. *Cell*. 1995;82: 773–783. doi:10.1016/0092-8674(95)90474-3
287. Cowles CR, Snyder WB, Burd CG, Emr SD. Novel Golgi to vacuole delivery pathway in yeast: identification of a sorting determinant and required transport component. *The EMBO Journal*. 1997;16: 2769–2782. doi:10.1093/emboj/16.10.2769
288. Cowles CR, Odorizzi G, Payne GS, Emr SD. The AP-3 adaptor complex is essential for cargo-selective transport to the yeast vacuole. *Cell*. 1997;91: 109–118.
289. Stepp JD, Huang K, Lemmon SK. The yeast adaptor protein complex, AP-3, is essential for the efficient delivery of alkaline phosphatase by the alternate pathway to the vacuole. *Journal of Cell Biology*. 1997;139: 1761–1774.
290. Kretzschmar D, Poeck B, Roth H, Ernst R, Keller A, Porsch M, et al. Defective pigment granule biogenesis and aberrant behavior caused by mutations in the *Drosophila* AP-3beta adaptin gene ruby. *Genetics*. 2000;155: 213–223.
291. Mullins C, Hartnell LM, Bonifacino JS. Distinct requirements for the AP-3 adaptor complex in pigment granule and synaptic vesicle biogenesis in *Drosophila melanogaster*. *Mol Gen Genet*. 2000;263: 1003–1014. doi:10.1007/PL00008688
292. Feng L, Novak EK, Hartnell LM, Bonifacino JS, Collinson LM, Swank RT. The Hermansky-Pudlak syndrome 1 (HPS1) and HPS2 genes independently contribute to the production and function of platelet dense granules, melanosomes, and lysosomes. *Blood*. 2002;99: 1651–1658. doi:10.1182/blood.V99.5.1651
293. Kantheti P, Qiao X, Diaz ME, Peden AA, Meyer GE, Carskadon SL, et al. Mutation in AP-3 delta in the mocha mouse links endosomal transport to storage deficiency in platelets, melanosomes, and synaptic vesicles. *Neuron*. 1998;21: 111–122.

294. Feng L, Seymour AB, Jiang S, To A, Peden AA, Novak EK, et al. The beta3A subunit gene (Ap3b1) of the AP-3 adaptor complex is altered in the mouse hypopigmentation mutant pearl, a model for Hermansky-Pudlak syndrome and night blindness. *Human Molecular Genetics*. 1999;8: 323–330.
295. Hermansky F, Pudlak P. Albinism associated with hemorrhagic diathesis and unusual pigmented reticular cells in the bone marrow: report of two cases with histochemical studies. *Blood*. 1959;14: 162–169.
296. Wei ML. Hermansky-Pudlak syndrome: a disease of protein trafficking and organelle function. *Pigment Cell Res*. 2006;19: 19–42. doi:10.1111/j.1600-0749.2005.00289.x
297. Wenham M, Grieve S, Cummins M, Jones ML, Booth S, Kilner R, et al. Two patients with Hermansky Pudlak syndrome type 2 and novel mutations in AP3B1. *Haematologica*. 2010;95: 333–337. doi:10.3324/haematol.2009.012286
298. Orlow SJ. Melanosomes are specialized members of the lysosomal lineage of organelles. *J Invest Dermatol*. 1995;105: 3–7.
299. Israels SJ, McMillan EM, Robertson C, Singhory S, McNicol A. The lysosomal granule membrane protein, LAMP-2, is also present in platelet dense granule membranes. *Thromb Haemost*. 1996;75: 623–629.
300. Peden AA. Localization of the AP-3 adaptor complex defines a novel endosomal exit site for lysosomal membrane proteins. *The Journal of Cell Biology*. 2004;164: 1065–1076. doi:10.1083/jcb.200311064
301. Dell'Angelica EC, Shotelersuk V, Aguilar RC, Gahl WA, Bonifacino JS. Altered trafficking of lysosomal proteins in Hermansky-Pudlak syndrome due to mutations in the beta 3A subunit of the AP-3 adaptor. *Molecular Cell*. 1999;3: 11–21. doi:10.1016/S1097-2765(00)80170-7
302. Peden AA. Assembly and function of AP-3 complexes in cells expressing mutant subunits. *The Journal of Cell Biology*. 2002;156: 327–336. doi:10.1083/jcb.200107140
303. Chapuy B, Tikkanen R, Mühlhausen C, Wenzel D, Figura von K, Höning S. AP-1 and AP-3 Mediate Sorting of Melanosomal and Lysosomal Membrane Proteins into Distinct Post-Golgi Trafficking Pathways. *Traffic*. 2008;9: 1157–1172. doi:10.1111/j.1600-0854.2008.00745.x
304. Dell'Angelica EC, Klumperman J, Stoorvogel W, Bonifacino JS. Association of the AP-3 adaptor complex with clathrin. *Science*. 1998;280: 431–434.
305. Dell'Angelica EC, Mullins C, Bonifacino JS. AP-4, a novel protein complex related

- to clathrin adaptors. *J Biol Chem*. 1999;274: 7278–7285.
306. Hirst J, Bright NA, Rous B, Robinson MS. Characterization of a fourth adaptor-related protein complex. *Mol Biol Cell*. 1999;10: 2787–2802.
307. Simmen T, Höning S, Icking A, Tikkanen R, Hunziker W. AP-4 binds basolateral signals and participates in basolateral sorting in epithelial MDCK cells. *Nature Cell Biology*. 2002;4: 154–159. doi:10.1038/ncb745
308. Burgos PV, Mardones GA, Rojas AL, daSilva LLP, Prabhu Y, Hurley JH, et al. Sorting of the Alzheimer's disease amyloid precursor protein mediated by the AP-4 complex. *Developmental Cell*. 2010;18: 425–436. doi:10.1016/j.devcel.2010.01.015
309. Hirst J, Irving C, Borner GHH. Adaptor protein complexes AP-4 and AP-5: new players in endosomal trafficking and progressive spastic paraplegia. *Traffic*. 2013;14: 153–164. doi:10.1111/tra.12028
310. Hirst J, Borner GHH, Antrobus R, Peden AA, Hodson NA, Sahlender DA, et al. Distinct and overlapping roles for AP-1 and GGAs revealed by the “knocksideways” system. *Curr Biol*. 2012;22: 1711–1716. doi:10.1016/j.cub.2012.07.012
311. Borner GHH, Antrobus R, Hirst J, Bhumbra GS, Kozik P, Jackson LP, et al. Multivariate proteomic profiling identifies novel accessory proteins of coated vesicles. *The Journal of Cell Biology*. 2012;197: 141–160. doi:10.1083/jcb.201111049
312. Hirst J, Barlow LD, Francisco GC, Sahlender DA, Seaman MNJ, Dacks JB, et al. The fifth adaptor protein complex. *Plos Biol*. 2011;9: e1001170. doi:10.1371/journal.pbio.1001170
313. Hirst J, Lui WW, Bright NA, Totty N, Seaman MN, Robinson MS. A family of proteins with gamma-adaptin and VHS domains that facilitate trafficking between the trans-Golgi network and the vacuole/lysosome. *Journal of Cell Biology*. 2000;149: 67–80.
314. Dell'Angelica EC, Puertollano R, Mullins C, Aguilar RC, Vargas JD, Hartnell LM, et al. GGAs: a family of ADP ribosylation factor-binding proteins related to adaptors and associated with the Golgi complex. *Journal of Cell Biology*. 2000;149: 81–94.
315. Takatsu H, Yoshino K, Nakayama K. Adaptor gamma ear homology domain conserved in gamma-adaptin and GGA proteins that interact with gamma-synergin. *Biochemical and Biophysical Research Communications*. 2000;271: 719–725. doi:10.1006/bbrc.2000.2700
316. Boman AL, Zhang CJ, Zhu X, Kahn RA. A family of ADP-ribosylation factor

- effectors that can alter membrane transport through the trans-Golgi. *Mol Biol Cell*. 2000;11: 1241–1255.
317. Poussu A, Lohi O, Lehto VP. Vear, a novel Golgi-associated protein with VHS and gamma-adaptin “ear” domains. *J Biol Chem*. 2000;275: 7176–7183.
318. Puertollano R, Randazzo PA, Presley JF, Hartnell LM, Bonifacino JS. The GGAs promote ARF-dependent recruitment of clathrin to the TGN. *Cell*. 2001;105: 93–102.
319. Misra S, Puertollano R, Kato Y, Bonifacino JS, Hurley JH. Structural basis for acidic-cluster-dileucine sorting-signal recognition by VHS domains. *Nature*. 2002;415: 933–937. doi:10.1038/415933a
320. Puertollano R, Aguilar RC, Gorshkova I, Crouch RJ, Bonifacino JS. Sorting of mannose 6-phosphate receptors mediated by the GGAs. *Science*. 2001;292: 1712–1716. doi:10.1126/science.1060750
321. Collins BM, Praefcke GJK, Robinson MS, Owen DJ. Structural basis for binding of accessory proteins by the appendage domain of GGAs. *Nat Struct Biol*. 2003;10: 607–613. doi:10.1038/nsb955
322. Miller GJ, Mattera R, Bonifacino JS, Hurley JH. Recognition of accessory protein motifs by the gamma-adaptin ear domain of GGA3. *Nat Struct Biol*. 2003;10: 599–606. doi:10.1038/nsb953
323. Doray B, Ghosh P, Griffith J, Geuze HJ, Kornfeld S. Cooperation of GGAs and AP-1 in packaging MPRs at the trans-Golgi network. *Science*. 2002;297: 1700–1703. doi:10.1126/science.1075327
324. Puertollano R, van der Wel NN, Greene LE, Eisenberg E, Peters PJ, Bonifacino JS. Morphology and dynamics of clathrin/GGA1-coated carriers budding from the trans-Golgi network. *Mol Biol Cell*. 2003;14: 1545–1557. doi:10.1091/mbc.02-07-0109
325. Puertollano R, Bonifacino JS. Interactions of GGA3 with the ubiquitin sorting machinery. *Nature Cell Biology*. 2004;6: 244–251. doi:10.1038/ncb1106
326. Scott PM, Bilodeau PS, Zhdankina O, Winistorfer SC, Hauglund MJ, Allaman MM, et al. GGA proteins bind ubiquitin to facilitate sorting at the trans-Golgi network. *Nature Cell Biology*. Nature Publishing Group; 2004;6: 8–259. doi:10.1038/ncb1107
327. He X, Li F, Chang W-P, Tang J. GGA proteins mediate the recycling pathway of memapsin 2 (BACE). *J Biol Chem*. 2005;280: 11696–11703. doi:10.1074/jbc.M411296200

328. Kornfeld S, Mellman I. The biogenesis of lysosomes. *Annu Rev Cell Biol.* 1989;5: 483–525. doi:10.1146/annurev.cb.05.110189.002411
329. A P Varki MLRSK. Identification of a variant of mucopolidosis III (pseudo-Hurler polydystrophy): a catalytically active N-acetylglucosaminylphosphotransferase that fails to phosphorylate lysosomal enzymes. *Proc Natl Acad Sci USA. National Academy of Sciences;* 1981;78: 7773.
330. Hasilik A, Waheed A, Figura von K. Enzymatic phosphorylation of lysosomal enzymes in the presence of UDP-N-acetylglucosamine. Absence of the activity in I-cell fibroblasts. *Biochemical and Biophysical Research Communications.* 1981;98: 761–767.
331. Tong PY, Gregory W, Kornfeld S. Ligand interactions of the cation-independent mannose 6-phosphate receptor. The stoichiometry of mannose 6-phosphate binding. *J Biol Chem.* 1989;264: 7962–7969.
332. Dahms NM, Kornfeld S. The cation-dependent mannose 6-phosphate receptor. Structural requirements for mannose 6-phosphate binding and oligomerization. *J Biol Chem.* 1989;264: 11458–11467.
333. Stein M, Zijderhand-Bleekemolen JE, Geuze H, Hasilik A, Figura von K. Mr 46,000 mannose 6-phosphate specific receptor: its role in targeting of lysosomal enzymes. *The EMBO Journal.* 1987;6: 2677–2681.
334. Campbell CH, Fine RE, Squicciarini J, Rome LH. Coated vesicles from rat liver and calf brain contain cryptic mannose 6-phosphate receptors. *J Biol Chem.* 1983;258: 2628–2633.
335. Lemansky P. Lysosomal enzyme precursors in coated vesicles derived from the exocytic and endocytic pathways. *The Journal of Cell Biology.* 1987;104: 1743–1748. doi:10.1083/jcb.104.6.1743
336. van Meel E, Klumperman J. Imaging and imagination: understanding the endo-lysosomal system. *Histochem Cell Biol.* 2008;129: 253–266. doi:10.1007/s00418-008-0384-0
337. Johnson KF, Kornfeld S. A His-Leu-Leu sequence near the carboxyl terminus of the cytoplasmic domain of the cation-dependent mannose 6-phosphate receptor is necessary for the lysosomal enzyme sorting function. *Journal of Biological Chemistry.* 1992;267: 17110–17115.
338. Johnson KF, Kornfeld S. The cytoplasmic tail of the mannose 6-phosphate/insulin-like growth factor-II receptor has two signals for lysosomal enzyme sorting in the Golgi. *Journal of Cell Biology.* 1992;119: 249–257.



339. Shiba T, Takatsu H, Nogi T, Matsugaki N, Kawasaki M, Igarashi N, et al. Structural basis for recognition of acidic-cluster dileucine sequence by GGA1. *Nature*. 2002;415: 937–941. doi:10.1038/415937a
340. Takatsu H, Katoh Y, Shiba Y, Nakayama K. Golgi-localizing, gamma-adaptin ear homology domain, ADP-ribosylation factor-binding (GGA) proteins interact with acidic dileucine sequences within the cytoplasmic domains of sorting receptors through their Vps27p/Hrs/STAM (VHS) domains. *J Biol Chem*. 2001;276: 28541–28545. doi:10.1074/jbc.C100218200
341. Zhu Y, Doray B, Poussu A, Lehto VP, Kornfeld S. Binding of GGA2 to the lysosomal enzyme sorting motif of the mannose 6-phosphate receptor. *Science*. 2001;292: 1716–1718. doi:10.1126/science.1060896
342. Honing S, Sosa M, Hille-Rehfeld A, Figura von K. The 46-kDa mannose 6-phosphate receptor contains multiple binding sites for clathrin adaptors. *J Biol Chem*. 1997;272: 19884–19890.
343. Mauxion F, Le Borgne R, Munier-Lehmann H, Hoflack B. A casein kinase II phosphorylation site in the cytoplasmic domain of the cation-dependent mannose 6-phosphate receptor determines the high affinity interaction of the AP-1 Golgi assembly proteins with membranes. *J Biol Chem*. 1996;271: 2171–2178.
344. Griffiths G. Mannose 6-Phosphate Receptors and ADP-ribosylation Factors Cooperate for High Affinity Interaction of the AP-1 Golgi Assembly Proteins with Membranes. *Journal of Biological Chemistry*. 1996;271: 2162–2170. doi:10.1074/jbc.271.4.2162
345. Le Borgne R, Schmidt A, Mauxion F, Griffiths G, Hoflack B. Binding of AP-1 Golgi adaptors to membranes requires phosphorylated cytoplasmic domains of the mannose 6-phosphate/insulin-like growth factor II receptor. *J Biol Chem*. 1993;268: 22552–22556.
346. Ghosh P, Dahms NM, Kornfeld S. Mannose 6-phosphate receptors: new twists in the tale. *Nat Rev Mol Cell Biol*. Nature Publishing Group; 2003;4: 202–213. doi:10.1038/nrm1050
347. Bai H, Doray B, Kornfeld S. GGA1 interacts with the adaptor protein AP-1 through a WNSF sequence in its hinge region. *J Biol Chem*. 2004;279: 17411–17417. doi:10.1074/jbc.M401158200
348. Umeda A, Meyerholz A, Ungewickell E. Identification of the universal cofactor (auxilin 2) in clathrin coat dissociation. *European Journal of Cell Biology*. 2000;79: 336–342. doi:10.1078/S0171-9335(04)70037-0

349. Greener T, Zhao X, Nojima H, Eisenberg E, Greene LE. Role of Cyclin G-associated Kinase in Uncoating Clathrin-coated Vesicles from Non-neuronal Cells. *Journal of Biological Chemistry*. 2000.
350. Morgan JR, Prasad K, Jin S, Augustine GJ, Lafer EM. Uncoating of clathrin-coated vesicles in presynaptic terminals: roles for Hsc70 and auxilin. *Neuron*. 2001;32: 289–300.
351. Korolchuk VI, Banting G. CK2 and GAK/auxilin2 Are Major Protein Kinases in Clathrin-Coated Vesicles. *Traffic*. Wiley Online Library; 2002;3: 428–439.
352. Zhou X, Fabian L, Bayraktar JL, Ding H-M, Brill JA, Chang HC. Auxilin is required for formation of Golgi-derived clathrin-coated vesicles during *Drosophila* spermatogenesis. *Development*. 2011;138: 1111–1120. doi:10.1242/dev.057422
353. Nakagawa T, Setou M, Seog D, Ogasawara K, Dohmae N, Takio K, et al. A novel motor, KIF13A, transports mannose-6-phosphate receptor to plasma membrane through direct interaction with AP-1 complex. *Cell*. 2000;103: 569–581.
354. Stenmark H. Rab GTPases as coordinators of vesicle traffic. *Nat Rev Mol Cell Biol*. 2009;10: 513–525. doi:10.1038/nrm2728
355. Lippé R, Miaczynska M, Rybin V, Runge A, Zerial M. Functional synergy between Rab5 effector Rabaptin-5 and exchange factor Rabex-5 when physically associated in a complex. *Mol Biol Cell*. *Am Soc Cell Biol*; 2001;12: 2219–2228. doi:10.1091/mbc.12.7.2219
356. Horiuchi H, Lippe R, McBride HM, Rubino M, Woodman P, Stenmark H, et al. A novel Rab5 GDP/GTP exchange factor complexed to Rabaptin-5 links nucleotide exchange to effector recruitment and function. *Cell*. 1997;90: 1149–1159.
357. Vitale G, Rybin V, Christoforidis S, Thornqvist P, McCaffrey M, Stenmark H, et al. Distinct Rab-binding domains mediate the interaction of Rabaptin-5 with GTP-bound Rab4 and Rab5. *The EMBO Journal*. 1998;17: 1941–1951. doi:10.1093/emboj/17.7.1941
358. Geuze HJ, Stoorvogel W, Strous GJ, Slot JW, Bleekemolen JE, Mellman I. Sorting of mannose 6-phosphate receptors and lysosomal membrane proteins in endocytic vesicles. *Journal of Cell Biology*. Rockefeller Univ Press; 1988;107: 2491–2501.
359. Díaz E, Pfeffer SR. TIP47: a cargo selection device for mannose 6-phosphate receptor trafficking. *Cell*. 1998;93: 433–443.
360. Carroll KS, Hanna J, Simon I, Krise J, Barbero P, Pfeffer SR. Role of Rab9 GTPase in facilitating receptor recruitment by TIP47. *Science*. American Association for the

- Advancement of Science; 2001;292: 1373–1376. doi:10.1126/science.1056791
361. Riederer MA, Soldati T, Shapiro AD, Lin J, Pfeffer SR. Lysosome biogenesis requires Rab9 function and receptor recycling from endosomes to the trans-Golgi network. *Journal of Cell Biology*. 1994;125: 573–582.
  362. Crump CM, Xiang Y, Thomas L, Gu F, Austin C, Tooze SA, et al. PACS-1 binding to adaptors is required for acidic cluster motif-mediated protein traffic. *The EMBO Journal*. 2001;20: 2191–2201. doi:10.1093/emboj/20.9.2191
  363. Wan L, Molloy SS, Thomas L, Liu G, Xiang Y, Rybak SL, et al. PACS-1 defines a novel gene family of cytosolic sorting proteins required for trans-Golgi network localization. *Cell*. 1998;94: 205–216.
  364. Braulke T, Bonifacino JS. Sorting of lysosomal proteins. *BBA - Molecular Cell Research*. Elsevier B.V; 2009;1793: 605–614. doi:10.1016/j.bbamcr.2008.10.016
  365. Lobel P, Fujimoto K, Ye RD, Griffiths G, Kornfeld S. Mutations in the cytoplasmic domain of the 275 kd mannose 6-phosphate receptor differentially alter lysosomal enzyme sorting and endocytosis. *Cell*. 1989;57: 787–796. doi:10.1016/0092-8674(89)90793-9
  366. Canfield WM, Johnson KF, Ye RD, Gregory W, Kornfeld S. Localization of the signal for rapid internalization of the bovine cation-independent mannose 6-phosphate/insulin-like growth factor-II receptor to amino acids 24-29 of the cytoplasmic tail. *J Biol Chem*. 1991;266: 5682–5688.
  367. Jadot M, Canfield WM, Gregory W, Kornfeld S. Characterization of the signal for rapid internalization of the bovine mannose 6-phosphate/insulin-like growth factor-II receptor. *J Biol Chem*. 1992;267: 11069–11077.
  368. Glickman JN, Conibear E, Pearse BM. Specificity of binding of clathrin adaptors to signals on the mannose-6-phosphate/insulin-like growth factor II receptor. *The EMBO Journal*. 1989;8: 1041–1047.
  369. Neiss WF. A coat of glycoconjugates on the inner surface of the lysosomal membrane in the rat kidney. *Histochemistry*. 1984;80: 603–608.
  370. Chen WJ, Goldstein JL, Brown MS. NPXY, a sequence often found in cytoplasmic tails, is required for coated pit-mediated internalization of the low density lipoprotein receptor. *J Biol Chem*. 1990;265: 3116–3123.
  371. Lai A, Sisodia SS, Trowbridge IS. Characterization of sorting signals in the beta-amyloid precursor protein cytoplasmic domain. *J Biol Chem*. 1995;270: 3565–3573.
  372. Trowbridge IS, Collawn JF, Hopkins CR. Signal-dependent membrane protein

- trafficking in the endocytic pathway. *Annu Rev Cell Biol.* 1993;9: 129–161.  
doi:10.1146/annurev.cb.09.110193.001021
373. Ohno H, Stewart J, Fournier MC, Bosshart H, Rhee I, Miyatake S, et al. Interaction of tyrosine-based sorting signals with clathrin-associated proteins. *Science.* 1995;269: 1872–1875. doi:10.1126/science.7569928
374. Ohno H, Fournier M-C, Poy G, Bonifacino JS. Structural determinants of interaction of tyrosine-based sorting signals with the adaptor medium chains. *J Biol Chem.* 1996;271: 29009–29015. doi:10.1074/jbc.271.46.29009
375. Boll W, Ohno H, Songyang Z, Rapoport I, Cantley LC, Bonifacino JS, et al. Sequence requirements for the recognition of tyrosine-based endocytic signals by clathrin AP-2 complexes. *The EMBO Journal.* 1996;15: 5789–5795.
376. Honing S, Griffith J, Geuze HJ, Hunziker W. The tyrosine-based lysosomal targeting signal in lamp-1 mediates sorting into Golgi-derived clathrin-coated vesicles. *The EMBO Journal.* 1996;15: 5230–5239.
377. Ohno H. Physiological Roles of Clathrin Adaptor AP Complexes: Lessons from Mutant Animals. *Journal of Biochemistry.* 2006;139: 943–948.  
doi:10.1093/jb/mvj120
378. Owen DJ, Evans PR. A structural explanation for the recognition of tyrosine-based endocytotic signals. *Science. American Association for the Advancement of Science;* 1998;282: 1327–1332. doi:10.1126/science.282.5392.1327
379. Royle SJ, Bobanović LK, Murrell-Lagnado RD. Identification of a Non-canonical Tyrosine-based Endocytic Motif in an Ionotropic Receptor . *Journal of Biological ...* 2002.
380. Royle SJ, Qureshi OS, Bobanović LK, Evans PR, Owen DJ, Murrell-Lagnado RD. Non-canonical YXXGPhi endocytic motifs: recognition by AP2 and preferential utilization in P2X4 receptors. *Journal of Cell Science.* 2005;118: 3073–3080.  
doi:10.1242/jcs.02451
381. Setiadi H, Disdier M, Green SA, Canfield WM, McEver RP. Residues throughout the cytoplasmic domain affect the internalization efficiency of P-selectin. *J Biol Chem.* 1995;270: 26818–26826.
382. Owen DJ, Setiadi H, Evans PR, McEver RP, Green SA. A Third Specificity-Determining Site in  $\mu$ 2 Adaptin for Sequences Upstream of Yxx $\Phi$  Sorting Motifs. *Traffic. Wiley Online Library;* 2001;2: 105–110.  
doi:10.1034/j.1600-0854.2001.020205.x

383. Kittler JT, Chen G, Kukhtina V, Vahedi-Faridi A, Gu Z, Tretter V, et al. Regulation of synaptic inhibition by phospho-dependent binding of the AP2 complex to a YECL motif in the GABAA receptor gamma2 subunit. *Proceedings of the National Academy of Sciences*. 2008;105: 3616–3621. doi:10.1073/pnas.0707920105
384. Tretter V, Revilla-Sanchez R, Houston C, Terunuma M, Havekes R, Florian C, et al. Deficits in spatial memory correlate with modified {gamma}-aminobutyric acid type A receptor tyrosine phosphorylation in the hippocampus. *Proceedings of the National Academy of Sciences*. 2009;106: 20039–20044. doi:10.1073/pnas.0908840106
385. Conner SD, Schmid SL. Identification of an adaptor-associated kinase, AAK1, as a regulator of clathrin-mediated endocytosis. *Journal of Cell Biology*. 2002;156: 921–929. doi:10.1083/jcb.200108123
386. Ricotta D, Conner SD, Schmid SL, Figura von K, Höning S. Phosphorylation of the AP2 mu subunit by AAK1 mediates high affinity binding to membrane protein sorting signals. *Journal of Cell Biology*. 2002;156: 791–795. doi:10.1083/jcb.200111068
387. Ohno H, Aguilar RC, Yeh D, Taura D, Saito T, Bonifacino JS. The medium subunits of adaptor complexes recognize distinct but overlapping sets of tyrosine-based sorting signals. *J Biol Chem*. 1998;273: 25915–25921.
388. Letourneur F, Klausner RD. A novel di-leucine motif and a tyrosine-based motif independently mediate lysosomal targeting and endocytosis of CD3 chains. *Cell*. 1992;69: 1143–1157.
389. Bentham M, Mazaleyrat S, Harris M. The di-leucine motif in the cytoplasmic tail of CD4 is not required for binding to human immunodeficiency virus type 1 Nef, but is critical for CD4 down-modulation. *J Gen Virol. Soc General Microbiol*; 2003;84: 2705–2713. doi:10.1099/vir.0.19274-0
390. Hunziker W, Fumey C. A di-leucine motif mediates endocytosis and basolateral sorting of macrophage IgG Fc receptors in MDCK cells. *The EMBO Journal*. 1994;13: 2963–2969.
391. Sheikh H, Isacke CM. A di-hydrophobic Leu-Val motif regulates the basolateral localization of CD44 in polarized Madin-Darby canine kidney epithelial cells. *J Biol Chem*. 1996;271: 12185–12190. doi:10.1074/jbc.271.21.12185
392. Bello V, Goding JW, Greengrass V, Sali A, Dubljevic V, Lenoir C, et al. Characterization of a Di-leucine-based Signal in the Cytoplasmic Tail of the Nucleotide-pyrophosphatase NPP1 That Mediates Basolateral Targeting but not Endocytosis. *Mol Biol Cell. Am Soc Cell Biol*; 2001;12: 3004–3015.

393. Pond L, Kuhn LA, Teyton L, Schutze M-P, Tainer JA, Jackson MR, et al. A role for acidic residues in di-leucine motif-based targeting to the endocytic pathway. *J Biol Chem. ASBMB*; 1995;270: 19989–19997. doi:10.1074/jbc.270.34.19989
394. Sandoval IV, Martinez-Arca S, Valdueza J, Palacios S, Holman GD. Distinct reading of different structural determinants modulates the dileucine-mediated transport steps of the lysosomal membrane protein LIMP-II and the insulin-sensitive glucose transporter GLUT4. *J Biol Chem*. 2000;275: 39874–39885. doi:10.1074/jbc.M006261200
395. Marks MS. Protein targeting by tyrosine- and di-leucine-based signals: evidence for distinct saturable components. *The Journal of Cell Biology*. 1996;135: 341–354. doi:10.1083/jcb.135.2.341
396. Rapoport I, Chen YC, Cupers P, Shoelson SE, Kirchhausen T. Dileucine-based sorting signals bind to the beta chain of AP-1 at a site distinct and regulated differently from the tyrosine-based motif-binding site. *The EMBO Journal*. 1998;17: 2148–2155. doi:10.1093/emboj/17.8.2148
397. Hofmann MW, Honing S, RODIONOV D, Dobberstein B, Figura von K, BAKKE O. The leucine-based sorting motifs in the cytoplasmic domain of the invariant chain are recognized by the clathrin adaptors AP1 and AP2 and their medium chains. *J Biol Chem*. 1999;274: 36153–36158.
398. Janvier K, Kato Y, Boehm M, Rose JR, Martina JA, Kim B-Y, et al. Recognition of dileucine-based sorting signals from HIV-1 Nef and LIMP-II by the AP-1 gamma-sigma1 and AP-3 delta-sigma3 hemicomplexes. *Journal of Cell Biology*. 2003;163: 1281–1290. doi:10.1083/jcb.200307157
399. Doray B, Lee I, Knisely J, Bu G, Kornfeld S. The gamma/sigma1 and alpha/sigma2 hemicomplexes of clathrin adaptors AP-1 and AP-2 harbor the dileucine recognition site. *Mol Biol Cell*. 2007;18: 1887–1896. doi:10.1091/mbc.E07-01-0012
400. Mattera R, Boehm M, Chaudhuri R, Prabhu Y, Bonifacino JS. Conservation and Diversification of Dileucine Signal Recognition by Adaptor Protein (AP) Complex Variants. *Journal of Biological Chemistry*. 2011;286: 2022–2030. doi:10.1074/jbc.M110.197178
401. Sitaram A, Dennis MK, Chaudhuri R, De Jesus-Rojas W, Tenza D, Setty SRG, et al. Differential recognition of a dileucine-based sorting signal by AP-1 and AP-3 reveals a requirement for both BLOC-1 and AP-3 in delivery of OCA2 to melanosomes. *Mol Biol Cell*. 2012;23: 3178–3192. doi:10.1091/mbc.E11-06-0509
402. Kelly BT, McCoy AJ, Späte K, Miller SE, Evans PR, Höning S, et al. A structural explanation for the binding of endocytic dileucine motifs by the AP2 complex.

- Nature. Nature Publishing Group; 2008;456: 976–979. doi:10.1038/nature07422
403. Honing S, Sandoval IV, Figura von K. A di-leucine-based motif in the cytoplasmic tail of LIMP-II and tyrosinase mediates selective binding of AP-3. *The EMBO Journal*. 1998;17: 1304–1314. doi:10.1093/emboj/17.5.1304
404. Bonifacino JS, Traub LM. Signals for sorting of transmembrane proteins to endosomes and lysosomes. *Annu Rev Biochem*. 2003;72: 395–447. doi:10.1146/annurev.biochem.72.121801.161800
405. McMahon HT, Boucrot E. Molecular mechanism and physiological functions of clathrin-mediated endocytosis. *Nat Rev Mol Cell Biol*. 2011;12: 517–533. doi:10.1038/nrm3151
406. Tian Y, Chang JC, Fan EY, Flajolet M, Greengard P. Adaptor complex AP2/PICALM, through interaction with LC3, targets Alzheimer's APP-CTF for terminal degradation via autophagy. *Proceedings of the National Academy of Sciences*. 2013. doi:10.1073/pnas.1315110110
407. Schneider A, Rajendran L, Honscho M, Gralle M, Donnert G, Wouters F, et al. Flotillin-Dependent Clustering of the Amyloid Precursor Protein Regulates Its Endocytosis and Amyloidogenic Processing in Neurons. *Journal of Neuroscience*. 2008;28: 2874–2882. doi:10.1523/JNEUROSCI.5345-07.2008
408. Cossec J-C, Simon A, Marquer C, Moldrich RX, Leterrier C, Rossier J, et al. Clathrin-dependent APP endocytosis and A $\beta$  secretion are highly sensitive to the level of plasma membrane cholesterol. *BBA - Molecular and Cell Biology of Lipids*. Elsevier B.V; 2010;1801: 846–852. doi:10.1016/j.bbalip.2010.05.010
409. Eehalt R, Keller P, Haass C, Thiele C, Simons K. Amyloidogenic processing of the Alzheimer beta-amyloid precursor protein depends on lipid rafts. *Journal of Cell Biology*. 2003;160: 113–123. doi:10.1083/jcb.200207113
410. Cam JA, Zerbinatti CV, Knisely JM, Hecimovic S, Li Y, Bu G. The low density lipoprotein receptor-related protein 1B retains beta-amyloid precursor protein at the cell surface and reduces amyloid-beta peptide production. *Journal of Biological Chemistry*. 2004;279: 29639–29646. doi:10.1074/jbc.M313893200
411. Wagner T, Pietrzik CU. The role of lipoprotein receptors on the physiological function of APP. *Exp Brain Res*. 2011;217: 377–387. doi:10.1007/s00221-011-2876-8
412. Sugimoto H, Sugahara M, Fölsch H, Koide Y, Nakatsu F, Tanaka N, et al. Differential recognition of tyrosine-based basolateral signals by AP-1B subunit mu1B in polarized epithelial cells. *Mol Biol Cell*. American Society for Cell

- Biology; 2002;13: 2374–2382. doi:10.1091/mbc.E01-10-0096
413. Horton AC, Ehlers MD. Neuronal polarity and trafficking. *Neuron*. 2003;40: 277–295. doi:10.1016/S0896-6273(03)00629-9
414. Simons M, Ikonen E, Tienari PJ, Cid-Arregui A, Mönning U, Beyreuther K, et al. Intracellular routing of human amyloid protein precursor: axonal delivery followed by transport to the dendrites. *J Neurosci Res*. Wiley Subscription Services, Inc., A Wiley Company; 1995;41: 121–128. doi:10.1002/jnr.490410114
415. Tienari PJ, De Strooper B, Ikonen E, Simons M, Weidemann A, Czech C, et al. The beta-amyloid domain is essential for axonal sorting of amyloid precursor protein. *The EMBO Journal*. 1996;15: 5218–5229.
416. Margeta MA, Wang GJ, Shen K. Clathrin adaptor AP-1 complex excludes multiple postsynaptic receptors from axons in *C. elegans*. *Proceedings of the National Academy of Sciences*. 2009;106: 1632–1637. doi:10.1073/pnas.0812078106
417. Matsuda S, Miura E, Matsuda K, Kakegawa W, Kohda K, Watanabe M, et al. Accumulation of AMPA Receptors in Autophagosomes in Neuronal Axons Lacking Adaptor Protein AP-4. *Neuron*. 2008;57: 730–745. doi:10.1016/j.neuron.2008.02.012
418. Matsuda S, Yuzaki M. AP-4: autophagy-four mislocalized proteins in axons. *Autophagy*. 2008;4: 815–816.
419. Lorenzen A, Samosh J, Vandewark K, Anborgh PH, Seah C, Magalhaes AC, et al. Rapid and Direct Transport of Cell Surface APP to the Lysosome defines a novel selective pathway. *Mol Brain*. 2010;3: 11. doi:10.1186/1756-6606-3-11
420. Tang W, Tam JH, Seah C, Chiu J, Tyrer A, Cregan SP, et al. Arf6 controls beta-amyloid production by regulating macropinocytosis of the Amyloid Precursor Protein to lysosomes. *Mol Brain*. 2015;8: 41. doi:10.1186/s13041-015-0129-7
421. Kerr MC, Lindsay MR, Luetterforst R, Hamilton N, Simpson F, Parton RG, et al. Visualisation of macropinosome maturation by the recruitment of sorting nexins. *Journal of Cell Science*. 2006;119: 3967–3980. doi:10.1242/jcs.03167
422. Racoosin EL, Swanson JA. Macropinosome maturation and fusion with tubular lysosomes in macrophages. *Journal of Cell Biology*. 1993;121: 1011–1020.
423. Donaldson JG. Multiple Roles for Arf6: Sorting, Structuring, and Signaling at the Plasma Membrane. *Journal of Biological Chemistry*. 2003;278: 41573–41576. doi:10.1074/jbc.R300026200
424. Sannerud R, Declerck I, Peric A, Raemaekers T, Menendez G, Zhou L, et al. ADP



- ribosylation factor 6 (ARF6) controls amyloid precursor protein (APP) processing by mediating the endosomal sorting of BACE1. *Proceedings of the National Academy of Sciences*. 2011;108: E559–68. doi:10.1073/pnas.1100745108
425. Zhang Y, Ivanova E, Bi A, Pan ZH. Ectopic Expression of Multiple Microbial Rhodopsins Restores ON and OFF Light Responses in Retinas with Photoreceptor Degeneration. *J Neurosci*. 2009;29: 9186–9196. doi:10.1523/JNEUROSCI.0184-09.2009
426. Nixon RA, Cataldo AM. Lysosomal system pathways: genes to neurodegeneration in Alzheimer's disease. *J Alzheimers Dis*. 2006;9: 277–289.
427. Nixon RA, Yang D-S. Autophagy failure in Alzheimer's disease--locating the primary defect. *Neurobiology of Disease*. 2011;43: 38–45. doi:10.1016/j.nbd.2011.01.021
428. Cataldo AM, Nixon RA. Enzymatically active lysosomal proteases are associated with amyloid deposits in Alzheimer brain. *Proc Natl Acad Sci USA*. 1990;87: 3861–3865.
429. Cataldo AM, Thayer CY, Bird ED, Wheelock TR, Nixon RA. Lysosomal proteinase antigens are prominently localized within senile plaques of Alzheimer's disease: evidence for a neuronal origin. *Brain Research*. 1990;513: 181–192. doi:10.1016/0006-8993(90)90456-L
430. Cataldo AM, Barnett JL, Mann DM, Nixon RA. Colocalization of lysosomal hydrolase and beta-amyloid in diffuse plaques of the cerebellum and striatum in Alzheimer's disease and Down's syndrome. *J Neuropathol Exp Neurol*. 1996;55: 704–715.
431. Cataldo AM, Barnett JL, Peterhoff CM, Troncoso JC, Pieroni C, Nixon RA, et al. Endocytic pathway abnormalities precede amyloid beta deposition in sporadic Alzheimer's disease and Down syndrome: differential effects of APOE genotype and presenilin mutations. *Am J Pathol*. 2000;157: 277–286.
432. Chen X, Wagener JF, Morgan DH, Hui L, Ghribi O, Geiger JD. Endolysosome mechanisms associated with Alzheimer's disease-like pathology in rabbits ingesting cholesterol-enriched diet. *J Alzheimers Dis*. 2010;22: 1289–1303. doi:10.3233/JAD-2010-101323
433. Yang D-S, Stavrides P, Mohan PS, Kaushik S, Kumar A, Ohno M, et al. Reversal of autophagy dysfunction in the TgCRND8 mouse model of Alzheimer's disease ameliorates amyloid pathologies and memory deficits. *Brain*. 2011;134: 258–277. doi:10.1093/brain/awq341

434. Cataldo AM, Barnett JL, Pieroni C, Nixon RA. Increased neuronal endocytosis and protease delivery to early endosomes in sporadic Alzheimer's disease: neuropathologic evidence for a mechanism of increased beta-amyloidogenesis. *J Neurosci.* 1997;17: 6142–6151.
435. Cataldo AM, Mathews PM, Boiteau AB, Hassinger LC, Peterhoff CM, Jiang Y, et al. Down syndrome fibroblast model of Alzheimer-related endosome pathology: accelerated endocytosis promotes late endocytic defects. *Am J Pathol.* 2008;173: 370–384. doi:10.2353/ajpath.2008.071053
436. Mathews PM, Guerra CB, Jiang Y, Grbovic OM, Kao BH, Schmidt SD, et al. Alzheimer's disease-related overexpression of the cation-dependent mannose 6-phosphate receptor increases Abeta secretion: role for altered lysosomal hydrolase distribution in beta-amyloidogenesis. *Journal of Biological Chemistry.* 2002;277: 5299–5307. doi:10.1074/jbc.M108161200
437. Cataldo AM, Hamilton DJ, Nixon RA. Lysosomal abnormalities in degenerating neurons link neuronal compromise to senile plaque development in Alzheimer disease. *Brain Research.* 1994;640: 68–80. doi:10.1016/0006-8993(94)91858-9
438. Cataldo AM, Barnett JL, Berman SA, Li J, Quarless S, Bursztajn S, et al. Gene expression and cellular content of cathepsin D in Alzheimer's disease brain: evidence for early up-regulation of the endosomal-lysosomal system. *Neuron.* 1995;14: 671–680.
439. Cataldo AM, Petanceska S, Terio NB, Peterhoff CM, Durham R, Mercken M, et al. Abeta localization in abnormal endosomes: association with earliest Abeta elevations in AD and Down syndrome. *NBA.* 2004;25: 1263–1272. doi:10.1016/j.neurobiolaging.2004.02.027
440. Braak H, Braak E. Staging of Alzheimer's disease-related neurofibrillary changes. *NBA.* 1995;16: 271–8– discussion 278–84. doi:10.1016/0197-4580(95)00021-6
441. Cataldo AM, Peterhoff CM, Schmidt SD, Terio NB, Duff K, Beard M, et al. Presenilin mutations in familial Alzheimer disease and transgenic mouse models accelerate neuronal lysosomal pathology. *J Neuropathol Exp Neurol.* 2004;63: 821–830.
442. Yang DS, Stavrides P, Mohan PS, Kaushik S, Kumar A, Ohno M, et al. Reversal of autophagy dysfunction in the TgCRND8 mouse model of Alzheimer's disease ameliorates amyloid pathologies and memory deficits. *Brain.* 2010;134: 258–277. doi:10.1093/brain/awq341
443. Butler D, Hwang J, Estick C, Nishiyama A, Kumar SS, Baveghems C, et al. Protective Effects of Positive Lysosomal Modulation in Alzheimer's Disease

- Transgenic Mouse Models. Ikezu T, editor. PLoS ONE. 2011;6: e20501.  
doi:10.1371/journal.pone.0020501.t003
444. Yu WH, Cuervo AM, Kumar A, Peterhoff CM, Schmidt SD, Lee J-H, et al. Macroautophagy--a novel Beta-amyloid peptide-generating pathway activated in Alzheimer's disease. *Journal of Cell Biology*. 2005;171: 87–98. doi:10.1083/jcb.200505082
445. Nixon RA, Wegiel J, Kumar A, Kumar A, Yu WH, Peterhoff C, et al. Extensive involvement of autophagy in Alzheimer disease: an immuno-electron microscopy study. *J Neuropathol Exp Neurol*. 2005;64: 113–122.
446. DeWitt DA, Silver J. Regenerative failure: a potential mechanism for neuritic dystrophy in Alzheimer's disease. *Experimental Neurology*. 1996;142: 103–110. doi:10.1006/exnr.1996.0182
447. Grace EA, Rabiner CA, Busciglio J. Characterization of neuronal dystrophy induced by fibrillar amyloid beta: implications for Alzheimer's disease. *NSC*. 2002;114: 265–273. doi:10.1016/S0306-4522(02)00241-5
448. Hu X, Crick SL, Bu G, Frieden C, Pappu RV, Lee J-M. Amyloid seeds formed by cellular uptake, concentration, and aggregation of the amyloid-beta peptide. *Proceedings of the National Academy of Sciences*. 2009;106: 20324–20329. doi:10.1073/pnas.0911281106
449. Su Y, Chang PT. Acidic pH promotes the formation of toxic fibrils from beta-amyloid peptide. *Brain Research*. 2001;893: 287–291.
450. Liu R-Q, Zhou Q-H, Ji S-R, Zhou Q, Feng D, Wu Y, et al. Membrane localization of beta-amyloid 1-42 in lysosomes: a possible mechanism for lysosome labilization. *J Biol Chem*. 2010;285: 19986–19996. doi:10.1074/jbc.M109.036798
451. Yanagisawa K. Pathological significance of ganglioside clusters in Alzheimer's disease. *Journal of Neurochemistry*. 2011;116: 806–812. doi:10.1111/j.1471-4159.2010.07006.x
452. Yamamoto N, Hirabayashi Y, Amari M, Yamaguchi H, Romanov G, Van Nostrand WE, et al. Assembly of hereditary amyloid beta-protein variants in the presence of favorable gangliosides. *FEBS Letters*. 2005;579: 2185–2190. doi:10.1016/j.febslet.2005.03.013
453. Yamamoto N, Yokoseki T, Shibata M, Yamaguchi H, Yanagisawa K. Suppression of Abeta deposition in brain by peripheral administration of Fab fragments of anti-seed antibody. *Biochemical and Biophysical Research Communications*. 2005;335: 45–47. doi:10.1016/j.bbrc.2005.06.208

454. Keilani S, Lun Y, Stevens AC, Williams HN, Sjoberg ER, Khanna R, et al. Lysosomal dysfunction in a mouse model of Sandhoff disease leads to accumulation of ganglioside-bound amyloid- $\beta$  peptide. *Journal of Neuroscience*. 2012;32: 5223–5236. doi:10.1523/JNEUROSCI.4860-11.2012
455. Yuyama K, Yamamoto N, Yanagisawa K. Chloroquine-induced endocytic pathway abnormalities: Cellular model of GM1 ganglioside-induced A $\beta$  fibrillogenesis in Alzheimer's disease. *FEBS Letters*. 2006;580: 6972–6976. doi:10.1016/j.febslet.2006.11.072
456. Hui L, Chen X, Geiger JD. Endolysosome involvement in LDL cholesterol-induced Alzheimer's disease-like pathology in primary cultured neurons. *Life Sci*. 2012;91: 1159–1168. doi:10.1016/j.lfs.2012.04.039
457. Nixon RA. Niemann-Pick Type C disease and Alzheimer's disease: the APP-endosome connection fattens up. *Am J Pathol*. 2004;164: 757–761. doi:10.1016/S0002-9440(10)63163-X
458. Bodovitz S, Klein WL. Cholesterol modulates alpha-secretase cleavage of amyloid precursor protein. *Journal of Biological Chemistry*. 1996;271: 4436–4440.
459. Malnar M, Hecimovic S, Mattsson N, Zetterberg H. Bidirectional links between Alzheimer's disease and Niemann-Pick type C disease. *Neurobiology of Disease*. 2014;72 Pt A: 37–47. doi:10.1016/j.nbd.2014.05.033
460. Malnar M, Kosicek M, Mitterreiter S, Omerbasic D, Lichtenthaler SF, Goate A, et al. Niemann-Pick type C cells show cholesterol dependent decrease of APP expression at the cell surface and its increased processing through the beta-secretase pathway. *Biochim Biophys Acta*. 2010;1802: 682–691. doi:10.1016/j.bbadis.2010.05.006
461. Malnar M, Kosicek M, Lisica A, Posavec M, Krolo A, Njavro J, et al. Cholesterol-depletion corrects APP and BACE1 mistrafficking in NPC1-deficient cells. *Biochim Biophys Acta*. 2012;1822: 1270–1283. doi:10.1016/j.bbadis.2012.04.002
462. Mattsson N, Zetterberg H, Bianconi S, Yanjanin NM, Fu R, Månsson J-E, et al. Gamma-secretase-dependent amyloid-beta is increased in Niemann-Pick type C: a cross-sectional study. *Neurology*. Lippincott Williams & Wilkins; 2011;76: 366–372. doi:10.1212/WNL.0b013e318208f4ab
463. Tam JH, Pasternak SH. Amyloid and Alzheimer's disease: inside and out. *Can J Neurol Sci*. 2012;39: 286–298.
464. Knauer MF, Soreghan B, Burdick D, Kosmoski J, Glabe CG. Intracellular accumulation and resistance to degradation of the Alzheimer amyloid A $\beta$ /beta

- protein. *Proc Natl Acad Sci USA*. 1992;89: 7437–7441.
465. Wertkin AM, Turner RS, Pleasure SJ, Golde TE, Younkin SG, Trojanowski JQ, et al. Human neurons derived from a teratocarcinoma cell line express solely the 695-amino acid amyloid precursor protein and produce intracellular beta-amyloid or A4 peptides. *Proc Natl Acad Sci USA. National Academy of Sciences*; 1993;90: 9513–9517.
466. Martin BL, Schrader-Fischer G, Busciglio J, Duke M, Paganetti P, Yankner BA. Intracellular accumulation of beta-amyloid in cells expressing the Swedish mutant amyloid precursor protein. *Journal of Biological Chemistry*. 1995;270: 26727–26730.
467. Takahashi RH, Milner TA, Li F, Nam EE, Edgar MA, Yamaguchi H, et al. Intra-neuronal Alzheimer abeta42 accumulates in multivesicular bodies and is associated with synaptic pathology. *Am J Pathol*. 2002;161: 1869–1879.
468. Takahashi RH, Takahashi RH, Almeida CG, Kearney PF, Yu F, et al. Oligomerization of Alzheimer's beta-amyloid within processes and synapses of cultured neurons and brain. *Journal of Neuroscience*. 2004;24: 3592–3599. doi:10.1523/JNEUROSCI.5167-03.2004
469. Cataldo AM, Hamilton DJ, Barnett JL, Paskevich PA, Nixon RA. Properties of the endosomal-lysosomal system in the human central nervous system: disturbances mark most neurons in populations at risk to degenerate in Alzheimer's disease. *J Neurosci*. 1996;16: 186–199.
470. Tu H, Nelson O, Bezprozvanny A, Wang Z, Lee S-F, Hao Y-H, et al. Presenilins Form ER Ca<sup>2+</sup> Leak Channels, a Function Disrupted by Familial Alzheimer's Disease-Linked Mutations. *Cell*. 2006;126: 981–993. doi:10.1016/j.cell.2006.06.059
471. Lee J-H, Yu WH, Kumar A, Lee S, Mohan PS, Peterhoff CM, et al. Lysosomal proteolysis and autophagy require presenilin 1 and are disrupted by Alzheimer-related PS1 mutations. *Cell*. 2010;141: 1146–1158. doi:10.1016/j.cell.2010.05.008
472. Esselens C, Oorschot V, Baert V, Raemaekers T, Spittaels K, Serneels L, et al. Presenilin 1 mediates the turnover of telencephalin in hippocampal neurons via an autophagic degradative pathway. *Journal of Cell Biology*. 2004;166: 1041–1054. doi:10.1083/jcb.200406060
473. Neely KM, Green KN, LaFerla FM. Presenilin is necessary for efficient proteolysis through the autophagy-lysosome system in a  $\gamma$ -secretase-independent manner. *Journal of Neuroscience. Society for Neuroscience*; 2011;31: 2781–2791. doi:10.1523/JNEUROSCI.5156-10.2010

474. Zhang X, Garbett K, Veeraraghavalu K, Wilburn B, Gilmore R, Mirnics K, et al. A role for presenilins in autophagy revisited: normal acidification of lysosomes in cells lacking PSEN1 and PSEN2. *Journal of Neuroscience*. Society for Neuroscience; 2012;32: 8633–8648. doi:10.1523/JNEUROSCI.0556-12.2012
475. Coen K, Flannagan RS, Baron S, Carraro-Lacroix LR, Wang D, Vermeire W, et al. Lysosomal calcium homeostasis defects, not proton pump defects, cause endo-lysosomal dysfunction in PSEN-deficient cells. *The Journal of Cell Biology*. Rockefeller Univ Press; 2012;198: 23–35. doi:10.1083/jcb.201201076
476. Coffey EE, Beckel JM, Laties AM, Mitchell CH. Lysosomal alkalization and dysfunction in human fibroblasts with the Alzheimer's disease-linked presenilin 1 A246E mutation can be reversed with cAMP. *Neuroscience*. 2014;263: 111–124. doi:10.1016/j.neuroscience.2014.01.001
477. Stoka V, Turk B, Schendel SL, Kim TH, Cirman T, Snipas SJ, et al. Lysosomal protease pathways to apoptosis. Cleavage of bid, not pro-caspases, is the most likely route. *Journal of Biological Chemistry*. American Society for Biochemistry and Molecular Biology; 2001;276: 3149–3157. doi:10.1074/jbc.M008944200
478. Roberg K, Johansson U, Ollinger K. Lysosomal release of cathepsin D precedes relocation of cytochrome c and loss of mitochondrial transmembrane potential during apoptosis induced by oxidative stress. *Free Radical Biology and Medicine*. 1999;27: 1228–1237.
479. Johansson A-C, Steen H, Ollinger K, Roberg K. Cathepsin D mediates cytochrome c release and caspase activation in human fibroblast apoptosis induced by staurosporine. *Cell Death and Differentiation*. Nature Publishing Group; 2003;10: 1253–1259. doi:10.1038/sj.cdd.4401290
480. D'Andrea MR, Nagele RG, Wang HY, Peterson PA, Lee DH. Evidence that neurones accumulating amyloid can undergo lysis to form amyloid plaques in Alzheimer's disease. *Histopathology*. 2001;38: 120–134.
481. Rajendran L, Hoshino M, Zahn TR, Keller P, Geiger KD, Verkade P, et al. Alzheimer's disease beta-amyloid peptides are released in association with exosomes. *Proc Natl Acad Sci USA*. 2006;103: 11172–11177. doi:10.1073/pnas.0603838103
482. Danzer KM, Kranich LR, Ruf WP, Cagsal-Getkin O, Winslow AR, Zhu L, et al. Exosomal cell-to-cell transmission of alpha synuclein oligomers. *Molecular Neurodegeneration*. 2012;7: 42. doi:10.1186/1750-1326-7-42
483. Alvarez-Erviti L, Seow Y, Schapira AH, Gardiner C, Sargent IL, Wood MJA, et al. Lysosomal dysfunction increases exosome-mediated alpha-synuclein release and

- transmission. *Neurobiology of Disease*. 2011;42: 360–367. doi:10.1016/j.nbd.2011.01.029
484. Blott EJ, Griffiths GM. Secretory lysosomes. *Nature reviews Molecular cell biology*. 2002;3: 122–131. doi:10.1038/nrm732
485. Jaiswal JK, Andrews NW, Simon SM. Membrane proximal lysosomes are the major vesicles responsible for calcium-dependent exocytosis in nonsecretory cells. *Journal of Cell Biology*. 2002;159: 625–635. doi:10.1083/jcb.200208154
486. Defour A, Sreetama SC, Jaiswal JK. Imaging cell membrane injury and subcellular processes involved in repair. *J Vis Exp*. 2014. doi:10.3791/51106
487. Arantes RME. A Role for Synaptotagmin VII-Regulated Exocytosis of Lysosomes in Neurite Outgrowth from Primary Sympathetic Neurons. *Journal of Neuroscience*. 2006;26: 4630–4637. doi:10.1523/JNEUROSCI.0009-06.2006
488. Stinchcombe JC, Griffiths GM. Regulated secretion from hemopoietic cells. *Journal of Cell Biology*. 1999;147: 1–6.
489. Andrews NW. Regulated secretion of conventional lysosomes. *Trends in Cell Biology*. 2000;10: 316–321.
490. Dell'Angelica EC, Mullins C, Caplan S, Bonifacino JS. Lysosome-related organelles. *FASEB J*. 2000;14: 1265–1278.
491. Burgoyne RD, Morgan A. Secretory granule exocytosis. *Physiological Reviews*. 2003;83: 581–632. doi:10.1152/physrev.00031.2002
492. Griscelli C, Prunieras M. Pigment dilution and immunodeficiency: a new syndrome. *Int J Dermatol*. 1978;17: 788–791.
493. Aslan D, Sari S, Derinöz O, Dalgıç B. Griscelli syndrome: description of a case with Rab27A mutation. *Pediatr Hematol Oncol*. Informa UK Ltd UK; 2006;23: 255–261. doi:10.1080/08880010500506909
494. Bizario JCS, Feldmann J, Castro FA, Ménasché G, Jacob CMA, Cristofani L, et al. Griscelli syndrome: characterization of a new mutation and rescue of T-cytotoxic activity by retroviral transfer of RAB27A gene. *J Clin Immunol*. 2004;24: 397–410. doi:10.1023/B:JOCI.0000029119.83799.cb
495. Gomi H, Mori K, Itohara S, Izumi T. Rab27b is expressed in a wide range of exocytic cells and involved in the delivery of secretory granules near the plasma membrane. *Mol Biol Cell*. 2007;18: 4377–4386. doi:10.1091/mbc.E07-05-0409
496. Zhao S, Torii S, Yokota-Hashimoto H, Takeuchi T, Izumi T. Involvement of

- Rab27b in the regulated secretion of pituitary hormones. *Endocrinology*. 2002;143: 1817–1824.
497. Bahadoran P, Aberdam E, Mantoux F, Buscà R, Bille K, Yalman N, et al. Rab27a: A key to melanosome transport in human melanocytes. *Journal of Cell Biology*. 2001;152: 843–850.
498. Hume AN, Collinson LM, Rapak A, Gomes AQ, Hopkins CR, Seabra MC. Rab27a regulates the peripheral distribution of melanosomes in melanocytes. *Journal of Cell Biology*. 2001;152: 795–808. doi:10.1083/jcb.152.4.795
499. Stinchcombe JC, Barral DC, Mules EH, Mules EH, Booth S, Hume AN, et al. Rab27a is required for regulated secretion in cytotoxic T lymphocytes. *Journal of Cell Biology*. 2001;152: 825–834. doi:10.1038/nature11801
500. Ostrowski M, Carmo NB, Krumeich S, Fanget I, Raposo G, Savina A, et al. Rab27a and Rab27b control different steps of the exosome secretion pathway : *Nature Cell Biology*. *Nature Cell Biology*. 2010;12: 19–30– sup pp 1–13. doi:10.1038/ncb2000
501. Izumi T. Physiological roles of Rab27 effectors in regulated exocytosis. *Endocr J*. 2007;54: 649–657.
502. Marks MS, Heijnen HFG, Raposo G. Lysosome-related organelles: unusual compartments become mainstream. *Current Opinion in Cell Biology*. 2013;25: 495–505. doi:10.1016/j.ceb.2013.04.008
503. Sanal O, Ersoy F, Tezcan I, Metin A, Yel L, Ménasché G, et al. Griscelli disease: genotype-phenotype correlation in an array of clinical heterogeneity. *J Clin Immunol*. 2002;22: 237–243.
504. Strom M, Hume AN, Tarafder AK, Barkagianni E, Seabra MC. A family of Rab27-binding proteins. Melanophilin links Rab27a and myosin Va function in melanosome transport. *Journal of Biological Chemistry*. 2002;277: 25423–25430. doi:10.1074/jbc.M202574200
505. Ménasché G, Ho CH, Sanal O, Feldmann J, Tezcan I, Ersoy F, et al. Griscelli syndrome restricted to hypopigmentation results from a melanophilin defect (GS3) or a MYO5A F-exon deletion (GS1). *Journal of Clinical Investigation*. 2003;112: 450–456. doi:10.1172/JCI18264
506. Wu XS, Wu XS, Tsan GL, Hammer JA. Melanophilin and myosin Va track the microtubule plus end on EB1. *Journal of Cell Biology*. 2005;171: 201–207. doi:10.1083/jcb.200503028
507. Wu X, Kocher B, Wei Q, Hammer JA. Myosin Va associates with microtubule-rich domains in both interphase and dividing cells. *Cell Motil Cytoskeleton*. 1998;40:



- 286–303. doi:10.1002/(SICI)1097-0169(1998)40:3<286::AID-CM7>3.0.CO;2-B
508. Wu X, Bowers B, Wei Q, Kocher B, Hammer JA. Myosin V associates with melanosomes in mouse melanocytes: evidence that myosin V is an organelle motor. *Journal of Cell Science*. 1997;110 ( Pt 7): 847–859.
509. Provance DW, Wei M, Ipe V, Mercer JA. Cultured melanocytes from dilute mutant mice exhibit dendritic morphology and altered melanosome distribution. *Proc Natl Acad Sci USA*. 1996;93: 14554–14558.
510. Johnson JL, Monfregola J, Napolitano G, Kiosses WB, Catz SD. Vesicular trafficking through cortical actin during exocytosis is regulated by the Rab27a effector JFC1/Slp1 and the RhoA-GTPase-activating protein Gem-interacting protein. *Mol Biol Cell*. 2012;23: 1902–1916. doi:10.1091/mbc.E11-12-1001
511. Malacombe M, Bader M-F, Gasman S. Exocytosis in neuroendocrine cells: new tasks for actin. *Biochim Biophys Acta*. 2006;1763: 1175–1183. doi:10.1016/j.bbamcr.2006.09.004
512. Aunis D, Bader MF. The cytoskeleton as a barrier to exocytosis in secretory cells. *J Exp Biol*. 1988;139: 253–266.
513. Südhof TC, Rizo J. Synaptic vesicle exocytosis. *Cold Spring Harbor Perspectives in Biology*. 2011;3. doi:10.1101/cshperspect.a005637
514. Ye S, Karim ZA, Hawas Al R, Pessin JE, Filipovich AH, Whiteheart SW. Syntaxin-11, but not syntaxin-2 or syntaxin-4, is required for platelet secretion. *Blood*. 2012;120: 2484–2492. doi:10.1182/blood-2012-05-430603
515. Stadt zur U, Schmidt S, Kasper B, Beutel K, Diler AS, Henter J-I, et al. Linkage of familial hemophagocytic lymphohistiocytosis (FHL) type-4 to chromosome 6q24 and identification of mutations in syntaxin 11. *Human Molecular Genetics*. 2005;14: 827–834. doi:10.1093/hmg/ddi076
516. Bryceson YT, Rudd E, Zheng C, Edner J, Ma D, Wood SM, et al. Defective cytotoxic lymphocyte degranulation in syntaxin-11 deficient familial hemophagocytic lymphohistiocytosis 4 (FHL4) patients. *Blood*. 2007;110: 1906–1915. doi:10.1182/blood-2007-02-074468
517. Elstak ED, Neeft M, Nehme NT, Voortman J, Cheung M, Goodarzifard M, et al. The munc13-4-rab27 complex is specifically required for tethering secretory lysosomes at the plasma membrane. *Blood*. 2011;118: 1570–1578. doi:10.1182/blood-2011-02-339523
518. Côte M, Ménager MM, Burgess A, Mahlaoui N, Picard C, Schaffner C, et al. Munc18-2 deficiency causes familial hemophagocytic lymphohistiocytosis type 5

and impairs cytotoxic granule exocytosis in patient NK cells. *J Clin Invest.* 2009;119: 3765–3773. doi:10.1172/JCI40732

519. Stadt zur U, Rohr J, Seifert W, Koch F, Grieve S, Pagel J, et al. Familial hemophagocytic lymphohistiocytosis type 5 (FHL-5) is caused by mutations in Munc18-2 and impaired binding to syntaxin 11. *Am J Hum Genet.* 2009;85: 482–492. doi:10.1016/j.ajhg.2009.09.005

## Chapter 2

### 2 The Amyloid Precursor Protein is rapidly transported from the Golgi apparatus to the lysosome and where it is processed into beta-amyloid.

Alzheimer's disease (AD) is characterized by cerebral deposition of  $\beta$ -amyloid peptide ( $A\beta$ ).  $A\beta$  is produced by sequential cleavage of the Amyloid Precursor Protein (APP) by  $\beta$ - and  $\gamma$ -secretases. Many studies have demonstrated that the internalization of APP from the cell surface can regulate  $A\beta$  production although the exact organelle in which  $A\beta$  is produced remains contentious. A number of recent studies suggest that intracellular trafficking also plays a role in regulating  $A\beta$  production, but these pathways are relatively under studied.

Using APP tagged with photoactivatable Green Fluorescent Protein (paGFP), we show that APP is rapidly trafficked from the Golgi apparatus to the lysosome where it is rapidly cleared. Chloroquine and the highly selective  $\gamma$ -secretase inhibitor L685, 458 cause the accumulation of APP in lysosomes implying that APP is being cleaved by secretases in the lysosome. The Swedish mutation dramatically increases the rate of lysosomal APP processing, which is also inhibited by chloroquine and L685, 458. Lysosomal transport of APP is reduced by siRNA knockdown of AP-3 and reduces secreted  $A\beta$  by more than a third.

These data suggests that AP-3 mediates rapid delivery of APP to lysosomes, and that the lysosome is a likely site of  $A\beta$  production.

#### 2.1 Introduction

Alzheimer's disease is the leading cause of dementia in adults [1]. A neuropathological hallmark of AD is the accumulation of  $\beta$ -amyloid ( $A\beta$ ) in plaques in the brain [2].  $A\beta$  is produced through sequential cleavage of amyloid precursor protein (APP) by secretases. Cleavage by  $\beta$ -secretase removes the N-terminal ectodomain, leaving a 99 residue C-terminal fragment (CTF) containing  $A\beta$  [3-5]. The CTF is then processed by  $\gamma$ -secretase [6] to produce  $A\beta$  species ranging from 39 to 43 residues in length [7]. The 42-amino acid form of  $A\beta$  ( $A\beta_{42}$ ) has a higher propensity to aggregate, is toxic to cells in culture, and is the dominant component of amyloid plaques [8-11].

Many experiments suggest that the production of A $\beta$  occurs in the endosomal/lysosomal system. Work in our laboratory has demonstrated that lysosomes are highly enriched in APP and  $\gamma$ -secretase proteins (composed of at least presenilin, APH1, PEN-2 and nicastrin) and  $\gamma$ -secretase activity (the ability to cleave APP to produce A $\beta$ ) [12,13]. Others have also described APP and  $\gamma$ -secretase activity in lysosome-related autophagosomes and phagosomes [14,15]. In agreement with these findings, deacidification of the endosomal/lysosomal system decreases A $\beta$  production [16,17]. When proteolysis is blocked with protease inhibitors or by presenilin knock-out (which abolishes  $\gamma$ -secretase activity), amyloidogenic fragments of APP accumulate in lysosomes [18-20].

While many studies have shown that endocytosis of APP is crucial for A $\beta$  production [21-23], a number of studies have suggested that the intracellular trafficking of APP might also play an important role in A $\beta$  generation. For example, A $\beta$  production is decreased in MDCK cells when APP is sorted to the basolateral membrane [24]. More recent studies demonstrate that A $\beta$  production is decreased by retrograde sorting of APP from endosomes to the trans-Golgi network (TGN) [25-27]. Because the TGN serves as sorting station for nascent cargo from the ER and protein recycled from endosomes [28], an understanding the trafficking of APP into and out of the Golgi will increase our understanding of A $\beta$  production.

While cell-surface proteins are amenable to many labeling techniques, intracellular proteins are more difficult to track. Photoactivatable-Green Fluorescent Protein (paGFP) has provided a new tool to examine intracellular trafficking. paGFP is a form of GFP that has low basal fluorescence, but develops strong, stable green fluorescence after being activated by 413 nm laser light [29,30]. Constructs using paGFP [30,31] have been used to examine the turnover of peroxisomes [32] and autophagosomes [33] and to examine actin dynamics in neuronal dendritic spines [34].

Fluorescent protein tags have previously been used to examine movement of APP containing vesicles [35,36], including tubular-vesicular structures emanating from the Golgi apparatus [37].

APP-paGFP constructs have been used to visualize APP undergoing fast axonal transport [38] and to image the trafficking of APP out of the perinuclear region, although these authors did not identify the compartments involved [39,40].

Our aim was to examine the trafficking of APP from the Golgi apparatus and to identify downstream compartments and identify sites of cleavage. We used targeted activation of APP-paGFP in the Golgi apparatus (identified using Galactosyltransferase fused to Cyan Fluorescent Protein (GalT-CFP) [41], and followed activated APP-paGFP using confocal microscopy fluorescence imaging to intracellular compartments labeled with compartment marker proteins fused to red fluorescent proteins including Rab5 (early endosomes) [42-44], Rab9 (late endosomes) [45,46] and LAMP1 (lysosomes) [47,48]. Tracking the disappearance of green fluorescent APP-paGFP from these downstream compartments allows us to examine the intracellular site of cleavage and degradation; essentially performing pulse chase experiments in single cells. Surprisingly, we show that a large fraction of APP traffics rapidly to LAMP1-labeled lysosomes within seconds after photoactivation in the Golgi, and is subsequently cleaved by a  $\gamma$ -secretase-like activity. This pathway is mediated by an interaction between APP and Adaptor Protein 3 (AP-3). Knocking down AP-3 blocks lysosomal transport and reduces A $\beta$  secretion into the media by about 33%. This suggests that direct lysosomal transport of APP is an important source of A $\beta$ .

## 2.2 Materials and Methods

### 2.2.1 Antibodies

The antibodies used were: Rabbit anti-APP C-terminal (1:1000, Cat. No. A8717; Sigma), mouse anti-HA (1:1000, Cat. No. 12CA5; Roche); mouse anti- $\gamma$ -adaplin (Cat No. 610386; BD Bioscience). The AP-3  $\delta$ 3 subunit- mouse- SA4 (1:1000), developed by Peden et al. [117] was obtained from the Developmental Studies Hybridoma Bank, created by the NICHD of the NIH and maintained at The University of Iowa, Department of Biology, Iowa City, IA 52242.

Secondary antibodies used were donkey anti-mouse HRP (1: 10 000, Cat No. 711-0350150, Jackson Immunoresearch) and goat-anti rabbit HRP (1: 10 000; Biorad).  $\alpha$ -tubulin was stained using a mouse monoclonal antibody (Cat No. T5168, Sigma). For immunostaining, donkey anti-rabbit Alexa Fluor 488 (A-11034; Invitrogen) and goat anti-mouse Alex Fluor 546 (A-11003; Invitrogen).

### 2.2.2 Cell Culture and Transfection

SN56 cells (a gift from Dr. Jane Rylett) were cultured in Dulbecco's Modified Eagle medium (DMEM) (Gibco) supplemented with 10% v/v of fetal bovine serum (FBS; Gibco) and 50  $\mu$ g/ml of penicillin/streptomycin (P/S), in 5% CO<sub>2</sub> at 37°C. Cells were subcultured every 3 days. For confocal studies,  $5 \times 10^5$  cells were seeded on to glass-bottomed culture dishes (MatTek) the day before transfection in DMEM supplemented with 10% FBS. Cells were transiently transfected using Lipofectamine (Invitrogen) according to manufacturer's instructions. To differentiate the cells, the media was replaced 24 hours after transfection with DMEM supplemented with 50  $\mu$ g/ml P/S and 1 mM dibutyryl cyclic AMP (dbcAMP; Sigma). Cells were differentiated for 24 hours and imaged or harvested. Primary cortical neurons were prepared from embryonic day 15 CD1 mouse embryos as described previously [118].

For silencing RNA (siRNA) mediated knockdown of the  $\delta$  subunit of AP-3, the Stealth Select 3 RNAi™ set (Invitrogen) was used. Sequence 3 of this set was found to knockdown the  $\delta$ 3 subunit (5'GAGAAGCUGCCUGUCCAGAAACAUA3'). The ubiquitously expressed  $\gamma$ 1

subunit of AP-1 was knocked down using 5'UAAUUAUCAUUCAUAGCU3' with a 3' TT overhang. Stealth RNAi™ siRNA Negative Control Med GC (12935-300; Invitrogen) was used as a control. The control RNAi was tagged on the 5' end with Alexa 647 to determine which cells were transfected with siRNA. For each 35 mm dish, 200nM of siRNA was transfected using Lipofectamine 2000 according to manufacturer's instructions. During the knockdown experiments, 1nM of negative control siRNA was co transfected with the siRNA against  $\delta 3$  or  $\gamma 1$  to confirm the transfection of siRNA into the cell.

### 2.2.3 DNA Constructs

A cDNA encoding APP 750 fused to yellow fluorescent protein (YFP) was a kind gift from Dr. Bradley Hyman (Massachusetts General Hospital). Constructs expressing full length or shortened (last 112 amino acids) APP ( $\beta$ APP) with an amino terminal hemagglutinin (HA) tag and enhanced cyan FP (eCFP) on the carboxy terminus were generated as previously described [50]. The plasmids encoding photoactivatable GFP (paGFP) was a kind gift of Dr. Jennifer Lippincott-Schwartz [30].  $\beta$ APP was recloned such that paGFP is placed on the C-terminal cytoplasmic tail of the protein. The Swedish mutation (KM670/671NL) was introduced into the  $\beta$ APP-ECFP construct using PCR [50], and was recloned into the paGFP vector.

Rab5-mRFP, Rab9-mCherry, and LAMP1-mRFP were generated as previously described [50]. The VSVG-paGFP construct was purchased from Addgene (<http://www.addgene.org>).

### 2.2.4 Confocal Microscopy

A Zeiss LSM-510 META laser- scanning microscope using a Zeiss 63 $\times$  1.4 numerical aperture oil immersion lens was used to obtain images (Carl Zeiss, Oberkochen, Germany). The optical section thickness was typically 1  $\mu$ m. To visualize Alexa Fluor 488 and paGFP fluorescence, the samples were excited with a 488 nm laser and filtered using a band pass (BP) 500-530-nm emission filter set. For Alexa Fluor 546, mCherry and mRFP fluorescence, a 543 nm excitation laser and BP 560-615 filter set were used. To collect ECFP fluorescence, a BP 475-525 emission filter set was used after excitation with a 458 nm lasers. Alexa Fluor 647 fluorescence was imaged using 633 nm excitation lasers, and a LP 650 filter.

### 2.2.5 Live Cell Imaging

For live cell imaging, the cells were washed twice with PBS, and the culture media was replaced with 37°C Hank's Balanced Salt Solution (HBSS; Cat. No. 14025-092, Invitrogen). To maintain a constant temperature of 37°C, the 35 mm plate was placed on a heated stage (heated insert P; PeCon GmbH) connected to a Tempcontrol 37-2 digital 2-channel (PeCon GmbH).

Using the Ziess Physiology package, regions of interest (ROI) were selected in the Golgi apparatus, which was demarcated by GalT-CFP fluorescence and these were carefully monitored during the experiment to ensure that they remained over the Golgi apparatus if the cell or the Golgi apparatus apparatus moved. In a typical experiment, cells were imaged approximately every 30 seconds. For the first 15 minutes, ROIs in the Golgi apparatus were irradiated with 405 nm laser light to photoactivate APP-paGFP before imaging. After the initial 15-minute pulse period, images were taken without irradiation and the movement/degradation of paGFP fluorescence was followed for approximately 45 minutes.

To inhibit APP-paGFP cleavage, cells were treated with chloroquine (Cat. No. C6628, Sigma) or L685, 458 (Cat. No. 565771, EMD Millipore). Cells were treated with 100  $\mu$ M chloroquine 30 minutes before imaging to deacidify lysosomes. Deacidification of lysosomes was confirmed using 75nM Lysosensor™ Green (Cat. No. L-7534, Invitrogen). To inhibit cleavage using a specific  $\gamma$ -secretase inhibitor, SN56 cells were treated with 0.5  $\mu$ M L685, 458 for 24 h before imaging.

### 2.2.6 Colocalization Analysis

Colocalization analysis was performed on using Imaris 7.0 Imaris Colocalization module (Biplane). Imaris software was used to create IsoSurfaces corresponding to the paGFP and RFP fluorescence channels following the manufacturer's directions ([www.bitplane.com](http://www.bitplane.com) *webcite*) [119]. This is a computer assisted method to set fluorescence intensity thresholds to detect fluorescence in an organellar distribution that can then be used to automatically follow fluorescence intensity and colocalization over time. The co-localization of APP and LAMP1 over time was plotted using Prism 5.0 software (Graphpad, La Jolla CA) and curves were fit



using the nonlinear regression by least squares to fit a one phase exponential decay.

To colocalize AP-3 $\delta$  and APP we adopted a strategy we have previously employed [50] and described by Hutcheon *et al.* [120] (also discussed in [121,122]), which sets thresholds based on a fixed percentage of the brightest pixels in an image. This allows for the identification of positive pixels that is unbiased (it does not require the judgment of the observer on an image to image basis) and is relatively unaffected by parameters of image acquisition or the level of protein expression. To colocalize AP-3 $\delta$  and APP, the brightest 2% of pixels was selected, and the percentage of pixels colocalized was recorded [50]. Prism Graphpad 5.0b was used for all graphing and statistical analysis. A One-way ANOVA was performed with a Dunn's post-hoc test, and P values under 0.05 were considered significant.

### 2.2.7 Immunostaining

SN56 cells or mouse cortical neurons were fixed for 15 minutes with 4% paraformaldehyde (Alfa Aesar; Cat No. 43368). Cells were permeabilized for 5 minutes with 0.1% TritonX-100 in PBS and blocked with 2% BSA for 1 h. Cells were incubated with primary antibodies overnight at 4°C, washed twice with PBS, and stained with secondary antibody for 1 h. After staining, confocal plates were store at 4°C in PBS, and coverslips were mounted on glass slides with ImmunoMount (Fisher) and stored at 4°C.

### 2.2.8 Proximity Ligation Assay (PLA)

SN56 cells were transiently transfected with  $\beta$ APP-eCFP, and fixed for 15 minutes with 4% paraformaldehyde at room temperature. Cells were permeabilized and blocked in the same manner as immunostaining. PLA was performed using a commercially available kit (Duolink; Olink Bioscience) according to manufacturer's instructions. Briefly, primary antibodies were washed off cells with PBS, and species specific PLA secondary probes were applied to cells. If secondary PLA probes are within 40 nm of each other, their complementary DNA strands are ligated and are amplified. Complementary fluorescent oligonucleotides bind to the amplified sequence, which results in a fluorescent dot where there are two interacting proteins.

### 2.2.9 Cell Lysis and Western Blots

SN56 cells ( $1.5 \times 10^6$  cells) were seeded on 60 mm tissue culture dishes (Becton Dickinson) and transfected with plasmids or siRNA using Lipofectamine 2000 according to manufacturer's instructions. Cells were harvested in lysis buffer (1% Nonidet P-40, 150 mM NaCl, 50 mM Tris-Cl) supplemented with pepstatin and complete protease inhibitor cocktail (Roche). Lysates were clarified by centrifugation at 13,000 g for 20 min. To facilitate equal loading, the amount of total protein was determined by bicinchoninic acid (BCA; Thermo Fisher Scientific). Samples were electrophoresed on SDS-PAGE and transferred to PVDF membranes (Cat No. 162-01777; Biorad). Densitometry was performed in ImageJ (NIH), and was normalized to  $\alpha$ -tubulin band density. Graphs were plotted in Prism 5.0b (Graphpad, La Jolla, CA), a one-way ANOVA was performed with a Tukey's post-hoc test. Results were significant if  $p < 0.05$ .

## 2.3 Results

### 2.3.1 APP-paGFP can be followed as it traffics from the Golgi apparatus to LAMP1-labeled compartments

In order to study the intracellular trafficking of APP from the Golgi apparatus in live cells, we generated expression constructs (Figure 2.1) containing full length APP (FL-APP) fused to an N-terminal HA epitope tag and photoactivatable Green Fluorescent Protein (paGFP) at its C-terminal cytoplasmic tail. To avoid any confounding effects of uncharacterized N-terminal APP cleavage and sorting signals [49], we also examined a shortened construct (referred to as  $\beta$ APP) fused to the C-terminal 112 amino acids of APP containing both the  $\beta$ - and  $\gamma$ -cleavage sites. This construct also contains an N-terminal HA- epitope tag.  $\beta$ APP-CFP colocalizes with full length FL-APP-GFP and has the same subcellular distribution as endogenous APP in primary neurons [50]. These constructs are cleaved by secretases (Figure 2.2) and produce A $\beta$  (ELISA data below). In fixed cells, the N-terminal HA-tag of these constructs are well colocalized with the C-terminal Fluorescent protein tag, implying that much of the intracellular APP is trafficked before cleavage (Figure 2.3). We have previously demonstrated that  $\beta$ APP-CFP and FL-APP-GFP are also trafficked to the cell surface and internalized to endosomes and lysosomes [50]. After photoactivation of  $\beta$ APP-paGFP and FL-APP-paGFP constructs, regions or compartments exhibiting APP accumulation of Golgi-derived APP are predicted to appear as regions of increased green fluorescence. At sites where  $\gamma$ -cleavage occurs, cleavage is expected to release the APP C-terminal and its paGFP tag into the cytoplasm, decreasing the fluorescent signal over time.

**Figure 2.1:** Schematic of constructs.

APP constructs were generated including the full length APP 751 fused to paGFP on its C-terminus. A shorter construct consisting of the C-terminal 112 amino acids of APP fused to paGFP. Both constructs include a linker with includes an N-terminal HA epitope tag, and both constructs contain  $\alpha$ -,  $\beta$ - and  $\gamma$ - cleavage sites. Cleavage at the  $\gamma$ -site will release the C-terminal tail of APP along with the paGFP tag into the cytoplasm.

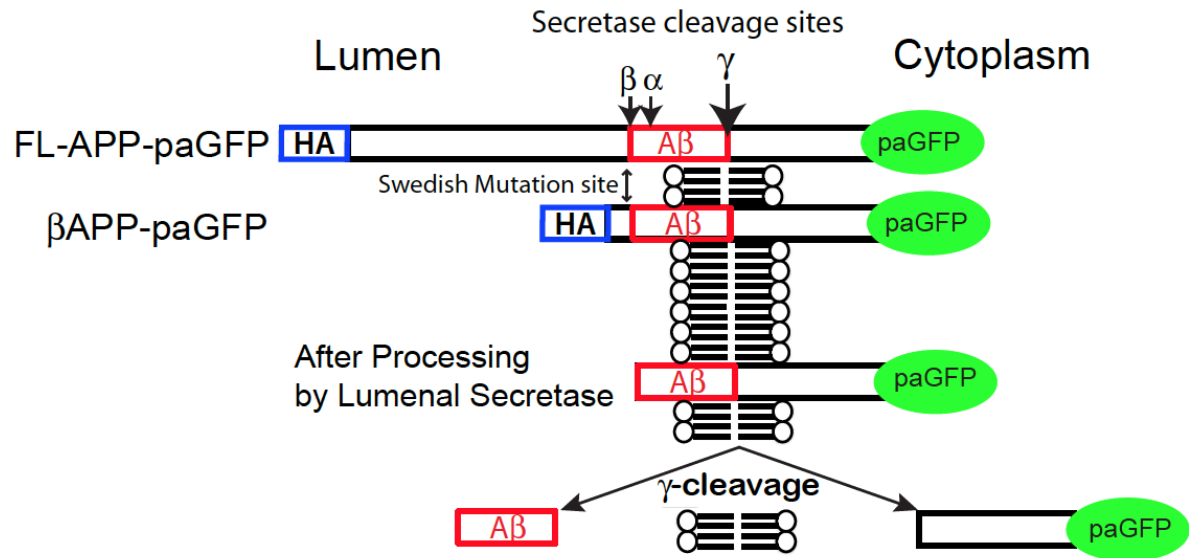


Figure 2.1

**Figure 2.2:** Cleavage of  $\beta$ APP-paGFP

$\beta$ APP-paGFP and full-length APP are cleaved by that  $\gamma$ -secretase in a similar manner. SN56 cells were transiently transfected with plasmids expressing GFP, full-length APP-paGFP (FL-APP-paGFP), or  $\beta$ APP-paGFP. Twenty-four hours before harvesting protein for western blotting, cells were treated with DMSO or with L685, 458. Cell lysate was run on a 12% SDS polyacrylamide gel, and transferred onto nitrocellulose membrane. Membrane was probed for APP using APP C-terminal antibody (Sigma). Membranes were reprobed for  $\alpha$ -tubulin, as a loading control. Full length APP-paGFP is cleaved to produce fragments of the predicted size, with a  $\beta$ -cleaved fragment at ~37 kDa (which is GFP (27kDa) the 10 kDa  $\beta$ -cleaved APP). The addition of the  $\gamma$ -secretase inhibitor L685, 458 causes the accumulation of the 37 kDa band. This pattern is repeated for the shorter  $\beta$ APP-paGFP construct.

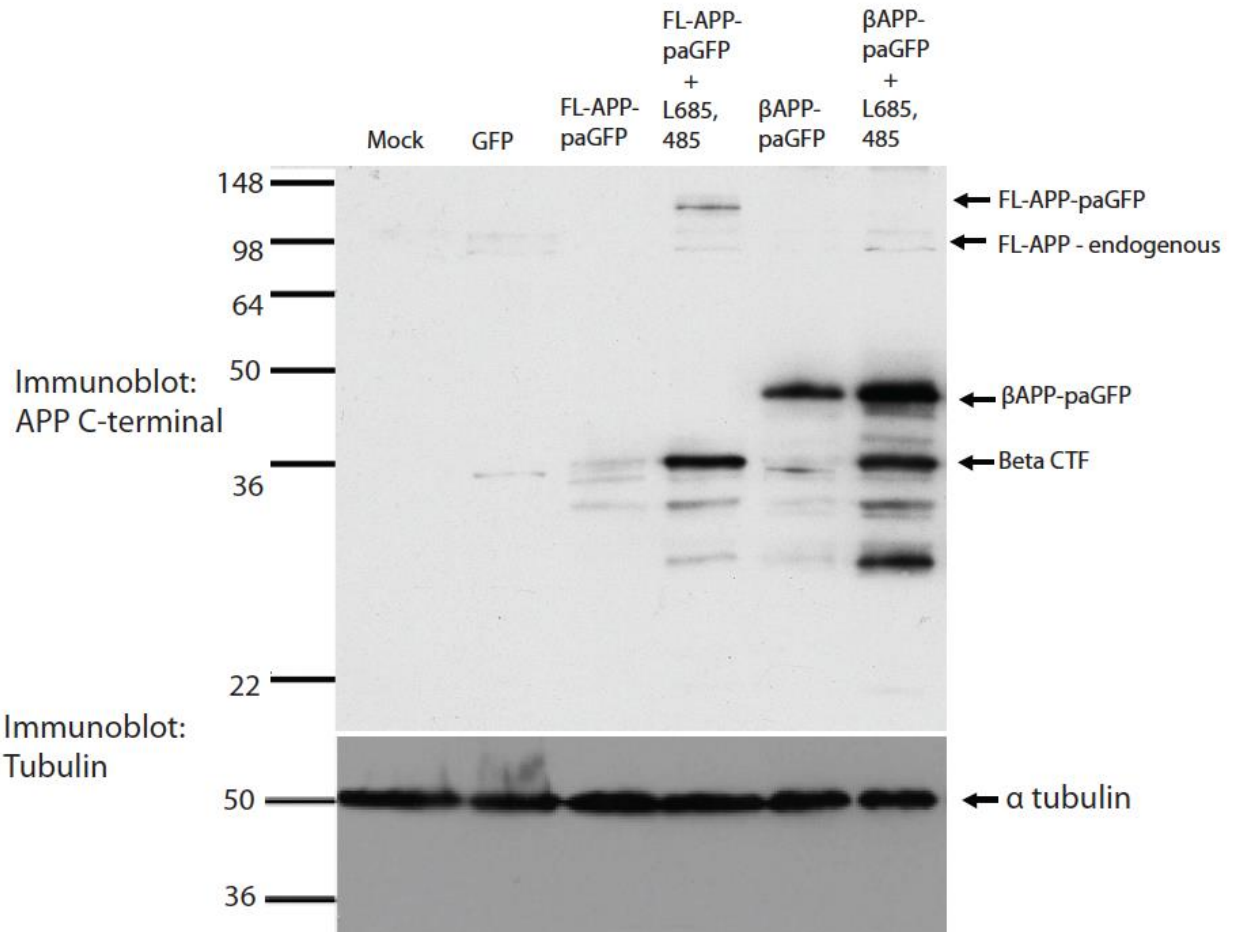


Figure 2.2

**Figure 2.3:** Colocalization of HA-tag and  $\beta$ APP-CFP

Most of the trafficked APP in the cell is uncleaved. SN56 cells were transiently transfected with plasmids expressing  $\beta$ APP-CFP, and immunostained with an anti-HA antibody, which binds to the HA-epitope on the N-terminus of the construct. In the merged image, it is possible to see that there is extensive colocalization of the N-terminal HA and the C-terminal CFP tag, implying that much of the intracellular APP is being trafficked uncleaved.



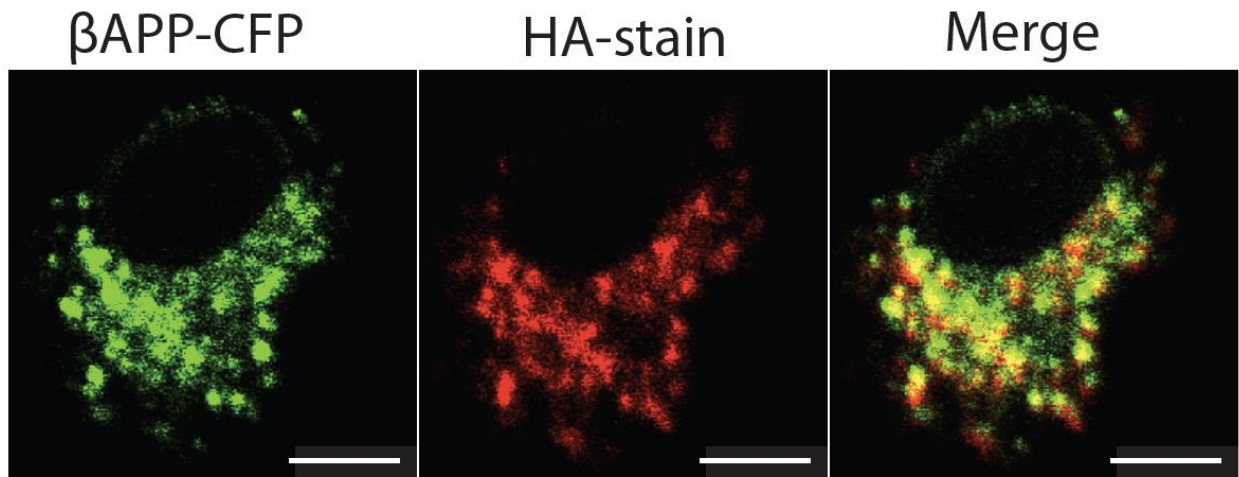


Figure 2.3

These studies were performed in the SN56 cell line, which is a hybrid cell created by fusing dissociated embryonic mouse septal neurons with N18TG2 neuroblastoma cells. SN56 cells were chosen because they are easily transfectable, have a neuronal morphology, and have a cholinergic phenotype when differentiated [51,52]. For each experiment, SN56 cells were co-transfected with an APP-paGFP construct along with a marker of the Golgi apparatus (GalT-CFP) [41] and subcellular compartment marker fused to a modified red fluorescent protein (mRFP or mCherry). Compartment markers were LAMP1 (lysosomes), Rab5 (early endosomes) and Rab9 (late endosomes). LAMP1 is a 120kDa protein that is localized to the limiting membrane of lysosomes [47,48]. Rab5 localizes to the early endosomal membrane and is involved in homogenous or heterogenous vesicle fusion [42-44]. Rab9 localizes to late endosomal membrane and evidence suggests that Rab9 is involved in returning cargo from the late endosome to the Golgi [45,53]. Although many authors use Rab7 as a late endosomal marker, Rab7 also labels lysosomes extensively [54]. Before imaging, SN56 cells were differentiated for 24 hours in serum free DMEM supplemented with dbcAMP. Cells with normal morphology, no inclusions, and normal compartment marker distribution were imaged live on a Zeiss LSM510 laser scanning confocal microscope. Regions of interests (ROIs; the irradiation targets, typically  $0.1-0.2 \mu\text{m}^2$ ) were drawn on the Golgi apparatus using the Zeiss Physiology package. During a 15-minute photoactivation period, cells were alternately imaged and then briefly irradiated with 405 nm laser light (25 mW) for 20 iterations (typically 2 seconds) within each of the ROI's to photoactivate APP-paGFP to produce a video time course. The irradiation targets were carefully monitored throughout the experiments to ensure that they did not drift outside the Golgi apparatus. Because of the very small irradiation targets, and APP's rapid movement through the Golgi apparatus, multiple rounds of photoactivation were required to create a strong green fluorescent signal. Images were acquired after each photoactivation cycle, approximately every 30 seconds, and colocalization analysis was performed using Imaris software (Bitplane). After the initial photoactivation period, cells were imaged for up to an hour to follow the movement of APP out of the Golgi and its clearance.

When we started these experiments, we expected APP to move primarily to the cell surface and

then to be internalized into lysosomes after 30 minutes to 1 hour. Instead, within seconds of photoactivation, activated bright green fluorescent APP-paGFP colocalized with LAMP1-mRFP, implying rapid transport to lysosomes. A typical experiment is shown in Video 2.1, where  $\beta$ APP-paGFP from the Golgi apparatus (blue) and can be seen moving within seconds to lysosomes (red). After 15 minutes of alternately photoactivating and imaging, cells were imaged (chased) for a further hour. During the chase period most of the green fluorescent APP disappeared, suggesting that it was being cleared.

In these experiments, both photoactivated FL-APP-paGFP and  $\beta$ APP-paGFP appear to be rapidly colocalized with the LAMP-1 compartment (Figure 2.4a; top and middle panels). To confirm that this trafficking occurs in neurons, we then transfected GalT-CFP,  $\beta$ APP-paGFP and LAMP1-mRFP into primary mouse cortical neurons. After photoactivating  $\beta$ APP-paGFP in the Golgi, green fluorescence appears within 30 seconds to a minute in LAMP1-mRFP labeled compartments. (Figure 2.4a; bottom panel). To further demonstrate that the LAMP1 compartment rapidly received photoactivated APP-paGFP, we performed imaging at high magnification in closely cropped cells with  $\beta$ APP-paGFP. In the earliest time points, it was possible to observe green fluorescent APP-paGFP arriving rapidly within LAMP1 compartments (Figure 2.4b). We quantitated the fraction of fluorescent activated paGFP colocalized with LAMP-mRFP after 15 minutes of photoactivation, we found that  $34 \pm 5$  % (Mean  $\pm$  SEM) of FL-APP and  $34 \pm 4$  % of  $\beta$ APP was colocalized with LAMP1 (not statistically different) (Figure 2.4c). Because the trafficking of the shorter construct was indistinguishable and generated brighter images, the  $\beta$ APP-paGFP construct was used for the remainder of these experiments. Enlarged images from these experiments along with colocalization analysis are shown in Figure 2.5. These images are very similar to the trafficking of LAMP1-paGFP from the Golgi to lysosomes reported by Patterson et al. [30].

To rule out the possibility that transport to the LAMP1 compartment was due to overexpression of the paGFP tag, we examined the transport of the Vesicular Stomatitis Virus Glycoprotein (VSVG); a classic secretory trafficking protein. VSVG was tagged with paGFP at its cytoplasmic C-terminus [55,56] similar to our APP constructs. We transfected SN56 cells VSVG-paGFP.

These cells were subjected to the same imaging protocol as  $\beta$ APP-paGFP transfected cells. After the 15-minute pulse-period, VSVG-paGFP appeared on the cell surface and exhibited minimal transport to a LAMP1 compartment (Figure 2.4d), in concordance with previous results [31,56]. Therefore, we conclude the paGFP tag did not alter the trafficking of APP.

To verify the accuracy of  $\beta$ APP-paGFP photoactivation in the Golgi apparatus and that we were not photoactivating  $\beta$ APP-paGFP in nearby structures, SN56 cells were transfected with GalT-CFP,  $\beta$ APP-paGFP and LAMP1-mRFP and pretreated with nocodazole and/or cytochalasin D to block transport out of the Golgi [57]. Cells were then photoactivated and imaged for 15 minutes using the Golgi apparatus marker GalT-CFP as a target, and a Z-stack was taken immediately after the photoactivation period. During the entire experiment, photoactivated APP-paGFP remained almost exclusively within the Golgi apparatus (Figure 2.4e; Video 2.2). Inspection of the post-irradiation Z-stack also revealed that photoactivated  $\beta$ APP-paGFP was localized principally within the Golgi apparatus, with almost no fluorescence evident in other compartments or at the cell surface (Figure 2.4f).

**Figure 2.4:** APP is rapidly trafficked from the Golgi apparatus to LAMP1-labeled compartment.

Photoactivation targets were drawn on the Golgi apparatus (white dots with arrows). For 15 minutes, cells were alternately imaged and irradiated (photoactivated) with 405 nm laser light within the targets. White arrowheads point to APP-paGFP colocalized with Lamp1-mRFP. Scale Bar = 5  $\mu$ m. a) Demonstrates rapid transport of Full length-APP- paGFP (top panel) and  $\beta$ APP-paGFP (middle panel) from Golgi apparatus to a LAMP1-labeled compartment. The same trafficking occurs in mouse primary neurons (lower panel) (See Video 2.1). b) Higher magnification images of  $\beta$ APP-paGFP trafficking rapidly to a LAMP1 labeled compartment. Scale Bar = 1  $\mu$ m. c) Comparison of the colocalization of activated FL-APP-paGFP (n = 9) and activated  $\beta$ APP-paGFP (n = 8). d) SN56 cells transiently transfected with the secretory protein Vesicular Stomatitis Virus Glycoprotein-paGFP (VSVG-paGFP), GalT-CFP (blue), and LAMP1-mRFP (red) to demonstrate that very little of the green photoactivated VSVG-paGFP arrives in the LAMP1 compartment; paGFP does not alter trafficking. Scale bars = 5  $\mu$ m. e) Transfected SN56 cells were treated for 5 minutes with nocodazole before imaging (See Video 2.2). Scale bars = 5  $\mu$ m. f) Z-stack of the same cell taken immediately following 15 minutes of photoactivation demonstrating that green signal remains inside the Golgi.

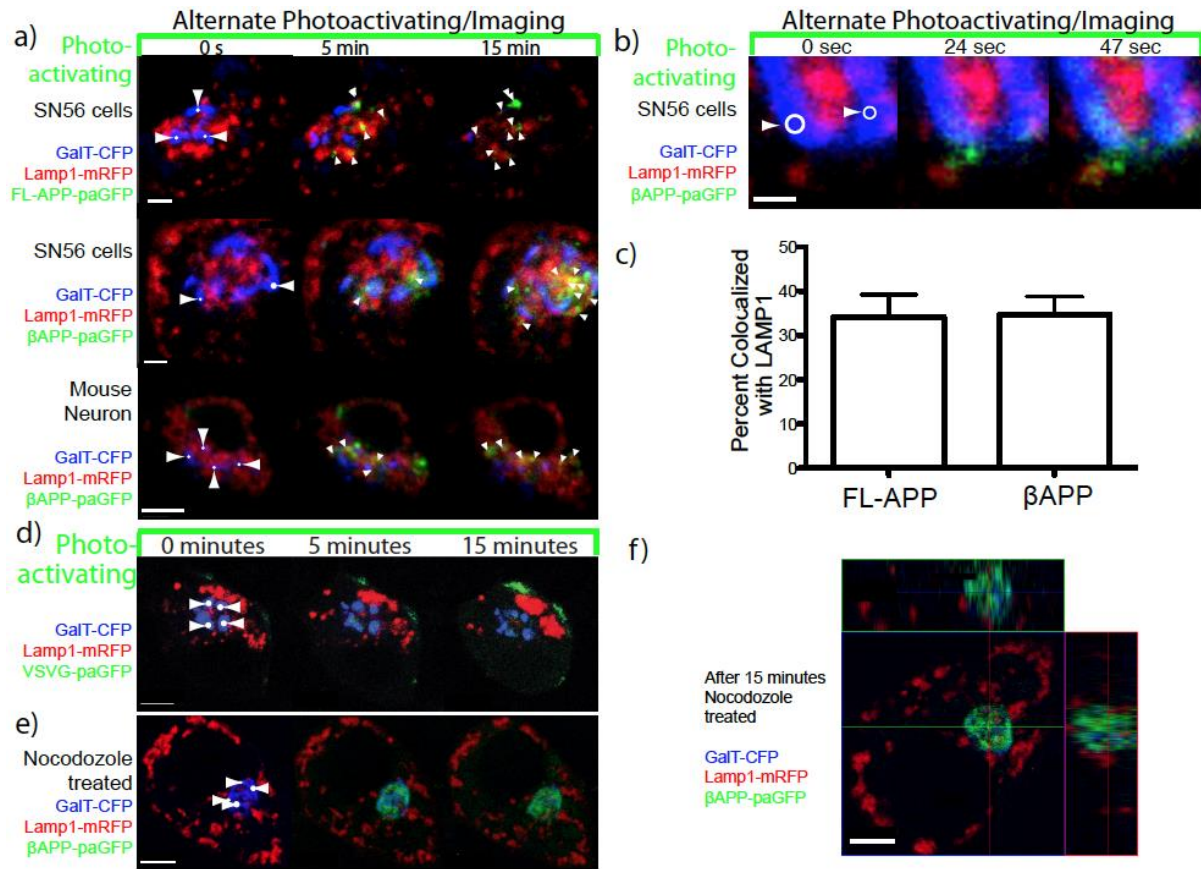


Figure 2.4

**Figure 2.5:** Enlarged images of APP trafficking

Colocalization of photo-activated APP-paGFP with LAMP1. SN56 cells were transiently transfected with plasmids expressing GFP,  $\beta$ APP-paGFP and GalT-CFP. a) Shows the initial image of an SN56 cell before photoactivation, with the Golgi apparatus labeled blue (GalT-CFP) and lysosomes labeled red with LAMP1-mRFP. Thresholds were set in the red and blue channels to identify the Golgi apparatus and Lysosomes using Imaris software, and a colocalization channel is generated and overlaid in white. Although the Golgi apparatus and Lysosomes are closely apposed, the fluorescent protein markers demonstrate minimal colocalization. Panel b shows the same cell after 15 minutes of Golgi-targeted photoactivation with activated  $\beta$ APP-paGFP in green and lysosomes labeled red with LAMP1-mRFP. The inset is magnified as figure c. Panel c shows the red LAMP1-mRFP and green photoactivated  $\beta$ APP-paGFP channels separately. Thresholds were set in the red and green channels to identify the lysosomes and the majority of the APP fluorescent signal using Imaris software, and a colocalization channel is generated and overlaid in white. This channel demonstrates extensive colocalization of APP-paGFP and LAMP1. Furthermore, many regions of APP labeled fluorescence have the same shape as the underlying LAMP1 label, implying that they are indeed colocalized in these confocal images.

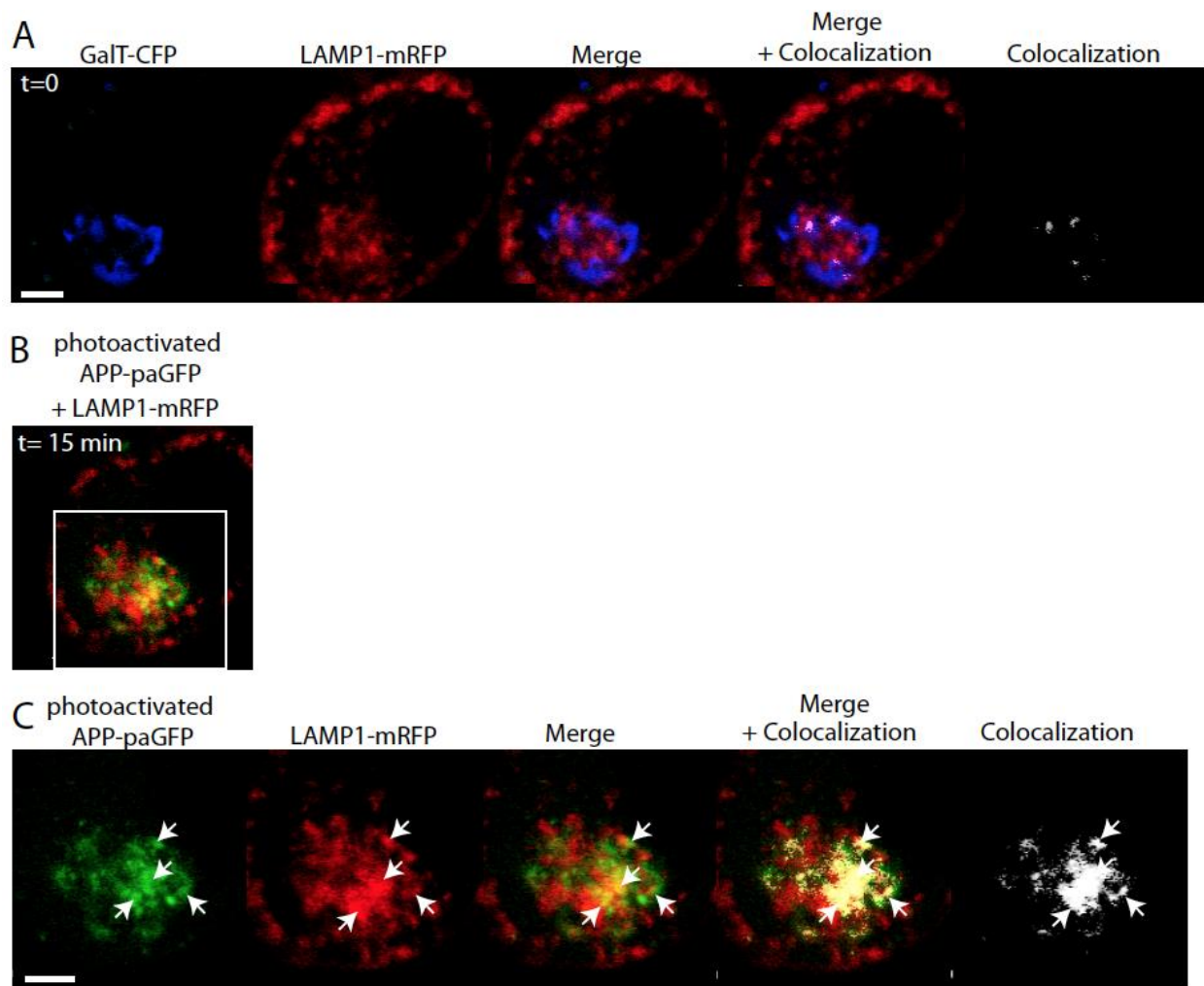


Figure 2.5



### 2.3.2 APP-paGFP traffics preferentially to lysosomes from the Golgi apparatus

Next, we examined APP trafficking from the Golgi apparatus to early and late endosomes. In these experiments,  $\beta$ APP-paGFP was co-transfected with GalT-CFP along with either Rab5-mRFP (early endosomes) or Rab9-mCherry (late endosomes). Rab5 is highly associated with early endosomal membranes and is routinely used as a marker for early endosomes [42,43]. Rab9 localizes to late endosomal membrane and evidence suggests that Rab9 is involved in returning cargo from the late endosome to the Golgi [45,46,54]. Rab7 is also a late endosomal marker [45], but Rab7 also defines a population of lysosomes [54]. Therefore, to avoid mis-identification of late endosomes as lysosomes we chose Rab9 as our late endosomal marker.

Cells were then alternately irradiated with 405 nm within targets placed over the Golgi apparatus and imaged to produce a time course of images. In these experiments, a small amount of  $\beta$ APP-paGFP can be seen colocalizing with Rab9 and Rab5 (Figure 2.6a and b; respectively) at the end of the photoactivation period. At the end of the 15-minute pulse period,  $37 \pm 5\%$  (Mean  $\pm$  SEM) of photoactivated  $\beta$ APP-paGFP colocalized with LAMP1 labeled compartments. Trafficking to Rab9 and Rab5 compartments was significantly lower at  $17 \pm 4\%$  and  $6 \pm 3\%$ , respectively ( $p < 0.05$ ) (Figure 2.6c). Although some LAMP1 labeling is found in early and late endosomes, the fact that significantly more APP was co-localized with LAMP1 than Rab5 or Rab9 suggests that APP is in *bona fide* lysosomes.

**Figure 2.6:** APP is primarily transported to a LAMP1 compartment.

SN56 cells were cotransfected with plasmids expressing APP-paGFP, GalT-CFP (blue), and a compartment marker (red). Photoactivation targets were drawn on the Golgi apparatus (white dots with arrows).  $\beta$ APP-paGFP trafficking was visualized from the Golgi apparatus to Rab 9 labelled late endosomes (a) and Rab 5 labelled early endosomes (b). Scale bars represent 5  $\mu$ m. c) Percent of APP-paGFP fluorescence colocalized with respective compartment markers after 15 minutes of photoactivation in the Golgi (circles: LAMP1 (n = 9), squares: Rab9 (n = 10), triangles: Rab5 (n = 7)). Error bars represent standard deviation. (\* =  $p < 0.05$ ).

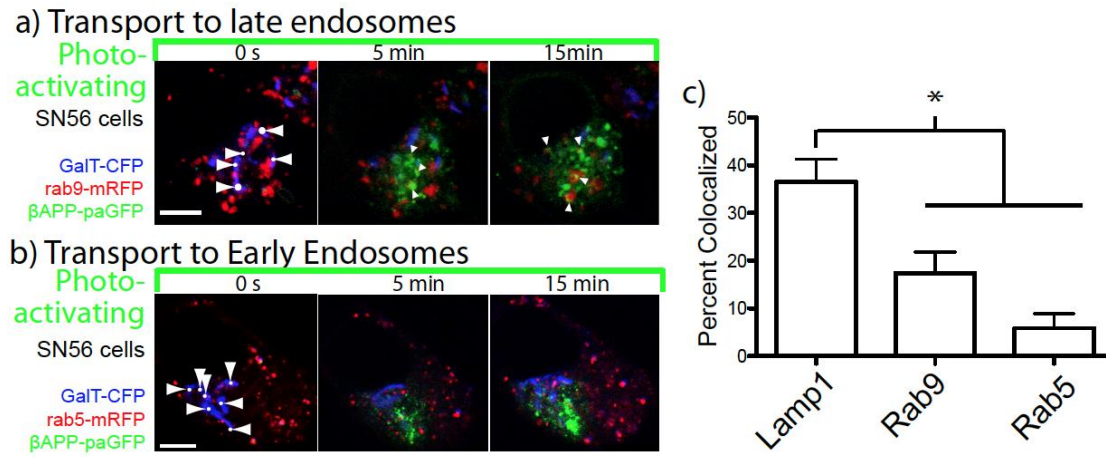


Figure 2.6

### 2.3.3 APP-paGFP is cleaved in a LAMP1 positive compartment

Subcellular fractionation has shown that  $\gamma$ -secretase proteins and APP are *bona fide* residents of the lysosomal membrane [13]. Furthermore, *in vitro* assays revealed that  $\gamma$ -secretase has an acidic optimal pH (4.5-5) [13]. Therefore, we hypothesized that inhibiting  $\gamma$ -secretase or lysosomal enzyme function could inhibit both secretase cleavage and nonspecific degradation of  $\beta$ APP, which would result in paGFP fluorescence accumulation at the lysosome membrane. Therefore, we followed the extinction of paGFP fluorescence from LAMP1 positive vesicles after the end of the photoactivation period. We found that there was nearly complete extinction of photoactivated  $\beta$ APP-paGFP (Figure 2.7a; Video 2.1) and FL-APP-paGFP (Figure 2.8) fluorescence from the LAMP1 compartment within 1 hour. First we examined the effects of nonspecific inhibition of lysosomal function, using chloroquine. Chloroquine has been reported to alkalinize the endosomal/ lysosomal system and to inhibit APP clearance and A $\beta$  production [17,58,59]. Cells were treated with 100  $\mu$ M chloroquine for 30 minutes before imaging. The increase in pH was confirmed by loss of LysoSensor Green signal (a pH-dependent fluorescent probe, Invitrogen) from LAMP1 compartments Figure 2.9. As in the untreated control cells,  $\beta$ APP-paGFP fluorescent signal was observed trafficking directly from the Golgi apparatus to LAMP1-mRFP labeled lysosomes (Figure 2.7b, Video 2.3). However, in cells treated with chloroquine, there was an accumulation of  $\beta$ APP-paGFP fluorescence in LAMP1-labeled compartments.

Next we assessed the ability of the highly potent and specific  $\gamma$ -secretase inhibitor L685,458 [60] to block the cleavage of  $\beta$ APP-paGFP. SN56 cells were pretreated with 0.5  $\mu$ M of L685,458 for 24 hours before imaging. L685,458 treatment caused marked accumulation of photoactivated  $\beta$ APP-paGFP in lysosomes during the photoactivation phase, and significantly reduced the clearance of APP from lysosomes. (Figure 2.7c; Video 2.4).

We hypothesized that if APP were cleaved at the lysosomal membrane by secretase enzymes, the cytoplasmic tail of APP along with activated paGFP would be released into the cytoplasm resulting in loss of fluorescence from this compartment. Furthermore, this process would appear with kinetics order greater than 0. In contrast, the loss of fluorescence due to photobleaching would be directly proportional to the amount of time that the fluorophore was irradiated, and should therefore fall off linearly, with 0 order kinetics. To quantitate APP-paGFP clearance from the lysosome after the photoactivation period, we measured the number of pixels of APP-paGFP fluorescence colocalized with LAMP1-mRFP using Imaris software for each time point, normalizing the highest value of colocalization (after the photoactivation period) to 100%. In these experiments, FL-APP-paGFP and  $\beta$ APP-paGFP disappear from the lysosomes with non-linear kinetics. The disappearance of  $\beta$ APP-paGFP was modeled using Prism 5 (GraphPad, La Jolla, CA) from the lysosome can be accurately modeled using the integrated rate equation for a first order reaction ( $k=0.00153 \text{ sec}^{-1}$ ,  $r^2=0.96$ ) (Figure 2.7d). We attempted to model the data with two and three phase exponential decay curves, but these resulted in worse fit. This suggests that APP is cleaved with first order kinetics in lysosomal compartments, suggesting enzymatic clearance.

Because of our long imaging protocol, some of the loss fluorescence from activated paGFP could be the result of photobleaching. Therefore, we constructed photobleaching curves using enhanced-GFP (EGFP), as EGFP and paGFP have nearly identical photobleaching characteristics [30]. SN56 cells were transiently transfected with EGFP, and fixed with 4% paraformaldehyde. Cells were then imaged using the same imaging protocol, as in the previous live cell imaging experiments. The normalized number of green pixels at each time point was quantitated, and plotted on the same graph as our  $\beta$ APP-paGFP clearance data (Figure 2.7d).  $\beta$ APP-paGFP fluorescence decayed faster and became significantly lower than GFP fluorescence (One-way ANOVA; Tukey's Post Hoc;  $p<0.05$ ). Therefore, the loss of  $\beta$ APP-paGFP fluorescence appears to be the result of a first order enzymatic reaction (Figure 2.7d).

Next, we quantified the effect of inhibitors on APP clearance (Figure 2.7e). After chloroquine treatment, photoactivated APP-paGFP in the lysosome decreased linearly over time during the

chase phase, suggesting that it was not cleared by an enzymatic cleavage. There was no significant difference from loss of fluorescence due to photobleaching (One-way ANOVA; Tukey's Post Hoc  $p < 0.05$ ) (Figure 2.7e). In cells treated with L685,458 or chloroquine, the loss of  $\beta$ APP-paGFP fluorescence from lysosomes during the chase phase was also not significantly different from the rate of loss of GFP fluorescence due to photobleaching (One-way ANOVA; Tukey's Post Hoc;  $p < 0.05$ ) (Figure 2.7e). Cells treated with L685,458 also consistently exhibited accumulation of photoactivated  $\beta$ APP-paGFP at the cell surface (Figure 2.7c middle and right panels). This is in agreement with a previous study that showed APP internalization was decreased by treatment with  $\gamma$ -secretase inhibitors [61,62]. Our data therefore suggests that  $\beta$ APP-paGFP clearance from lysosomes is performed by both a pH-dependent protease (as expected for a  $\beta$ -secretase) and by the  $\gamma$ -secretase. The accumulation of APP in these LAMP1 compartments following inhibition of proteases suggests that they represent terminal lysosomes and not an endosomal intermediate.

**Figure 2.7:** APP is processed in the lysosome by a  $\gamma$ -secretase like activity.

SN56 cells were transiently transfected with  $\beta$ APP-paGFP, GalT-CFP, and LAMP1-mRFP. Cells were alternately photoactivated with 405 nm light and imaged in the Golgi for 15 minutes, and then imaged every 30 seconds for 1 hour. a) Shows the accumulation of photoactivated APP-paGFP in the lysosome after 15 minutes, followed by its near complete clearance after 45 minutes. Arrowheads denote areas of colocalization (See Video 2.1). b) Transiently transfected SN56 cells were pretreated with 100  $\mu$ M chloroquine for 30 minutes prior to imaging. After chloroquine treatment APP is still visible in lysosomes after 45 minutes (See Video 2.3). c) Cells treated with 0.5  $\mu$ M L685, 458 ( $\gamma$ -secretase inhibitor) overnight prior to photoactivating/imaging. L685, 458 treatment substantially increases the accumulation of photoactivated  $\beta$ APP-paGFP in lysosomes, and substantially decreases its clearance. Scale bars represent 5  $\mu$ m (See Video 2.4). d) Cleavage of  $\beta$ APP-paGFP was determined by measuring the loss of FL-APP (black open triangles) and  $\beta$ APP-paGFP (black closed circles) from LAMP1 labeled compartments. Values were averaged and normalized to begin at 100%. Overlaid in green squares is the loss of fluorescence of EGFP in the identical imaging protocol. Error bars represent SEM. (\* =  $p < 0.05$ ). (e) Shows the clearance of photoactivated APP-paGFP cells that were treated with 100  $\mu$ M chloroquine for 30 minutes before imaging (n = 9) or with 0.5  $\mu$ M L685, 458 ( $\gamma$ -secretase inhibitor) (n = 9). Error bars represent SEM.

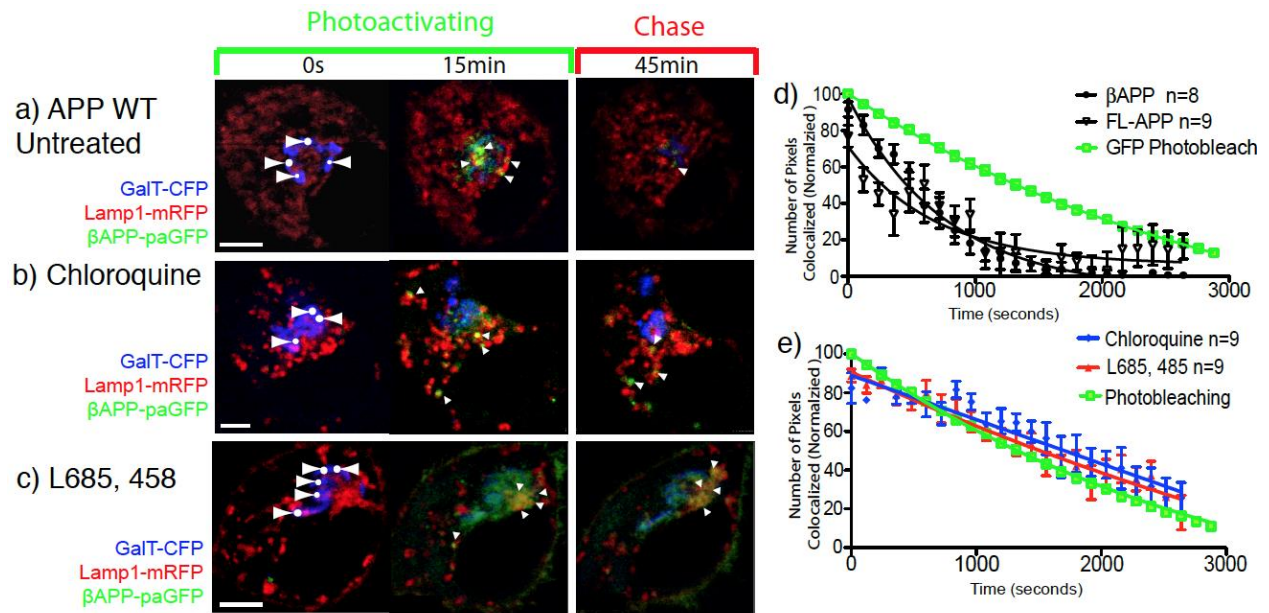


Figure 2.7



**Figure 2.8:** Trafficking of full-length APP-paGFP to LAMP1-mRFP labelled compartments

SN56 cells were transfected with GalT-CFP, FL-APP-paGFP, and LAMP1-mRFP. Cells were photoactivated in the GalT labelled compartments and imaged for 15-minutes for 15-minutes. The cells were chased for a further 45-minutes to follow the clearance of APP from the cell. The images shown below are from the 0, 15, and 45-minute time points. Scale bar represents 5 $\mu$ m. White arrows point to colocalized pixels between FL-APP-paGFP and LAMP1-mRFP.

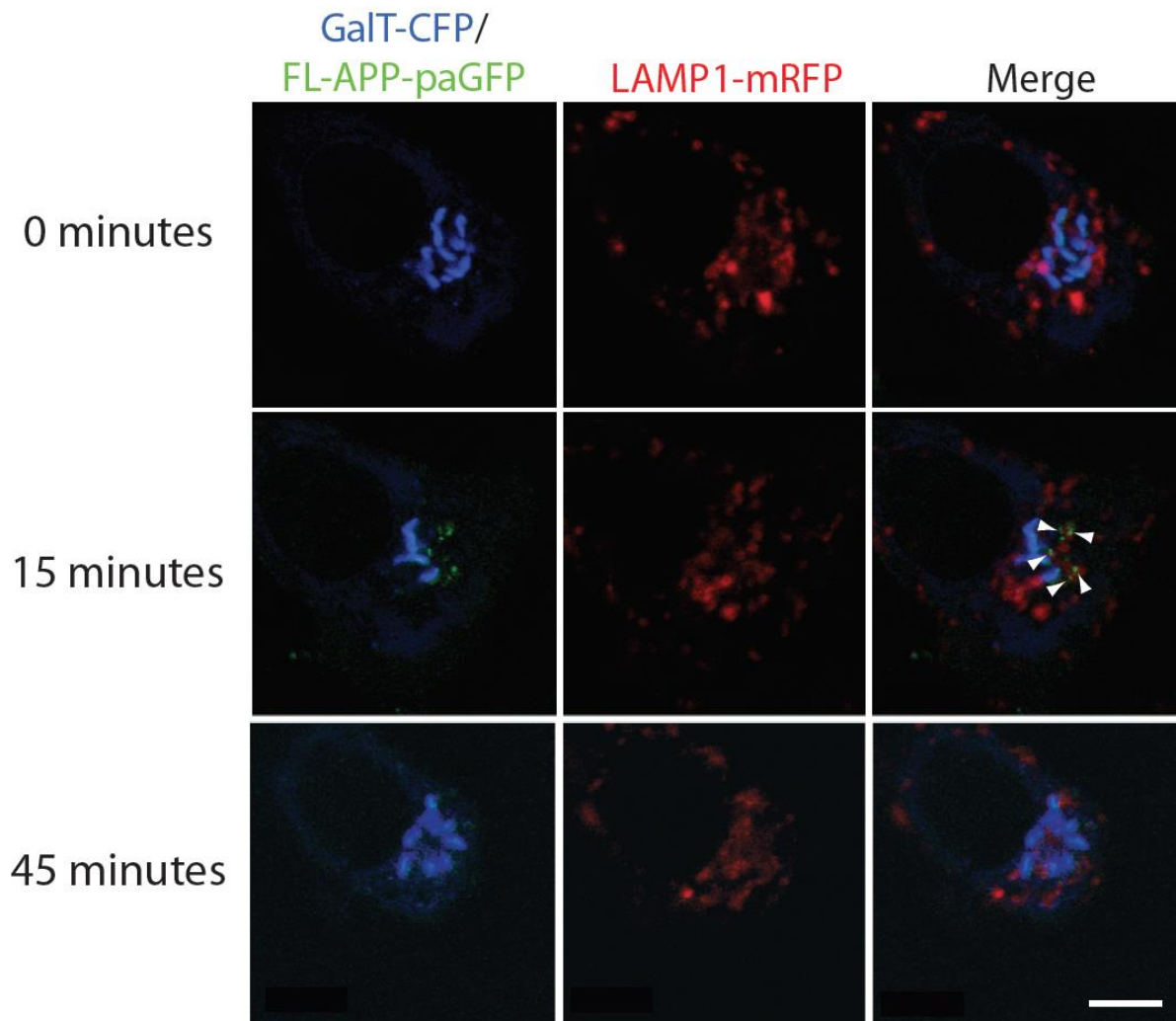


Figure 2.8

**Figure 2.9:** De-acidification of lysosomes with chloroquine.

SN56 cells were preloaded with 75nm Lysosensor™ Green after transfection with LAMP1-mRFP. The cells were imaged by confocal microscopy before and after treatment with chloroquine. Scale bars represent 5µm.

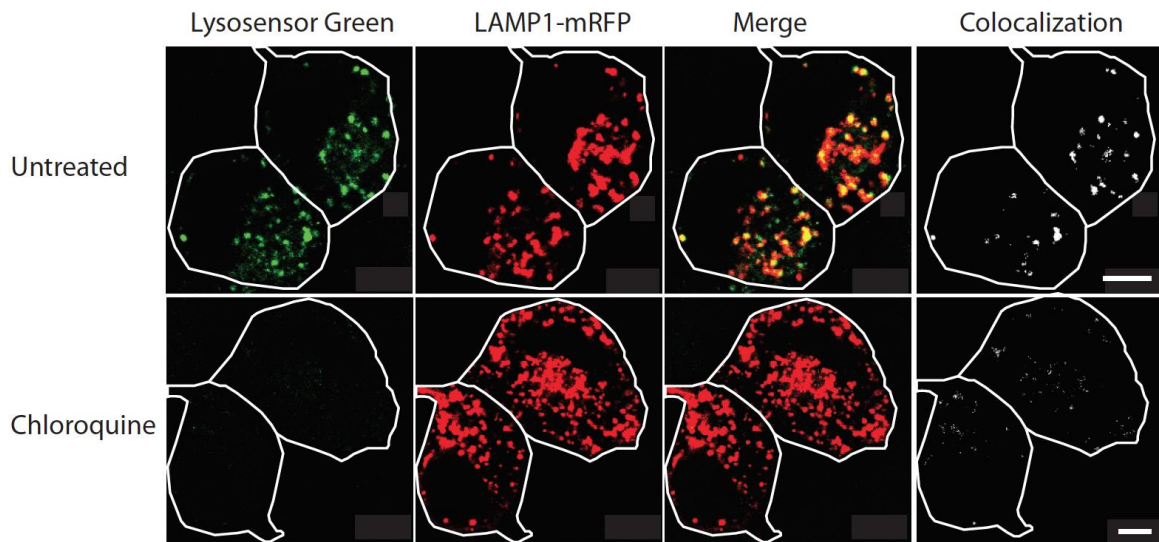


Figure 2.9

**Figure 2.10:** Cleavage of  $\beta$ APPsw-paGFP

$\beta$ APP-paGFP,  $\beta$ APPsw-paGFP, and full-length APP-paGFP are cleaved by that  $\gamma$ -secretase in a similar manner. SN56 cells were transiently transfected with plasmids expressing GFP, FL-APP-paGFP,  $\beta$ APP-paGFP, or  $\beta$ APPsw-paGFP. Twenty-four hours before harvesting protein for western blotting, cells were treated with DMSO or with L685, 458. Cell lysate was run on a 12% SDS polyacrylamide gel, and transferred onto nitrocellulose membrane. Membrane was probed for APP using APP C-terminal antibody (Sigma). Membranes were reprobbed for  $\alpha$ -tubulin, as a loading control.

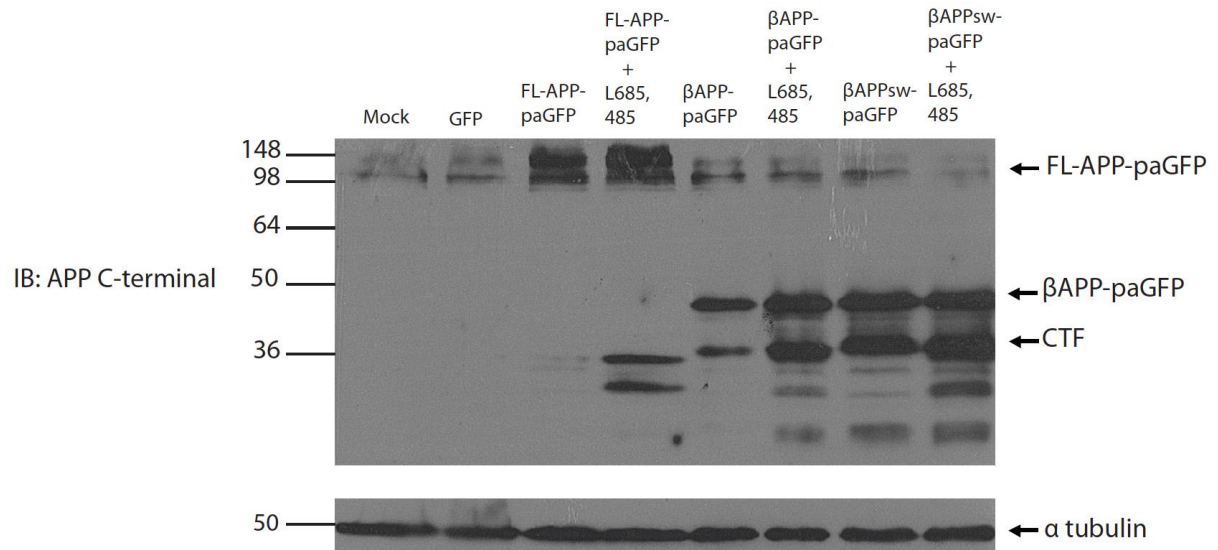


Figure 2.10

### 2.3.4 The Swedish mutation dramatically increases APP clearance from the lysosome, but not the Golgi apparatus

The Swedish mutation ( $\beta$ APP<sup>sw</sup>) is a double mutation at codons APP 670/671 (numbered in APP695) adjacent to the  $\beta$ -secretase cleavage site that increases the rate of  $\beta$ -cleavage of APP by up to a factor of 10, and has been suggested to alter the trafficking of APP [22,63,64]. To examine the effect of the Swedish mutation on intracellular APP trafficking, we transiently transfected SN56 cells with  $\beta$ APP<sup>sw</sup>-paGFP along with plasmids expressing compartment markers for the Golgi apparatus and lysosomes. Protein from SN56 cells transfected with  $\beta$ APP-paGFP, FL-APP-paGFP, or  $\beta$ APP<sup>sw</sup>-paGFP was harvested and separated by SDS-PAGE. By SDS-PAGE, the expression level of  $\beta$ APP-paGFP and  $\beta$ APP<sup>sw</sup>-paGFP was similar (Figure 2.10). The pulse-chase paradigm, as performed with wild-type  $\beta$ APP-paGFP, was performed on these cells, targeting the GalT-CFP labeled Golgi apparatus to photoactivate  $\beta$ APP<sup>sw</sup>-paGFP. Unlike cells transfected with the wild type construct, green fluorescence did not accumulate in cells transfected with  $\beta$ APP<sup>sw</sup>-paGFP in a LAMP1-labeled compartment. Instead, these cells rapidly developed diffuse green fluorescence throughout the entire cell body (Figure Figure 2.11a; Video 2.5). The diffuse cytoplasmic appearance of paGFP fluorescence suggests that APP is being rapidly cleaved, with the APP C-terminal fused to paGFP diffusing rapidly into the cytosol. This likely reflects the higher rate of  $\beta$ -cleavage of Swedish mutation [65,66].

It has previously been suggested that secretase cleavage of the APP<sup>sw</sup> might occur in the Golgi apparatus. In order to examine APP cleavage in the Golgi apparatus, we repeated this experiment after treating the cells with nocodazole and cytochalasin D (Figure 2.11b; Video 2.6). In dramatic contrast to untreated cells, virtually all of the paGFP fluorescence remains localized to the Golgi apparatus during the photoactivation period. Cells were then followed for up to 1-hour post photoactivation, during which most of the green signal remains in the Golgi apparatus. It was not possible to quantify the clearance of  $\beta$ APP<sup>sw</sup>-paGFP from the Golgi apparatus in this experiment, because of photobleaching of the GalT-CFP marker. Although it is not possible to say from this data that there is no cleavage of APP in the Golgi apparatus, the Golgi apparatus does not appear to facilitate the majority of APP processing.

In order to examine lysosomal processing of  $\beta$ APP<sup>sw</sup>-paGFP, we treated cells with chloroquine and L685,458. After treatment with chloroquine, there was rapid trafficking of  $\beta$ APP<sup>sw</sup>-paGFP signal to the lysosome where it accumulated in the photoactivation phase and then gradually decreased in brightness in the chase phase (Figure 2.11; Video 2.7). This result was also seen after treatment with the  $\gamma$ -secretase inhibitor L685, 458 (Figure 2.11b; Video 2.8). The loss of fluorescence signal in the chase phase as linear for both of these treatments was not significantly different from GFP photobleaching (Figure 2.11c and 2.9d). Together, these data suggest that the Swedish mutation accelerates the cleavage of APP at the lysosomal membrane, but does not have an effect on APP trafficking to the lysosome.



**Figure 2.11:** The Swedish mutation causes rapid clearance of APP from lysosomes.

SN56 cells were transiently transfected with  $\beta$ APP<sup>sw</sup>-paGFP, GalT-CFP, and LAMP1-mRFP. Scale bars represent 5  $\mu$ m. a)  $\beta$ APP<sup>sw</sup>-paGFP was photoactivated for 15 minutes in the GalT-CFP labeled compartment, and chased for 45 minutes.  $\beta$ APP<sup>sw</sup> is cleaved nearly instantaneously and appears in the cytoplasm. b) Cells were treated for 5 minutes before imaging with 66  $\mu$ M nocodazole and 10  $\mu$ M cytochalasin. GalT-CFP is false colored red to provide better contrast, and LAMP1-mRFP has been false coloured blue. Photoactivated  $\beta$ APP<sup>sw</sup>-paGFP accumulates in the Golgi and does not appear to be cleaved. c) Cells were treated acutely with 100  $\mu$ M chloroquine (See Video 2.7) which results in photoactivated  $\beta$ APP<sup>sw</sup>-paGFP accumulating in lysosomes. White arrowheads represent  $\beta$ APP<sup>sw</sup>-paGFP colocalized with LAMP1-mRFP d) Cells were treated with 0.5  $\mu$ M L658, 458 (See Video 2.8), which also causes photoactivated  $\beta$ APP<sup>sw</sup>-paGFP to appear in lysosomes. Scale bars represent 5  $\mu$ m. Quantitation of colocalized green pixels with LAMP1-mRFP show that the clearance of  $\beta$ APP<sup>sw</sup>-paGFP from the lysosome proceeds linearly after treatment with e) chloroquine (n = 8), or with f) L658, 458 (n = 9). Error bars represent standard deviation.

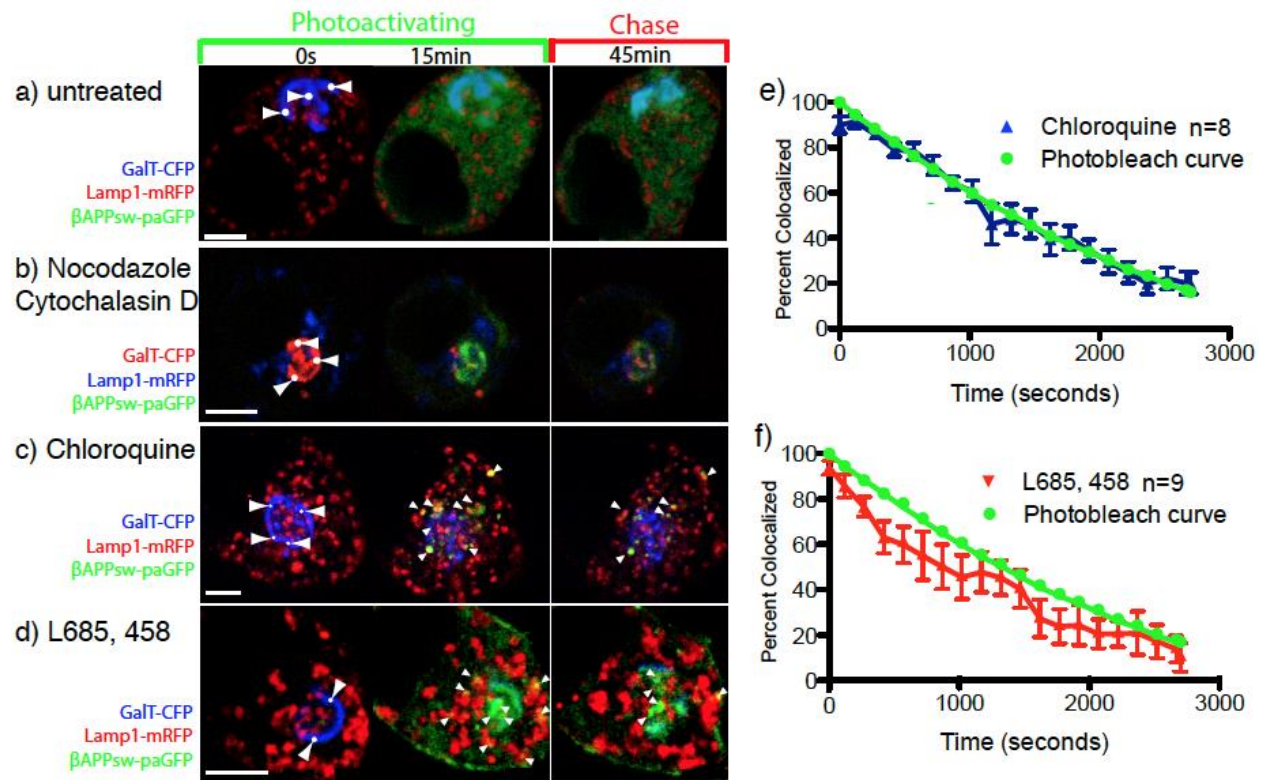


Figure 2.11

### 2.3.5 APP interacts with adaptor protein AP-3

AP-3 is an adaptor protein that is integral to the direct delivery of lysosomal membrane proteins (LMPs) from the Golgi apparatus [67-71]. First, we sought to determine whether APP and AP-3 colocalize in neurons. Cortical neurons dissected from E15 mice were immunostained (DIV7) for the APP C-terminal and AP-3  $\delta$  subunit, demonstrating colocalization. When analyzed by Imaris,  $42 \pm 3\%$  (Mean $\pm$ SEM) of APP fluorescence was colocalized with AP-3 signal. We then depleted the  $\delta$  subunit of AP-3 in SN56 cells using siRNA, as this has been shown to cause instability and degradation of the entire AP-3 complex [72]. We found that cells transfected with this siRNA expressed only  $22 \pm 12\%$  (Mean $\pm$ SD) of the AP-3  $\delta$  subunit on Western blots ( $p < 0.05$ ), while cells transfected with a control siRNA showed no significant change in AP-3  $\delta$  expression (Figure 2.12a and b). We also observed this effect by immunostaining; cells transfected with siRNA (visualized by the Alexa fluor 647 label on the 5' end of the control oligonucleotide) showed a marked decrease in AP-3 $\delta$  staining while untransfected cells, or cells transfected with fluorescently labelled negative control siRNA only were unaffected (Figure 2.12c).

To determine whether APP and AP-3 interact using the *in situ* proximity ligation assay (iPLA) which allows the study of low affinity interactions in-situ and has comparable accuracy to co-immunoprecipitation [73,74]. Briefly, iPLA employs species-specific secondary antibodies bearing complementary DNA strands. If the two antibodies are within 40 nm, the DNA strands will hybridize, and the resulting sequence can be replicated, amplified, and labelled with fluorescent oligonucleotides. Pairs of interacting proteins were detected as red fluorescent dots/ $\mu\text{m}^3$ .

SN56 cells were transfected with  $\beta$ APP-CFP, and iPLA was used to determine the proximity of APP and AP-3. Cells mock transfected or transfected with negative control siRNA both demonstrate an interaction between APP and AP-3 (Figure 2.13b). Conversely, cells transfected with siRNA against AP-3  $\delta$  showed a marked decrease (approximately 98%) in fluorescent puncta signifying decreased interaction (Figure 2.13b and c).

**Figure 2.12:** Knockdown of AP3 and AP1 by siRNA.

a) SN56 cells were transfected with fluorescently-tagged control siRNA or AP-3 $\delta$  and fluorescently tagged siRNA. Western blot demonstrating that AP-3 $\delta$  siRNA decreases AP-3 $\delta$  protein. Blots were stripped and re-probed with anti-tubulin antibody as a loading control. b) Western blots (from a) were scanned and analyzed using densitometry (ImageJ) and graphed. Error bars represents standard error of the mean. (\* $p < 0.05$ ). c) SN56 cells were transfected with fluorescently tagged control siRNA or anti-AP-3 $\delta$  and fluorescently tagged siRNA (purple). Cells were the immunostained to detect AP-3 $\delta$  (red). Fluorescent images overlaid with white light images to delimit the cell body. (scale bars represents 5  $\mu\text{m}$ ). d) SN56 cells were transfected with control siRNA or siRNA against AP-1 $\gamma$ . Western blot demonstrating that AP-1 $\gamma$  siRNA decreases AP-1 protein. Blots were stripped and re-probed with anti-tubulin antibody as a loading control. e) Western blots (from d) were scanned and analyzed using densitometry (ImageJ) and graphed. Error bars represents standard error of the mean. (\*= $p < 0.05$ ).

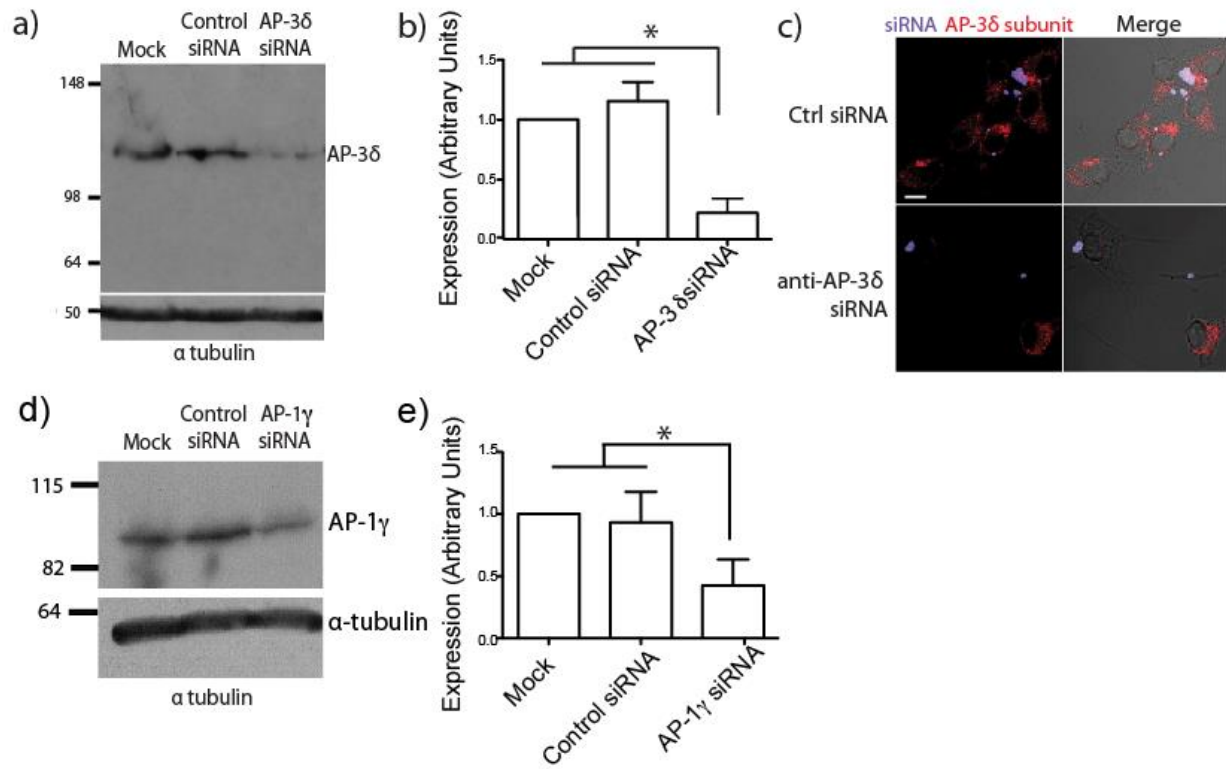


Figure 2.12

**Figure 2.13:** AP-3 $\delta$  and APP colocalize and interact.

a) E15 mouse neurons were cultured and immunostained with antibodies against AP-3 $\delta$  (SA4; red) and APP (APP C-terminal; green). Arrowheads point to colocalized pixels. Scale bars represent 5  $\mu$ m. Inset shows magnified view of the cell body. b) Proximity ligation assay (PLA) demonstrates the interaction of APP and AP-3 $\delta$ . Cells were transiently transfected with  $\beta$ APP-CFP with no siRNA, control siRNA or AP-3 $\delta$  siRNA. Cells were stained with mouse anti- AP-3 $\delta$  and rabbit anti-APP C-terminal antibodies. These were detected with secondary antibodies conjugated to complementary DNA sequences. When proteins are within 40 nm, DNA is ligated and replicated and detected by in-situ fluorescent red dots. AP-3 $\delta$  siRNA substantially reduces the number of red dots. (scale bars represent 10  $\mu$ m) c) Quantification of PLA fluorescent dots in SN56 cells normalized to cell volume (\*p < 0.05).

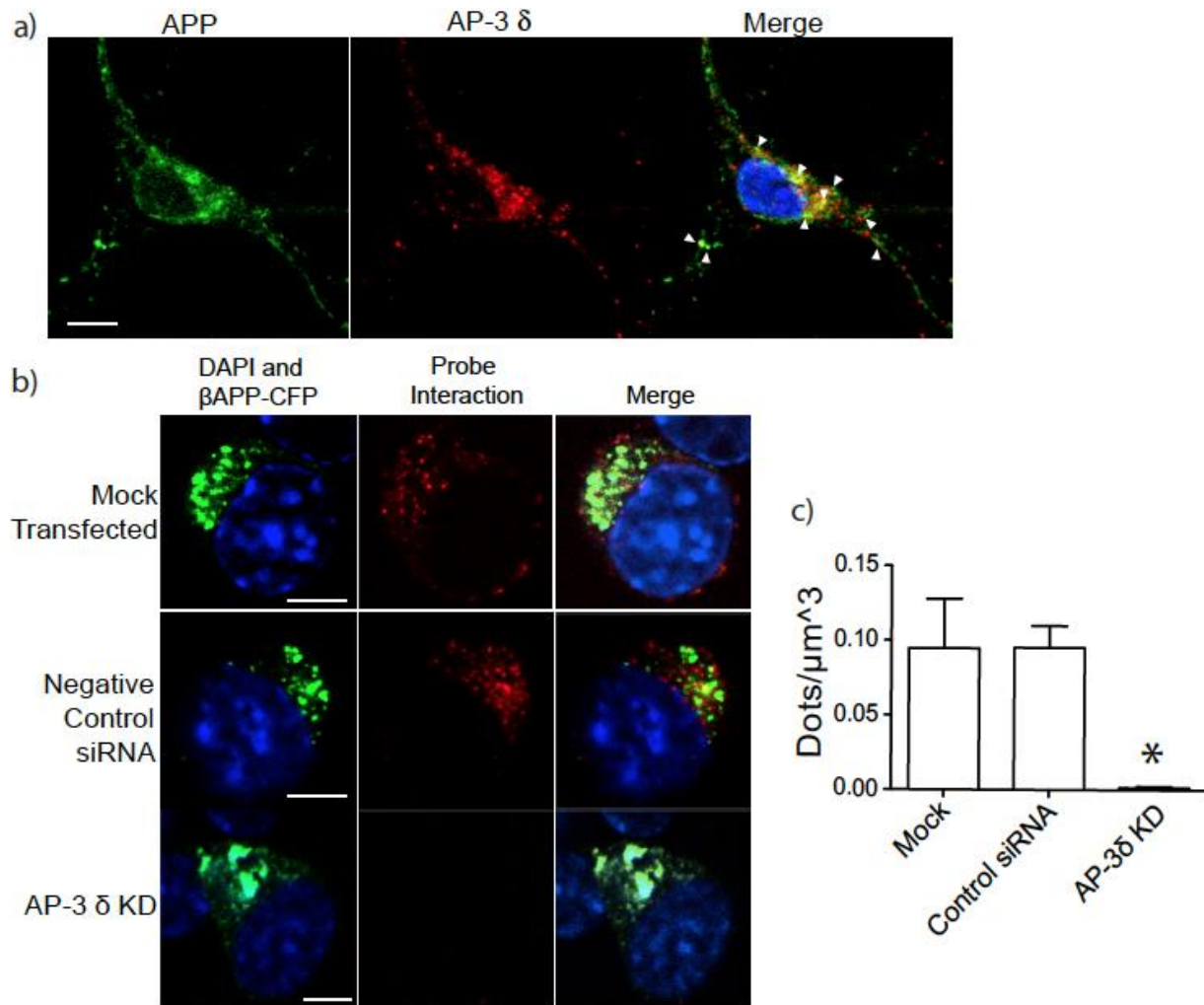


Figure 2.13

### 2.3.6 AP-3 Knockdown Disrupts Trafficking of APP to Lysosomes

We hypothesized that we could disrupt the trafficking of APP to lysosomes by siRNA mediated knockdown of AP-3. As a control, we examined the effect of AP-1 knockdown by siRNA (both AP-1a and AP-1b isoforms) (Figure 2.14). AP-1 belongs to the heterotetrameric family of adaptor proteins, which includes AP-1, AP-2, AP-3, and AP-4. AP-1 mediates the cell surface trafficking and basolateral sorting in epithelial cells [75,76]. As before, we co-transfected cells with  $\beta$ APP-paGFP, GalT-CFP and LAMP1-mRFP with the addition of siRNA against either AP-1 $\gamma$ , AP-3 $\delta$ , or a control siRNA. In cells transfected with active siRNA, a small amount of fluorescently tagged negative control siRNA was included as a marker to identify transfected cells. Cells were photoactivated in irradiation targets placed over the Golgi apparatus, and transport of APP was imaged over a 15-minute period and then analyzed for colocalization of photoactivated APP and LAMP1-mRFP. We found that cells transfected with control siRNA alone did not change  $\beta$ APP-paGFP trafficking to lysosomes, as compared to cells not transfected with siRNA ( $37\pm 5\%$  vs  $37\pm 5\%$ ). However, the siRNA against  $\delta 3$  reduced APP transit to the lysosome to  $16 \pm 3\%$  after 15 minutes of photoactivation. AP-1 $\gamma$  knockdown did not change the trafficking of APP from the TGN to lysosomes ( $34\pm 4\%$ ; Mean $\pm$ SEM) (Figure 2.14a and b). Therefore, AP-3 mediates rapid transport of APP to the lysosome, while AP-1 is not involved in the direct trafficking of APP to lysosomes, at least on the timescale examined here.

To determine the effect of AP-1 knockdown and AP-3 knockdown on APP processing, SN56 cells were transfected with  $\beta$ APP<sub>sw</sub>-CFP and with negative control siRNA, AP-1 siRNA, AP-3 siRNA or a combination of AP-1 and AP-3 siRNAs. Two days after differentiation, culture medium was taken from the cells and analyzed for A $\beta$ 40 and A $\beta$ 42 by ELISA (Invitrogen) (Figure 2.15a). AP-1 siRNA did not significantly alter the levels of A $\beta$  40 [ $106\%\pm 7\%$  (mean $\pm$ SEM)], as compared to control. AP-3 siRNA and combined AP-3 and AP-1 siRNAs reduced the levels of A $\beta$ 40  $54\pm 3\%$  and  $63\pm 6\%$ , respectively ( $p < 0.5$ ). For A $\beta$ 42 (Figure 2.15d), the control siRNA raised A $\beta$ 42 production slightly to  $141\pm 12\%$  (not significant) while siRNAs against AP-1 reduced A $\beta$ 42 levels in the medium to  $75\pm 14\%$  (not significant). Inhibitory siRNA



to AP-3 alone or AP-1 and AP-3 together reduced the levels of A $\beta$ 42 to 64 $\pm$ 13 and 46 $\pm$ 11% respectively (P<0.5) (Figure 2.15b). Therefore, AP-3 KD reduced the levels of A $\beta$ 40 and 42 in the media, and this effect was increased when AP-1 was knocked down as well.

**Figure 2.14:** AP-3 mediates direct trafficking of APP to lysosomes.

a) SN56 cells were transfected with  $\beta$ APP-paGFP, LAMP1-mRFP, GalT-CFP (n=9), and either control siRNA (n=9), siRNA against AP-3 $\delta$  mRNA (n=10) or siRNA against AP-1 $\gamma$  (n=9). Cells were alternately photoactivated with 405 nm light and imaged in the Golgi for 15 minutes (scale bar represents 5  $\mu$ m). White arrowheads in the merged image (far right panel) denote colocalized pixels. Scale bars represent 5  $\mu$ m. b) Percent of  $\beta$ APP-paGFP colocalizing with LAMP1-mRFP at the end of the 15-minute photoactivation period. (\* =  $p < 0.05$ ; Error bars represent standard deviation).

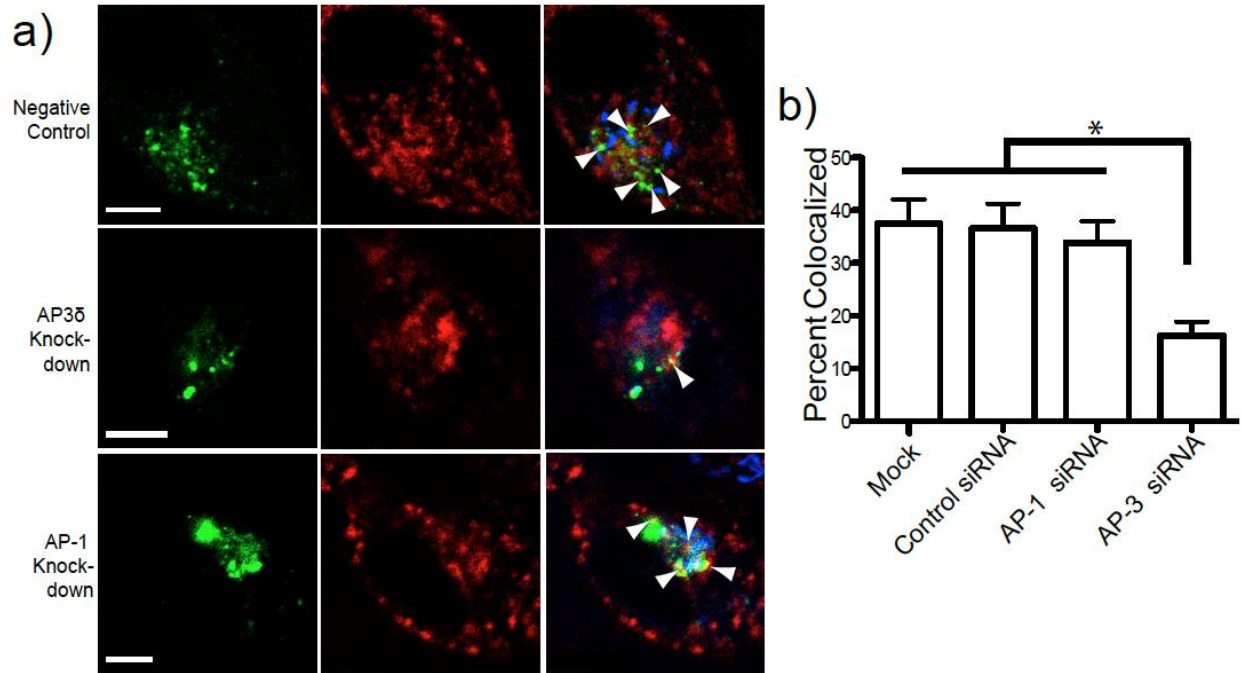


Figure 2.14

**Figure 2.15:** AP-3 mediates processing to A $\beta$ .

SN56 cells were transfected with  $\beta$ APP-paGFP, LAMP1-mRFP, GalT-CFP, and either control siRNA, siRNA against AP-3 $\delta$  mRNA or siRNA against AP-1 $\gamma$ . a) SN56 cells were co-transfected a plasmid expressing  $\beta$ APP<sup>swe</sup>-CFP and with control siRNAs, siRNA against AP-1 $\gamma$ , siRNA against AP-1 $\gamma$  and AP-3 $\delta$  combined, or siRNA against AP-3 $\delta$ . Conditioned media was analyzed for a) A $\beta$ 40 or b) A $\beta$ 42 by ELISA. Experiments were performed 4 times, with each experiment consisting of 2 replicates. (\* indicates significantly different from control.  $p < 0.05$ ; \*\* indicates significantly different from control and either AP-1 or AP-3 alone  $p < 0.05$ ) Error bars represent SEM.

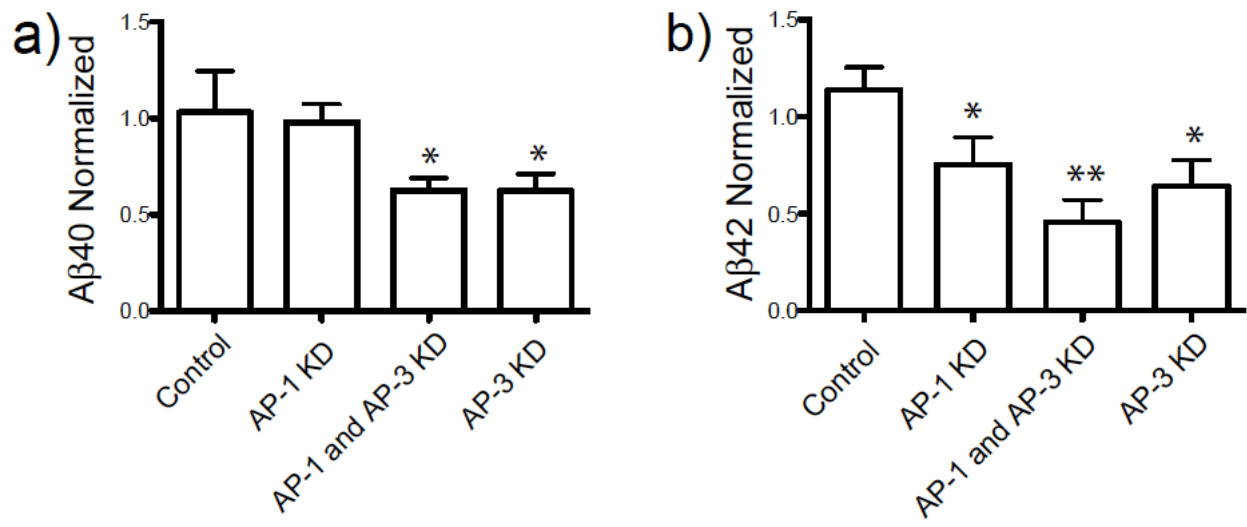


Figure 2.15

## 2.4 Discussion

In this work, we demonstrate the use of paGFP to study the intracellular trafficking of and clearance of APP. While paGFP has been used before to examine APP trafficking [39,40,70], this is the first report to follow APP from the Golgi apparatus into identified downstream compartments and examine its clearance pharmacologically. Although we had expected APP to traffic to the lysosome primarily via the plasma membrane, instead we observed rapid transport of APP to a LAMP1 compartment within seconds, similar to the behavior of LAMP1 [30]. Furthermore, we were able to follow the clearance of  $\beta$ APP-paGFP in from lysosomes, essentially performing a pulse-chase experiment in this organelle in single cells. We show that  $\beta$ APP-paGFP is cleared from the lysosome with first order kinetics, which is faster than the linear loss of fluorescence observed during photobleaching. The clearance of APP from lysosomes is sensitive to both chloroquine, a nonspecific inhibitor of lysosomal function, and L684, 458, a specific gamma-secretase inhibitor. The direct trafficking of APP to this LAMP1 positive compartment is decreased by AP-3 knockdown. The depletion of AP-3 or AP-3 and AP-1 together results in a substantial reduction of A $\beta$  in the media.

Because intracellular compartment markers localizations are not absolute, lysosomal markers can be found in endosomal compartments and vice versa [77,78]. However, several features suggest that APP is moving to a *bona fide* lysosomal compartment. APP appears to be moving primarily to LAMP1 positive compartments, with less moving to compartments labeled with Rab5 and Rab9 (early and late) labeled compartments, suggesting that the main compartment receiving APP is LAMP1 positive and negative for Rab5 and Rab9. Furthermore, after the inhibition of degradation of APP with chloroquine or L685, 458, APP moves to LAMP1-labeled compartments and accumulates in these compartments, implying that they are terminal compartments of the endosomal lysosomal system. Furthermore, that AP-3 knockdown reduces the production and secretion of A $\beta$ 42 by 36% and A $\beta$ 40 by 47% suggests that the lysosome is a major site of APP processing and A $\beta$  production. These features suggest that APP is delivered predominantly to lysosomes.

Prior to this study, most APP trafficking studies suggested that APP primarily moved to the lysosome via the cell surface [79], however the evidence presented here suggests APP can traffic intracellularly from the Golgi to lysosomes. Kuentzel *et al.* found that less than ~20% of nascent APP is transported to the plasma membrane [80], suggesting that this direct lysosomal pathway maybe a major processing pathway of APP. LMPs are known to traffic to the lysosome by at least 2 different pathways. Some LMPs, like lysosomal acid phosphatase, transit first to the cell surface, and then cycle between the plasma membrane and endosomes repetitively before transport to the lysosome [81]. Other proteins, such as LAMP-1, transit intracellularly from the Golgi apparatus to lysosomes, without appearing at the cell surface [82,83]. Our work is in agreement with of Castor *et al.*, who also demonstrated using a temperature-block paradigm that APP in the Golgi apparatus rapidly appears in a LAMP1-positive compartment rapidly after being released from the Golgi [84]. APP now has at least 4 distinct pathways to the lysosome : one from the cell surface through endocytosis into endosomes [85], one directly to lysosomes from the cell surface [50], one through autophagosomes [86], and finally the direct transport from the Golgi apparatus demonstrated here. This suggests that APP is a normal resident Lysosomal Membrane Protein.

This work is not intended to minimize the importance of APP's cell surface trafficking. Indeed, AP-1 knockdown, which is predicted to interfere with APP trafficking to the cell surface, is able to substantially reduce A $\beta$  production indicates that cell surface APP is still a significant source of A $\beta$ . APP transiting to the cell surface is likely not being well visualized in this study for a number of reasons including: 1) activated APP-paGFP arriving at the membrane is diluted by a large amount of non-fluorescent APP already at the membrane, 2) APP has a relatively short half life at the membrane, estimated at 10 minutes [21,85] and 3) we are imaging confocal sections and therefore seeing only a small fraction of the cell membrane itself. Indeed, Golgi apparatus-photoactivated  $\beta$ APP-paGFP becomes visible at the plasma membrane when internalization is inhibited with a  $\gamma$ -secretase inhibitor [61,87], demonstrating that APP can transit rapidly to the cell surface [80].

Several studies have suggested the presence of  $\gamma$ -cleavage in the lysosome. Our own studies have

demonstrated that  $\gamma$ -secretase proteins and activity are present in highly purified lysosomes. Although many studies have observed  $\gamma$ -secretase function at neutral pH, we have found that  $\gamma$ -secretase activity within isolated lysosomal membranes possesses an acidic optimal pH [13]. Our findings are in agreement with previous findings that show a marked accumulation of APP in lysosomes after disruption of lysosomal pH, and inhibit the production of A $\beta$  [17]. Furthermore, many other studies have documented the accumulation of APP fragments in lysosomes after inhibition of lysosomal enzymes or inactivation of PS1 [16,18,20,88], suggesting a critical role for lysosomes in  $\gamma$ -secretase cleavage of APP. However, this is the first study to visualize accumulation of APP CTFs at the lysosomal membrane using a highly selective  $\gamma$ -secretase inhibitor [89-91].

Some investigators have suggested that APP (particularly APP<sup>sw</sup>) undergoes cleavage in the Golgi apparatus and in post-Golgi vesicles [63,92]. Our data appears to show APP and APP<sup>sw</sup> accumulating stably in the Golgi apparatus when trafficking is blocked pharmacologically. Although it is impossible to rule out some processing of APP in the Golgi apparatus with these experiments, these data suggest that the Golgi apparatus is not a major site of A $\beta$  production.

It is interesting that chloroquine and L684, 458 produce similar results. To our knowledge, chloroquine has never been shown to specifically affect the  $\gamma$ -secretase directly in cell free assays. Although our own data has suggests that  $\gamma$ -secretase functions at an acidic pH in the lysosome [13], most authors use a neutral pH [93] or mildly acidic pH [94] for this enzyme. However, efficient  $\gamma$ -secretase function requires the removal of the luminal domain of APP by  $\beta$ -cleavage [95]. The  $\beta$ -secretase is known to transit to the late endosomal/lysosomal compartments [96,97].  $\beta$ -cleavage may also be performed by lysosomal cathepsins [98,99]. With a pH optimum below 4.5 [5,100],  $\beta$ -secretase (like cathepsins) would function optimally in the lysosome. Therefore, the accumulation of APP in the lysosome after chloroquine could be by non-specifically inhibiting a luminal pH dependent  $\beta$ -secretase or  $\beta$ -like cleaving enzyme, which then secondarily inhibits  $\gamma$ -cleavage. When  $\beta$ -cleavage is accelerated by the APP<sup>sw</sup> mutation, APP-paGFP is cleared so rapidly that it cannot be imaged in the lysosome. This suggests that, rather than being a tightly controlled regulatory enzyme, the  $\gamma$ -secretase behaves more like a



“proteasome of the membrane” whose job is to remove transmembrane stubs of proteins from the membrane [101].

Our results also demonstrate that lysosomal trafficking of APP may be an important mechanism of regulating APP cleavage. Specifically AP-3 knockdown reduces lysosomal trafficking of APP from the Golgi apparatus and reduces A $\beta$  production and this effect is additive to AP-1 knock down. A wide range of other proteins likely also likely regulate APP processing by altering its trafficking including GGA1 [102,103], X11a, Fe65 [104,105], AP-4 [106], VPS35 [25] and SorLa [26,27,39]. These studies suggest that control of APP processing by intracellular trafficking may be crucial for regulating A $\beta$  production.

These findings may have broad importance for the pathophysiology of AD. This is because the lysosome’s biochemical milieu and acidic pH make it the ideal environment for the nucleation of amyloid fibrils [107,108]. In fact, the lysosome has been proposed to be a site of A $\beta$  aggregate seeding [109-111]. This development of A $\beta$  aggregates has been shown to disrupt synapses [112] and membranes [113], and can lead to lysosomal rupture leading to cell death [114,115]. A $\beta$  may be secreted in exosomes, which are intraluminal vesicles released from the endosomal/lysosomal system [58,116]. Therefore, A $\beta$  and its higher-order aggregates may be produced, nucleated, and secreted from lysosomes. The lysosome sits at a crossroad, as a site for the production and degradation of A $\beta$ , as well as its fibrillogenesis. This work points to the importance of the lysosomal system in APP processing and its regulation in developing therapeutic treatments for AD.

## 2.5 References

1. Mebane-Sims I. 2009 Alzheimer's disease facts and figures. *Alzheimers Dement.* 2009;5: 234–270. doi:10.1016/j.jalz.2009.03.001
2. Nelson PT, Braak H, Markesbery WR. Neuropathology and cognitive impairment in Alzheimer disease: a complex but coherent relationship. *J Neuropathol Exp Neurol.* 2009;68: 1–14. doi:10.1097/NEN.0b013e3181919a48
3. Lin X, Koelsch G, Wu S, Downs D, Dashti A, Tang J. Human aspartic protease memapsin 2 cleaves the beta-secretase site of beta-amyloid precursor protein. *Proc Natl Acad Sci USA.* 2000;97: 1456–1460.
4. Hussain I, Powell D, Howlett DR, Tew DG. Identification of a Novel Aspartic Protease (Asp 2) as  $\beta$ -Secretase. *Molecular and Cellular* .... 1999.
5. Vassar R, Bennett BD, Babu-Khan S, Kahn S, Mendiaz EA, Denis P, et al. Beta-secretase cleavage of Alzheimer's amyloid precursor protein by the transmembrane aspartic protease BACE. *Science.* 1999;286: 735–741.
6. Periz G, Fortini ME. Functional reconstitution of gamma-secretase through coordinated expression of presenilin, nicastrin, Aph-1, and Pen-2. *J Neurosci Res.* 2004;77: 309–322. doi:10.1002/jnr.20203
7. Golde TE. The Abeta hypothesis: leading us to rationally-designed therapeutic strategies for the treatment or prevention of Alzheimer disease. *Brain Pathology.* 2005;15: 84–87. doi:10.1111/j.1750-3639.2005.tb00104.x
8. Lambert MP, Barlow AK, Chromy BA, Edwards C, Freed R, Liosatos M, et al. Diffusible, nonfibrillar ligands derived from Abeta1-42 are potent central nervous system neurotoxins. *Proc Natl Acad Sci USA.* 1998;95: 6448–6453.
9. Pike CJ, Burdick D, Walencewicz AJ, Glabe CG, Cotman CW. Neurodegeneration induced by beta-amyloid peptides in vitro: the role of peptide assembly state. *J Neurosci.* 1993;13: 1676–1687.
10. Iwatsubo T, Odaka A, Suzuki N, Mizusawa H, Nukina N, Ihara Y. Visualization of A beta 42(43) and A beta 40 in senile plaques with end-specific A beta monoclonals: evidence that an initially deposited species is A beta 42(43). *Neuron.* 1994;13: 45–53.
11. Gravina SA, Ho L, Eckman CB, Long KE, Otvos L, Younkin LH, et al. Amyloid beta protein (A beta) in Alzheimer's disease brain. Biochemical and immunocytochemical analysis with antibodies specific for forms ending at A beta 40 or A beta 42(43). *Journal*

- of Biological Chemistry. 1995;270: 7013–7016.
12. Bagshaw RD, Pasternak SH, Mahuran DJ, Callahan JW. Nicastrin is a resident lysosomal membrane protein. *Biochemical and Biophysical Research Communications*. 2003;300: 615–618.
  13. Pasternak SH, Bagshaw RD, Guiral M, Zhang S, Ackerley CA, Pak BJ, et al. Presenilin-1, nicastrin, amyloid precursor protein, and gamma-secretase activity are co-localized in the lysosomal membrane. *J Biol Chem*. 2003;278: 26687–26694. doi:10.1074/jbc.M212192200
  14. Yu WH, Kumar A, Peterhoff C, Shapiro Kulnane L, Uchiyama Y, Lamb BT, et al. Autophagic vacuoles are enriched in amyloid precursor protein-secretase activities: implications for beta-amyloid peptide over-production and localization in Alzheimer's disease. *Int J Biochem Cell Biol*. 2004;36: 2531–2540. doi:10.1016/j.biocel.2004.05.010
  15. Jutras I, Laplante A, Boulais J, Brunet S, Thinakaran G, Desjardins M. Gamma-secretase is a functional component of phagosomes. *J Biol Chem*. 2005;280: 36310–36317. doi:10.1074/jbc.M504069200
  16. Siman R, Mistretta S, Durkin JT, Savage MJ, Loh T, Trusko S, et al. Processing of the beta-amyloid precursor. Multiple proteases generate and degrade potentially amyloidogenic fragments. *J Biol Chem*. 1993;268: 16602–16609.
  17. Schrader-Fischer G, Paganetti PA. Effect of alkalizing agents on the processing of the beta-amyloid precursor protein. *Brain Research*. 1996;716: 91–100. doi:10.1016/0006-8993(96)00002-9
  18. Golde T, Estus S, Younkin L, Selkoe D, Younkin S. Processing of the amyloid protein precursor to potentially amyloidogenic derivatives. *Science*. 1992;255: 728–730. doi:10.1126/science.1738847
  19. Higaki J, Quon D, Zhong Z, Cordell B. Inhibition of beta-amyloid formation identifies proteolytic precursors and subcellular site of catabolism. *Neuron*. 1995;14: 651–659.
  20. Chen F, Yang DS, Petanceska S, Yang A, Tandon A, Yu G, et al. Carboxyl-terminal fragments of Alzheimer beta-amyloid precursor protein accumulate in restricted and unpredicted intracellular compartments in presenilin 1-deficient cells. *Journal of Biological Chemistry*. 2000;275: 36794–36802. doi:10.1074/jbc.M006986200
  21. Koo EH, Squazzo SL. Evidence that production and release of amyloid beta-protein involves the endocytic pathway. *J Biol Chem*. 1994;269: 17386–17389.
  22. Perez RG, Squazzo SL, Koo EH. Enhanced release of amyloid beta-protein from codon 670/671 “Swedish” mutant beta-amyloid precursor protein occurs in both secretory and endocytic pathways. *J Biol Chem*. 1996;271: 9100–9107.

23. Grbovic OM. Rab5-stimulated Up-regulation of the Endocytic Pathway Increases Intracellular  $\beta$ -Cleaved Amyloid Precursor Protein Carboxyl-terminal Fragment Levels and A $\beta$  Production. *Journal of Biological Chemistry*. 2003;278: 31261–31268. doi:10.1074/jbc.M304122200
24. Capell A, Meyn L, Fluhrer R, Teplow DB, Walter J, Haass C. Apical sorting of beta-secretase limits amyloid beta-peptide production. *Journal of Biological Chemistry*. 2002;277: 5637–5643. doi:10.1074/jbc.M109119200
25. Wen L, Tang F-L, Hong Y, Luo S-W, Wang C-L, He W, et al. VPS35 haploinsufficiency increases Alzheimer's disease neuropathology. *Journal of Cell Biology*. Rockefeller Univ Press; 2011;195: 765–779.
26. Rogaeva E, Meng Y, Lee JH, Gu Y, Kawarai T, Zou F, et al. The neuronal sortilin-related receptor SORL1 is genetically associated with Alzheimer disease. *Nat Genet*. 2007;39: 168–177. doi:10.1038/ng1943
27. Andersen OM, Reiche J, Schmidt V, Gotthardt M, Spoelgen R, Behlke J, et al. Neuronal sorting protein-related receptor sorLA/LR11 regulates processing of the amyloid precursor protein. *Proc Natl Acad Sci USA*. 2005;102: 13461–13466. doi:10.1073/pnas.0503689102
28. Gu F, Crump CM, Thomas G. Trans-Golgi network sorting. *Cell Mol Life Sci*. 2001;58: 1067–1084.
29. Patterson GH, Lippincott-Schwartz J. Selective photolabeling of proteins using photoactivatable GFP. *Methods*. 2004;32: 445–450. doi:10.1016/j.ymeth.2003.10.006
30. Patterson GH, Patterson GH, Lippincott-Schwartz J. A photoactivatable GFP for selective photolabeling of proteins and cells. *Science*. American Association for the Advancement of Science; 2002;297: 1873–1877. doi:10.1126/science.1074952
31. Hirschberg K, Miller CM, Ellenberg J, Presley JF, Siggia ED, Phair RD, et al. Kinetic analysis of secretory protein traffic and characterization of golgi to plasma membrane transport intermediates in living cells. *The Journal of Cell Biology*. 1998;143: 1485–1503.
32. Kim PK, Mullen RT, Schumann U, Lippincott-Schwartz J. The origin and maintenance of mammalian peroxisomes involves a de novo PEX16-dependent pathway from the ER. *Journal of Cell Biology*. 2006;173: 521–532. doi:10.1083/jcb.200601036
33. Hailey DW, Rambold AS, Satpute-Krishnan P, Mitra K, Sougrat R, Kim PK, et al. Mitochondria supply membranes for autophagosome biogenesis during starvation. *Cell*. 2010;141: 656–667. doi:10.1016/j.cell.2010.04.009
34. Honkura N, Matsuzaki M, Noguchi J, Ellis-Davies GCR, Kasai H. The subspine

- organization of actin fibers regulates the structure and plasticity of dendritic spines. *Neuron*. 2008;57: 719–729. doi:10.1016/j.neuron.2008.01.013
35. Bhalla A, Vetanovetz CP, Morel E, Chamoun Z, Di Paolo G, Small SA. The location and trafficking routes of the neuronal retromer and its role in amyloid precursor protein transport. *Neurobiology of Disease*. 2012;47: 126–134. doi:10.1016/j.nbd.2012.03.030
  36. Fjorback AW, Seaman M, Gustafsen C, Mehmedbasic A, Gokool S, Wu C, et al. Retromer binds the FANSHY sorting motif in SorLA to regulate amyloid precursor protein sorting and processing. *Journal of Neuroscience*. 2012;32: 1467–1480. doi:10.1523/JNEUROSCI.2272-11.2012
  37. Ludwig A, Blume J, Diep T-M, Yuan J, Mateos JM, Leuthäuser K, et al. Calsyntenins mediate TGN exit of APP in a kinesin-1-dependent manner. *Traffic*. 2009;10: 572–589. doi:10.1111/j.1600-0854.2009.00886.x
  38. Scott DA, Das U, Tang Y, Roy S. Mechanistic logic underlying the axonal transport of cytosolic proteins. *Neuron*. 2011;70: 441–454. doi:10.1016/j.neuron.2011.03.022
  39. Schmidt V, Sporbert A, Rohe M, Reimer T, Rehm A, Andersen OM, et al. SorLA/LR11 regulates processing of amyloid precursor protein via interaction with adaptors GGA and PACS-1. *J Biol Chem*. 2007;282: 32956–32964. doi:10.1074/jbc.M705073200
  40. Herl L, Thomas AV, Lill CM, Banks M, Deng A, Jones PB, et al. Mutations in amyloid precursor protein affect its interactions with presenilin/gamma-secretase. *Mol Cell Neurosci*. 2009;41: 166–174. doi:10.1016/j.mcn.2009.02.008
  41. Storrie B, White J, Röttger S, Stelzer EH, Saganuma T, Nilsson T. Recycling of golgi-resident glycosyltransferases through the ER reveals a novel pathway and provides an explanation for nocodazole-induced Golgi scattering. *Journal of Cell Biology*. 1998;143: 1505–1521.
  42. Chavrier P, Parton RG, Hauri HP, Simons K, Zerial M. Localization of low molecular weight GTP binding proteins to exocytic and endocytic compartments. *Cell*. 1990;62: 317–329.
  43. Gorvel JP, Chavrier P, Zerial M, Gruenberg J. rab5 controls early endosome fusion in vitro. *Cell*. 1991;64: 915–925.
  44. Bucci C, Parton RG, Mather IH, Stunnenberg H, Simons K, Hoflack B, et al. The small GTPase rab5 functions as a regulatory factor in the early endocytic pathway. *Cell*. 1992;70: 715–728. doi:10.1016/0092-8674(92)90306-W
  45. Soldati T, Rancaño C, Geissler H, Pfeffer SR. Rab7 and Rab9 are recruited onto late endosomes by biochemically distinguishable processes. *J Biol Chem*. 1995;270: 25541–25548. Available:

<http://eutils.ncbi.nlm.nih.gov/entrez/eutils/elink.fcgi?dbfrom=pubmed&id=7592724&retmode=ref&cmd=prlinks>

46. Aivazian D, Serrano RL, Pfeffer S. TIP47 is a key effector for Rab9 localization. *Journal of Cell Biology*. 2006;173: 917–926. doi:10.1083/jcb.200510010
47. Chen JW, Murphy TL, Willingham MC, Pastan I, August JT. Identification of two lysosomal membrane glycoproteins. *The Journal of Cell Biology*. 1985;101: 85–95.
48. Howe CL, Granger BL, Hull M, Green SA, Gabel CA, Helenius A, et al. Derived protein sequence, oligosaccharides, and membrane insertion of the 120-kDa lysosomal membrane glycoprotein (lgp120): identification of a highly conserved family of lysosomal membrane glycoproteins. *Proc Natl Acad Sci USA*. 1988;85: 7577–7581.
49. Muresan V, Varvel NH, Lamb BT, Muresan Z. The cleavage products of amyloid-beta precursor protein are sorted to distinct carrier vesicles that are independently transported within neurites. *Journal of Neuroscience*. 2009;29: 3565–3578. doi:10.1523/JNEUROSCI.2558-08.2009
50. Lorenzen A, Samosh J, Vandewark K, Anborgh PH, Seah C, Magalhaes AC, et al. Rapid and Direct Transport of Cell Surface APP to the Lysosome defines a novel selective pathway. *Mol Brain*. 2010;3: 11. doi:10.1186/1756-6606-3-11
51. Hammond DN, Wainer BH, Tonsgard JH, Heller A. Neuronal properties of clonal hybrid cell lines derived from central cholinergic neurons. *Science*. American Association for the Advancement of Science; 1986;234: 1237–1240. doi:10.1126/science.3775382
52. Pedersen WA, Kloczewiak MA, Blusztajn JK. Amyloid beta-protein reduces acetylcholine synthesis in a cell line derived from cholinergic neurons of the basal forebrain. *Proc Natl Acad Sci USA*. 1996;93: 8068–8071.
53. Díaz E, Pfeffer SR. TIP47: a cargo selection device for mannose 6-phosphate receptor trafficking. *Cell*. 1998;93: 433–443.
54. Bucci C, Thomsen P, Nicoziani P, McCarthy J, van Deurs B. Rab7: a key to lysosome biogenesis. *Mol Biol Cell*. 2000;11: 467–480.
55. Presley JF, Cole NB, Schroer TA, Hirschberg K, Zaal KJ, Lippincott-Schwartz J. ER-to-Golgi transport visualized in living cells. *Nature*. 1997;389: 81–85. doi:10.1038/38001
56. Sevier CS, Weisz OA, Davis M, Machamer CE. Efficient export of the vesicular stomatitis virus G protein from the endoplasmic reticulum requires a signal in the cytoplasmic tail that includes both tyrosine-based and di-acidic motifs. *Mol Biol Cell*. 2000;11: 13–22.

57. Samson F, Donoso JA, Heller-Bettinger I, Watson D, Himes RH. Nocodazole action on tubulin assembly, axonal ultrastructure and fast axoplasmic transport. *J Pharmacol Exp Ther.* 1979;208: 411–417.
58. Vingtdeux V, Hamdane M, Loyens A, Gelé P, Drobeck H, Bégard S, et al. Alkalinizing drugs induce accumulation of amyloid precursor protein by-products in luminal vesicles of multivesicular bodies. *J Biol Chem.* 2007;282: 18197–18205. doi:10.1074/jbc.M609475200
59. Vingtdeux V, Hamdane M, Bégard S, Loyens A, Delacourte A, Beauvillain J-C, et al. Intracellular pH regulates amyloid precursor protein intracellular domain accumulation. *Neurobiology of Disease.* 2007;25: 686–696. doi:10.1016/j.nbd.2006.09.019
60. Shearman MS, Beher D, Clarke EE, Lewis HD, Harrison T, Hunt P, et al. L-685,458, an Aspartyl Protease Transition State Mimic, Is a Potent Inhibitor of Amyloid  $\beta$ -Protein Precursor  $\gamma$ -Secretase Activity. *Biochemistry.* 2000;39: 8698–8704. doi:10.1021/bi0005456
61. Tarassishin L, Yin YI, Bassit B, Li Y-M. Processing of Notch and amyloid precursor protein by gamma-secretase is spatially distinct. *Proc Natl Acad Sci USA.* 2004;101: 17050–17055. doi:10.1073/pnas.0408007101
62. Kaether C. Presenilin-1 affects trafficking and processing of betaAPP and is targeted in a complex with nicastrin to the plasma membrane. *The Journal of Cell Biology.* 2002;158: 551–561. doi:10.1083/jcb.200201123
63. Thinakaran G, Teplow DB, Siman R, Greenberg B, Sisodia SS. Metabolism of the "Swedish" amyloid precursor protein variant in neuro2a (N2a) cells. Evidence that cleavage at the "beta-secretase" site occurs in the golgi apparatus. *J Biol Chem.* 1996;271: 9390–9397.
64. De Strooper B, Craessaerts K, van Leuven F, Van den Berghe H. Exchanging the extracellular domain of amyloid precursor protein for horseradish peroxidase does not interfere with alpha-secretase cleavage of the beta-amyloid region, but randomizes secretion in Madin-Darby canine kidney cells. *J Biol Chem.* 1995;270: 30310–30314.
65. Mullan M, Crawford F, Axelman K, Houlden H, Lilius L, Winblad B, et al. A pathogenic mutation for probable Alzheimer's disease in the APP gene at the N-terminus of beta-amyloid. *Nat Genet.* 1992;1: 345–347. doi:10.1038/ng0892-345
66. Citron M, Oltersdorf T, Haass C, McConlogue L, Hung AY, Seubert P, et al. Mutation of the beta-amyloid precursor protein in familial Alzheimer's disease increases beta-protein production. *Nature.* 1992;360: 672–674. doi:10.1038/360672a0
67. Gupta SN, Kloster MM, Rodionov DG, Bakke O. Re-routing of the invariant chain to

- the direct sorting pathway by introduction of an AP3-binding motif from LIMP II. *European Journal of Cell Biology*. 2006;85: 457–467. doi:10.1016/j.ejcb.2006.02.001
68. Ihrke G, Kyttala A, Russell MRG, Rous BA, Luzio JP. Differential Use of Two AP-3-mediated Pathways by Lysosomal Membrane Proteins. *Traffic*. 2004;5: 946–962. doi:10.1111/j.1600-0854.2004.00236.x
69. Le Borgne R, Alconada A, Bauer U, Hoflack B. The mammalian AP-3 adaptor-like complex mediates the intracellular transport of lysosomal membrane glycoproteins. *J Biol Chem*. 1998;273: 29451–29461.
70. Rohrer J, Schweizer A, Russell D, Kornfeld S. The targeting of Lamp1 to lysosomes is dependent on the spacing of its cytoplasmic tail tyrosine sorting motif relative to the membrane. *The Journal of Cell Biology*. 1996;132: 565–576.
71. Rous BA, Reaves BJ, Ihrke G, Briggs JAG, Gray SR, Stephens DJ, et al. Role of adaptor complex AP-3 in targeting wild-type and mutated CD63 to lysosomes. *Mol Biol Cell*. 2002;13: 1071–1082. doi:10.1091/mbc.01-08-0409
72. Kantheti P, Qiao X, Diaz ME, Peden AA, Meyer GE, Carskadon SL, et al. Mutation in AP-3 delta in the mocha mouse links endosomal transport to storage deficiency in platelets, melanosomes, and synaptic vesicles. *Neuron*. 1998;21: 111–122.
73. Greenberg JI, Shields DJ, Barillas SG, Acevedo LM, Murphy E, Huang J, et al. A role for VEGF as a negative regulator of pericyte function and vessel maturation. *Nature*. 2008;456: 809–813. doi:10.1038/nature07424
74. Cai J, Chen Z, Ruan Q, Han S, Liu L, Qi X, et al.  $\gamma$ -Secretase and presenilin mediate cleavage and phosphorylation of vascular endothelial growth factor receptor-1. *Journal of Biological Chemistry*. 2011;286: 42514–42523. doi:10.1074/jbc.M111.296590
75. Folsch H. The AP-1A and AP-1B clathrin adaptor complexes define biochemically and functionally distinct membrane domains. *The Journal of Cell Biology*. 2003;163: 351–362. doi:10.1083/jcb.200309020
76. Gravotta D, Carvajal-Gonzalez JM, Mattera R, Deborde S, Banfelder JR, Bonifacino JS, et al. The clathrin adaptor AP-1A mediates basolateral polarity. *Developmental Cell*. 2012;22: 811–823. doi:10.1016/j.devcel.2012.02.004
77. Saftig P, Klumperman J. Lysosome biogenesis and lysosomal membrane proteins: trafficking meets function. *Nature Publishing Group*; 2009;: 1–13. doi:10.1038/nrm2745
78. Bagshaw RD, Mahuran DJ, Callahan JW. A proteomic analysis of lysosomal integral membrane proteins reveals the diverse composition of the organelle. *Mol Cell Proteomics*. 2005;4: 133–143. doi:10.1074/mcp.M400128-MCP200



79. Thinakaran G, Koo EH. Amyloid Precursor Protein Trafficking, Processing, and Function. *Journal of Biological Chemistry*. 2008;283: 29615–29619. doi:10.1074/jbc.R800019200
80. Kuentzel SL, Ali SM, Altman RA, Greenberg BD, Raub TJ. The Alzheimer beta-amyloid protein precursor/protease nexin-II is cleaved by secretase in a trans-Golgi secretory compartment in human neuroglioma cells. *Biochem J*. 1993;295 ( Pt 2): 367–378.
81. Braun M, Waheed A, Figura von K. Lysosomal acid phosphatase is transported to lysosomes via the cell surface. *The EMBO Journal*. 1989;8: 3633–3640.
82. Barriocanal JG, Bonifacino JS, Yuan L, Sandoval IV. Biosynthesis, glycosylation, movement through the Golgi system, and transport to lysosomes by an N-linked carbohydrate-independent mechanism of three lysosomal integral membrane proteins. *Journal of Biological Chemistry*. 1986;261: 16755–16763.
83. D'Souza MP, August JT. A kinetic analysis of biosynthesis and localization of a lysosome-associated membrane glycoprotein. *Archives of Biochemistry and Biophysics*. 1986;249: 522–532.
84. Caster AH, Kahn RA. Recruitment of the Mint3 adaptor is necessary for export of the amyloid precursor protein (APP) from the Golgi complex. *J Biol Chem*. 2013;288: 28567–28580. doi:10.1074/jbc.M113.481101
85. Koo EH, Squazzo SL, Selkoe DJ, Koo CH. Trafficking of cell-surface amyloid beta-protein precursor. I. Secretion, endocytosis and recycling as detected by labeled monoclonal antibody. *Journal of Cell Science*. 1996;109 ( Pt 5): 991–998.
86. Yu WH, Cuervo AM, Kumar A, Peterhoff CM, Schmidt SD, Lee J-H, et al. Macroautophagy--a novel Beta-amyloid peptide-generating pathway activated in Alzheimer's disease. *Journal of Cell Biology*. 2005;171: 87–98. doi:10.1083/jcb.200505082
87. Kaether C, Lammich S, Edbauer D, Ertl M, Rietdorf J, Capell A, et al. Presenilin-1 affects trafficking and processing of  $\beta$ APP and is targeted in a complex with nicastrin to the plasma membrane. *Journal of Cell Biology*. Rockefeller Univ Press; 2002;158: 551–561.
88. Haass C, Koo EH, Mellon A, Hung AY, Selkoe DJ. Targeting of cell-surface beta-amyloid precursor protein to lysosomes: alternative processing into amyloid-bearing fragments. *Nature*. 1992;357: 500–503. doi:10.1038/357500a0
89. Pratt KG, Zhu P, Watari H, Cook DG, Sullivan JM. A novel role for {gamma}-secretase: selective regulation of spontaneous neurotransmitter release from

- hippocampal neurons. *Journal of Neuroscience*. 2011;31: 899–906.  
doi:10.1523/JNEUROSCI.4625-10.2011
90. Sharples RA, Vella LJ, Nisbet RM, Naylor R, Perez K, Barnham KJ, et al. Inhibition of gamma-secretase causes increased secretion of amyloid precursor protein C-terminal fragments in association with exosomes. *The FASEB Journal*. 2008;22: 1469–1478.  
doi:10.1096/fj.07-9357com
  91. Tian G. Linear Non-competitive Inhibition of Solubilized Human gamma -Secretase by Pepstatin A Methylester, L685458, Sulfonamides, and Benzodiazepines. *Journal of Biological Chemistry*. 2002;277: 31499–31505. doi:10.1074/jbc.M112328200
  92. Haass C, Koo EH, Capell A, Teplow DB, Selkoe DJ. Polarized sorting of beta-amyloid precursor protein and its proteolytic products in MDCK cells is regulated by two independent signals. *The Journal of Cell Biology*. 1995;128: 537–547.
  93. Ye W, Selkoe DJ, Wolfe MS. Activity-dependent isolation of the presenilin- gamma -secretase complex reveals nicastrin and a gamma substrate. *Proc Natl Acad Sci USA*. 2002;99: 2720–2725. doi:10.1073/pnas.052436599
  94. Winkler E, Hobson S, Fukumori A, Dümpelfeld B, Luebbers T, Baumann K, et al. Purification, Pharmacological Modulation, and Biochemical Characterization of Interactors of Endogenous Human  $\gamma$ -Secretase †. *Biochemistry*. American Chemical Society; 2009;48: 1183–1197. doi:10.1021/bi801204g
  95. Struhl G, Adachi A. Requirements for presenilin-dependent cleavage of notch and other transmembrane proteins. *Molecular Cell*. 2000;6: 625–636. doi:10.1016/S1097-2765(00)00061-7
  96. Koh YH, Arnim von CAF, Hyman BT, Tanzi RE, Tesco G. BACE is degraded via the lysosomal pathway. *J Biol Chem*. 2005;280: 32499–32504.  
doi:10.1074/jbc.M506199200
  97. Kinoshita A, Whelan CM, Smith CJ, Mikhailenko I, Rebeck GW, Strickland DK, et al. Demonstration by fluorescence resonance energy transfer of two sites of interaction between the low-density lipoprotein receptor-related protein and the amyloid precursor protein: role of the intracellular adapter protein Fe65. *Journal of Neuroscience*. 2001;21: 8354–8361.
  98. Hook VYH, Kindy M, Reinheckel T, Peters C, Hook G. Genetic cathepsin B deficiency reduces beta-amyloid in transgenic mice expressing human wild-type amyloid precursor protein. *Biochemical and Biophysical Research Communications*. 2009;386: 284–288.  
doi:10.1016/j.bbrc.2009.05.131
  99. Schechter I, Ziv E. Kinetic properties of cathepsin D and BACE 1 indicate the need to

- search for additional beta-secretase candidate(s). 2008;389: 313–320.  
doi:10.1515/BC.2008.025
100. Grüniger-Leitch F, Schlatter D, Küng E, Nelböck P, Döbeli H. Substrate and inhibitor profile of BACE (beta-secretase) and comparison with other mammalian aspartic proteases. *J Biol Chem*. 2002;277: 4687–4693. doi:10.1074/jbc.M109266200
  101. Kopan R, Ilagan MXG. Gamma-secretase: proteasome of the membrane? *Nat Rev Mol Cell Biol*. 2004;5: 499–504. doi:10.1038/nrm1406
  102. Arnim von CAF, Tangredi MM, Peltan ID, Lee BM, Irizarry MC, Kinoshita A, et al. Demonstration of BACE (beta-secretase) phosphorylation and its interaction with GGA1 in cells by fluorescence-lifetime imaging microscopy. *Journal of Cell Science*. 2004;117: 5437–5445. doi:10.1242/jcs.01422
  103. Arnim von CAF. GGA1 Acts as a Spatial Switch Altering Amyloid Precursor Protein Trafficking and Processing. *Journal of Neuroscience*. 2006;26: 9913–9922. doi:10.1523/JNEUROSCI.2290-06.2006
  104. King GD, Perez RG, Steinhilb ML, Gaut JR, Turner RS. X11 $\alpha$  modulates secretory and endocytic trafficking and metabolism of amyloid precursor protein: mutational analysis of the yenpty sequence. *Neuroscience*. 2003;120: 143–154. doi:10.1016/S0306-4522(03)00284-7
  105. McLoughlin DM, Miller CCJ. The FE65 proteins and Alzheimer's disease. *J Neurosci Res*. 2008;86: 744–754. doi:10.1002/jnr.21532
  106. Burgos PV, Mardones GA, Rojas AL, daSilva LLP, Prabhu Y, Hurley JH, et al. Sorting of the Alzheimer's disease amyloid precursor protein mediated by the AP-4 complex. *Developmental Cell*. 2010;18: 425–436. doi:10.1016/j.devcel.2010.01.015
  107. Su Y, Chang PT. Acidic pH promotes the formation of toxic fibrils from beta-amyloid peptide. *Brain Research*. 2001;893: 287–291.
  108. Waschuk SA, Elton EA, Darabie AA, Fraser PE, McLaurin JA. Cellular membrane composition defines A beta-lipid interactions. *J Biol Chem*. 2001;276: 33561–33568. doi:10.1074/jbc.M103598200
  109. Hu X, Crick SL, Bu G, Frieden C, Pappu RV, Lee J-M. Amyloid seeds formed by cellular uptake, concentration, and aggregation of the amyloid-beta peptide. *Proceedings of the National Academy of Sciences*. 2009;106: 20324–20329. doi:10.1073/pnas.0911281106
  110. Tam JH, Pasternak SH. Amyloid and Alzheimer's disease: inside and out. *Can J Neurol Sci*. 2012;39: 286–298.

111. LaFerla FM, Green KN, Oddo S. Intracellular amyloid-beta in Alzheimer's disease. *Nat Rev Neurosci.* 2007;8: 499–509. doi:10.1038/nrn2168
112. Takahashi RH, Milner TA, Li F, Nam EE, Edgar MA, Yamaguchi H, et al. Intraneuronal Alzheimer abeta42 accumulates in multivesicular bodies and is associated with synaptic pathology. *Am J Pathol.* 2002;161: 1869–1879.
113. McLaurin J, Chakrabartty A. Membrane disruption by Alzheimer beta-amyloid peptides mediated through specific binding to either phospholipids or gangliosides. Implications for neurotoxicity. *J Biol Chem.* 1996;271: 26482–26489. doi:10.1074/jbc.271.43.26482
114. Yang AJ, Chandswangbhuvana D, Margol L, Glabe CG. Loss of endosomal/lysosomal membrane impermeability is an early event in amyloid Abeta1-42 pathogenesis. *J Neurosci Res.* 1998;52: 691–698. doi:10.1002/(SICI)1097-4547(19980615)52:6<691::AID-JNR8>3.0.CO;2-3
115. Liu R-Q, Zhou Q-H, Ji S-R, Zhou Q, Feng D, Wu Y, et al. Membrane localization of beta-amyloid 1-42 in lysosomes: a possible mechanism for lysosome labilization. *J Biol Chem.* 2010;285: 19986–19996. doi:10.1074/jbc.M109.036798
116. Rajendran L, Honsho M, Zahn TR, Keller P, Geiger KD, Verkade P, et al. Alzheimer's disease beta-amyloid peptides are released in association with exosomes. *Proc Natl Acad Sci USA.* 2006;103: 11172–11177. doi:10.1073/pnas.0603838103
117. Peden AA. Localization of the AP-3 adaptor complex defines a novel endosomal exit site for lysosomal membrane proteins. *The Journal of Cell Biology.* 2004;164: 1065–1076. doi:10.1083/jcb.200311064
118. Fortin A, Cregan SP, MacLaurin JG, Kushwaha N, Hickman ES, Thompson CS, et al. APAF1 is a key transcriptional target for p53 in the regulation of neuronal cell death. *Journal of Cell Biology.* 2001;155: 207–216. doi:10.1083/jcb.200105137
119. Zhang H, Xing L, Rossoll W, Wichterle H, Singer RH, Bassell GJ. Multiprotein complexes of the survival of motor neuron protein SMN with Gemins traffic to neuronal processes and growth cones of motor neurons. *Journal of Neuroscience.* 2006;26: 8622–8632. doi:10.1523/JNEUROSCI.3967-05.2006
120. Hutcheon B, Brown LA, Poulter MO. Digital analysis of light microscope immunofluorescence: high-resolution co-localization of synaptic proteins in cultured neurons. *J Neurosci Methods.* 2000;96: 1–9.
121. Holmes KD, Babwah AV, Dale LB, Poulter MO, Ferguson SSG. Differential regulation of corticotropin releasing factor 1alpha receptor endocytosis and trafficking by beta-arrestins and Rab GTPases. *Journal of Neurochemistry.* 2006;96: 934–949. doi:10.1111/j.1471-4159.2005.03603.x

122. Hutcheon B, Fritschy JM, Poulter MO. Organization of GABA receptor alpha-subunit clustering in the developing rat neocortex and hippocampus. *Eur J Neurosci.* 2004;19:2475–2487. doi:10.1111/j.0953-816X.2004.03349.x

## Chapter 3

### 3 Tyrosine Binding Protein sites regulate the intracellular trafficking and processing of Amyloid Precursor Protein through a novel lysosome-directed pathway

The amyloid hypothesis posits that the production of  $\beta$ -amyloid ( $A\beta$ ) aggregates leads to neurodegeneration and cognitive decline associated with AD.  $A\beta$  is produced by sequential cleavage of the amyloid precursor protein (APP) by  $\beta$ - and  $\gamma$ -secretase. While nascent APP is well known to transit to the endosomal/ lysosomal system via the cell surface, we have recently shown that APP can also traffic to lysosomes intracellularly via its interaction with AP-3.

Because AP-3 interacts with cargo protein via interaction with tyrosine motifs, we mutated the three tyrosines motif in the cytoplasmic tail of APP. Here, we show that the YTSI motif interacts with AP-3, and phosphorylation of the serine in this motif disrupts the interaction and decreases APP trafficking to lysosomes. Furthermore, we show that phosphorylation at this motif can decrease the production of neurotoxic  $A\beta$  42. This demonstrates that reducing APP trafficking to lysosomes may be a strategy to reduce  $A\beta$  42 in Alzheimer's disease.

#### 3.1 Introduction

Alzheimer's disease (AD) is characterized by the accumulation of extracellular plaques in the brains of AD patients composed of  $\beta$ -amyloid ( $A\beta$ ) peptides.  $A\beta$  is derived from the amyloid precursor protein (APP), a type 1 transmembrane glycoprotein. To produce  $A\beta$ , APP is cleaved first by the  $\beta$ -secretase, which releases the soluble APP $\beta$  ectodomain, leaving a 99-residue  $\beta$ -carboxyl terminal fragment ( $\beta$ CTF). The  $\beta$ CTF is then cleaved by  $\gamma$ -secretase to produce  $A\beta$  species varying from 38-43 residues and an APP intracellular domain. Currently, the subcellular localization of these cleavage events is unclear. For example the Golgi apparatus, plasma membrane, and autophagosomes [1-4] have been implicated in  $A\beta$  production. However, many studies show that nascent APP is cleaved after endocytosis from the cell surface into endosomes and subsequently into lysosomes [2,5-8]. We have recently shown that APP can also transit directly into lysosomes from the cell surface via macropinosomes [9,10]. We have also

shown that APP and  $\gamma$ -secretase proteins are *bona fide* resident proteins of lysosome [11-13]. Furthermore,  $\gamma$ -secretase has an acidic optimal pH [11], and disruption of endosomal/lysosomal pH by chloroquine or ammonium chloride decreases the production of A $\beta$  [14-16].

Although many studies have examined the cell surface trafficking of APP, few have examined APP's intracellular transport. The advent of photo-activatable fluorescent proteins (pa-GFP) provided a new tool to study the intracellular behavior of proteins [17-19]. Recently, we demonstrated that a paGFP tag could be used to follow the intracellular trafficking of APP from the Golgi. We uncovered a previously unknown direct trafficking pathway for APP from the Golgi to the lysosome (via an interaction with the adaptor protein, AP-3), where it is cleaved to form A $\beta$  [20].

AP-3 is a heterotetrameric adaptor protein, which consists of a  $\beta$ 3,  $\delta$ 3,  $\mu$ 3, and  $\sigma$ 3 domains. The  $\mu$ 3 domain of AP-3 recognizes tyrosine motifs of the form YXX $\Theta$  (where  $\Theta$  is a bulky amino acid and X is any amino acid) [21]. APP contains two YXX $\Theta$  motifs at <sup>709</sup>YTSI<sup>712</sup> and <sup>738</sup>YENP<sup>741</sup> (using APP 751 numbering). These motifs interact with other known members of the heterotetrameric adaptor protein family (AP-1, AP-2, and AP-4) [4,22-24]. The YENP motif is part of a larger motif that contains an NPXY motif (<sup>738</sup>GYENPTY<sup>743</sup>)(Figure 3.1a), which has been shown to be involved in endocytosis [6,8,25,26].

While the role of these tyrosine mutations in APP internalization is well documented, the effect of these mutations on the intracellular trafficking from the Golgi to lysosomes remains to be elucidated. Here, we use paGFP-tagged APP and live cell imaging to examine the role of these cytoplasmic tyrosine motifs on the intracellular trafficking of APP. We show that the mutation of Y709A or Y743A disrupt the transit of APP from the Golgi to the lysosome in live cells. Furthermore, the <sup>709</sup>YTSI<sup>712</sup> motif is responsible for the interaction of APP with AP-3. This interaction can be disrupted by phosphorylation of serine within the <sup>709</sup>YTSI<sup>712</sup> (S711), which can be phosphorylated by protein kinase C (PKC) [27,28], and decreases lysosomal transport from the Golgi. Furthermore, we demonstrate that PKC $\epsilon$  activation can divert APP away from lysosomes; possibly by S711 phosphorylation.

## 3.2 Materials and Methods

### 3.2.1 Antibodies and Chemicals

Antibodies used were Mouse Anti-HA (Sigma, H9658), AP-3 (SA4, Developmental Studies Hybridoma Bank) and APP C-terminal (Sigma, A8717). The PKC activator Phorbol-12-myristate-13-acetate (PMA) was purchased from Sigma (P8139) and 8-[2-(2-pentyl-cyclopropylmethyl)-cyclopropyl]-octanoic acid (DCP-LA) was purchased from (Sigma, D5318). Staurosporine was purchased from Millipore (Cat No. 569397). Gö6976 was purchased from Tocris Bioscience (Cat. No. 2253).

### 3.2.2 Cell Culture

SN56 cells were maintained Dulbecco's minimal Eagle's medium (DMEM, Invitrogen) supplemented with 10% fetal bovine serum and 50ug/ml of penicillin/streptomycin, in an incubator at 37°C with 5% CO<sub>2</sub>. Cells were split every 3-4 days; depending on confluency. For microscopy, cells were seeded on glass-bottomed culture dishes (MatTek) one day before transfection. Cells were transfected using Lipofectamine 2000 (Invitrogen) following manufactures directions. After a 24hrs, cells were differentiated in DMEM using 1mM dibutyrl cyclic AMP (dbcAMP; Sigma) and imaged or fixed.

### 3.2.3 Plasmid Constructs

A plasmid encoding the last 112 amino acids of APP with paGFP and CFP C-terminal tags was previously designed [9,20]. The N-terminal of our construct is tagged with a HA epitope to facilitate cell-surface internalization experiments. Mutations were generated using a site-directed mutagenesis kit (Stratagene) and subsequently sequenced to ensure accuracy. Rab5-mRFP and LAMP1-mRFP were generated as previously described [9].

### 3.2.4 Confocal Microscopy

Images were captured with a Zeiss LSM (laser-scanning microscope) -510 META with a Zeiss 63× 1.4 numerical aperture oil immersion lens (Carl Zeiss, Oberkochen, Germany). The thickness of each optical section was set to 1 μM. Cyan fluorescent protein (CFP) was excited



with a 458 nm laser and filtered with a BP 475-525 filter set. Alexa Fluor 488 and paGFP fluorescence were excited with a 488 nm laser and filtered using a band pass (BP) 500-530-nm emission filter set. Alexa Fluor 546, proximity ligation assay (PLA) red detection agent, mCherry, and mRFP fluorescence were excited with a 543 nm laser and filtered with a BP 560–615nm of LP 560nm filter set.

### 3.2.5 Live-Cell Imaging

Images were taken using a Zeiss LSM-510 META laser-scanning microscope using a Zeiss 63x 1.4 numerical aperture oil immersion lens (Carl Zeiss, Germany). Live cell imaging was performed as previously described [20,29]. Briefly, SN56 cells were washed with PBS and transferred to with pre-warmed to 37°C Hank's Balanced Salt Solution (HBSS; Cat. No. 14025–092, Invitrogen). The confocal plates were placed on a heated stage (PeCon GmbH) connected to a Tempcontrol 37-2 digital 2-channel (PeCon GmbH), to maintain the cells at 37°C. ROIs were drawn over the Golgi apparatus as demarcated by GalT-CFP fluorescence, using the Zeiss Physiology package. As the cell can move and shift during the imaging period, the locations of these ROI were carefully monitored to ensure they remained over the Golgi for the duration of the photo-activation period. During typical experiments, the cell was alternatively imaged and photo-activated for the 15-minutes.  $\beta$ APP-paGFP was photoactivated with a 25 mW 405 nm laser, set to maximum power in the pre-specified ROIs. The bleaching for each individual ROI took approximately 50msecs. There were typically 4 ROIs drawn per cell for an approximately 4sec total photoactivation time. A time delay between frames was set accordingly to photoactivate and capture an image every 30 seconds.

### 3.2.6 Colocalization Analysis

Colocalization analysis was performed using Imaris 7.0 Imaris Colocalization module (Biplane) as previously described [20,29]. To analyze the vesicular trafficking of  $\beta$ APP in live cells, Imaris was used to create IsoSurfaces corresponding to paGFP and LAMP1-mRFP or Rab5-mRFP fluorescence, following manufacturer's instructions. This is a semi-automated method that defines organelle distribution based on fluorescence intensity and estimated vesicle size. APP vesicles and the compartment vesicles were demarcated using Imaris, and the amount of

colocalization was calculated as a percentage of material ( $\beta$ APP-paGFP) within the compartment. The percentage of material value takes into account the number of pixels colocalized, as well as the intensity of each individual pixel.

For images of fixed cells, the top 2% of the brightest pixels from each channel were thresholded, and the colocalization was determined in Imaris [9]. The percentage of material colocalized was recorded and plotted in Prism Graphpad 5.0b. Prism Graphpad 5.0b was used for all graphing and statistical analysis. A One-way ANOVA was performed with a Bonferroni post-hoc test, and P values under 0.05 were considered significant.

### 3.2.7 Proximity Ligation Assay

PLA was performed using a commercially available kit (Duolink; Olink Bioscience) according to manufacturer's instructions. Briefly, cells were permeabilized with 0.01% Triton in PBS and blocked with 2% BSA/PBS and stained with primary antibodies overnight at 4°C. AP-3 $\delta$  was probed with the mouse SA4 antibody (DSHB) and APP was probed with the rabbit APP C-terminal (Sigma). Cells were washed and incubated with species-specific secondary antibodies, with covalently attached single-stranded oligonucleotides. When antibodies are within 40nm, the oligonucleotides are ligated and amplified. These are then detected by fluorescent oligonucleotides.

Z-stacks were captured by confocal microscopy and the number of dots per cell was normalized to cell volume. The results were graphed using Prism and one-way ANOVA was performed with a Tukey's post hoc test. P-values less than 0.05 were significant.

### 3.2.8 Internalization Assay

APP internalization was studied as previously described [9,10]. Briefly, anti-HA antibody was labeled using a Zenon 647 labeling kit (Invitrogen), as per manufacturer's instructions. Cells were washed with PBS and labeled with the antibody conjugate for 30 minutes on ice to tag cell-surface  $\beta$ APP-CFP. The cells washed with PBS and the cells were incubated in pre-warmed HBSS at 37°C and moved to an incubator at 37°C with 5% CO<sub>2</sub> for 15 minutes. After 15 minutes, cells were fixed with 4% PFA, and imaged using confocal microscopy.

### 3.2.9 A $\beta$ 40 and A $\beta$ 42 ELISA

SN56 cells were transfected with  $\beta$ APP<sup>sw</sup>-paGFP ( $\beta$ APP bearing the Swedish mutation),  $\beta$ APP<sup>sw</sup> S711A-paGFP, or  $\beta$ APP<sup>sw</sup> S711E-paGFP. One set of cells transfected with  $\beta$ APP<sup>sw</sup>-paGFP and treated with DCP-LA. Cells were differentiated as described above and cell culture media was collected two days after differentiation. Cell culture media was centrifuged at 200 RPM for 10 minutes at 4°C to remove large cellular debris and detached cells. A $\beta$ 40 and A $\beta$ 42 were detected with the A $\beta$ 40 ELISA Kit (KHB3482) or A $\beta$ 42 Ultrasensitive ELISA Kit (KHB3544) from Life Technologies, according to manufacturer's instructions.

## 3.3 Results

### 3.3.1 Tyrosine Motifs and the Intracellular trafficking of APP

We have previously followed the intracellular trafficking of  $\beta$ APP-paGFP from the Golgi apparatus [20]. This shortened construct consists of the last 112 amino acids of APP; including the  $\beta$ -cleavage site. We use a shortened construct to avoid the possibility that trafficking might be altered by currently undefined luminal sequences on APP [30]. In our previous experiments we demonstrated that the shortened  $\beta$ APP-paGFP construct has the same trafficking pattern as full-length APP-paGFP [9,20]. Furthermore, the shortened construct also undergoes  $\beta$ - and  $\gamma$ -cleavage [20]. The shorter construct was used for these experiments because they are more easily expressed, which results in a stronger and more easily detectable fluorescence signal. The photoactivatable GFP (paGFP) is a form of GFP with low fluorescence after synthesis, but develops green fluorescence after irradiation with 405 nm light [18,19]. Using the  $\beta$ APP-paGFP chimera we have previously demonstrated a direct trafficking pathway from the Golgi apparatus to the lysosome [20].

We had previously demonstrated that the trafficking of APP from the Golgi to lysosomes is dependent on an interaction between APP and AP-3. The interaction of AP-3 to cargo depends on cytosolic tyrosine motifs of the form YXX $\Theta$  [21]. To determine the effect of tyrosine mutations on intracellular APP trafficking, we introduced Y709A, Y738A, and Y743A mutations into  $\beta$ APP-paGFP (see Figure 3.1a).  $\beta$ APP-paGFP was transfected into SN56 cells along with the Golgi apparatus marker (Galactosyltransferase-CFP, GalT-CFP) and a marker of lysosomes (lysosome associated membrane protein 1, LAMP1-mRFP) or early endosomes (Rab5-mRFP). After differentiation, cells were transferred to a heated stage (set at 37 °C) on a Zeiss LSM510 confocal microscope. Regions of interest (ROI) were then drawn on the Golgi apparatus using the GalT-CFP fluorescence as a target. Each imaging cycle consists of a brief irradiation of these the ROI with 405nm laser light at full power (25 mW for 20 iterations per imaging cycle) (for a demonstration of this technique, see videos at the Journal of Visual experimentation

<http://www.jove.com/video/53153/imaging-the-intracellular-trafficking-of-app-with->

[photoactivatable-gfp](#) [29]), followed by imaging of the cell. These cycles were repeated over a 15-minute period (See Video 3.1). In each imaging cycle, a small amount of APP-GFP was activated in the Golgi apparatus and could then be seen as it traffics. The final images in these time courses are shown in Figure 3.1b and 3.1c. Using Imaris software, we set thresholds to delimit green fluorescence (photo-activated  $\beta$ APP-paGFP) and red fluorescence (compartment markers) to generate a colocalization channel (Figure 3.1 b and c bottom panels). We then quantitated the amount of green fluorescence co-localized with the red signal (lysosomes or early endosomes) (Figure 3.1d).

In these experiments, WT  $\beta$ APP rapidly appeared in LAMP1-mRFP labeled compartments ( $30 \pm 5\%$  SEM,  $n=5$  independent experiments, 23 cells total) (Figure 3.1b and Video 3.1). In our previous paper, we demonstrated that this transport was abolished by nocadazole and was therefore dependent upon microtubule-related active transport and did not occur through diffusion or accidental irradiation of endosomes or lysosomes [20,29]. It is important to note that the resolution limit of confocal microscopy does not allow us to visualize the small trafficking vesicles emanating from the Golgi. In contrast, the Y709A and Y743A mutations caused a significant decrease ( $p<0.05$ , two-way ANOVA; Bonferroni post hoc) in  $\beta$ APP-paGFP colocalization with LAMP1-mRFP after 15 minutes ( $11 \pm 4\%$  SEM,  $n=5$  independent experiments, 21 cells total, and  $12 \pm 1\%$  SEM,  $n=3$  independent experiments 10 cells total, respectively) (Figure 3.1b and Video 3.2 and 3.4, respectively). The Y738A mutation did not significantly reduce trafficking to lysosomes as compared to WT  $\beta$ APP ( $p>0.05$ ,  $n=4$  independent experiments, 11 cells total) (Figure 3.1b, d and Video 3.3).

We also analyzed cells transfected with Rab5 to determine whether tyrosine mutations shift APP into earlier compartments in the endosomal/lysosomal pathway. In these experiments, relatively small amounts of wild type  $\beta$ APP trafficked to early endosomes ( $9 \pm 2\%$  SEM,  $n=5$  independent experiments, 16 cells total) (Figure 3.1c). In contrast, the Y709A and Y743A significantly increased trafficking to the early endosome, ( $25 \pm 3\%$  SEM,  $n=4$  independent experiments 16 cells total, and  $29 \pm 7\%$  SEM,  $n=3$  independent experiments 11 cells total), while the Y738A mutation did not ( $21 \pm 4\%$  SEM,  $n=4$  independent experiments 16 cells total, Figure 3.1c and d)

( $p < 0.05$ , two way ANOVA; Bonferroni post hoc). Therefore, the Y709A and Y743A both reduce the intracellular trafficking of APP to lysosomes.

**Figure 3.1:** Tyrosine mutations modulate the intracellular trafficking of APP.

a) Depiction of the carboxyl terminal of APP, with APP 751 numbering. The tyrosines and serines studied in this paper are shown, and the tyrosine motifs underlined. SN56 cells were transiently transfected with wild type APP or APP with mutations Y709A, Y738A, or Y743A tagged with paGFP. Each cell was subjected to 15-minutes of sequential imaging. Before each image, the cell was photo-activated within the Golgi (blue). b) Trafficking of APP to lysosomes (LAMP-1) and c) early endosomes (Rab5) was studied. The top panels show representative images from each cell after 15 minutes of photo-activation (Scale bars represent 5 $\mu$ m). The bottom panels depict colocalized pixels. The white border demarcates the edge of the cell and was drawn based on the white light images. Triangles point to colocalized pixels. d) Using a semi-automated method, the APP vesicles and LAMP1 or Rab5 vesicles were selected and the means were plotted using Prism 5.0b. Error bars represent SEM (\*=p<0.05).

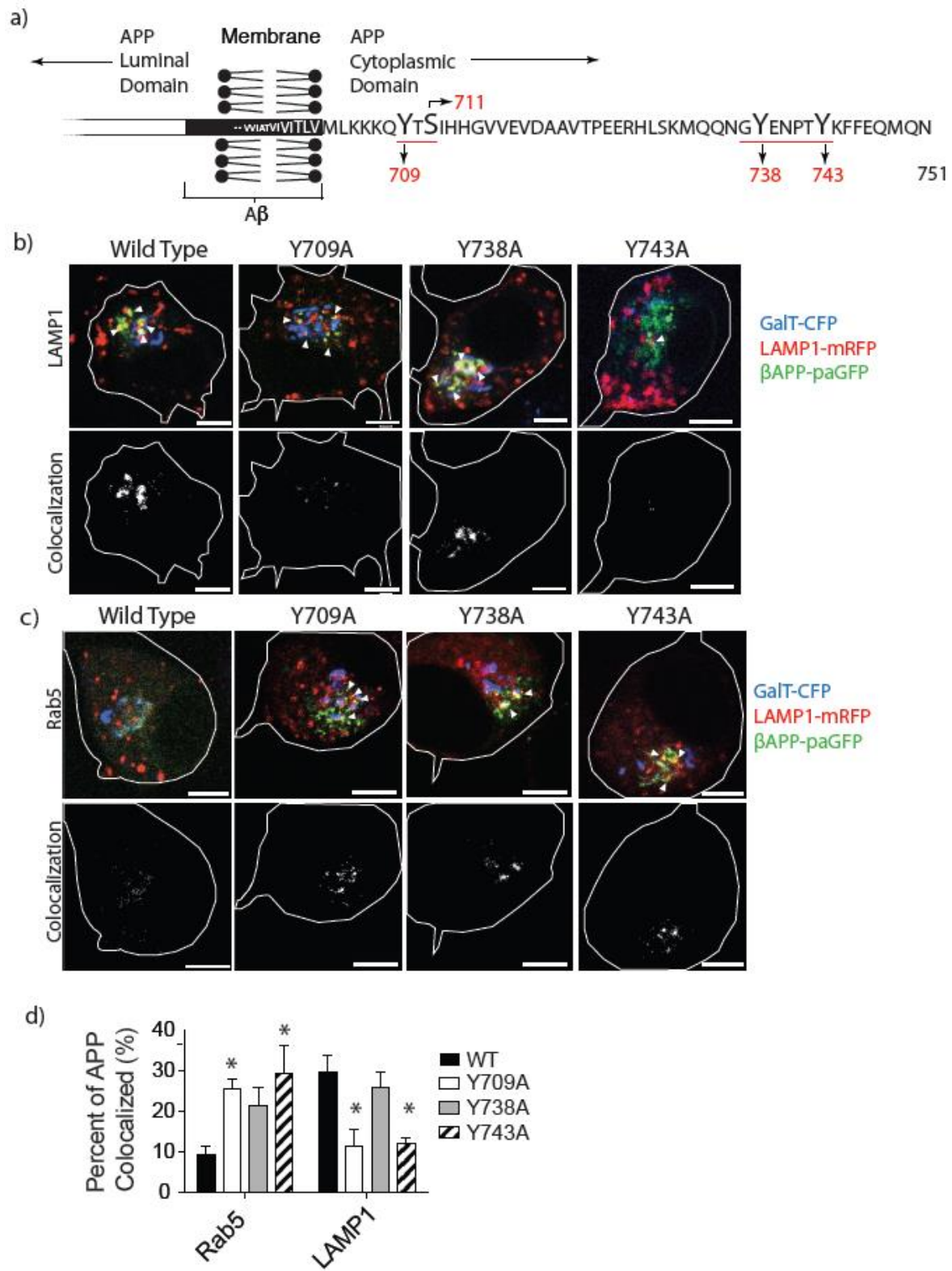


Figure 3.1



### 3.3.2 Amyloid Precursor Protein Internalization

Mutagenesis of tyrosine-based trafficking motifs has been shown to alter the endocytosis of APP [6,8,31]. We have shown that APP can be internalized into lysosomes by two pathways, one by way of early endosomes and a second pathway directly from the cell surface [9,10]. To determine if internalization into early endosomes was affected by mutations in C-terminal tyrosines, SN56 cells were transfected with  $\beta$ APP-CFP constructs and Rab5-mRFP. Our  $\beta$ APP-CFP constructs are tagged on the N-terminal with a HA epitope to facilitate internalization experiments.  $\beta$ APP-CFP was surface-labelled on ice with a Zenon-647 anti-HA antibody conjugate. After a 15-minute internalization at 37 °C,  $28 \pm 2\%$  (SEM; n=5 independent experiments, 73 cells total) of wild type  $\beta$ APP-CFP was internalized into Rab5 positive endosomes (Figure 3.2a). The Y709A mutation did not significantly affect the internalization of  $\beta$ APP into early endosomes ( $23 \pm 2\%$  SEM, n=5 independent experiments, 55 cells total) (Figure 3.2b, e). However, the Y738A and Y743A mutations significantly reduced the internalization of  $\beta$ APP into early endosomes ( $19 \pm 1\%$  SEM, n=5 independent experiments, 62 cells total and  $14 \pm 2\%$  SEM, n=4 independent experiments, 53 total cells, respectively,  $p > 0.05$ ) (Figure 3.2c, e) [10].

To follow the direct trafficking of APP to lysosomes, SN56 cells were transfected with  $\beta$ APP and LAMP1-mRFP, surface-labeled on ice with a fluorescent HA-antibody conjugate. This was followed by a 15-minute internalization period at 37 °C before fixation. In cells expressing wild type  $\beta$ APP,  $21 \pm 1\%$  SEM (n=5 independent experiments, 83 cells total) of  $\beta$ APP was internalized into LAMP1 labeled vesicles (Figure 3.3a and e). The Y709A and Y738 mutations did not significantly change the internalization of  $\beta$ APP into lysosomes ( $p > 0.05$ ,  $19 \pm 1\%$  SEM, n=5 independent experiments 70 cells total, and  $23 \pm 2\%$  SEM, n=7 independent experiments 95 cells total, respectively) (Figure 3.3b, c, and e). However, the Y743A mutation reduced internalization to  $12 \pm 1\%$  SEM ( $p < 0.05$ , n=6 independent experiments 78 total cells) (Figure 3.3d and e). Therefore, the Y743A mutation disrupts  $\beta$ APP internalization to both Rab5 and LAMP1 compartments, while the Y709A mutation has no effect on internalization.

**Figure 3.2:** Tyrosine disrupts internalization into early endosomes.

SN56 cells were transfected with  $\beta$ APP-CFP (with or without tyrosine mutations) and Rab5-mRFP. The HA-tag on our  $\beta$ APP-CFP construct was fluorescently labeled using an anti HA-Zenon conjugate. a-d) Representative images of  $\beta$ APP-CFP, bearing one of the tyrosine mutations, internalized into Rab5-mRFP compartments after 15-minutes. The edge of the cell is shown by the white border, and was drawn based on white-light images. Triangles point to colocalized pixels. Scale bars represent 5 $\mu$ m. e) The percentage of APP co-localized with Rab5 was quantified using Imaris and graphed (\*=p<0.05, error bars represent SEM).

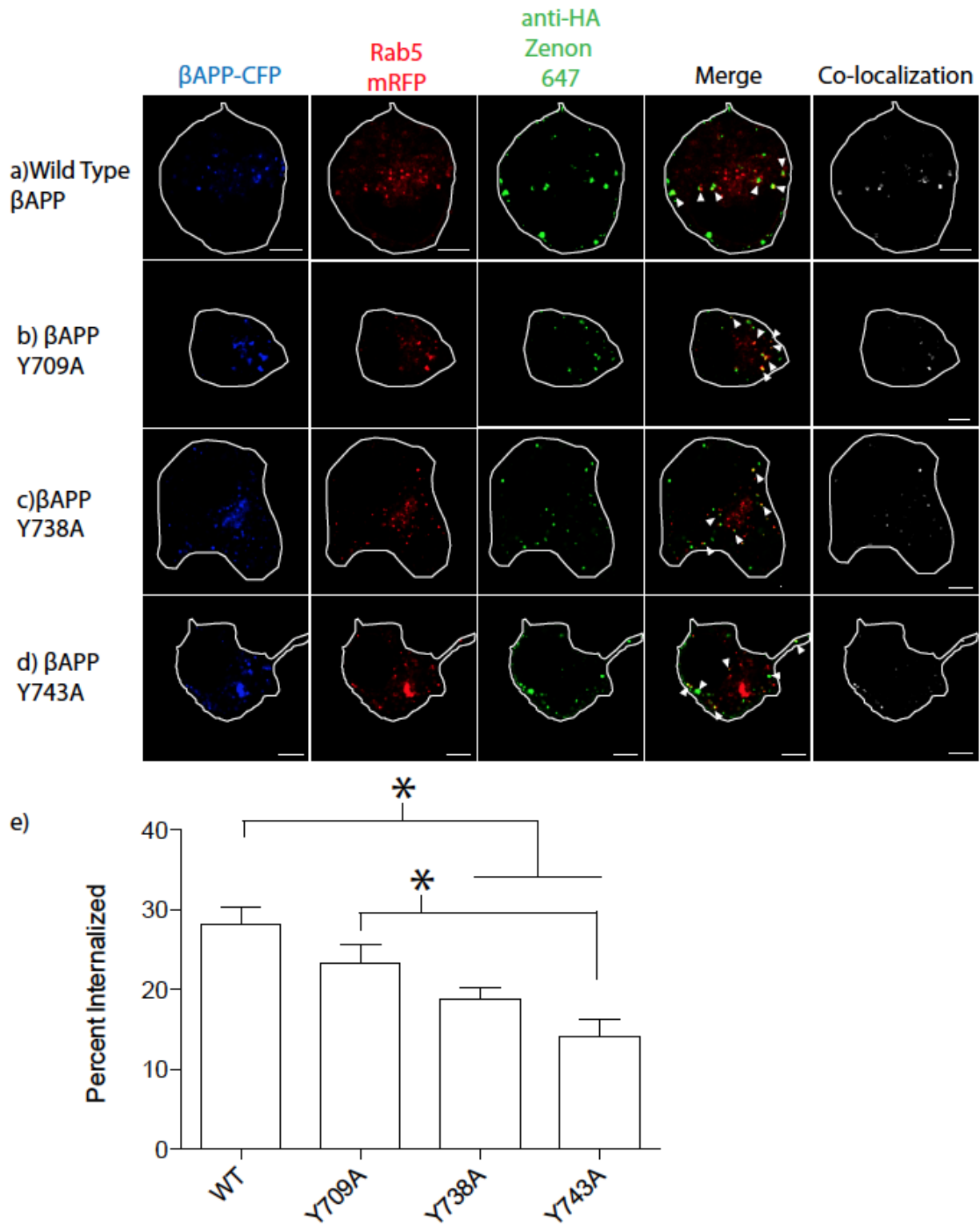


Figure 3.2

**Figure 3.3:** Y743A disrupts internalization into lysosomes.

SN56 cells were transfected with  $\beta$ APP-CFP (with or without tyrosine mutations) and Lamp1-mRFP. The HA-tag was fluorescently labeled using the anti HA-Zenon conjugate. The cells were incubated at 37°C for 15 minutes and fixed and imaged. a-d) Representative images of  $\beta$ APP-CFP, bearing one of the tyrosine mutations, internalized into LAMP1-mRFP compartments after 15-minutes. The edge of the cell is shown by the white border, and was drawn based on white-light images. Triangles point to colocalized pixels. Scale bars represent 5 $\mu$ m. e) APP co-localized with Lamp1 was quantified using Imaris and graphed (\*= $p < 0.05$ , error bars represent SEM).

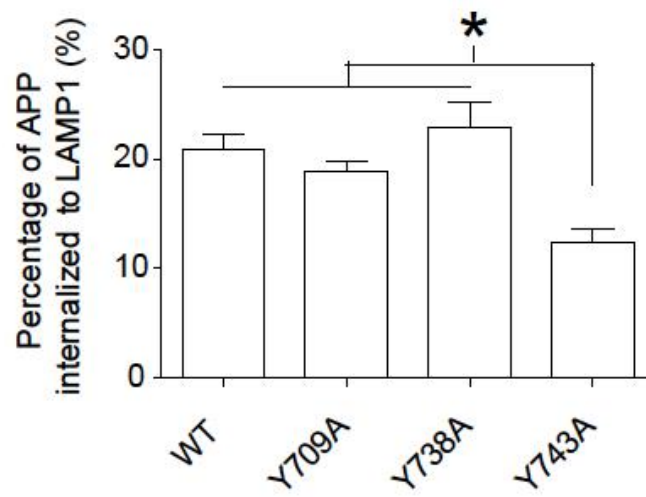
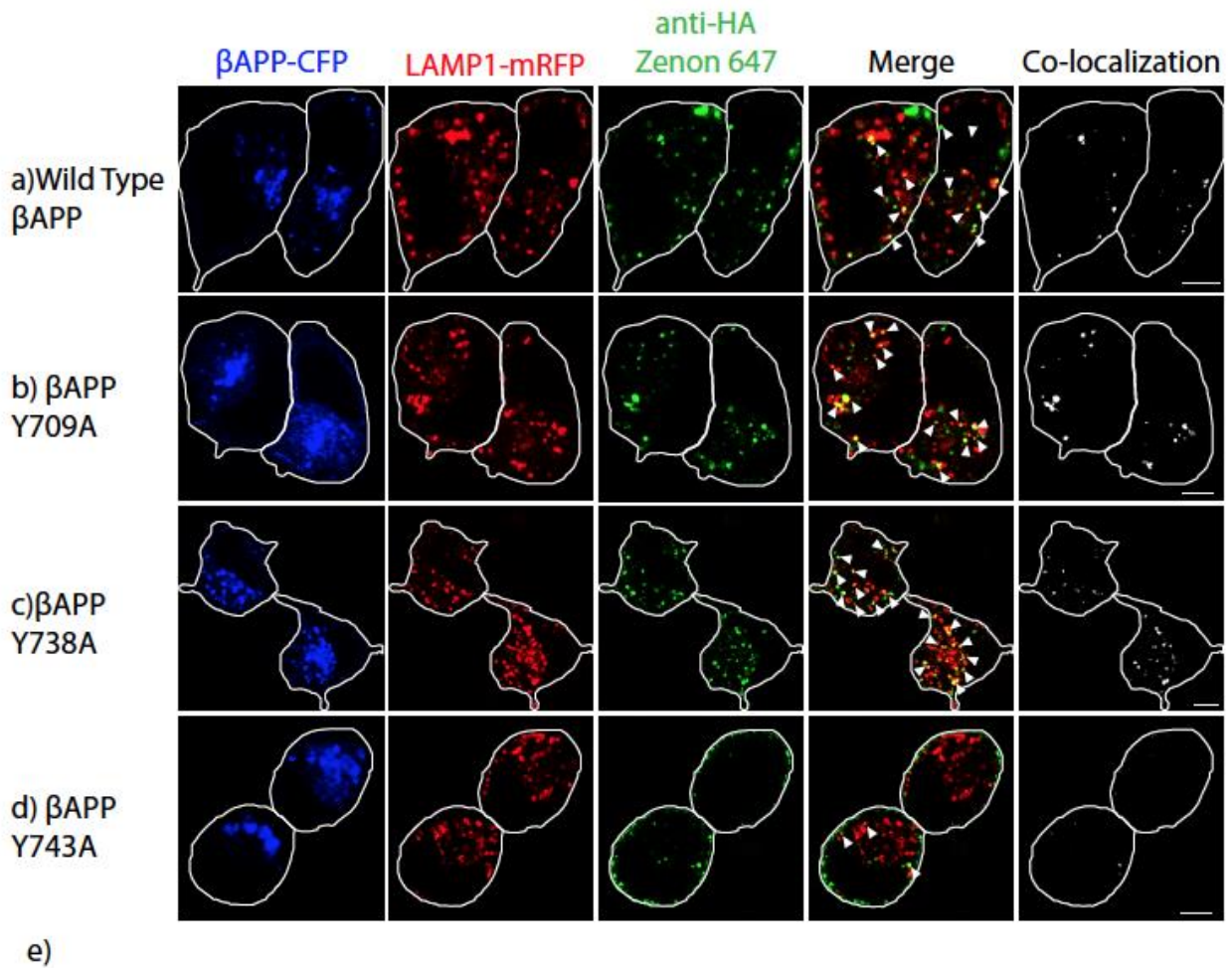


Figure 3.3

### 3.3.3 Amyloid Precursor Protein and AP-3 Interaction

Previously, we demonstrated that rapid trafficking of APP to lysosomes is dependent on APP interaction with AP-3 [20]. To determine the tyrosine motif responsible for the APP/AP-3 interaction, we performed an *in situ* proximity ligation (iPLA) assay with  $\beta$ APP-CFP bearing one of the cytoplasmic tyrosine mutations. Briefly, if the proteins of interest are within 40 nm of each other, antibody-conjugated single-stranded oligonucleotides anneal and can undergo rolling circle amplification. The amplification product is detected by hybridization with fluorescent oligonucleotides, which can be visualized by confocal microscopy. iPLA has been used to confirm protein-protein interactions *in situ*, including weak or transient interactions that are undetectable by co-immunoprecipitation [32-34].

SN56 cells were transfected with  $\beta$ APP-CFP with or without tyrosine mutations and iPLA was performed after fixation. A 3D-stack of images of each cell was acquired by confocal microscopy. The  $\beta$ APP-CFP /AP-3 interaction was quantified by counting the number of spots per  $\mu\text{m}^3$ . In cells transfected with WT  $\beta$ APP-CFP, cells had  $0.037 \pm 0.006$  dots/ $\mu\text{m}^3$  SEM (n=3 independent experiments, 28 cells total). The Y738A and Y743A mutations did not significantly alter  $\beta$ APP-CFP interaction with AP-3 ( $0.03 \pm 0.004$  dots/ $\mu\text{m}^3$  SEM n=3 independent experiments, 36 cells total and  $0.03 \pm 0.007$  dots/ $\mu\text{m}^3$  SEM n=3 independent experiments, 32 cells total, respectively) (Figure 3.4a and b). However, the Y709A mutation significantly decreased the interaction of  $\beta$ APP-CFP with AP-3 ( $0.02 \pm 0.004$  dots/ $\mu\text{m}^3$  SEM, n=3 independent experiments, 40 cells total) (Figure 3.4a and b). Therefore, it appears that the Y709A mutation disrupts the interaction of APP with AP-3 to prevent APP delivery to lysosomes.

**Figure 3.4:** Tyrosine motif mutations affect on APP/AP-3 interaction.

SN56 cells were transfected with plasmids expressing wild type APP or APP with mutations Y709A, Y738A, or Y743A. Cells were fixed and iPLA was performed to detect interaction between APP with AP-3 $\delta$ . a) Representative images are shown. The white border shows edge of the cell and was drawn based on the white light images. Scale bars represent 5 $\mu$ m. b) The dots per cell was counted using Imaris, normalized to cell volume, and graphed in Prism 5.0b ( $p < 0.05$ ). SN56 cells were transfected with plasmids expressing wild type APP or APP bearing phosphomimetic (S711E) or dephosphomimetic (S711A) mutations. Cells were fixed and iPLA was performed to determine if there was an interaction between APP and AP-3. c) Representative images of APP/AP-3 $\delta$  interaction. The white border shows edge of the cell and was drawn based on the white light images. Scale bars represent 5 $\mu$ m. d) The number of spots per cell was counted and normalized to cell volume. Error bars represent SEM and \*=  $p < 0.05$ .

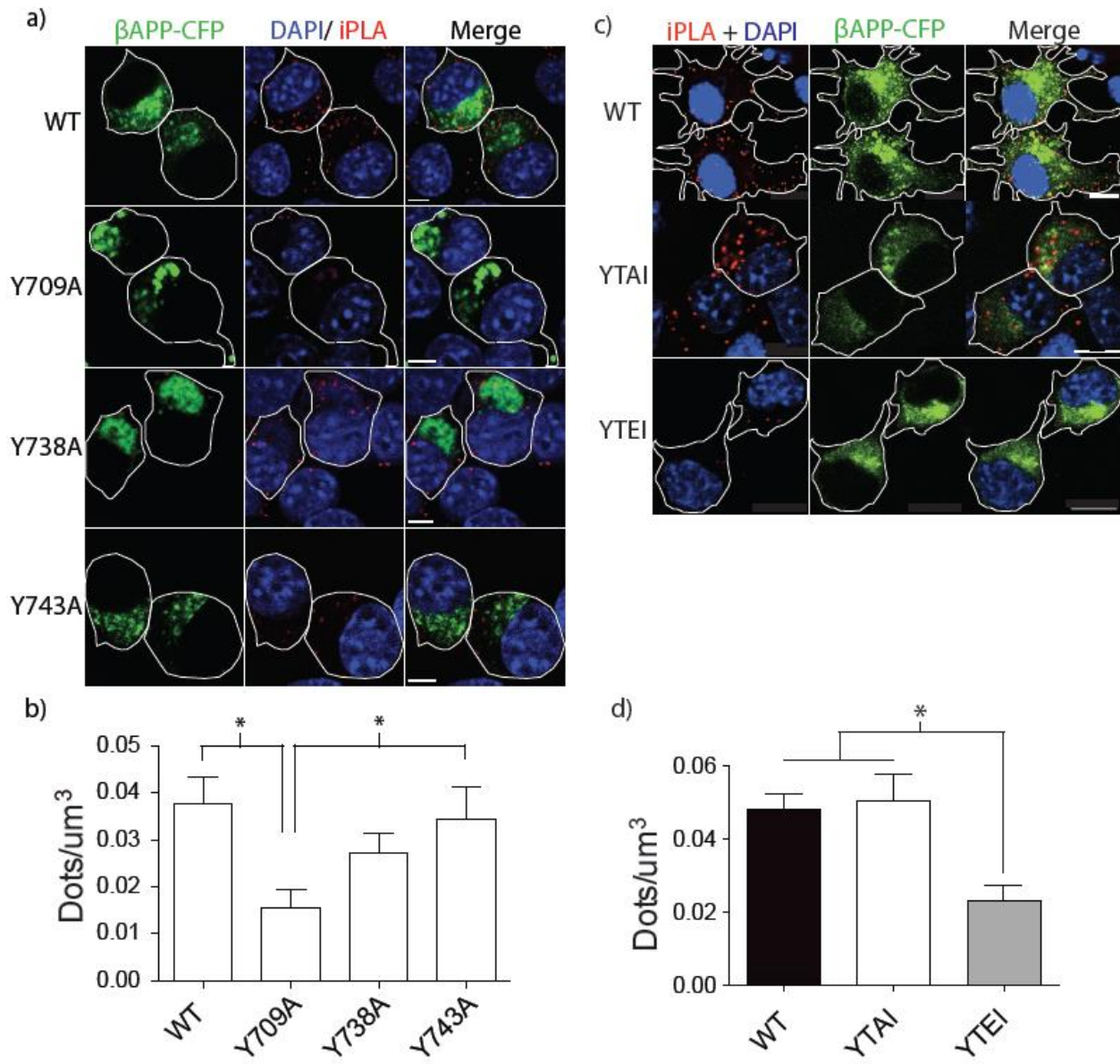


Figure 3.4



### 3.3.4 Pseudo-phosphorylation of Serine 711

The <sup>709</sup>YTSI<sup>712</sup> motif is involved in APP endocytosis, basolateral (intracellular) sorting, and cell surface delivery [6,23,35,36]. In the YTSI motif, the tyrosine and serine have been found to be phosphorylated in the brains of AD patients [27,37]. While the effect of Y709 phosphorylation on APP trafficking is unclear, S711 phosphorylation has recently been shown to regulate the intracellular trafficking of APP [38]. Pseudo-phosphorylation of the S711 residue of APP was shown to increase APP retrieval to the Golgi from the endosomal system and increased non-amyloidogenic processing of APP [38,39]. Furthermore, The S711 residue is the only residue in the APP C-terminus that can be phosphorylated by PKC [27,28]. To test if S711 phosphorylation affects the interaction of APP with AP-3, we introduced dephosphomimetic (S711A) and phosphomimetic (S711E) mutations to the  $\beta$ APP-CFP construct to determine their effect using iPLA. We show that  $\beta$ APP S711E-CFP interacted poorly with AP-3 ( $0.02 \pm 0.004$  dots/ $\mu\text{m}^3$  SEM, n=4 independent experiments, 46 cells total), as compared to WT  $\beta$ APP-CFP ( $0.05 \pm 0.004$  dots/ $\mu\text{m}^3$  SEM, n=4 independent experiments, 51 cells total) (Figure 3.4c and d). The dephosphomimetic (S711A) mutation did not significantly alter the interaction of  $\beta$ APP with AP-3 (Figure 3.4c and d, n= 3 independent experiments, 34 cells total). Therefore, pseudo-phosphorylation of  $\beta$ APP, at S711, disrupts its interaction with AP-3.

To determine the effect of these phosphomimetic mutations on  $\beta$ APP trafficking to lysosomes, we introduced the S711A and S711E mutations into our  $\beta$ APP-paGFP construct. We photo-activated  $\beta$ APP-paGFP in the Golgi and followed its transport into downstream compartments. The S711A mutation did not significantly disrupt  $\beta$ APP trafficking to lysosomes, as compared to WT  $\beta$ APP-paGFP (one-way ANOVA, n= p>0.05) ( $25 \pm 4\%$  SEM n= 4 independent experiments, 13 cells total compared to  $30 \pm 4\%$  SEM, n=5 independent experiments, 23 cells total) (Figure 3.5a and c and Video 3.5). However, the S711E mutation, which disrupts  $\beta$ APP interaction with AP-3, also significantly decreased the amount of  $\beta$ APP trafficked to LAMP1 compartments ( $17 \pm 3\%$  SEM, n=4 independent experiments, 17 cells total), as compared to WT APP (Figure 3.5a and c and Video 3.6). To determine if S711 mutations disrupts trafficking to early endosomes,

we repeated the intracellular trafficking experiments with Rab5-mRFP, a marker for early endosomes. In these experiment, there was no significant difference in the amount of  $\beta$ APP delivered to early endosomes with both mutations (Figure 3.5b and c). Therefore, phosphorylation of S711 impedes  $\beta$ APP delivery to lysosomes likely through disrupting the  $\beta$ APP/AP-3 interaction.

### 3.3.5 PKC Activation Controls Intracellular Trafficking of APP

S711 residue can be phosphorylated by PKC [27,28]. PKC agonists are known to increase the non-amyloidogenic processing of APP by increasing  $\alpha$ -secretase cleavage of APP [40,41]. S711 phosphorylation has also been reported to increase the interaction of APP with members of the retromer complex, and to divert APP from the lysosome to the Golgi [38]. Phosphorylation of S711 has also been suggested to increase the secretory trafficking from the Golgi [39]. Therefore, we asked whether S711 phosphorylation could disrupt Golgi to lysosome transport, through disrupting the APP and AP-3 interaction.

To examine the effects of PKC activation on  $\beta$ APP trafficking, SN56 cells were transfected with  $\beta$ APP-paGFP, GalT-CFP, and a marker for the endosomes or lysosomes. After a one-hour incubation with 300nM the PKC activator Phorbol-12-myristate-13-acetate (PMA), APP was photo-activated in the Golgi apparatus to follow the transport of APP to downstream compartments (Figure 3.6a). In untreated cells,  $30 \pm 4\%$  SEM (n=5 independent experiments, 23 cells total) of nascent  $\beta$ APP-paGFP is delivered to lysosomes. However, cells treated with 300nM PMA traffic  $18 \pm 3\%$  SEM (n=4 independent experiments, 10 cells total) of APP to lysosomes (one-way ANOVA, Bonferroni post hoc,  $p < 0.05$ ) (Figure 3.6c). Consistent with phosphomimetic mutations to the YTSI motif, PMA treatment significantly increased the amount of  $\beta$ APP-paGFP directed towards Rab5 (early endosome) labeled compartments (WT=  $9 \pm 2\%$  SEM, n=5 independent experiments, 16 cells total vs. PMA treated  $26 \pm 6\%$  SEM, n=5 independent experiments, 16 cells total) (Figure 3.6b and c).

**Figure 3.5:** S711E disrupts trafficking to lysosomes.

SN56 cells were transfected with plasmids expressing wild type APP, S711E, or S711A. Concomitantly, plasmids expressing LAMP1-mRFP or Rab5-mRFP and GalT-CFP were also transfected. a) Representative images depicting trafficking of APP S711A or S711E to lysosomes (LAMP1-mRFP) after photo-activation in GalT-CFP labeled compartments. b) Representative images showing the delivery of APP S711A or S711E to early endosomes after photo-activation. The edge of the cell is defined by the white line, and was drawn based on the white light images. Scale bars represent 5 $\mu$ m. Triangles with circles denote photo-activation sites at time 0. Triangles alone point to colocalized pixels. c) The percentage of APP colocalized with either LAMP1 or Rab5 was quantified with Imaris. Error bars denote SEM. \*=p<0.05.

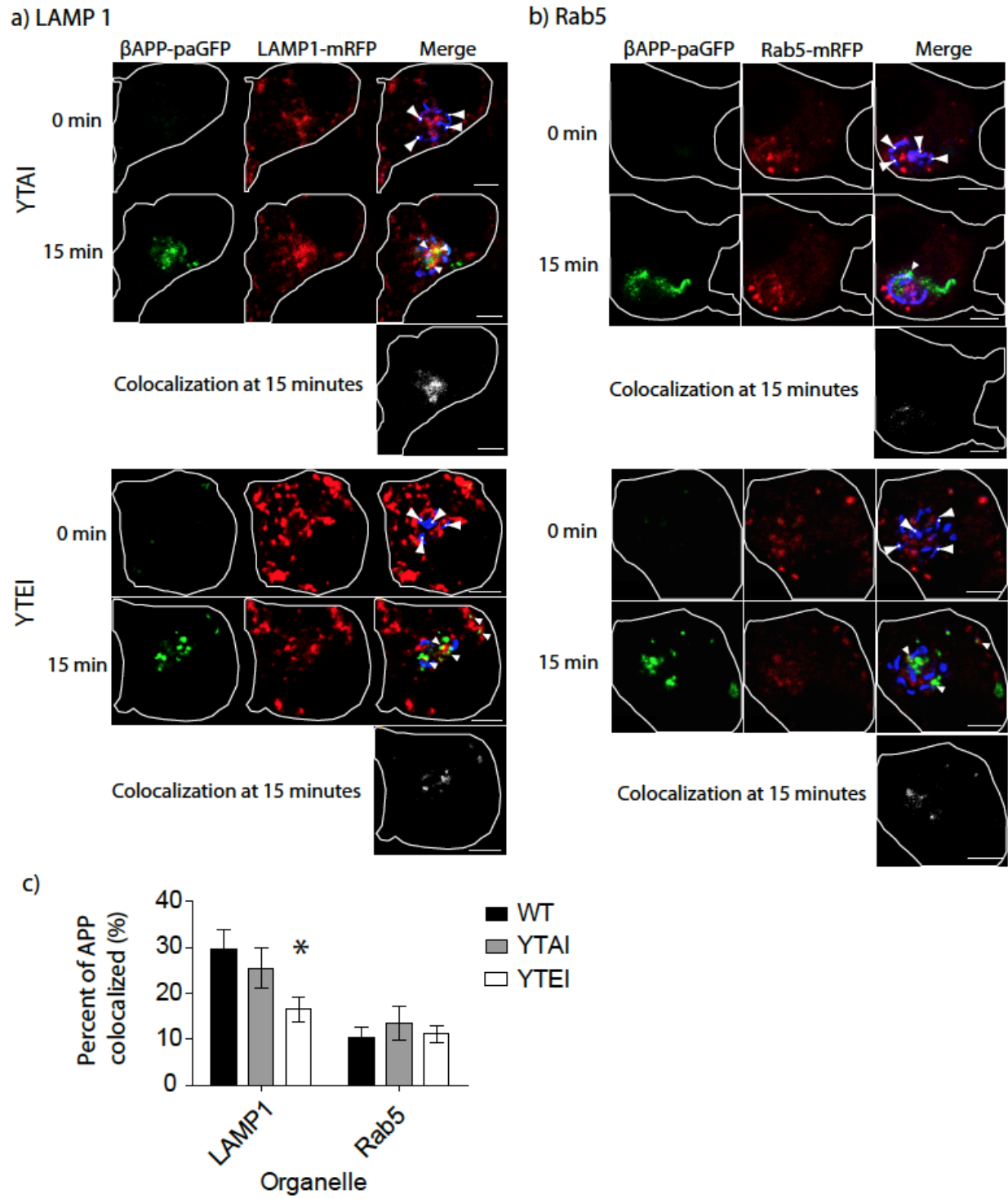
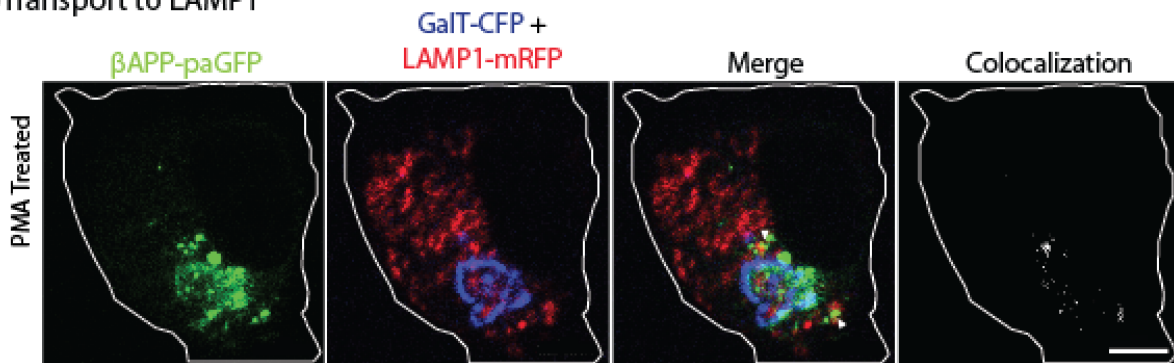


Figure 3.5

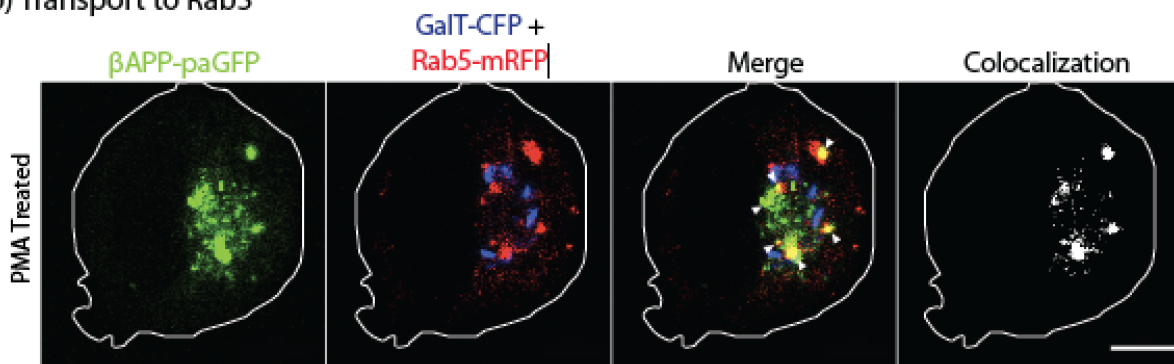
**Figure 3.6:** PMA treatment alters the intracellular trafficking of APP.

SN56 cells transiently transfected with  $\beta$ APP-paGFP were treated or not treated with 300nM PMA for 1-hour before imaging. Cells were photo-activated in the Golgi (GalT-CFP) for 15 minutes. Video of the live cells was taken during this 15-minute period to follow the trafficking of APP. Frames from the beginning and the end of the time course are shown here for transport to a) lysosomes (LAMP1) and b) early endosomes (Rab5). Far-right panels show colocalized pixels between the  $\beta$ APP-paGFP and LAMP1-mRFP channels. The edge of the cell is defined by the white line, and was drawn based on the white light images. Triangles alone point to colocalized pixels. Scale bars represent 5 $\mu$ m. c) The amount of APP colocalized with each compartment was quantified using Imaris at the 15-minute time point, and the results were plotted using Prism 5.0b. Error bars represent SEM and \* denotes  $p < 0.05$ .

## a) Transport to LAMP1



## b) Transport to Rab5



c)

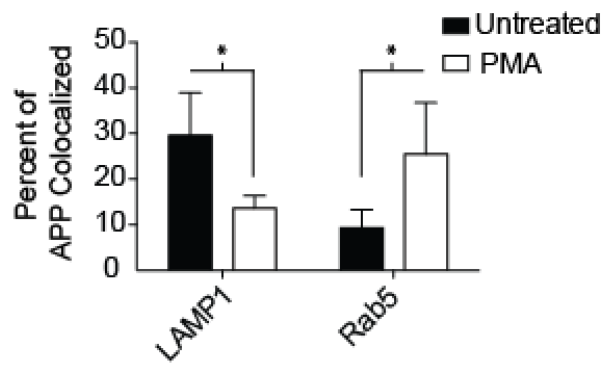


Figure 3.6

We also examined staurosporine treatment to inhibit PKC activity before PMA treatment. Staurosporine (1 $\mu$ M) pre-treatment restored the trafficking of APP to lysosomes (35  $\pm$  6% SEM, n=4 independent experiments, 12 cells total) (Figure 3.7a and b). Importantly, staurosporine treatment alone did not disrupt the trafficking of APP (31  $\pm$  5% SEM, n=4 independent experiments, 11 cells total). Therefore, activation of PKC diverts APP away from lysosomes and towards early endosomes.

PMA and other phorbol esters activate PKCs through binding to the diacylglycerol (DAG) binding site on PKC, and can activate conventional ( $\alpha$ ,  $\beta$ I,  $\beta$ II, and  $\gamma$ ) and novel PKCs ( $\delta$ ,  $\epsilon$ ,  $\eta$ , and  $\theta$ ). PKC $\alpha$  and PKC $\epsilon$  have both been suggested to regulate APP metabolism [42-45]. To specifically examine PKC $\alpha$  and other conventional PKC's, we pretreated the cells with Gö6976 (inhibitor of conventional PKCs (PKC $\alpha$ ,  $\beta$ I,  $\beta$ II, and  $\gamma$ ). Transfected SN56 cells were pretreated with Gö6976 before stimulation with PMA. In these experiments, Gö6976 pretreatment was unable block the effects of PMA (reducing  $\beta$ APP-paGFP delivery to lysosome; Gö6976 and PMA 18  $\pm$  4% SEM n= 3 independent experiments 10 cells total vs. PMA only 18  $\pm$  3% SEM n=4 independent experiments 10 cells total) (Figure 3.7a and b). This suggests that conventional PKCs are not major contributors in the diverting APP away from lysosomes.

Therefore, we turned our attention to the novel PKC family. However, we could not find a specific inhibitor the nPKCs. Instead, we turned to a specific agonist for nPKC $\epsilon$ . Previous studies have suggested that PKC $\epsilon$  promotes non-amyloidogenic cleavage of APP [44-46]. Recently, 8-[2-(2-pentyl-cyclopropylmethyl)-cyclopropyl]-octanoic acid (DCP-LA) was found to specifically activate PKC $\epsilon$  over other isoforms of PKC [47]. In fact, 500nM DCP-LA has previously been shown to strongly and specifically activate PKC $\epsilon$  and decrease A $\beta$  production in SH-SY5Y cells [46]. We treated our transfected SN56 cells with 500nM DCP-LA, to determine if DCP-LA mediated activation of PKC $\epsilon$  could regulate the trafficking of APP. DCP-LA significantly reduced targeting of  $\beta$ APP-paGFP to lysosomes (13  $\pm$  3% SEM, n=4 independent experiments, 15 cells total), which was not significantly different from cells treated with PMA (p>0.05) (Figure 3.8a and c, Video 3.7). In addition, treatment of SN56 cells with DCP-LA increased

delivery of APP to early endosomes, as seen with PMA treatment (Figure 3.8b and c) (WT=  $9 \pm 2\%$  SEM vs. DCP-LA treated  $30 \pm 2\%$  SEM n=4 independent experiments, 12 cells total). Moreover, pretreatment of transfected cells with staurosporine abrogated the effect of DCP-LA on trafficking of  $\beta$ APP-paGFP to lysosomes ( $32 \pm 2\%$  SEM, n=3 independent experiments, 9 cells total). However, pretreatment with Gö6976 ( $13 \pm 3\%$  SEM, n=4 independent experiments, 10 cells total) (Figure 3.8d and e) could not abolish the effects of DCP-LA treatment. These data suggests that the trafficking of APP away from lysosomes and towards early endosomes is regulated by PKC $\epsilon$ .

PKC $\epsilon$  activation by DCP-LA can decrease A $\beta$  production and reduce amyloid deposition in mice [44,46]. To determine if we could recapitulate these results, we transfected cells with  $\beta$ APP-paGFP bearing the Swedish familial mutation ( $\beta$ APP<sup>sw</sup>-paGFP) and treated the cells with DCP-LA. Cells were also transfected with either  $\beta$ APP<sup>sw</sup>-paGFP YTAI or  $\beta$ APP<sup>sw</sup>-paGFP YTEI to determine if pseudophosphorylation at S711 could modulate A $\beta$  production. Cell-culture media was gathered from three independent experiments and analyzed by ELISA for A $\beta$  40 or 42. A $\beta$  42 production was not significantly reduced by transfection with APP bearing the YTAI mutation. However, transfection of APP bearing the YTEI mutation or treatment with DCP-LA significantly decreased A $\beta$  42 by ~30% (Figure 3.8f). Therefore, it appears that phosphorylation of APP at S711 decreases the production of A $\beta$  42 by reducing lysosomal trafficking of APP. There was no significant change in A $\beta$ 40 secreted into culture media.



**Figure 3.7:** Staurosporine but not Gö6976 treatment restores trafficking of APP to lysosomes.

SN56 cells were pretreated for 1 hour with staurosporine or Gö6976 for 1 hour before treatment with PMA. Cells were imaged as previously stated. Depicted in a) are representative images of cells treated with PMA, with or without the indicated inhibitors. These images were taken from live cell video of photo-activated cells 15 minutes after the start of imaging. Far-right panels show colocalized pixels between the  $\beta$ APP-paGFP and LAMP1-mRFP channels. The edge of the cell is defined by the white line, and was drawn based on the white light images. Triangles point to colocalized pixels. Scale bars represent 5 $\mu$ m. b) The amount of APP colocalized with LAMP-mRFP was quantified using Imaris and plotted using Prism. Error bars represent SEM and \* denotes  $p < 0.05$  as compared to untreated cells and cells treated with staurosporine and PMA.

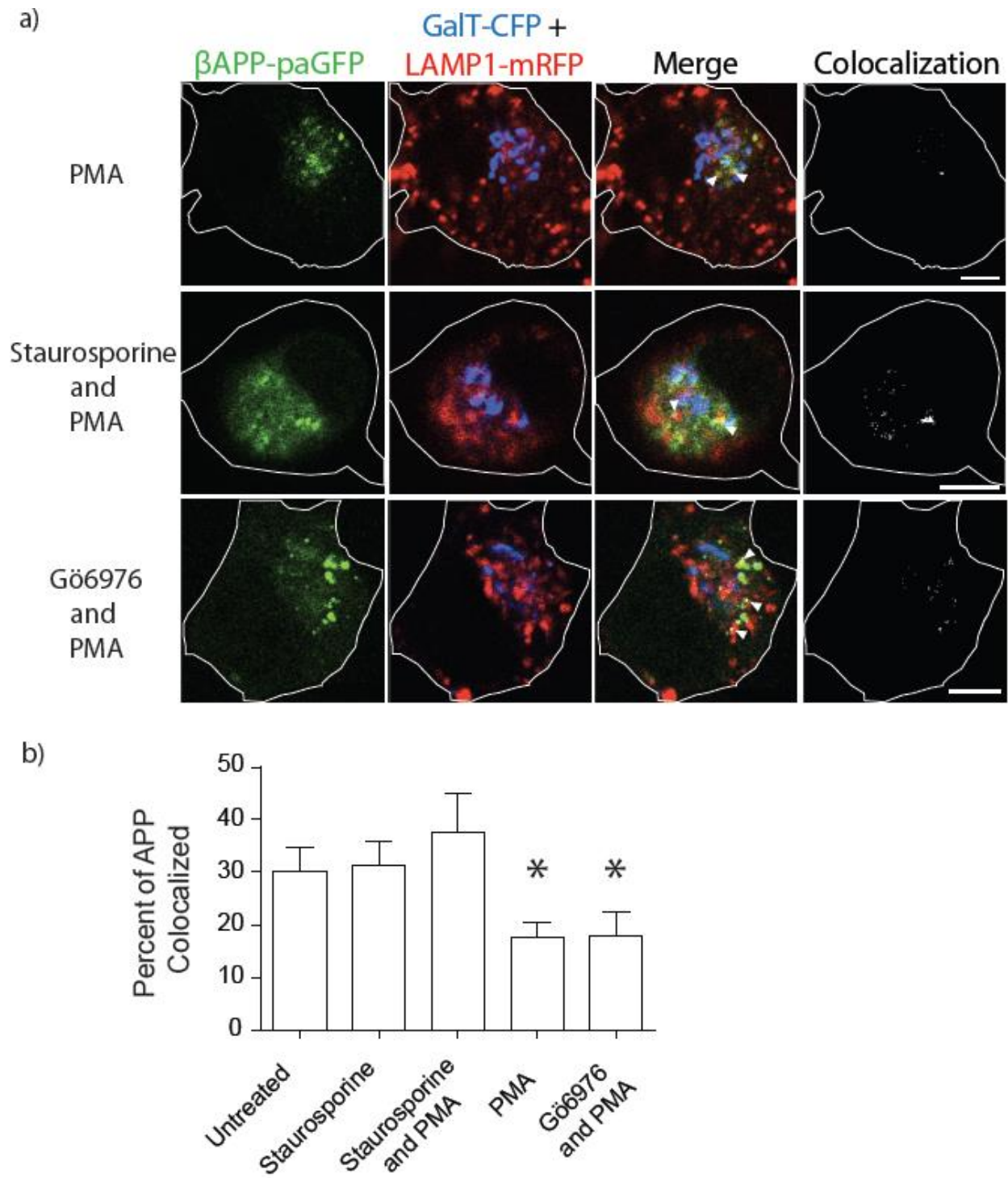
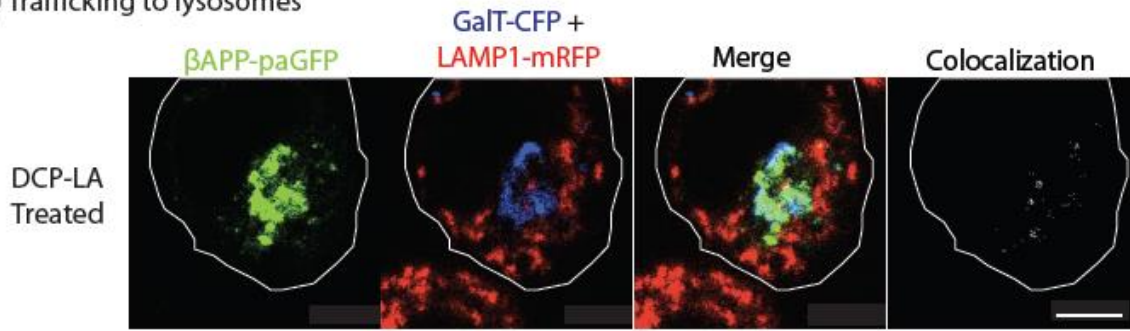


Figure 3.7

**Figure 3.8:** DCP-LA treatment of SN56 cells diverts APP into early endosome compartments.

Cells were transfected with  $\beta$ APP-paGFP, GalT-CFP, and **a)** LAMP1-mRFP or **b)** Rab5-mRFP. Cells were pre-treated with DCP-LA for one hour before imaging, and photo-activated within the Golgi. Far-right panels show colocalized pixels between the  $\beta$ APP-paGFP and LAMP1-mRFP channels. The edge of the cell is defined by the white line, and was drawn based on the white light images. Triangles point to colocalized pixels. Scale bars represent  $5\mu\text{m}$ . **c)** The amount of APP colocalized with each compartment, with or without DCP-LA treatment, was measured using Imaris and was plotted using Prism 5.0b. **d)** SN56 cells were treated with  $1\mu\text{M}$  staurosporine or  $1\mu\text{M}$  Gö6976 before treatment with DCP-LA. The amount of APP colocalized with LAMP1 was measured using Imaris and plotted using Prism 5.0b. \* denotes  $p < 0.05$  as compared to untreated. Representative images from the end of the photo-activation period are shown in **e)**. Images in the far-right panel show colocalized pixels between the LAMP1-mRFP and  $\beta$ APP-paGFP channels. Triangles point to colocalized pixels. Scale bars represent  $5\mu\text{m}$ . **f)** SN56 cells were transfected with  $\beta$ APP<sub>sw</sub>-paGFP and treated with DMSO or DCP-LA. Two other wells of cells were transfected with  $\beta$ APP<sub>sw</sub>-paGFP containing either the YTEI and YTAI mutation. The media was collected from the cells and used ELISA to analyze the amount of A $\beta$ 42. Error bars in both graphs represent SEM. \* denotes  $p < 0.05$  as compared to DMSO treated cells.

a) Trafficking to lysosomes



b) Trafficking to early endosomes

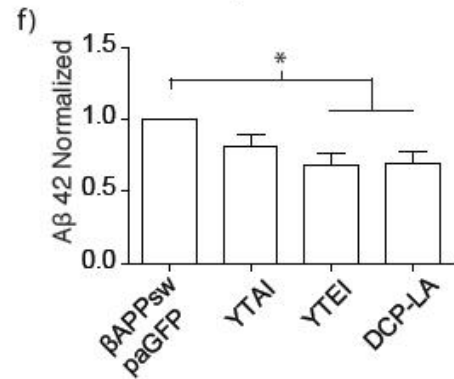
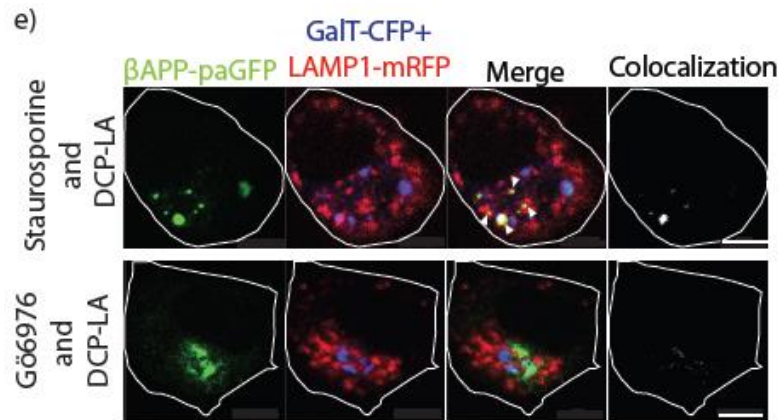
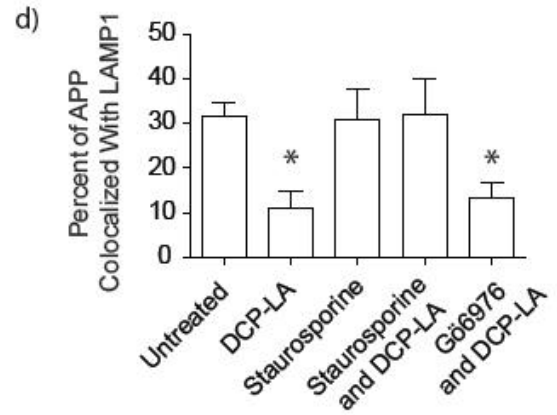
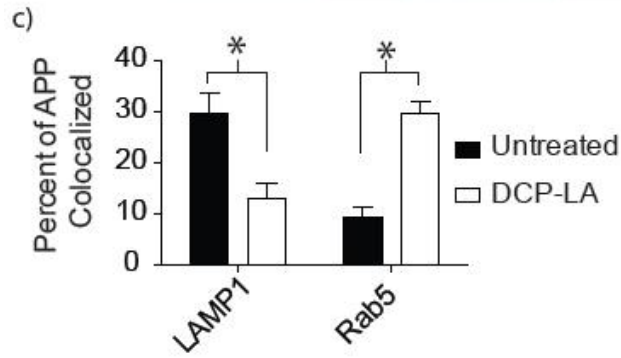
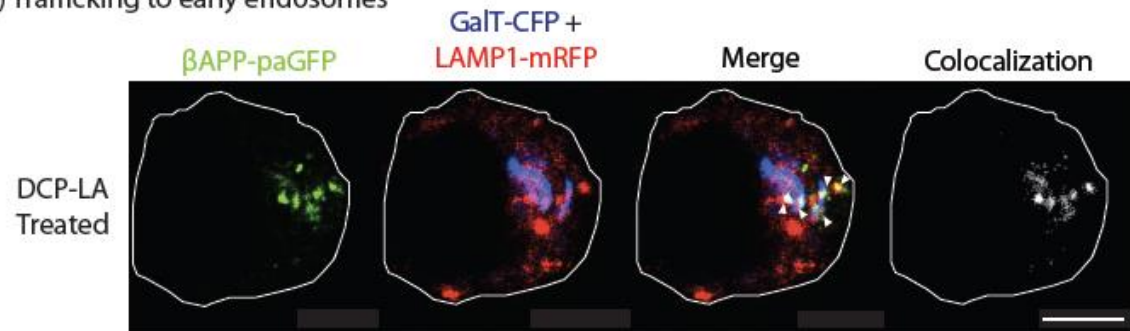


Figure 3.8

### 3.4 Discussion

In our previous study, we showed that siRNA-mediated knockdown of AP-3 can disrupt the trafficking of APP to lysosomes [20]. In the present study, the Y709A decreased intracellular trafficking to the lysosome while the Y743A mutations significantly decreased the fraction of APP delivered to lysosomes from the cell surface and by intracellular trafficking (Figure 3.1 and Figure 3.3). The YTSI motif was critical for APP and AP-3 interaction (Figure 3.4), and phosphorylating the serine residue in this motif reduced intracellular trafficking of APP to lysosomes and reduced A $\beta$ 42 production (Figure 3.5-3.8).

The YTSI motif is a canonical YXX $\theta$  motif. These motifs have roles in endocytosis, lysosomal sorting, basolateral sorting, and retrograde sorting to the Golgi [21]. The YTSI motif has been shown to regulate the endocytosis of a APP- transferrin receptor chimera [6]. However, internalization experiments with APP show that the Y709A mutation to APP did not disrupt endocytosis [8 and Figure 3.2]. The YTSI motif can also interact with AP-1 to sort APP to the basolateral membrane [23].

Interestingly, recent studies have shown that the YTSI motif of APP can also regulate the transit of APP through the Golgi [38,39]. Using a pseudophosphorylation strategy, similar to the one used here, a phosphomimetic (S711E) increased the retrograde trafficking of APP to the TGN, and decreases the trafficking of APP lysosomes. Conversely, a dephosphomimetic mutant decreased retrograde trafficking to the TGN and increases trafficking of APP to lysosomes. The enhanced retrograde trafficking of APP to the TGN was mediated by an enhanced interaction between APP and VPS-35 (a member of the retromer protein trafficking complex) [48,49], reducing APP delivery to lysosomes. Our findings concur with this data, in that pseudophosphorylation of the serine disrupts the interaction of APP and AP-3 and lowers the amount of APP trafficked to lysosomes (Figure 3.4 and 3.5). These findings suggest that phosphorylation of APP at S711 enhances the interaction of APP with the retromer complex [38] and destabilize its interaction with AP-3.

Phorbol ester stimulation of PKC is well known to increase the secretion of the APP N-terminal domain and decrease the production of A $\beta$  [42,43,45,46,50]. Both PKC $\alpha$  and PKC $\epsilon$  have been implicated in regulating the metabolism of APP [43,46,51,52]. In agreement with these findings, PMA or DCP-LA treatment reduced lysosomal trafficking seen with the phosphomimetic S711E (Figure 3.6 and 3.8). Gö6976, an inhibitor of conventional PKCs, did not reduce lysosomal targeting (Figure 3.7). While there was no specific pharmacological inhibitor of PKC $\epsilon$ , a specific agonist of PKC $\epsilon$  (DCP-LA) also diverted APP trafficking away from lysosomes (Figure 3.8). Furthermore, DCP-LA treatment or the phosphomimetic YTEI lowered the production of A $\beta$ <sub>42</sub>, suggesting a shift to non-amyloidogenic processing of APP (Figure 3.8f). Previous literature suggests PKC $\epsilon$ , an novel PKC, promotes non-amyloidogenic cleavage of APP [44-46]. DCP-LA also decreased A $\beta$  secreted in cell culture [46], and reduce the plaque burden in transgenic mouse models of APP [44]. Furthermore, in AD patients, PKC $\epsilon$  protein levels were decreased fibroblasts and neurons [53].

While we show here that phosphorylation of S711 may control intracellular lysosomal trafficking, it does not explain all of the observed behaviors related to PKC activation. Specifically, the phosphomimetic did not increase APP trafficking to early endosomes, as seen with PMA and DCP-LA treatments, which suggests other targets of PKC $\epsilon$  are also involved in APP sorting. PKC is known to regulate other steps in protein trafficking and proteolysis. PKC can also phosphorylate AP-2 in the  $\mu$ 2 domain and regulate the endocytosis of NA<sup>+</sup>/K<sup>+</sup> ATPase [54].

PKC $\epsilon$ , in particular, may also regulate secretory activity from the Golgi after being recruited to the Golgi apparatus [55]. In addition to regulation of Golgi export to the secretory pathway, PKC $\epsilon$  also regulates the recycling of  $\beta$ 1-integrins by phosphorylating vimentin (an integral part of intermediate filaments) [56,57]. While the data presented here suggest a role for APP phosphorylation in lysosomal trafficking and non-amyloidogenic metabolism, PKCs can interact with a large number of proteins; so many other regulatory events might be participating. For example, PKCs may influence the distribution of ADAM-10; a putative  $\alpha$ -secretase [58] and are

proposed to regulate proteolytic processing by secretase enzymes directly. ADAM 10 and 17 [59,60].

Although the alteration of APP processing by PKC has long been recognized, the effects of PKC on the intracellular trafficking of APP are less well understood. Before the advent of photo-activatable fluorescent proteins, the intracellular trafficking of APP, of any protein, was very difficult to visualize. Here, using paGFP that APP can transit directly from the Golgi directly to lysosomes. Furthermore we showing that PKC $\epsilon$  redirects APP from this novel pathway away from the lysosome and reduces A $\beta$  42 production. This is the mirror image of retromer dysfunction in AD, which is proposed to increased APP levels in the endosomal/lysosomal pathway and increased A $\beta$  production [61]. These experiments demonstrate that this novel direct-to lysosome pathway can be regulated pharmacologically and that reducing APP transit to the lysosome is a strategy to lower A $\beta$  42 production.

### 3.5 References

1. Greenfield JP, Tsai J, Gouras GK, Hai B, Thinakaran G, Checler F, et al. Endoplasmic reticulum and trans-Golgi network generate distinct populations of Alzheimer beta-amyloid peptides. *Proc Natl Acad Sci USA*. 1999;96: 742–747.
2. Cirrito JR, Kang J-E, Lee J, Stewart FR, Verges DK, Silverio LM, et al. Endocytosis Is Required for Synaptic Activity-Dependent Release of Amyloid- $\beta$  In Vivo. *Neuron*. 2008;58: 42–51. doi:10.1016/j.neuron.2008.02.003
3. Petanceska SS, Seeger M, Checler F, Gandy S. Mutant presenilin 1 increases the levels of Alzheimer amyloid beta-peptide A $\beta$ 42 in late compartments of the constitutive secretory pathway. *Journal of Neurochemistry*. 2000;74: 1878–1884.
4. Tian Y, Chang JC, Fan EY, Flajolet M, Greengard P. Adaptor complex AP2/PICALM, through interaction with LC3, targets Alzheimer's APP-CTF for terminal degradation via autophagy. *Proceedings of the National Academy of Sciences*. 2013. doi:10.1073/pnas.1315110110
5. Thinakaran G, Koo EH. Amyloid Precursor Protein Trafficking, Processing, and Function. *Journal of Biological Chemistry*. 2008;283: 29615–29619. doi:10.1074/jbc.R800019200
6. Lai A, Sisodia SS, Trowbridge IS. Characterization of sorting signals in the beta-amyloid precursor protein cytoplasmic domain. *J Biol Chem*. 1995;270: 3565–3573.
7. Lai A, Sisodia SS, Trowbridge IS. Characterization of sorting signals in the beta-amyloid precursor protein cytoplasmic domain. *J Biol Chem*. 1995;270: 3565–3573.
8. Perez RG, Soriano S, Hayes JD, Ostaszewski B, Xia W, Selkoe DJ, et al. Mutagenesis identifies new signals for beta-amyloid precursor protein endocytosis, turnover, and the generation of secreted fragments, including A $\beta$ 42. *J Biol Chem*. 1999;274: 18851–18856.
9. Lorenzen A, Samosh J, Vandewark K, Anborgh PH, Seah C, Magalhaes AC, et al. Rapid and Direct Transport of Cell Surface APP to the Lysosome defines a novel selective pathway. *Mol Brain*. 2010;3: 11. doi:10.1186/1756-6606-3-11
10. Tang W, Tam JH, Seah C, Chiu J, Tyrer A, Cregan SP, et al. Arf6 controls beta-amyloid production by regulating macropinocytosis of the Amyloid Precursor Protein to lysosomes. *Mol Brain*. 2015;8: 41. doi:10.1186/s13041-015-0129-7
11. Pasternak SH, Bagshaw RD, Guiral M, Zhang S, Ackerley CA, Pak BJ, et al. Presenilin-1, nicastrin, amyloid precursor protein, and gamma-secretase activity are co-localized in the



- lysosomal membrane. *J Biol Chem.* 2003;278: 26687–26694.  
doi:10.1074/jbc.M212192200
12. Bagshaw RD, Pasternak SH, Mahuran DJ, Callahan JW. Nicastrin is a resident lysosomal membrane protein. *Biochemical and Biophysical Research Communications.* 2003;300: 615–618.
  13. Pasternak SH, Callahan JW, Mahuran DJ. The role of the endosomal/lysosomal system in amyloid-beta production and the pathophysiology of Alzheimer's disease: reexamining the spatial paradox from a lysosomal perspective. *J Alzheimers Dis.* 2004;6: 53–65.
  14. Caporaso GL, Gandy SE, Buxbaum JD, Greengard P. Chloroquine inhibits intracellular degradation but not secretion of Alzheimer beta/A4 amyloid precursor protein. *Proc Natl Acad Sci USA.* 1992;89: 2252–2256.
  15. Haass C, Hung AY, Schlossmacher MG, Teplow DB, Selkoe DJ. beta-Amyloid peptide and a 3-kDa fragment are derived by distinct cellular mechanisms. *J Biol Chem.* 1993;268: 3021–3024.
  16. Schrader-Fischer G, Paganetti PA. Effect of alkalizing agents on the processing of the beta-amyloid precursor protein. *Brain Research.* 1996;716: 91–100. doi:10.1016/0006-8993(96)00002-9
  17. Hirschberg K, Miller CM, Ellenberg J, Presley JF, Siggia ED, Phair RD, et al. Kinetic analysis of secretory protein traffic and characterization of golgi to plasma membrane transport intermediates in living cells. *The Journal of Cell Biology.* 1998;143: 1485–1503.
  18. Patterson GH, Patterson GH, Lippincott-Schwartz J. A photoactivatable GFP for selective photolabeling of proteins and cells. *Science. American Association for the Advancement of Science;* 2002;297: 1873–1877. doi:10.1126/science.1074952
  19. Patterson GH, Lippincott-Schwartz J. Selective photolabeling of proteins using photoactivatable GFP. *Methods.* 2004;32: 445–450. doi:10.1016/j.ymeth.2003.10.006
  20. Tam JH, Seah C, Pasternak SH. The Amyloid Precursor Protein is rapidly transported from the Golgi apparatus to the lysosome and where it is processed into beta-amyloid. *Mol Brain. BioMed Central Ltd;* 2014;7: 54. doi:10.1186/s13041-014-0054-1
  21. Bonifacino JS, Traub LM. Signals for sorting of transmembrane proteins to endosomes and lysosomes. *Annu Rev Biochem.* 2003;72: 395–447.  
doi:10.1146/annurev.biochem.72.121801.161800
  22. Burgos PV, Mardones GA, Rojas AL, daSilva LLP, Prabhu Y, Hurley JH, et al. Sorting of the Alzheimer's disease amyloid precursor protein mediated by the AP-4 complex. *Developmental Cell.* 2010;18: 425–436. doi:10.1016/j.devcel.2010.01.015

23. Icking A, Amaddii M, Ruonala M, Höning S, Tikkanen R. Polarized Transport of Alzheimer Amyloid Precursor Protein Is Mediated by Adaptor Protein Complex AP1-1B. *Traffic*. 2006;8: 285–296. doi:10.1111/j.1600-0854.2006.00526.x
24. Schneider A, Rajendran L, Honsho M, Gralle M, Donnert G, Wouters F, et al. Flotillin-Dependent Clustering of the Amyloid Precursor Protein Regulates Its Endocytosis and Amyloidogenic Processing in Neurons. *Journal of Neuroscience*. 2008;28: 2874–2882. doi:10.1523/JNEUROSCI.5345-07.2008
25. Davis CG, Lehrman MA, Russell DW, Anderson RG, Brown MS, Goldstein JL. The J.D. mutation in familial hypercholesterolemia: amino acid substitution in cytoplasmic domain impedes internalization of LDL receptors. *Cell*. 1986;45: 15–24.
26. Chen WJ, Goldstein JL, Brown MS. NPXY, a sequence often found in cytoplasmic tails, is required for coated pit-mediated internalization of the low density lipoprotein receptor. *J Biol Chem*. 1990;265: 3116–3123.
27. Suzuki T, Nairn AC, Gandy SE, Greengard P. Phosphorylation of Alzheimer amyloid precursor protein by protein kinase C. *NSC*. 1992;48: 755–761. doi:10.1016/0306-4522(92)90264-3
28. Gandy S, Czernik AJ, Greengard P. Phosphorylation of Alzheimer disease amyloid precursor peptide by protein kinase C and Ca<sup>2+</sup>/calmodulin-dependent protein kinase II. *Proc Natl Acad Sci USA*. 1988;85: 6218–6221.
29. Tam JH, Pasternak SH. Imaging the Intracellular Trafficking of APP with Photoactivatable GFP. *J Vis Exp*. 2015;: 1–9. doi:10.3791/53153
30. Muresan V, Varvel NH, Lamb BT, Muresan Z. The cleavage products of amyloid-beta precursor protein are sorted to distinct carrier vesicles that are independently transported within neurites. *Journal of Neuroscience*. 2009;29: 3565–3578. doi:10.1523/JNEUROSCI.2558-08.2009
31. Lai A, Gibson A, Hopkins CR, Trowbridge IS. Signal-dependent trafficking of beta-amyloid precursor protein-transferrin receptor chimeras in madin-darby canine kidney cells. *J Biol Chem*. 1998;273: 3732–3739.
32. Cai J, Chen Z, Ruan Q, Han S, Liu L, Qi X, et al. -Secretase and Presenilin Mediate Cleavage and Phosphorylation of Vascular Endothelial Growth Factor Receptor-1. *Journal of Biological Chemistry*. 2011;286: 42514–42523. doi:10.1074/jbc.M111.296590
33. Greenberg JI, Shields DJ, Barillas SG, Acevedo LM, Murphy E, Huang J, et al. A role for VEGF as a negative regulator of pericyte function and vessel maturation. *Nature*. 2008;456: 809–813. doi:10.1038/nature07424
34. Gajadhar A, Guha A. A proximity ligation assay using transiently transfected, epitope-

- tagged proteins: application for in situ detection of dimerized receptor tyrosine kinases. *BioTechniques*. 2010;48: 145–152. doi:10.2144/000113354
35. Dilsizoglu Senol A, Tagliafierro L, Huguet L, Gorisse-Hussonnois L, Chasseigneaux S, Allinquant B. PAT1 inversely regulates the surface Amyloid Precursor Protein level in mouse primary neurons. *BMC Neurosci*. BioMed Central Ltd; 2015;16: 10. doi:10.1186/s12868-015-0152-8
  36. Zheng P, Eastman J, Vande Pol S, Pimplikar SW. PAT1, a microtubule-interacting protein, recognizes the basolateral sorting signal of amyloid precursor protein. *Proc Natl Acad Sci USA*. National Academy of Sciences; 1998;95: 14745–14750.
  37. Lee M-S, Kao S-C, Lemere CA, Xia W, Tseng H-C, Zhou Y, et al. APP processing is regulated by cytoplasmic phosphorylation. *Journal of Cell Biology*. 2003;163: 83–95. doi:10.1083/jcb.200301115
  38. Vieira SI, Rebelo S, Esselmann H, Wiltfang J, Lah J, Lane R, et al. Retrieval of the Alzheimer's amyloid precursor protein from the endosome to the TGN is S655 phosphorylation state-dependent and retromer-mediated. *Molecular Neurodegeneration*. 2010;5: 40. doi:10.1186/1750-1326-5-40
  39. Vieira SI, Rebelo S, Domingues SC, Cruz e Silva EF, Cruz e Silva OAB. S655 phosphorylation enhances APP secretory traffic. *Mol Cell Biochem*. 2009;328: 145–154. doi:10.1007/s11010-009-0084-7
  40. Skovronsky DM, Moore DB, Milla ME, Doms RW, Lee VM. Protein kinase C-dependent alpha-secretase competes with beta-secretase for cleavage of amyloid-beta precursor protein in the trans-golgi network. *Journal of Biological Chemistry*. 2000;275: 2568–2575. doi:10.1074/jbc.275.4.2568
  41. Lammich S, Kojro E, Postina R, Gilbert S, Pfeiffer R, Jasionowski M, et al. Constitutive and regulated alpha-secretase cleavage of Alzheimer's amyloid precursor protein by a disintegrin metalloprotease. *Proc Natl Acad Sci USA*. 1999;96: 3922–3927.
  42. Benussi L, Govoni S, Gasparini L, Binetti G, Trabucchi M, Bianchetti A, et al. Specific role for protein kinase C alpha in the constitutive and regulated secretion of amyloid precursor protein in human skin fibroblasts. *Neuroscience Letters*. 1998;240: 97–101.
  43. Kinouchi T, Sorimachi H, Maruyama K, Mizuno K, Ohno S, Ishiura S, et al. Conventional protein kinase C (PKC)-alpha and novel PKC epsilon, but not -delta, increase the secretion of an N-terminal fragment of Alzheimer's disease amyloid precursor protein from PKC cDNA transfected 3Y1 fibroblasts. *FEBS Letters*. 1995;364: 203–206.
  44. Hongpaisan J, Sun M-K, Alkon DL. PKC  $\epsilon$  activation prevents synaptic loss, A $\beta$  elevation, and cognitive deficits in Alzheimer's disease transgenic mice. *Journal of*

- Neuroscience. 2011;31: 630–643. doi:10.1523/JNEUROSCI.5209-10.2011
45. Yeon SW, Jung MW, Ha MJ, Kim SU, Huh K, Savage MJ, et al. Blockade of PKC $\epsilon$  Activation Attenuates Phorbol Ester-Induced Increase of  $\alpha$ -Secretase-Derived Secreted Form of Amyloid Precursor Protein. *Biochemical and Biophysical Research Communications*. 2001;280: 782–787. doi:10.1006/bbrc.2000.4181
  46. Nelson TJ, Cui C, Luo Y, Alkon DL. Reduction of beta-amyloid levels by novel protein kinase C(epsilon) activators. *J Biol Chem*. 2009;284: 34514–34521. doi:10.1074/jbc.M109.016683
  47. Kanno T. The linoleic acid derivative DCP-LA selectively activates PKC- $\epsilon$ , possibly binding to the phosphatidylserine binding site. *The Journal of Lipid Research*. 2006;47: 1146–1156. doi:10.1194/jlr.M500329-JLR200
  48. Vieira SI, Rebelo S, Esselmann H, Wiltfang J, Lah J, Lane R, et al. Retrieval of the Alzheimer's amyloid precursor protein from the endosome to the TGN is S655 phosphorylation state-dependent and retromer-mediated. *Molecular Neurodegeneration*. 2010;5: 40. doi:10.1186/1750-1326-5-40
  49. Bonifacino JS, Hurley JH. Retromer. *Current Opinion in Cell Biology*. 2008;20: 427–436. doi:10.1016/j.ceb.2008.03.009
  50. Gabuzda D, Busciglio J, Yankner BA. Inhibition of beta-amyloid production by activation of protein kinase C. *Journal of Neurochemistry*. 1993;61: 2326–2329. doi:10.1111/j.1471-4159.1993.tb07479.x
  51. Lanni C, Mazzucchelli M, Porrello E, Govoni S, Racchi M. Differential involvement of protein kinase C alpha and epsilon in the regulated secretion of soluble amyloid precursor protein. *European Journal of Biochemistry*. 2004;271: 3068–3075. doi:10.1111/j.1432-1033.2004.04240.x
  52. Racchi M, Mazzucchelli M, Pascale A, Sironi M, Govoni S. Role of protein kinase C[alpha] in the regulated secretion of the amyloid precursor protein. *Mol Psychiatry*. Nature Publishing Group; 2003;8: 209–216. doi:10.1038/sj.mp.4001204
  53. Khan TK, Khan TK, Sen A, Sen A, Hongpaisan J, Lim CS, et al. PKC $\epsilon$  deficits in Alzheimer's disease brains and skin fibroblasts. *J Alzheimers Dis*. 2015;43: 491–509. doi:10.3233/JAD-141221
  54. Chen Z, Krmar RT, Dada L, Efendiev R, Leibiger IB, Pedemonte CH, et al. Phosphorylation of adaptor protein-2 mu2 is essential for Na<sup>+</sup>,K<sup>+</sup>-ATPase endocytosis in response to either G protein-coupled receptor or reactive oxygen species. 2006;35: 127–132. doi:10.1165/rcmb.2006-0044OC
  55. Lehel C, Olah Z, Jakab G, Anderson WB. Protein kinase C epsilon is localized to the

- Golgi via its zinc-finger domain and modulates Golgi function. *Proc Natl Acad Sci USA*. 1995;92: 1406–1410.
56. Ivaska J, Whelan RDH, Watson R, Parker PJ. PKC epsilon controls the traffic of beta1 integrins in motile cells. *The EMBO Journal*. 2002;21: 3608–3619. doi:10.1093/emboj/cdf371
  57. Ivaska J, Vuoriluoto K, Huovinen T, Izawa I, Inagaki M, Parker PJ. PKCepsilon-mediated phosphorylation of vimentin controls integrin recycling and motility. *The EMBO Journal*. 2005;24: 3834–3845. doi:10.1038/sj.emboj.7600847
  58. Saraceno C, Marcello E, Di Marino D, Borroni B, Claeysen S, Perroy J, et al. SAP97-mediated ADAM10 trafficking from Golgi outposts depends on PKC phosphorylation. *Cell Death Dis*. 2014;5: e1547. doi:10.1038/cddis.2014.492
  59. Ohtsu H, Dempsey PJ, Eguchi S. ADAMs as mediators of EGF receptor transactivation by G protein-coupled receptors. *Am J Physiol, Cell Physiol*. 2006;291: C1–10. doi:10.1152/ajpcell.00620.2005
  60. Lemjabbar-Alaoui H, Sidhu SS, Mengistab A, Gallup M, Basbaum C. TACE/ADAM-17 Phosphorylation by PKC-Epsilon Mediates Premalignant Changes in Tobacco Smoke-Exposed Lung Cells. Rich B, editor. *PLoS ONE*. 2011;6: e17489. doi:10.1371/journal.pone.0017489.g008
  61. Retromer in Alzheimer disease, Parkinson disease and other neurological disorders. 2015;16: 126–132. doi:10.1038/nrn3896

## Chapter 4

### 4 Lysosomal secretion of beta-amyloid in neuronal cells

One of the hallmarks of Alzheimer's disease is the presence of amyloid plaques in the brain. The major constituent of these plaques is  $\beta$ -amyloid ( $A\beta$ ).  $A\beta$  is known to bind to receptors on the cell surface and mediate many of its cytotoxic effects. Work from our lab and others suggest that  $A\beta$  is produced through amyloidogenic cleavage in the endosomal/lysosomal system. However, the mechanism behind the secretion of  $A\beta$ , from intracellular stores, into the extracellular space is unknown. Lysosomes are known to undergo exocytosis in a number of cell types, including neurons. Therefore, lysosomes may serve to produce and secrete  $A\beta$  into the extracellular space.

Here, using total internal reflection fluorescence microscopy (TIR-FM), we show that a population of lysosomes are localized to the cell surface and can undergo exocytosis in SN56 cells. Furthermore, we show that SN56 cells transfected with mutants of Rab27b can decrease the number of lysosomes at the cell surface and decrease lysosomal exocytosis. Furthermore, these mutants can also decrease the amount of  $A\beta$  secreted into the cell culture media. Taken together, these data suggest that lysosomal exocytosis is capable of  $A\beta$  secretion, and may prove to be an important therapeutic target for limiting the effect of extracellular  $A\beta$  aggregates.

#### 4.1 Introduction

Alzheimer's disease (AD) is the most common neurodegenerative disease in adults. The Amyloid Hypothesis states that the  $\beta$ -amyloid ( $A\beta$ ) production is a critical early event in the pathogenesis of AD. In fact, amyloid deposition is required for a neuropathological diagnosis of AD. Although  $A\beta$  was identified more than 30 years ago, there is no consensus as to how it is secreted [1]. While it is widely accepted that neuronal activity results in Amyloid secretion, to date  $A\beta$  is not found in synaptic vesicles [2]. Although full-length APP and BACE are present in synaptic vesicles, only APP was demonstrated to be secreted from synaptic vesicles [3].  $A\beta$  has been shown to be secreted in exosomes (intraluminal vesicles from the endosomal/lysosomal system) suggesting that these compartments might be responsible for  $A\beta$  secretion [3,4].

A $\beta$  is produced by the sequential cleavage of APP by  $\beta$  and  $\gamma$ -secretase.  $\beta$ -secretase cleaves APP in ectodomain and leaves a 99-residue carboxy-terminal fragment, which is a substrate for  $\gamma$ -secretase. Work in our lab has shown that  $\gamma$ -secretase protein complex is present in lysosomes and  $\gamma$ -secretase's catalytic activity functions at an acidic optimal pH [5]. Alkalization lysosomal pH also lowers A $\beta$  production [6]. Acidic environments, similar to those in lysosomes, have been shown to promote A $\beta$  aggregation [7]. In addition, disruption of APP trafficking to lysosomes has been shown to decrease A $\beta$  production [8-11]. The lysosomes promote formation of amyloid seeds that promote A $\beta$  aggregation [12], and many have proposed the lysosome as an important early site of aggregation [13-16]. This evidence suggests that the lysosome might be a source of secreted A $\beta$ .

Although lysosomes are widely viewed as digestive organelles, modified lysosomes (lysosome-related organelles, LROs) are responsible for secretion in many cell types. LROs share a number similarities with lysosomes (organelle markers, low pH, hydrolases), but have cell-type specific tasks that allow them to perform varied tasks, such as skin pigmentation and clotting [reviewed in 17,18]. For example many dedicated-secretory cells (natural killer cells, melanocytes, lymphocytes, platelets) use secretory LROs as important secretory granules (lytic granules, melanosomes, azurophilic granules, platelet-dense granules) [17-30]. More recently, studies in cells that are not dedicated secretory cells have also demonstrated the use of lysosomal secretion, the secretion of conventional lysosomes can also be used for resealing damage to the plasma membrane damage [31].

Although secretory lysosomes have been documented in many cell types, there have been few reports of lysosomes playing a secretory role in neuronal cells [32,33]. Here we show, by TIRF microscopy, that a population of lysosomes sits docked on the plasma membrane in neuronal cells and primary mouse neurons are able to fuse with the plasma membrane following stimulation. Furthermore, lysosomes accumulated amyloid and are able to secrete endogenous A $\beta$  into the extracellular space in a Rab27 dependent manner.

## 4.2 Materials and Methods

### 4.2.1 Antibodies and Chemicals

Antibodies used were Mouse Anti-HA (Sigma, H9658), rabbit anti-LAMP1 (Sigma, L1418), rat anti-LAMP1 1D4B, APP C-terminal (Sigma, A8717), and anti-A $\beta$  (MOAB-2, Novus Biologicals, Cat. # NBP2-13075). HiLyte Fluor 488 A $\beta$ 42 (A $\beta$ 42-488) was purchased from Anaspec (Cat. # AS-60479-01). Bafilomycin was purchased from Calbiochem (CAS 88899-55-2).

### 4.2.2 Cell Culture

SN56 cells were maintained in Dulbecco's minimal Eagle's medium (DMEM, Invitrogen) with 10% fetal bovine serum (FBS) and 50ug/ml of penicillin/streptomycin. Cells were incubated in an incubator at 37°C with 5% CO<sub>2</sub>. SN56 cells were split every 3-4 days at approximately 90% confluence. To plate cells for imaging, SN56 cells were plated on glass bottom confocal plates one day before transfection. Transfections were performed using Lipofectamine 2000 according to manufacturer's instructions. In order to differentiate SN56 cells, transfection media was switched to DMEM with 1mM dibutyl cyclic AMP (dbcAMP; Sigma) 24 hours after transfection. Cells were differentiated for one day and imaged or fixed and stained for imaging.

### 4.2.3 Plasmid Constructs

Rab5-mRFP, LAMP1-mRFP, and  $\beta$ APP-CFP with the Swedish mutation have been described previously [9]. The design and use of the CatD-mChFP plasmid have been previously described [34,35]. mApple-LAMP1-phLuorin was a kind gift of Michael Davidson (Addgene plasmid # 54918). A construct encoding TIVAMP7 coupled to pHluorin was a gift from Dr. Thierry Gali. Rab27bWT-GFP was a kind gift from Gottfried Mieskes [36]. The Rab27b GFP-tagged mutants were obtained from Reinhard Jan [37].

### 4.2.4 Confocal Microscopy

Confocal microscopy images were obtained with a Zeiss LSM-510 META laser-scanning microscope using a Zeiss 63x 1.4 numerical aperture oil immersion lens (Carl Zeiss, Germany).



The thickness of the optical section was set to 1  $\mu\text{m}$ . To visualize Cyan fluorescent protein (CFP), CFP was excited with a 458 nm laser and filtered with a BP 475-525 filter set. pHluorin fluorescence was filtered a band pass (BP) 500-530-nm emission filter set after excitation with a 488 nm. mCherry and mRFP fluorescence were excited with a 543 nm laser and filtered with a BP 560–615nm of LP 560nm filter set. For fixed cells, the culture media was removed and cells were washed with PBS before being fixed with 4% paraformaldehyde. When staining with 1D4B for LAMP1 cells were permeabilized with 0.1% Triton in PBS. Non-specific binding was blocked with 2% BSA and stained for LAMP1. The rabbit-anti LAMP1 antibody required permeabilization with 1% saponin in 1% BSA in HBSS. Cells were stained with the rabbit-anti LAMP1 antibody after permeabilization.

For live cell imaging, SN56 cells were washed and were switched to pre-warmed to 37°C HBSS. Cells were kept at 37°C using a heated microscopy stage (PeCon GmbH) connected to a Tempcontrol 37-2 digital 2-channel (PeCon GmbH). To prevent reacidification, lysosomes were treated with 1  $\mu\text{M}$  of bafilomycin for 20 minutes. Lysosomal exocytosis was stimulated with 5  $\mu\text{M}$  of ionomycin. A time course was set to capture an image every minute to follow lysosomal exocytosis, as denoted by increased TIVAMP-pHluorin fluorescence.

To semi-quantitatively measure the amount of exocytosis after transfection with the Rab27b-GFP constructs, cells were treated with 5  $\mu\text{M}$  ionomycin for five minutes and immediately placed on ice. Cells were washed and fixed with 4% paraformaldehyde.

#### 4.2.5 Total internal reflection fluorescence microscopy (TIR-FM)

TIR-FM images were captured using a Leica AM TIRF MC using an HCX PL APO 63X oil immersion objective with numerical aperture of 1.47. In order to image the cell surface population of organelles. SN56 cells were plated on a glass-bottom confocal plate. Cells were fixed after transfection with the denoted plasmid.

For live cell trafficking experiments, SN56 cells were plated on a glass-bottom confocal plate. The differentiation media was removed and cells were washed with PBS. The media was replaced with HBSS pre-warmed to 37°C. The confocal plate was then transferred to the

microscope stage pre-warmed to 37°C. Live cell TIR-FM videos were acquired with a Leica AM TIRF MC using an HCX PL APO 100X oil immersion objective with numerical aperture of 1.47. All fluorescence emitted from 405/488/561 and 635nm lasers was captured after filtering through a Quad-band filter cube (Emission: BP 450/50, BP 525/36, BP 600/32, BP 705/72). To capture blue fluorescence protein (BFP) emission, BFP was excited with a 405 nm laser and could be detected using Quad-band filter cube. The microscope lacks a 458 nm laser, but excitation of CFP with a 405 nm laser was adequate for detecting CFP fluorescence. GFP and pHluorin were excited with a 488 nm laser. Dextran tetramethylrhodamine was excited with a 561 nm laser. Zenon 647 detection reagent was detected after excitation with a 635 nm laser.

To inject ionomycin onto the sample, a glass micropipette was attached to a FemtoJet microinjection system (Eppendorf, Mississauga, ON, Canada) and placed at the desired position over the cells. To capture rapid exocytic events, the imaging time for each wavelength was set to 50 ms. Due to hardware movement between wavelength, the total imaging time for one frame was 112ms. Video was captured for 3-5 minutes after ionomycin treatment. The videos were analyzed for exocytic vesicles one minute after ionomycin treatment.

#### 4.2.6 Counting vesicles at the cell surface

The number of vesicles in each TIR-FM image was quantified using a semi-automated method in Imaris using the built-in spot algorithm. The average size of the vesicle is determined by the user and Imaris searches for the vesicles in the image. The threshold can be manually adjusted, as required, to accurately select all vesicles. The Imaris program provides the number of vesicles. Using Imaris, a rough estimate of background can also be determined using a semi-automated method. The cell body typically has a higher level of noise than areas of the coverslip that are empty. IsoSurfaces can be created in Imaris based on this background fluorescence, which provides an estimate of cell size. From the IsoSurface, the approximate area of the cell touching the glass coverslip can be determined. By dividing the number of vesicles at the cell surface by the area of the cell on the glass, the number of vesicles per cell can be normalized to surface area.

#### 4.2.7 Detecting Exocytosis

Lysosomal exocytosis was detected by manually tracking lysosomes in single- or dual-colour images using ImageJ [38] and the ‘Manual Tracking’ plugin. A custom-written Matlab script (Mathworks, Natick, Massachusetts) was then used to detect putative exocytosis events. Briefly, the mean intensity of each lysosome was determined by averaging the pixel values around each manually tracked point, at each time point in the track, over a disk approximately the size of lysosomes in the image (radius of 5 pixels). Each track was then normalized to its minimum and maximum intensity, the intensity data smoothed over 10 time-points, and the derivative (slope) of the smoothed intensity graph calculated. Putative exocytosis events were defined as derivative values less than 2 times the standard deviation of the derivative plot (i.e. > 2 standard deviation decrease in lysosome intensity). Tracks containing putative exocytosis events were then flagged and manually curated to detect *bona fide* exocytosis events. To compare the proportion of vesicles secreted between luminal and membrane cargos, a  $\chi^2$  analysis was used to compare the luminal and membrane cargos.

#### 4.2.8 Neuronal Culture

All animal experiments were conducted in accordance with the University of Western Ontario Animal Care Committee. Alzheimer’s disease mice were B6C3-Tg (APP<sup>swe</sup>/PSEN1 $\Delta$ E9)85Dbo/J mice, which carry the human APP with Swedish mutation and human presenilin 1 gene with the DeltaE9 mutation. Primary cortical neurons were obtained from E18 embryos, as previously described [39]. Glass-bottom confocal plates (Matek) were coated with poly-L-lysine and seeded with neurons. The neurons were maintained in Neurobasal medium supplemented with 1X B25 and 0.8X N2 supplements, 2mM glutamax and 50U/mL penicillin/streptomycin (Life Technologies). Neurons were grown in a humidified incubator at 37°C with 5% CO<sub>2</sub>. Neurobasal media was replenished once every 4 days.

After 14 days *in vitro* (DIV), neurons were fixed with 4% paraformaldehyde HBSS supplemented with 4% sucrose for 15-minutes. Cells were stained for A $\beta$  and LAMP1 and imaged with confocal microscopy. Colocalization was analyzed as described below.

#### 4.2.9 Colocalization Analysis

Colocalization analysis was performed on using Imaris 7.2.1 Imaris Colocalization module (Biplane). For fixed cells, the brightest 2% of pixels from each channel was chosen and colocalized [9].

#### 4.2.10 APP internalization into lysosomes

We have previously shown that APP can be labelled on the cell surface and internalized rapidly into lysosomes [39]. SN56 cells were transfected with full-length APP-695 and LAMP1-YFP according to the protocol described above. After transfection and differentiation, the culture media was removed and cells were washed with PBS. To label APP on the cell surface, a Zenon Alexa Fluor 647 was conjugated with the 6E10 antibody. SN56 cells were placed on ice and labelled with the Zenon-6E10 conjugate. After labelling for 30 minutes, the bound antibody conjugate was internalized for one hour at 37°C. The exocytosis of internalized antibody was observed by TIR-FM after treatment with 5µM ionomycin.

#### 4.2.11 Staining of LAMP1 at the Cell Surface

SN56 cells transfected with Rab27b WT, T23N, N133I, or Q78L tagged with GFP. Cells were treated with 2.5µM ionomycin for five minutes and fixed with 4% PFA. After fixation, cells were stained for LAMP1 with the 1D4B antibody without permeabilization. Cells were imaged by confocal microscopy with the optical slice set to 5µm, in order to maximize the amount of fluorescence captured.

The relative fluorescence intensity was measured in ImageJ. Transfected cells were selected with the freeform drawing/selection tool. The area and mean fluorescence intensity was measured for each cell and plotted in Prism 5.0b.

#### 4.2.12 Aβ40 and Aβ42 ELISA

SN56 cells were transfected with βAPP<sup>sw</sup>-CFP (βAPP bearing the Swedish mutation). Cells were differentiated and cell culture media was collected two days after differentiation. To remove the large cellular debris, the collected media was spun at 200 G for 10 minutes at 4°C.

A $\beta$ 40 and A $\beta$ 42 were detected with the A $\beta$ 40 ELISA Kit (KHB3482) or A $\beta$ 42 Ultrasensitive ELISA Kit (KHB3544) from Life Technologies, and used according to manufacturer's instructions.

#### 4.2.13 Statistical Analysis

Prism Graphpad 5.0b was used for all graphing and statistical analysis. A One-way ANOVA was performed with a Bonferroni's post-hoc test, and P values <0.05 were considered significant.

### 4.3 Results

#### 4.3.1 Lysosomes at the cell surface

To determine whether lysosomes are membrane docked organelles in neuronal cells, we examined organelles in cultured SN56 cells neuronal cells. The SN56 cell line is a hybrid cell line generated by fusing dissociated embryonic mouse septal neurons with N18TG2 neuroblastoma cells. SN56 cells possess a neuronal morphology and cholinergic phenotype when differentiated and express endogenous APP [40,41]. SN56 cells were transfected with a panel of fluorescent-tagged organelle markers, including synaptophysin-GFP (synapses), LAMP1-mRFP (lysosomes), Cathepsin D -mCherryFP (CatD-ChFP, a luminal lysosomal enzyme), Rab5-mRFP (early endosomes), Rab9-chFP, (late endosomes), and Galactosyltransferase-CFP (GalT-CFP, trans-golgi network). SN56 cells were imaged using total internal reflection fluorescence microscopy (TIR-FM) to visualize organelles within 110nm of the cell surface and count the number of vesicles per  $\mu\text{m}^2$ . We found that lysosomes were docked at the plasma membrane, as shown by CatD-mChFP and LAMP1-mRFP fluorescence ( $0.14 \pm 0.016$  vesicles/ $\mu\text{m}^2$  SEM n=4 independent experiments, 59 cells total and  $0.28 \pm 0.050$  vesicles/ $\mu\text{m}^2$  SEM n=3 independent experiments, 39 cells total, respectively) (Figure 4.1a and b). CatD-chFP was found at the cell surface at similar levels to Rab5-mRFP ( $0.14 \pm 0.0082$  vesicles/ $\mu\text{m}^2$  SEM, n=4 independent experiments, 73 cells total), Rab7-mRFP ( $0.12 \pm 0.018$  vesicles/ $\mu\text{m}^2$  SEM, n=3 independent experiments, 41 cells total), Rab9-chFP ( $0.16 \pm 0.007$  vesicles/ $\mu\text{m}^2$  SEM, n=4 independent experiments, 60 cells total), and synaptophysin-GFP ( $0.16 \pm 0.0070$  vesicles/ $\mu\text{m}^2$  SEM, n=4 independent experiments, 60 cells total). As expected, no GalT-CFP fluorescence was detectable

at the cell surface. Interestingly, the numbers of LAMP1 positive vesicles at the cell surface are significantly higher than any other organelle marker. Therefore, in SN56 cells, lysosomes are among the resident organelles at the cell surface.

**Figure 4.1:** Neuronal lysosomes are found at the plasma membrane.

SN56 cells were transiently transfected with a panel of organelle markers (GalT-CFP, synaptophysin-GFP, Rab5 mRFP, Rab7-mRFP, Rab9-chFP, LAMP1-mRFP, or Cathepsin D-mChFP). **a)** Cells were imaged using TIR-FM to determine the number of vesicles within 110nm of the cell surface. Vesicles and cell area were determined using ImageJ and the number of vesicles per  $\mu\text{m}$ . **b)** TIR-FM images of LAMP1-mRFP and CatD-mChFP images at the cell surface are shown scale bars represent  $10\mu\text{m}$ . **c)** Cells were transfected with Rab27bWT-GFP, Rab27b Q78L-GFP, Rab27b N133I-GFP, or Rab27b T23N-GFP. TIR-FM imaging was used to determine if Rab27b mutants affected the number of lysosomes docked at the cell surface. Cells were stained for LAMP1 using 1D4B. Representative TIR-FM images (within 110nm of the cell surface) of cells transfected with Rab27b mutants and stained for LAMP1. Scale bars represent  $5\mu\text{m}$ . **d)** Using ImageJ, the number of vesicles was counted and normalized using cell area and graphed. Scaled bars represent SEM ( $*=p<0.05$ ). White lines denote the edge of individual cells.

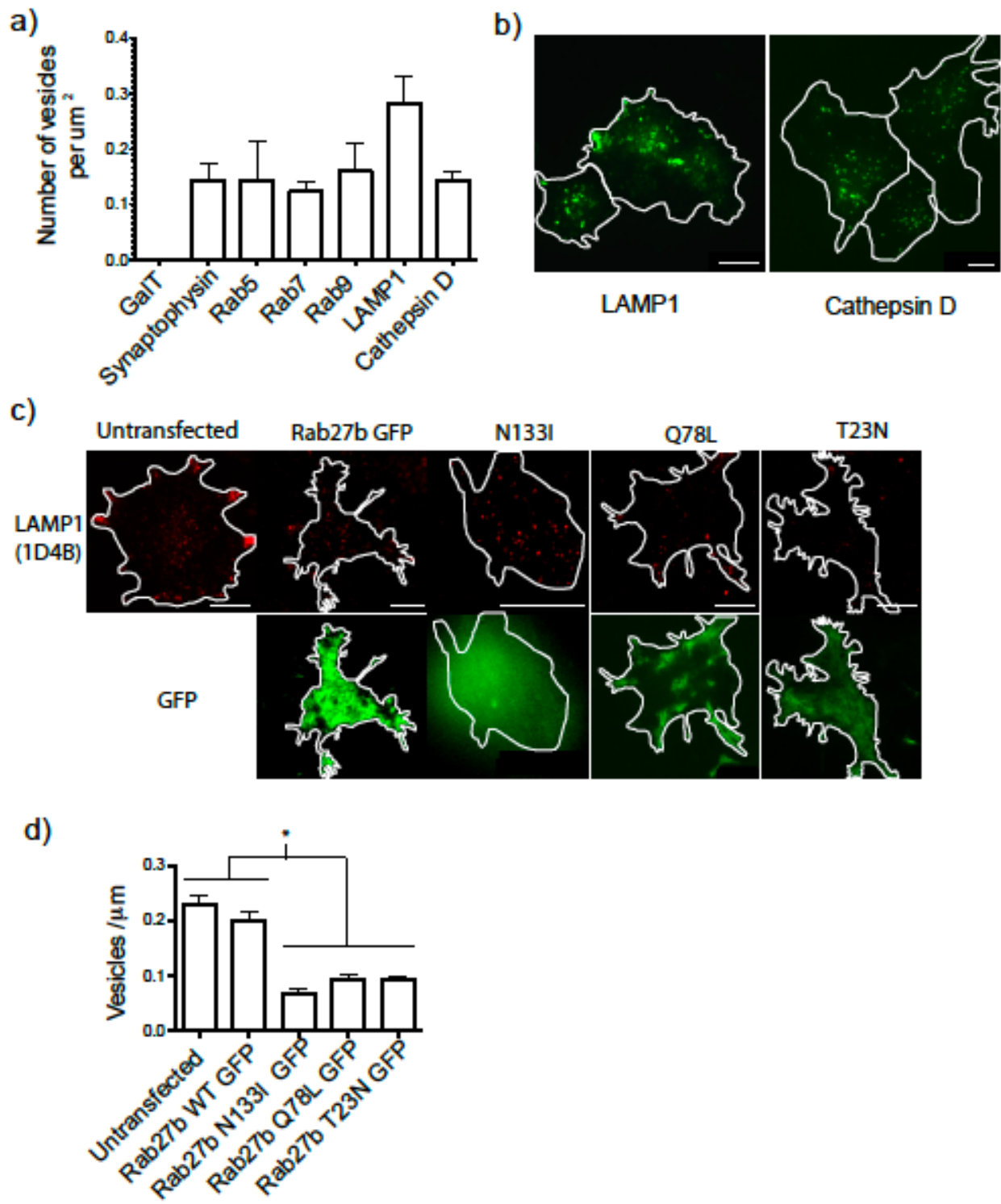


Figure 4.1



### 4.3.2 Rab27b Mutants Reduce Number of Lysosomes at Cell Surface

Rab27a and Rab27b have been implicated in the delivery and docking of lysosome-related organelles LROs to the cell surface in several cell types [42,43]. Rab27 is a regulatory protein that at rest is inactive and binds GDP. When Rab27 is activated, this GDP is exchanged for GTP, which is eventually hydrolyzed to GDP, moving the protein back to its inactive state. Rab27a silencing has been shown to decrease the number of dense-core vesicles at the plasma membrane of PC12 cells [43]. Rab27b has been shown to be involved in the proper distribution of melanosomes, docking of secretory granules, and exosome secretion [36,42,44,45]. As the Rab27b isoform is more highly expressed in the brain [42], we wanted to determine if Rab27b was important for lysosomal docking at the cell surface of neuronal cells. SN56 cells were transfected with Rab27bWT-GFP or with one of the following mutants; constitutively active, which is defective in GTP hydrolysis (Q78L) or dominant negative mutants defective in GTP binding (N133I or T23N) [45,46].

We then fixed the cells, stained them with an antibody against LAMP1, and imaged using TIR-FM. Cells transfected with wild-type (WT) Rab27b had  $0.20 \pm 0.014$  vesicles/ $\mu\text{m}^2$  SEM,  $n=8$  independent experiments, 90 cells total). This was not significantly different from the number of LAMP1 vesicles docked at the membrane of untransfected cells ( $0.23 \pm 0.015$  vesicles/ $\mu\text{m}^2$  SEM,  $n=3$  independent experiments, 54 cells total) (Figure 4.1c and d). However, transfection of Q78L, N133L, or T23N mutants all significantly reduced the number of docked lysosomes ( $0.095 \pm 0.0073$  vesicles/ $\mu\text{m}^2$  SEM,  $n=5$  independent experiments, 53 cells total,  $0.069 \pm 0.0092$  vesicles/ $\mu\text{m}^2$  SEM,  $n=3$  independent experiments, 30 cells total, and  $0.094 \pm 0.0053$  vesicles/ $\mu\text{m}^2$  SEM,  $n=3$  independent experiments, 32 cells total, respectively,  $p<0.05$ ) (Figure 4.1c and d). The reduced number of lysosomes in SN56 cells transfected with mutant versions of Rab27b suggests that Rab27b is involved in lysosome delivery to the cell surface.

**Figure 4.2:** Neuronal lysosomes can undergo stimulated exocytosis.

**a)** SN56 cells were transfected with Rab27b-GFP or one of its mutants. Cells were treated with 2.5 $\mu$ M ionomycin for 5 minutes and fixed. LAMP1 at the cell-surface was stained with 1D4B, without permeabilization. Scale bars represent 30 $\mu$ m. **b)** The fluorescence intensity was quantified for each cell in ImageJ, and graphed using Prism Graphpad. Error bars denote SEM. (\*= $p < 0.05$ ) **c)** Neuronal cells were cultured and stimulated with 2.5 $\mu$ m ionomycin and stained for cell-surface 1D4B. Cells treated with ionomycin show a prominent cell-surface stain for LAMP1. Scale bars represent 50 $\mu$ m.

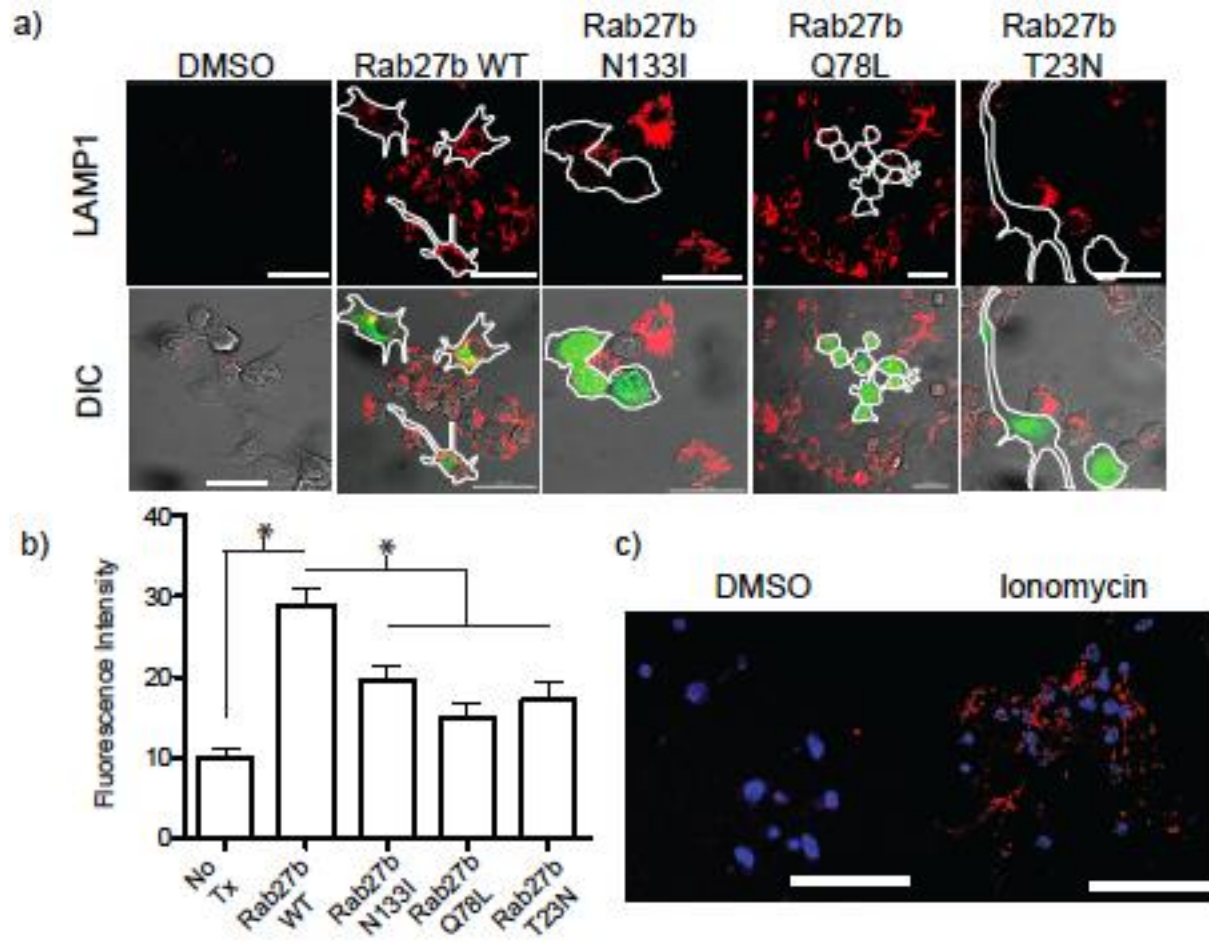


Figure 4.2

### 4.3.3 Rab27b Mutants Interfere with Lysosomal Exocytosis

We then sought to determine whether lysosomes were capable of secretion, and if Rab27b played a role in this lysosomal secretion. SN56 cells were transfected with Rab27b, or one of its mutants, and treated with 2.5 $\mu$ M ionomycin for 5 minutes. In order to only label the cell surface membrane of lysosomal origin, cells were fixed and stained without cell permeabilization. Because the antibody used targeted a luminal epitope on LAMP1 (1D4B) and the cells were not permeabilized, cells would only be stained if LAMP1 were placed on the plasma membrane. In this experiment cells treated with DMSO showed a low basal level of cell-surface LAMP1 staining (Figure 4.2a). However, cells transfected with Rab27b WT and treated with ionomycin demonstrated significantly increased cell-surface LAMP1 staining as compared to DMSO treated cells. We quantified the cell surface staining of LAMP1 on these cells by measuring the fluorescence in transfected cells, and these results are displayed in figure 4.2b. In accordance with the docking results in Figure 4.1, cells transfected with Rab27b mutants exhibited a significant decrease in cell-surface LAMP1 staining at the cell surface. To confirm our findings in neurons, primary mouse neurons were treated with 2.5 $\mu$ M ionomycin for 5 minutes and cell-surface stained with anti-LAMP1 antibody. Cells treated with ionomycin resulted in prominent cell surface staining of LAMP1. Conversely, there was little staining on control cells (Figure 4.2c). Therefore, the Rab27b mutants decrease the number of docked lysosomes at the cell surface and decrease number of lysosomes undergoing exocytosis in response to the calcium ionophore ionomycin.

### 4.3.4 Live-cell Video tracking of Lysosomal Secretion

#### 4.3.4.1 Lysosomal Cargo Release

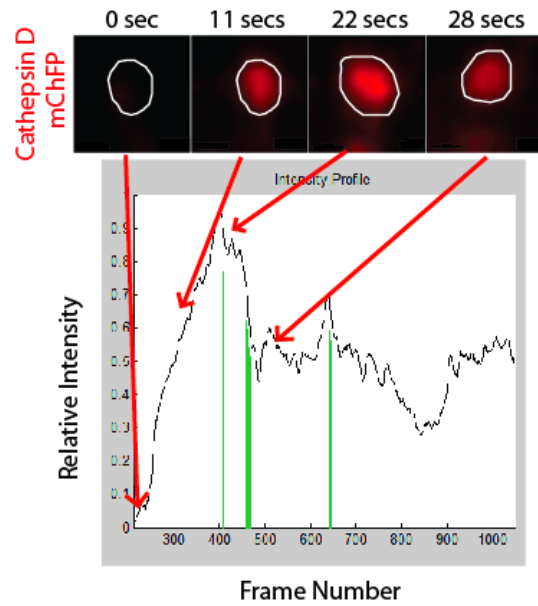
We performed live-cell imaging experiments in SN56 cells to visualize lysosome exocytosis. As previously shown, luminal and membrane cargo have different release kinetics [47]. Luminal contents, such as dextran, can be freely released, which makes luminal contents amenable for the detection of kiss-and-run and full exocytotic events. Conversely, membrane cargo is not released during exocytosis, but rather disperses longitudinally during full exocytosis. During kiss-and-run

exocytosis, the membrane cargo should remain concentrated on the lysosomal membrane [48]. To elucidate the underlying kinetics of lysosome exocytosis in SN56 cells, we transfected cells with CatD-mChFP or with LAMP1-mRFP, a membrane cargo. To increase the number of exocytic events, cells were treated with 5 $\mu$ M ionomycin and TIR-FM video was recorded. Immediately after treatment of ionomycin, there was a delay of 1-2 minutes before an increase in the number of exocytic events. Putative exocytic events were detected in a semi-automated method using ImageJ and Matlab and labelled as kiss and run exocytosis, full exocytosis, or not exocytic. Kiss-and-run fusions had a significant drop in vesicle intensity, however intensity did not drop to background (Figure 4.3a). Conversely, vesicle intensity also showed a significant drop in intensity to background levels (Figure 4.3b). From at least three independent experiments, a total of 719 CatD positive vesicles from 4 cells were tracked and a total of 192 LAMP1 positive vesicles were tracked from 3 cells. By  $\chi^2$  analysis, there was a significant relationship between the vesicular cargo and the type of exocytosis. As expected, there was a greater number of kiss-and-run exocytic events detected by the luminal (26.7% of CatD-mChFP events) cargo as compared to LAMP1-mRFP (8.33% of events). Concomitantly, there were fewer full fusions observed with CatD-mChFP cargo (2.4% of events) as compared to LAMP1-mRFP (9.9% of events). The decrease is likely due to a difficulty in detecting partial fusions with a membrane cargo.

**Figure 4.3:** Kiss-and-run exocytosis and Full exocytosis.

SN56 cells were transiently transfected with CatD-mRFP and treated with 5 $\mu$ m ionomycin and exocytosis was imaged using TIR-FM. Red arrows point to the corresponding frame on the graph. Green lines on the graph point to possible exocytosis events. A white line demarcates the edge of the vesicle. **a)** An example of a vesicle undergoing kiss-and-run exocytosis. **b)** A vesicle undergoing full exocytosis.

a) Kiss and Run exocytosis



b) Full exocytosis

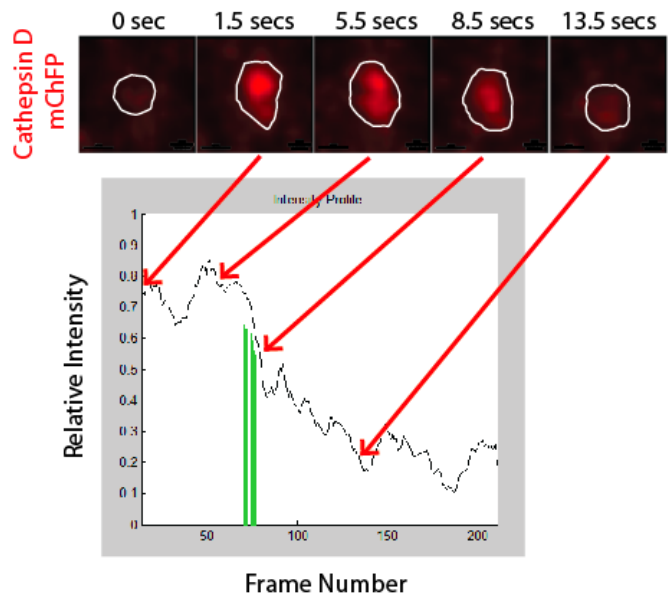


Figure 4.3

**Figure 4.4:** Detection of Lysosomal Secretion with pHluorin

SN56 cells were transiently transfected with plasmids expressing Lamp1-mRFP and VAMP7-pHluorin. **a)** Deacidification of lysosomes with 100 $\mu$ M chloroquine for 30 minutes revealed that TIVMP-pHluorin is colocalized with LAMP1-mRFP in SN56 cells. **b)** Cells were pre-treated for 20 minutes with 1 $\mu$ M bafilomycin, and lysosome exocytosis was stimulated with 5 $\mu$ M ionomycin. SN56 cells were imaged once every minute for 3 minutes. The image on the far right shows the merge of the two channels. Colocalized voxels are yellow and denoted by a white arrowhead. Scale bars represent 5 $\mu$ m.



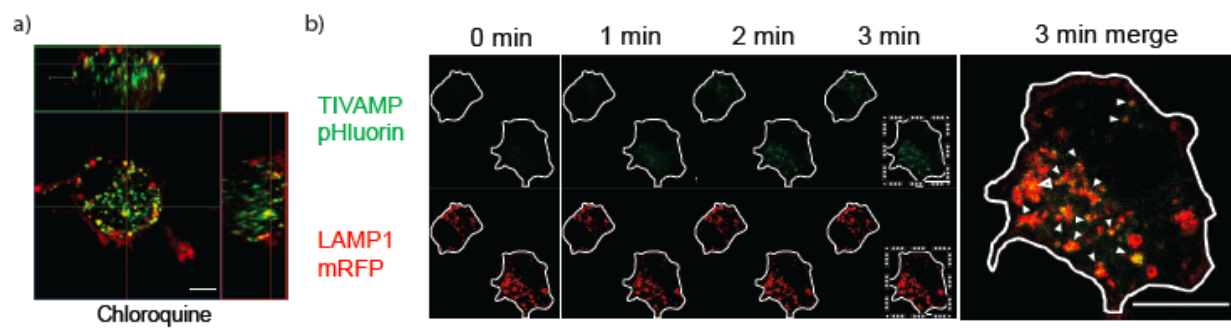


Figure 4.4

#### 4.3.4.2 pHluorin Detection of Secreting Lysosomes

To further confirm lysosomal exocytosis in a neuronal cell line, we turned to a construct encoding tetanus-insensitive vesicular membrane protein (TIVAMP) fused to a pH-sensitive mutant of GFP called pHluorin. Briefly, pHluorin is a mutant form of GFP that is relatively dark in the acidic environment of the lysosome. Neutralization of the luminal pH, for example by fusion with the plasma membrane, results in a dramatic increase in fluorescence [49]. Recent work has shown that TIVAMP is associated with lysosomes and is involved in lysosome exocytosis [23,50]. In order to confirm the colocalization of TIVAMP in lysosomes, LAMP1 in SN56 cells, cells were transfected with treated with 100 $\mu$ M chloroquine for 30 minutes to deacidify the lysosomal lumen. Cells were then imaged live using confocal microscopy, which revealed that LAMP1-mRFP and pHluorin were highly co-localized (Figure 4.4a).

To determine if lysosomes dock with the cell surface, SN56 cells transfected with LAMP1-mRFP and TIVAMP-pHluorin and were treated with bafilomycin for 20 minutes to prevent re-acidification after exocytosis. Therefore, TIVAMP-pHluorin in bafilomycin treated cells would specifically label lysosomes that have formed a pore or contacted the cell surface. Initially cells were treated with bafilomycin alone to confirm that this treatment would elevate pHluorin fluorescence, confocal images were taken immediately before and after bafilomycin treatment. Bafilomycin alone only resulted in a minor increase in pHluorin fluorescence. The same cell was then treated with 5 $\mu$ M ionomycin, and imaged once every minute for three minutes. Within one minute after the addition of ionomycin, LAMP1 vesicles began to fill with pHluorin fluorescence, and were filled by three minutes (Figure 4.4b).

Transfection of multiple plasmids into a cell may result in over-transfection or different ratios of constructs. In order to avoid some of the effects of over-transfection and to be certain that the TIVAMP and LAMP1 proteins were perfectly stoichiometrically co-localized, we obtained a chimeric protein that expresses pHluorin in the luminal domain and modified apple fluorescent protein (mAppleFP) (mApple-LAMP1-phLuorin). In between the two fluorescent proteins, there is a transmembrane domain and the sorting signal of the LAMP1. In SN56 cells, this protein

colocalized with LAMP1 detected with antibody 1D4B, which identifies a LAMP1 luminal epitope not present in the construct. Furthermore, chloroquine treatment deacidified lysosomes and increased fluorescence (Figure 4.5). Therefore, the mApple-LAMP1-phLuorin chimera was properly sorted to lysosomes and is responsive to changes in luminal pH. To follow the trafficking of mApple-LAMP1-phLuorin, transfected SN56 cells were imaged using TIR-FM. After treatment with 5 $\mu$ M ionomycin, exocytic vesicles could be visualized (Supplementary Video 1). In these movies, vesicles (red) can be seen coming up to the plasma membrane. Vesicles that come into communication with the plasma membrane have their luminal contents come to a more neutral pH, and also turn green.

**Figure 4.5:** Localization of mApple-LAMP1-pHluorin.

SN56 cells were transfected with a plasmid encoding the construct mApple-LAMP1-pHluorin. To confirm the correct targeting of this construct to lysosomes, SN56 cells were also transfected with LAMP1-CFP. Before treatment of cells with chloroquine, mApple fluorescence can be seen colocalizing with LAMP1-CFP fluorescence. After chloroquine treatment, the pHluorin increases in fluorescence due to deacidification of the lysosomal lumen. The green fluorescence can be detected in compartments positive for LAMP1-CFP and mApple. Scale bars represent 5  $\mu\text{m}$ .

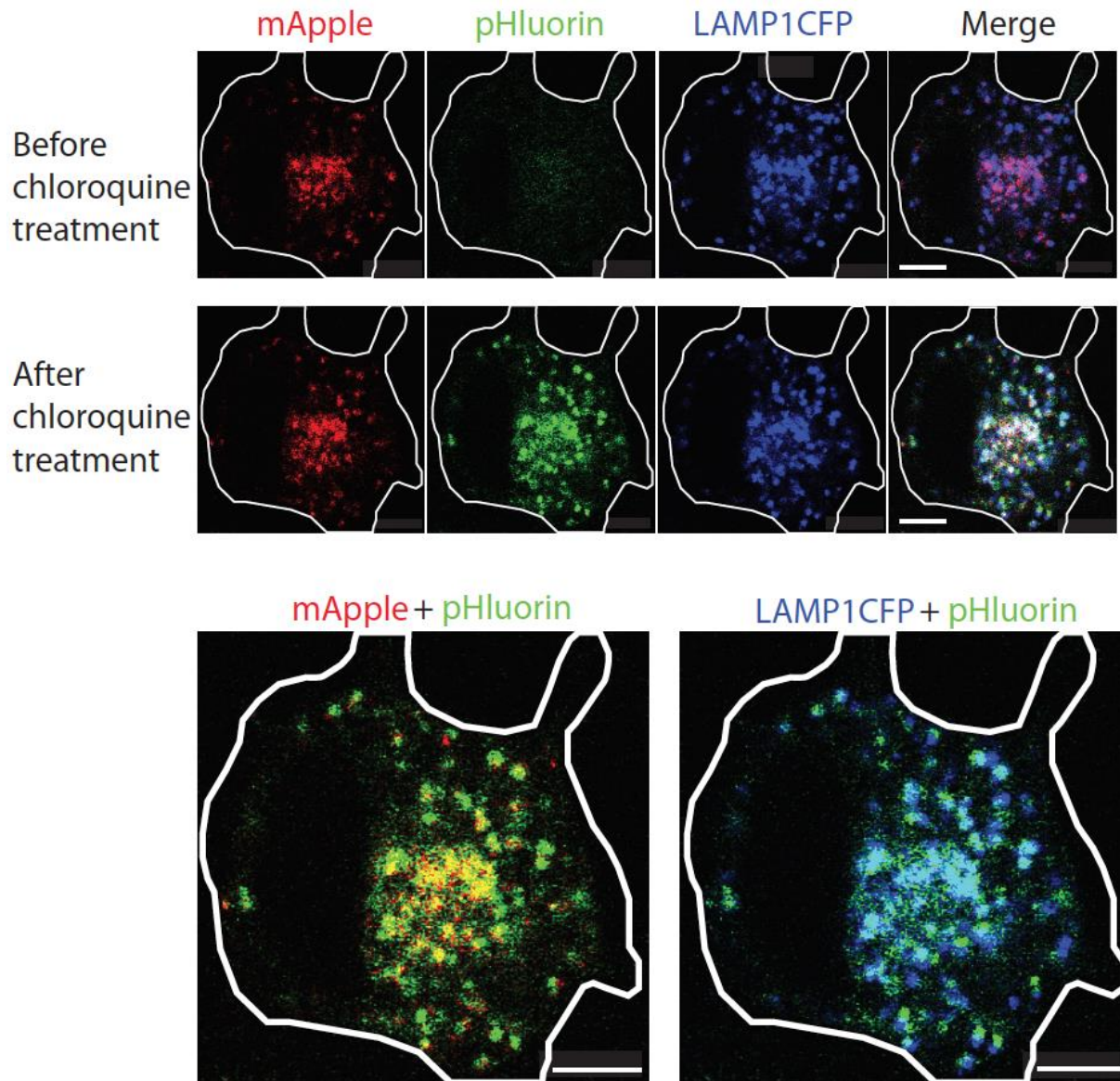


Figure 4.5

### 4.3.5 Intracellular Accumulation of A $\beta$

While extracellular aggregates of A $\beta$  are one of the hallmarks of AD, there is emerging evidence suggesting that intracellular aggregates of A $\beta$  may be pathologically relevant [51-54]. Previous work has demonstrated that these intracellular aggregates accumulate in the endosomal/lysosomal system [51,55-60]. To confirm the intracellular accumulation of A $\beta$  in lysosomes, we incubated SN56 cells with 250nM of HiLyte Fluor 488 A $\beta$ 42 (A $\beta$ 42-488) (Anaspec) and determined its colocalization with LAMP1-mRFP. As expected, 60% of A $\beta$ 42-488 colocalized with LAMP1 labeled compartments, suggesting that the majority of A $\beta$ 42-488 is localized to lysosomes (Figure 4.6a).

To determine if endogenously produced A $\beta$  could be detected intracellularly, we cultured cortical neurons harvested from newborn transgenic mice expressing human APP with the Swedish mutation and the deltaE9 mutation of the human PS1 gene. DIV7 cortical neurons were fixed and stained for A $\beta$  and LAMP1. Colocalization analysis found that  $55 \pm 4$  SEM% of A $\beta$  colocalized with LAMP1 labelled compartments (Figure 4.6b, n=3)

In order to follow the secretion of A $\beta$  in live cells, SN56 cells were transfected with full-length APP-695. After differentiation, cells were surface labelled with a Zenon-6E10 antibody conjugate and internalized for one hour. Our previous work has demonstrated that a portion of APP can be internalized into lysosomes after 15-minutes [9,39]. After labelling, live cells were treated with ionomycin and imaged by TIR-FM. Our analysis found that 2.4% of vesicles underwent full exocytosis and 18.5% of vesicles underwent kiss and run exocytosis.

**Figure 4.6:** A $\beta$  accumulates in lysosomes.

**a)** SN56 cells were transfected with LAMP1-mRFP. Cells were loaded with 250nM. HiLyte Fluor 488 A $\beta$ 42 (A $\beta$ 42-488) for 24 hours, and imaged. **b)** Primary cultured neurons from a mouse bearing PS1 delta exon 9 mutation and APP-Swe mutations were fixed and immunostained with and antibody against A $\beta$ . Scale bars represent 5 $\mu$ m.

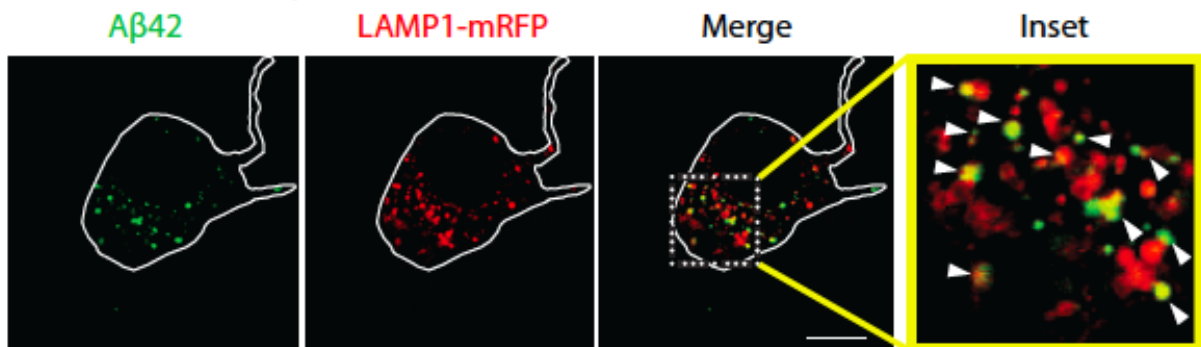
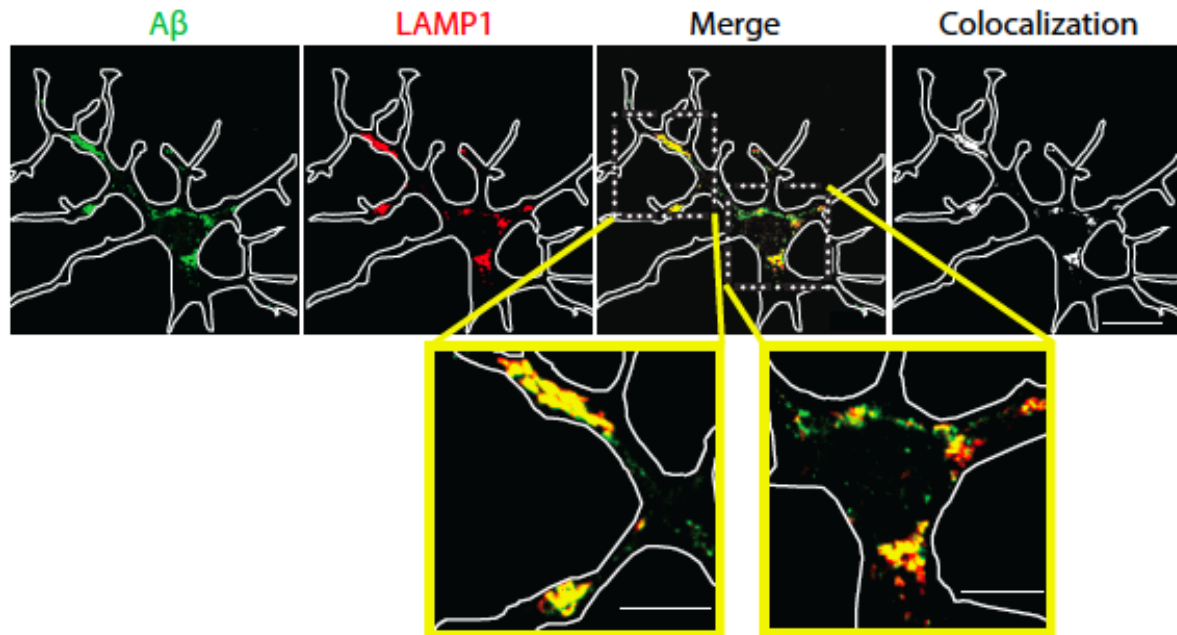
a) Loading of A $\beta$  into Lysosomes of SN56 cellsb) Detection of endogenous A $\beta$  in transgenic mouse neurons

Figure 4.6



#### 4.3.6 Rab27b Mutants Decrease A $\beta$ Secreted into Culture Media

To determine whether Rab27b affected A $\beta$  secretion into the media, SN56 cells were transfected with  $\beta$ APP-CFP with the Swedish mutation and a Rab27b-GFP mutant. Medium was collected after 48 hours and analyzed by ELISA. From each experiment, the amount of A $\beta$  secreted was normalized to that in cells that were only transfected with  $\beta$ APP-CFP. In these experiments, the amount of A $\beta$ 40 secreted is shown in Figure 4.7a, was significantly reduced by all 3 of the Rab27b mutants compared to controls (Q78L:  $67 \pm 12$  SEM %, N133I:  $61 \pm 6$  SEM %, T23N:  $61 \pm 9$  SEM %, n= 5). We determined the amount of A $\beta$  42 secreted by ELISA and found that only Rab27b construct bearing the T23N dominant negative mutation significantly reduced, as compared to Rab27b WT, the amount of A $\beta$  42 released to  $60 \pm 10$  SEM % as compared control (p<0.05). The amount of A $\beta$  42 released was not affected by the other mutants (Q78L:  $77 \pm 11$  SEM %, N133I:  $104 \pm 7$  SEM %, n= 4) (Figure 4.7a and b).

**Figure 4.7:** Rab27b inhibits A $\beta$  releases in SN56 cells.

Cells were transfected with Rab27bWT-GFP, Rab27b Q78L-GFP, Rab27b N133I-GFP, or Rab27b T23N-GFP. To determine if Rab27b affects A $\beta$  secretion, SN56 cells were transfected with Rab27b mutants and  $\beta$ APPswedish-CFP. Media was collected after 48 hours and **a)** A $\beta$ 40 and **b)** A $\beta$ 42 levels were determined by ELISA. (\*= $p < 0.05$ ).

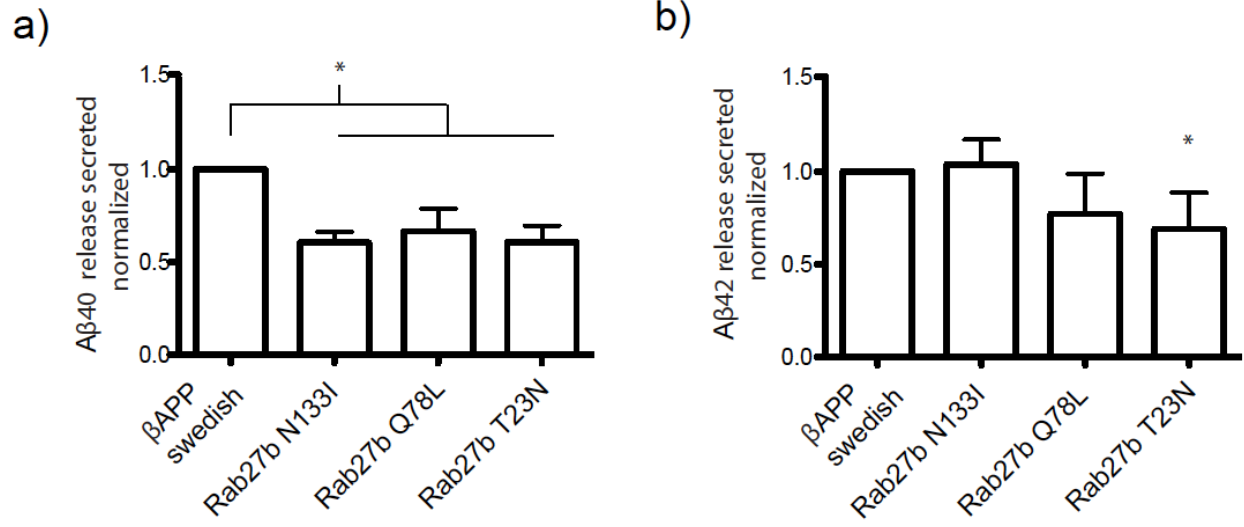


Figure 4.7

## 4.4 Discussion

Although lysosomes are commonly used for secretion in many cell types, little is known about secretory lysosomes in neurons. Here, we present data demonstrating that a population of lysosomes resides within 110 nm of the plasma membrane. After depolarization with ionomycin, the lysosomal marker LAMP1 can be imaged at the plasma membrane. These lysosomes are able to fuse with the plasma membrane, as indicated by a pH sensitive marker pHluorin, which demonstrates green fluorescence at neutral environment pH. Furthermore, these lysosomes contain neurotoxic A $\beta$ . Exocytosis can be imaged in live cells using TIRF microscopy, and occurs in neurons.

Although lysosomes are typically thought of as degradative organelles, lysosomes are able to contribute to secretion in many cell types [17]. Many authors have demonstrated that lysosomes are capable of secretion in professional secretory cells (platelets, neutrophils, melanocytes, and macrophages) [17,18]. In addition, conventional lysosomes fuse with the cell surface for plasma membrane wound sealing [61,62]. There is also evidence suggesting that neuronal lysosomes are secretory. For example, primary neurons isolated from sympathetic cervical ganglia depend on lysosomes for neurite extension [33].

Here, we used a semi-automated detection method to show that approximately 30% of tracked vesicles in SN56 cells are secretory as detected by CatD-mChFP. The majority of these secretory events appear to be kiss-and-run fusion (Figure 4.3a). Conversely, when exocytosis was detected with a membrane cargo there was a ~10% drop in the number of fusion events detected.

The decrease in number of detected in these events was due to the lower detection of kiss-and-run fusions. The difference in the proportion of vesicles detected is likely due to the difference in release kinetics of soluble and membrane cargo [47]. Soluble cargo would be expected to be released in partial and full fusions. In kiss-and-run fusions, there would be a drop in cargo fluorescence intensity, albeit not to background levels. Conversely, membrane cargo fluorescence would only decrease after complete fusions. During full fusions, membrane cargo

will diffuse laterally resulting in decrease fluorescence. However, during partial fusions, membrane cargo will stay concentrated in a vesicle, and not lead to a significant decrease in fluorescence [47].

Our data also show that Rab27b is involved in lysosomal docking and secretion. Previous work has shown that Rab27b is highly expressed in the brain [42,45]. Furthermore, over-expression of dominant-negative mutants of Rab27b into PC12 neuroendocrine cells decreased secretion from dense core granules [45]. In our studies, we show a decrease in the number of LAMP1 positive vesicles within 110nm of the membrane after transfection with constitutively-active and dominant-negative mutants of Rab27b, which suggests a deficit in vesicle docking or trafficking to the cell surface (Figure 4.1c). Consequently, there was also an observed decrease in the cell-surface labelled LAMP1 after ionomycin treatment (Figure 4.2a and b). The Rab27b mutants decreased the secretion of A $\beta$ 40 into the culture media, as determined by ELISA, even when in a constitutively active state (Figure 4.7a). Although we do not know the reason for active forms of regulatory GTPases to be inhibitory, it has been proposed that they can have indirect inhibitory effects by occupying/consuming other regulatory proteins. Interestingly, A $\beta$ 42 secretion was decreased only by the true dominant-negative Rab27b T23N mutant (Figure 4.7b), suggested that the negative effects seen in previous experiments were indirect..

The involvement of Rab27b in lysosomal secretion are in agreement with previous literature that demonstrated the importance of Rab27 and its effectors in granule secretion. Work from the They laboratory [44] demonstrated that Rab27b silencing by shRNA resulted in the perinuclear localization of CD63 (a late endosome/lysosome marker). These findings are echoed in melanocytes from patients with Griscelli syndrome (deficient in Rab27a). These melanocytes accumulate melanosomes in the perinuclear region, and melanosome sorting the cell periphery can be restored by the expression of exogenous Rab27a [63]. The Rab27-mediated trafficking and docking of lysosomes likely depends on a number of Rab27 effectors [reviewed in detail in 64,65]. For example, Rab27a interacts with melanophilin and interacts with the plus-end of the microtubule, which provides a possible mechanism for melanosome delivery to the periphery

[66]. Myosin Va also interacts with Rab27, and is involved in rearranging the actin at the cell periphery to capture and dock melanosomes [66].

Once at the membrane, Munc 13-4 proteins interact with Rab27a and are involved in the docking of lysosomes at the membrane [67]. Munc proteins also form a critical part of SNARE complex for synaptic vesicles and regulates synaptic vesicle fusion [68]. The formation of a unique SNARE complex for lysosome secretion in neurons. However, the protein participants remain unclear. One of the leading candidates is synaptotagmin 7, which is critical for lysosome-mediated neurite extension [33]. Previous work has also demonstrated that synaptotagmin 7 controls the fusion pore size, and silencing of synaptotagmin 7 leads to a higher proportion of full lysosomal fusions [47]. Synaptotagmin 7 can form SDS-resistant complexes with sensitive factor attachment protein 23 (SNAP23), TIVAMP, and syntaxin 4 [69]. TIVAMP has also been shown to be involved in lysosome secretion in neurons and astrocytes [32,50]. SNAP-23 and syntaxin 4 have also been implicated in lysosomal secretion in platelets [70]. However, the existence and physiological relevance of this complex in neurons and A $\beta$  secretion remains to be determined.

Work from our lab and others have demonstrated that endosomes and lysosomes are critical in the production of A $\beta$  [5,8,10,39]. Taken together with the current findings, these data suggest that lysosomes may be responsible for the production and secretion of A $\beta$ . The acidic environment of the lysosomes is conducive to the aggregation of A $\beta$  [7]. A $\beta$  is also known to accumulate intracellularly and form seeds that can promote the extracellular formation of fibrils [12]. Recent work has also demonstrated that A $\beta$  can be secreted in association with exosomes (intraluminal vesicles in endosomes and lysosomes) [4]. Furthermore, APP, APP CTFs, ADAM10 and BACE have also been detected in exosomes [71]. Interestingly, A $\beta$  can be detected in multi-vesicular bodies from the brains of AD patients and transgenic mice [55,56]. While the evidence for lysosomal production and secretion of A $\beta$  is compelling, at least one study has identified full-length APP and BACE on the synaptic vesicle membrane [3]. It was shown that full-length APP can be secreted from synaptic vesicles, although the secretion of A $\beta$  and other cleavage products was never directly identified [3].

The work presented here suggests that A $\beta$  is produced, stored, and secreted from lysosomes in a Rab27b dependent manner. However, the physiological significance of this pathway is unclear. The secretion of A $\beta$  from lysosomes may simply be an attempt for neurons to clear themselves of indigestible A $\beta$ . Intraluminal accumulation of A $\beta$  has been demonstrated to destabilize the lysosomal membrane and cause the leakage of luminal contents to the cytosol [72], with the release of lysosomal contents into the cytosol leading to cell death [73-75]. Alternatively, release may modulate brain activity. For example, A $\beta$  release has also been increased in response to synaptic activity and can modulate synaptic activity [76]. The A $\beta$  secretion in response to synaptic activity can be inhibited by blocking endocytosis [77]. Therefore, the lysosomal secretion of A $\beta$  appears to be physiologically and pathologically important and will need to be further explored.

## 4.5 References

1. Masters CL, Simms G, Weinman NA, Multhaup G, McDonald BL, Beyreuther K. Amyloid plaque core protein in Alzheimer disease and Down syndrome. *Proc Natl Acad Sci USA*. 1985;82: 4245–4249.
2. Marquez-Sterling NR, Lo AC, Sisodia SS, Koo EH. Trafficking of cell-surface beta-amyloid precursor protein: evidence that a sorting intermediate participates in synaptic vesicle recycling. *J Neurosci*. 1997;17: 140–151.
3. Groemer TW, Thiel CS, Holt M, Riedel D, Hua Y, Hüve J, et al. Amyloid precursor protein is trafficked and secreted via synaptic vesicles. *PLoS ONE*. 2011;6: e18754. doi:10.1371/journal.pone.0018754
4. Rajendran L, Honsho M, Zahn TR, Keller P, Geiger KD, Verkade P, et al. Alzheimer's disease beta-amyloid peptides are released in association with exosomes. *Proc Natl Acad Sci USA*. 2006;103: 11172–11177. doi:10.1073/pnas.0603838103
5. Pasternak SH, Bagshaw RD, Guiral M, Zhang S, Ackerley CA, Pak BJ, et al. Presenilin-1, nicastrin, amyloid precursor protein, and gamma-secretase activity are co-localized in the lysosomal membrane. *J Biol Chem*. 2003;278: 26687–26694. doi:10.1074/jbc.M212192200
6. Schrader-Fischer G, Paganetti PA. Effect of alkalizing agents on the processing of the beta-amyloid precursor protein. *Brain Research*. 1996;716: 91–100. doi:10.1016/0006-8993(96)00002-9

7. Su Y, Chang PT. Acidic pH promotes the formation of toxic fibrils from beta-amyloid peptide. *Brain Research*. 2001;893: 287–291.
8. Tam JH, Seah C, Pasternak SH. The Amyloid Precursor Protein is rapidly transported from the Golgi apparatus to the lysosome and where it is processed into beta-amyloid. *Mol Brain*. BioMed Central Ltd; 2014;7: 54. doi:10.1186/s13041-014-0054-1
9. Lorenzen A, Samosh J, Vandewark K, Anborgh PH, Seah C, Magalhaes AC, et al. Rapid and Direct Transport of Cell Surface APP to the Lysosome defines a novel selective pathway. *Mol Brain*. 2010;3: 11. doi:10.1186/1756-6606-3-11
10. Perez RG, Soriano S, Hayes JD, Ostaszewski B, Xia W, Selkoe DJ, et al. Mutagenesis identifies new signals for beta-amyloid precursor protein endocytosis, turnover, and the generation of secreted fragments, including Abeta42. *J Biol Chem*. 1999;274: 18851–18856.
11. Thinakaran G, Koo EH. Amyloid Precursor Protein Trafficking, Processing, and Function. *Journal of Biological Chemistry*. 2008;283: 29615–29619. doi:10.1074/jbc.R800019200
12. Hu X, Crick SL, Bu G, Frieden C, Pappu RV, Lee J-M. Amyloid seeds formed by cellular uptake, concentration, and aggregation of the amyloid-beta peptide. *Proceedings of the National Academy of Sciences*. 2009;106: 20324–20329. doi:10.1073/pnas.0911281106
13. Yang AJ, Knauer M, Burdick DA, Glabe C. Intracellular A beta 1-42 aggregates stimulate the accumulation of stable, insoluble amyloidogenic fragments of the amyloid precursor protein in transfected cells. *Journal of Biological Chemistry*. 1995;270: 14786–14792.
14. Yang AJ, Chandswangbhuvana D, Shu T, Henschen A, Glabe CG. Intracellular accumulation of insoluble, newly synthesized abetan-42 in amyloid precursor protein-transfected cells that have been treated with Abeta1-42. *Journal of Biological Chemistry*. 1999;274: 20650–20656.
15. Burdick D, Kosmoski J, Knauer MF, Glabe CG. Preferential adsorption, internalization and resistance to degradation of the major isoform of the Alzheimer's amyloid peptide, A beta 1-42, in differentiated PC12 cells. *Brain Research*. 1997;746: 275–284.
16. Knauer MF, Soreghan B, Burdick D, Kosmoski J, Glabe CG. Intracellular accumulation and resistance to degradation of the Alzheimer amyloid A4/beta protein. *Proc Natl Acad Sci USA*. 1992;89: 7437–7441.
17. Dell'Angelica EC, Mullins C, Caplan S, Bonifacino JS. Lysosome-related organelles. *FASEB J*. 2000;14: 1265–1278.
18. Marks MS, Heijnen HFG, Raposo G. Lysosome-related organelles: unusual compartments become mainstream. *Current Opinion in Cell Biology*. 2013;25: 495–505. doi:10.1016/j.ceb.2013.04.008



19. Raposo G, Marks MS. Melanosomes — dark organelles enlighten endosomal membrane transport. *Nat Rev Mol Cell Biol.* 2007;8: 786–797. doi:10.1038/nrm2258
20. Topham NJ, Hewitt EW. Natural killer cell cytotoxicity: how do they pull the trigger? *Immunology.* 2009;128: 7–15. doi:10.1111/j.1365-2567.2009.03123.x
21. Bossi G, Griffiths GM. Degranulation plays an essential part in regulating cell surface expression of Fas ligand in T cells and natural killer cells. *Nat Med.* 1999;5: 90–96. doi:10.1038/4779
22. de Saint Basile G, Ménasché G, Fischer A. Molecular mechanisms of biogenesis and exocytosis of cytotoxic granules. *Nature Publishing Group.* 2010;10: 568–579. doi:10.1038/nri2803
23. Marcet-Palacios M, Odemuyiwa SO, Coughlin JJ, Garofoli D, Ewen C, Davidson CE, et al. Vesicle-associated membrane protein 7 (VAMP-7) is essential for target cell killing in a natural killer cell line. *Biochemical and Biophysical Research Communications.* 2008;366: 617–623. doi:10.1016/j.bbrc.2007.11.079
24. Bryceson YT, Rudd E, Zheng C, Edner J, Ma D, Wood SM, et al. Defective cytotoxic lymphocyte degranulation in syntaxin-11 deficient familial hemophagocytic lymphohistiocytosis 4 (FHL4) patients. *Blood.* 2007;110: 1906–1915. doi:10.1182/blood-2007-02-074468
25. Stadt zur U, Rohr J, Seifert W, Koch F, Grieve S, Pagel J, et al. Familial hemophagocytic lymphohistiocytosis type 5 (FHL-5) is caused by mutations in Munc18-2 and impaired binding to syntaxin 11. *Am J Hum Genet.* 2009;85: 482–492. doi:10.1016/j.ajhg.2009.09.005
26. Stadt zur U, Schmidt S, Kasper B, Beutel K, Diler AS, Henter J-I, et al. Linkage of familial hemophagocytic lymphohistiocytosis (FHL) type-4 to chromosome 6q24 and identification of mutations in syntaxin 11. *Human Molecular Genetics.* 2005;14: 827–834. doi:10.1093/hmg/ddi076
27. Stinchcombe J. Linking Albinism and Immunity: The Secrets of Secretory Lysosomes. *Science.* 2004;305: 55–59. doi:10.1126/science.1095291
28. Stinchcombe JC, Barral DC, Mules EH, Mules EH, Booth S, Hume AN, et al. Rab27a is required for regulated secretion in cytotoxic T lymphocytes. *Journal of Cell Biology.* 2001;152: 825–834. doi:10.1038/nature11801
29. Stinchcombe JC, Griffiths GM. Regulated secretion from hemopoietic cells. *Journal of Cell Biology.* 1999;147: 1–6.
30. Stinchcombe JC, Griffiths GM. Secretory Mechanisms in Cell-Mediated Cytotoxicity. *Annu Rev Cell Dev Biol.* 2007;23: 495–517.

doi:10.1146/annurev.cellbio.23.090506.123521

31. Huynh C, Roth D, Ward DM, Kaplan J, Andrews NW. Defective lysosomal exocytosis and plasma membrane repair in Chediak-Higashi/beige cells. *Proc Natl Acad Sci USA*. 2004;101: 16795–16800. doi:10.1073/pnas.0405905101
32. Martinez-Arca S, Alberts P, Zahraoui A, Louvard D, Galli T. Role of tetanus neurotoxin insensitive vesicle-associated membrane protein (TI-VAMP) in vesicular transport mediating neurite outgrowth. *The Journal of Cell Biology*. 2000;149: 889–900.
33. Arantes RME. A Role for Synaptotagmin VII-Regulated Exocytosis of Lysosomes in Neurite Outgrowth from Primary Sympathetic Neurons. *Journal of Neuroscience*. 2006;26: 4630–4637. doi:10.1523/JNEUROSCI.0009-06.2006
34. Suchy M, Ta R, Li AX, Wojciechowski F, Pasternak SH, Bartha R, et al. A paramagnetic chemical exchange-based MRI probe metabolized by cathepsin D: design, synthesis and cellular uptake studies. *Org Biomol Chem*. The Royal Society of Chemistry; 2010;8: 2560–2566. doi:10.1039/b926639a
35. Ta R, Suchy M, Tam JH, Li AX, Martinez-Santesteban FS, Scholl TJ, et al. A dual magnetic resonance imaging/fluorescent contrast agent for Cathepsin-D detection. *Contrast Media Mol Imaging*. 2013;8: 127–139. doi:10.1002/cmimi.1502
36. Chen Y, Samaraweera P, Sun T-T, Kreibich G, Orlow SJ. Rab27b association with melanosomes: dominant negative mutants disrupt melanosomal movement. *J Invest Dermatol*. Nature Publishing Group; 2002;118: 933–940. doi:10.1046/j.1523-1747.2002.01754.x
37. Pavlos NJ, Grønborg M, Riedel D, Chua JJE, Boyken J, Kloepper TH, et al. Quantitative analysis of synaptic vesicle Rabs uncovers distinct yet overlapping roles for Rab3a and Rab27b in Ca<sup>2+</sup>-triggered exocytosis. *Journal of Neuroscience*. Society for Neuroscience; 2010;30: 13441–13453. doi:10.1523/JNEUROSCI.0907-10.2010
38. Schneider CA, Rasband WS, Eliceiri KW. NIH Image to ImageJ: 25 years of image analysis. *Nat Meth*. 2012;9: 671–675. doi:10.1038/nmeth.2089
39. Tang W, Tam JH, Seah C, Chiu J, Tyrer A, Cregan SP, et al. Arf6 controls beta-amyloid production by regulating macropinocytosis of the Amyloid Precursor Protein to lysosomes. *Mol Brain*. 2015;8: 41. doi:10.1186/s13041-015-0129-7
40. Pedersen WA, Kloczewiak MA, Blusztajn JK. Amyloid beta-protein reduces acetylcholine synthesis in a cell line derived from cholinergic neurons of the basal forebrain. *Proc Natl Acad Sci USA*. 1996;93: 8068–8071.
41. Hammond DN, Wainer BH, Tongsgard JH, Heller A. Neuronal properties of clonal hybrid cell lines derived from central cholinergic neurons. *Science*. American Association for the

- Advancement of Science; 1986;234: 1237–1240. doi:10.1126/science.3775382
42. Gomi H, Mori K, Itohara S, Izumi T. Rab27b is expressed in a wide range of exocytic cells and involved in the delivery of secretory granules near the plasma membrane. *Mol Biol Cell*. 2007;18: 4377–4386. doi:10.1091/mbc.E07-05-0409
  43. Tsuboi T, Fukuda M. Rab3A and Rab27A cooperatively regulate the docking step of dense-core vesicle exocytosis in PC12 cells. *Journal of Cell Science*. 2006;119: 2196–2203. doi:10.1242/jcs.02962
  44. Ostrowski M, Carmo NB, Krumeich S, Fanget I, Raposo G, Savina A, et al. Rab27a and Rab27b control different steps of the exosome secretion pathway : *Nature Cell Biology*. *Nature Cell Biology*. 2010;12: 19–30– sup pp 1–13. doi:10.1038/ncb2000
  45. Zhao S, Torii S, Yokota-Hashimoto H, Takeuchi T, Izumi T. Involvement of Rab27b in the regulated secretion of pituitary hormones. *Endocrinology*. 2002;143: 1817–1824.
  46. Hendrix A, Maynard D, Pauwels P, Braems G, Denys H, Van den Broecke R, et al. Effect of the secretory small GTPase Rab27B on breast cancer growth, invasion, and metastasis. *J Natl Cancer Inst*. Oxford University Press; 2010;102: 866–880. doi:10.1093/jnci/djq153
  47. Jaiswal JK, Chakrabarti S, Andrews NW, Simon SM. Synaptotagmin VII restricts fusion pore expansion during lysosomal exocytosis. *Plos Biol*. Public Library of Science; 2004;2: E233. doi:10.1371/journal.pbio.0020233
  48. Schmoranz J, Goulian M, Axelrod D, Simon SM. Imaging constitutive exocytosis with total internal reflection fluorescence microscopy. *The Journal of Cell Biology*. 2000;149: 23–32.
  49. Sankaranarayanan S, Ryan TA. Real-time measurements of vesicle-SNARE recycling in synapses of the central nervous system. *Nature Cell Biology*. 2000;2: 197–204. doi:10.1038/35008615
  50. Sato M, Yoshimura S, Hirai R, Goto A, Kunii M, Atik N, et al. The Role of VAMP7/TI-VAMP in Cell Polarity and Lysosomal Exocytosis in vivo. *Traffic*. 2011;12: 1383–1393. doi:10.1111/j.1600-0854.2011.01247.x
  51. Tam JH, Pasternak SH. Amyloid and Alzheimer's disease: inside and out. *Can J Neurol Sci*. 2012;39: 286–298.
  52. Skovronsky DM, Doms RW, Lee VM. Detection of a novel intraneuronal pool of insoluble amyloid beta protein that accumulates with time in culture. *Journal of Cell Biology*. The Rockefeller University Press; 1998;141: 1031–1039.
  53. Walsh DM, Tseng BP, Rydel RE, Podlisny MB, Selkoe DJ. The oligomerization of amyloid beta-protein begins intracellularly in cells derived from human brain.

- Biochemistry. 2000;39: 10831–10839. doi:10.1021/bi001048s
54. Wertkin AM, Turner RS, Pleasure SJ, Golde TE, Younkin SG, Trojanowski JQ, et al. Human neurons derived from a teratocarcinoma cell line express solely the 695-amino acid amyloid precursor protein and produce intracellular beta-amyloid or A4 peptides. *Proc Natl Acad Sci USA. National Academy of Sciences*; 1993;90: 9513–9517.
  55. Takahashi RH, Milner TA, Li F, Nam EE, Edgar MA, Yamaguchi H, et al. Intraneuronal Alzheimer abeta42 accumulates in multivesicular bodies and is associated with synaptic pathology. *Am J Pathol.* 2002;161: 1869–1879.
  56. Takahashi RH, Takahashi RH, Almeida CG, Kearney PF, Kearney PF, Yu F, et al. Oligomerization of Alzheimer's beta-amyloid within processes and synapses of cultured neurons and brain. *Journal of Neuroscience.* 2004;24: 3592–3599. doi:10.1523/JNEUROSCI.5167-03.2004
  57. Chen X, Wagener JF, Morgan DH, Hui L, Ghribi O, Geiger JD. Endolysosome mechanisms associated with Alzheimer's disease-like pathology in rabbits ingesting cholesterol-enriched diet. *J Alzheimers Dis.* 2010;22: 1289–1303. doi:10.3233/JAD-2010-101323
  58. Hui L, Chen X, Geiger JD. Endolysosome involvement in LDL cholesterol-induced Alzheimer's disease-like pathology in primary cultured neurons. *Life Sci.* 2012;91: 1159–1168. doi:10.1016/j.lfs.2012.04.039
  59. Cataldo AM, Hamilton DJ, Barnett JL, Paskevich PA, Nixon RA. Properties of the endosomal-lysosomal system in the human central nervous system: disturbances mark most neurons in populations at risk to degenerate in Alzheimer's disease. *J Neurosci.* 1996;16: 186–199.
  60. Cataldo AM, Petanceska S, Terio NB, Peterhoff CM, Durham R, Mercken M, et al. Abeta localization in abnormal endosomes: association with earliest Abeta elevations in AD and Down syndrome. *NBA.* 2004;25: 1263–1272. doi:10.1016/j.neurobiolaging.2004.02.027
  61. Jaiswal JK, Andrews NW, Simon SM. Membrane proximal lysosomes are the major vesicles responsible for calcium-dependent exocytosis in nonsecretory cells. *Journal of Cell Biology.* 2002;159: 625–635. doi:10.1083/jcb.200208154
  62. Bi GQ, Alderton JM, Steinhardt RA. Calcium-regulated exocytosis is required for cell membrane resealing. *Journal of Cell Biology.* 1995;131: 1747–1758.
  63. Bahadoran P, Aberdam E, Mantoux F, Buscà R, Bille K, Yalman N, et al. Rab27a: A key to melanosome transport in human melanocytes. *Journal of Cell Biology.* 2001;152: 843–850.
  64. Izumi T, Gomi H, Kasai K, Mizutani S, Torii S. The roles of Rab27 and its effectors in the

- regulated secretory pathways. *Cell Struct Funct.* 2003;28: 465–474.
65. Izumi T. Physiological roles of Rab27 effectors in regulated exocytosis. *Endocr J.* 2007;54: 649–657.
  66. Wu XS, Wu XS, Tsan GL, Hammer JA. Melanophilin and myosin Va track the microtubule plus end on EB1. *Journal of Cell Biology.* 2005;171: 201–207. doi:10.1083/jcb.200503028
  67. Elstak ED, Neeft M, Nehme NT, Voortman J, Cheung M, Goodarzifard M, et al. The munc13-4-rab27 complex is specifically required for tethering secretory lysosomes at the plasma membrane. *Blood.* 2011;118: 1570–1578. doi:10.1182/blood-2011-02-339523
  68. Südhof TC, Rizo J. Synaptic vesicle exocytosis. *Cold Spring Harbor Perspectives in Biology.* 2011;3. doi:10.1101/cshperspect.a005637
  69. Rao SK. Identification of SNAREs Involved in Synaptotagmin VII-regulated Lysosomal Exocytosis. *Journal of Biological Chemistry.* 2004;279: 20471–20479. doi:10.1074/jbc.M400798200
  70. Chen D, Lemons PP, Schraw T, Whiteheart SW. Molecular mechanisms of platelet exocytosis: role of SNAP-23 and syntaxin 2 and 4 in lysosome release. *Blood.* 2000;96: 1782–1788.
  71. Perez-Gonzalez R, Gauthier SA, Kumar A, Levy E. The Exosome Secretory Pathway Transports Amyloid Precursor Protein Carboxyl-terminal Fragments from the Cell into the Brain Extracellular Space. *Journal of Biological Chemistry.* 2012;287: 43108–43115. doi:10.1074/jbc.M112.404467
  72. Liu R-Q, Zhou Q-H, Ji S-R, Zhou Q, Feng D, Wu Y, et al. Membrane localization of beta-amyloid 1-42 in lysosomes: a possible mechanism for lysosome labilization. *J Biol Chem.* 2010;285: 19986–19996. doi:10.1074/jbc.M109.036798
  73. Stoka V, Turk B, Schendel SL, Kim TH, Cirman T, Snipas SJ, et al. Lysosomal protease pathways to apoptosis. Cleavage of bid, not pro-caspases, is the most likely route. *Journal of Biological Chemistry. American Society for Biochemistry and Molecular Biology;* 2001;276: 3149–3157. doi:10.1074/jbc.M008944200
  74. Roberg K, Johansson U, Ollinger K. Lysosomal release of cathepsin D precedes relocation of cytochrome c and loss of mitochondrial transmembrane potential during apoptosis induced by oxidative stress. *Free Radical Biology and Medicine.* 1999;27: 1228–1237.
  75. Johansson A-C, Steen H, Ollinger K, Roberg K. Cathepsin D mediates cytochrome c release and caspase activation in human fibroblast apoptosis induced by staurosporine. *Cell Death and Differentiation. Nature Publishing Group;* 2003;10: 1253–1259. doi:10.1038/sj.cdd.4401290

76. Kamenetz F, Tomita T, Hsieh H, Seabrook G, Borchelt D, Iwatsubo T, et al. APP processing and synaptic function. *Neuron*. 2003;37: 925–937. doi:10.1016/S0896-6273(03)00124-7
77. Cirrito JR, Kang J-E, Lee J, Stewart FR, Verges DK, Silverio LM, et al. Endocytosis Is Required for Synaptic Activity-Dependent Release of Amyloid- $\beta$  In Vivo. *Neuron*. 2008;58: 42–51. doi:10.1016/j.neuron.2008.02.003

## Chapter 5

### 5 Discussion

#### 5.1 Summary of Novel Observations

In this thesis, I set out to characterize the trafficking of APP and link this to A $\beta$  production and secretion. Although most APP processing experiments focused on internalization of APP to endosomes before processing, our laboratory has demonstrated that APP can also transit from the cell surface to lysosomes directly before processing into A $\beta$ . **1)** We have expanded these experiments to follow intracellular APP trafficking using APP tagged with a photoactivatable form of GFP. With this construct, we have characterized a novel trafficking pathway for APP to be transported directly from the Golgi apparatus to lysosomes, where it is processed into A $\beta$  by secretase-like enzymatic activities. **2)** This novel trafficking pathway is dependent on an interaction between AP-3 and APP. **3)** Furthermore, this interaction is mediated through an interaction with the YTSI motif in the cytoplasmic tail of APP and can be decreased by phosphorylation of the serine in they YTSI motif. **4)** Finally, we demonstrate that lysosomes are secretory organelles, even in neuronal systems, and are able to secrete their contents, including A $\beta$ .

The importance of protein sorting has been well recognized in AD [reviewed in 1,2], with many authors contending that APP sorting can directly control A $\beta$  production. One reason trafficking plays a role in A $\beta$  is because this process is dependent on amyloidogenic cleavage of APP by  $\beta$ - and  $\gamma$ -secretases. While the  $\gamma$ -secretase has been localized to the ER, Golgi, plasma membrane, and endosomes [reviewed in 3], the localization of  $\gamma$ -secretase activity is the most critical to understanding the production of A $\beta$ . Work in human embryonic kidney cells, transiently transfected with a fluorescent reporter of  $\gamma$ -secretase activity, suggests that  $\gamma$ -secretase activity is localized at endosomes and plasma membrane [4]. However, a careful isolation of lysosomes from rat livers revealed that APP and  $\gamma$ -secretase as full length proteins at the lysosomal membrane [5].

The role of APP trafficking to and from lysosomes can regulate the production of A $\beta$ . Inhibition of endocytosis or mutagenesis of APP internalization signals decreases the production of A $\beta$  [6,7]. Recent work has also demonstrated that retromer mediated recycling of APP from endosomes to the Golgi can lower the amount of A $\beta$  produced and likely plays an important role in AD pathology [8-11]. Therefore, an understanding of protein sorting is important for understanding pathology in AD.

## 5.2 APP intracellular trafficking

Much of our understanding of APP sorting comes from studies of internalization of APP from the cell surface, due to the ease of labeling APP exposed on the cell surface. This has led to the belief that *all* APP is first presented at the cell surface before internalization to endosomes, the putative site of A $\beta$  production [12]. Despite these confident claims, very few studies have actually followed the intracellular movement of APP. To follow the intracellular trafficking of APP, we took advantage of a photo-activatable mutant of GFP, which has almost no basal fluorescence [13,14]. We tagged a truncated version of APP (last 112 amino acids) with paGFP and transiently transfected SN56 cells with our  $\beta$ APP-paGFP construct. After accurate photoactivation within the TGN, we found that  $\beta$ APP-paGFP trafficked rapidly to lysosomes without transiting through the cell surface. Furthermore, APP accumulated in lysosomes, after alkalisation, and is not processed into A $\beta$ .

An intracellular pathway for APP between the Golgi and lysosomes has been previously suggested [15-17]. Kuentzel et al. [15] demonstrated that secretase release of the N-terminal domain occurs before APP appears at the cell surface, suggesting that secretase cleavage of APP may occur completely intracellularly. Unfortunately, the time course of A $\beta$  production was not followed in this study [15]. More recent findings suggest that APP is released from the Golgi apparatus to an endosomal intermediate before appearance at the cell surface [16,17]. These findings suggest that APP can trafficking directly to the endosomal and lysosomal system from the Golgi apparatus.



Our work suggests that APP is processed rapidly after appearance at the lysosomal membrane. SN56 cells treated with L685, 458 (a  $\gamma$ -secretase inhibitor) or chloroquine (an alkalinizing agent) caused an accumulation of photo-activated  $\beta$ APP-paGFP at the lysosomal membrane. APP has been postulated as a cell-surface receptor [18]. Indeed, antibodies against the extracellular domain of APP can activate intracellular signalling [19,20]. Full-length APP can also homodimerize and heterodimerize, with other members of the APP family, and participate in cell-cell adhesion [21]. Therefore, there may be a mechanism for the delivery of full-length APP from the lysosomal membrane to the cell surface. It has been suggested that APP can be sorted from endosomes into synaptic vesicles for delivery to the cell surface [22]. APP has been localized to synaptic vesicles and appears at the cell surface at sites of synaptic activity [22]. In studies with A2780 human ovarian cancer cells, Rab25 and Chloride Intracellular Channel Protein 3 (CLIC3) worked cooperatively to recycle  $\alpha 5 \beta 1$  integrin from late endosomes and lysosomes to the cell surface at the rear of migrating cell [23]. More recent work demonstrated that CLIC3 is also involved in the recycling of Matrix metalloproteinase-14 from late endosomes and lysosomes to cell surface [24]. Alternatively, a proportion of APP may be delivered to the cell surface from the Golgi. It has been demonstrated that the S655E phosphomimetic mutation can increase the APP export to the cell surface from the Golgi apparatus [25]. However, in our experiments, cell surface delivery of APP was never observed even with the S655E phosphomimetic mutation. The fluorescence of APP at the cell surface may be under the detection limit of our microscopy experiments.

The only situation where we observed significant cell surface APP was after treatment with L685, 458. L685, 458 is thought to be a transition state mimic and occupy the aspartyl-protease site of PS1 [26]. The inhibitor may disrupt the trafficking of APP by interfering with the interaction of APP and  $\gamma$ -secretase, which has been shown to be involved in APP trafficking [27-29]. PS1 and PS2 appear to be essential to the formation of vesicles from the TGN [28]. Furthermore, cells expressing various FAD mutants of PS1 decreased the formation of vesicles at the TGN and lowered the cell-surface levels of APP [28]. Interestingly, over-expression of phospholipase D1 interferes with the interaction of  $\gamma$ -secretase components, suggesting that an intact  $\gamma$ -secretase complex is required for proper APP trafficking [29]. PS1 and PS2 also appear

to be involved in APP internalization from the cell surface. Expression of non-functional PS1 delays the internalization of APP from the cell surface [30]. Therefore, the appearance of APP at the cell-surface, after treatment with L685, 458, may result from altered trafficking of APP from lysosomes to the cell surface. Alternatively, APP may accumulate at the cell surface due to disrupted internalization.

Indeed, a direct pathway between Golgi and lysosomes is well known for other lysosomal membrane proteins. For example, LAMP1 is transported directly from the Golgi to the lysosomes, without appearing at the cell surface [31,32]. The direct transport of lysosomal proteins is dependent on AP-3. When cells are deficient in AP-3, LMPs, such as LAMP1 and CD63, are still sorted to lysosomes. However, instead of a direct pathway, LMPs in AP-3 deficient cells are first delivered to the cell-surface before being internalized sorted to lysosomes [33,34]. In agreement with these findings, siRNA-mediated silencing of AP-3 in our SN56 cells decreased the amount of APP trafficking to lysosomes, and decreased the amount of A $\beta$  produced.

### 5.3 Manipulating the Intracellular Trafficking of APP

AP-3, and other members of the heterotetrameric adaptor protein family, are known to interact with tyrosine sorting motifs in the cytoplasmic domain of transmembrane proteins [35]. Previous work has demonstrated that mutagenesis of these motifs can disrupt internalization of APP from the cell surface [6,36]. Furthermore, the YTSI motif and the non-canonical YKFFE motif have been shown to interact with AP-1 and AP-4, respectively, and regulate intracellular APP trafficking [37,38]. In agreement with previous mutagenesis studies, our studies demonstrated that mutations to tyrosines in the GYENPTY internalization motif decreased internalization to early endosomes and lysosomes [6,36]. While the NPXY motif has been shown to be involved in cell-surface protein internalization through an interaction with AP-2 [39], the GYENPTY motif is critical for the interaction with various adaptor proteins. Many of these adaptors can control the metabolism of APP. For example, the APP interacting protein, Mint1, is important in APP internalization and A $\beta$  production [40]. Dab2, which also binds the NPTY motif, can interact

with AP-2, thereby linking APP to the clathrin endocytosis pathway [41]. Furthermore, APP can also interact with LRP, via a Fe65-intermediate, to facilitate APP internalization [42,43].

While previous work has carefully studied the internalization of APP, the role of these sorting motifs in APP egress from the Golgi is unstudied. In this thesis we presented evidence suggesting that these tyrosine motifs are critical in the intracellular trafficking of APP from the Golgi to the lysosome. Specifically, we showed that the Y709A and Y743A mutation decreased the delivery of APP to lysosomes, but increased early endosome localization. Furthermore, the Y738A and Y743A mutation prevented rapid internalization of APP from the cell surface to lysosomes. This suggests that Y743A mutation may participate in the trafficking of APP to the lysosome, while the Y709A and Y738A mutation work in specific sub-cellular locales. Furthermore, we demonstrated that the Y709A mutation could decrease interaction of APP with AP-3, which suggests the YTSI motif is critical for APP delivery from the Golgi to the lysosome.

Recently, there has been more interest in APP trafficking between the Golgi and endosomes, which has revealed a number of protein adaptors that regulate the trafficking of APP. However, many of these trafficking studies were performed in non-neuronal cells, therefore, the generalizability of these results to neuronal cells is unclear. In HeLa cells, APP can recruit Mint3 to the Golgi membrane and facilitates Golgi export of APP to LAMP1 labelled compartments [16]. Interestingly, these experiments demonstrated that Y687 was critical for Mint3 recruitment and rapid trafficking to LAMP1 compartments [16]. Conversely, our own experiments found no effect of Y687 trafficking from the Golgi to the lysosomes. These differences may be the result of differential expression of trafficking proteins in neuronal cells.

AP-4 has also been implicated in the delivery of APP to endosomes [37]. Silencing of AP-4 disrupts the delivery of APP from the Golgi to endosomes [37]. In support of these findings, the data presented here demonstrate that mutation of the YKFFE motif to AKFFE causes a decrease of APP sorting to lysosomes. However, other work has demonstrated that AP-4 cannot be recruited to the Golgi after APP expression [16]. Therefore, the role of AP-4 in APP trafficking remains to be determined.

While the studies mentioned above have focussed primarily on cytoplasmic sorting signals, a recent study has demonstrated that APP may depend on luminal sorting signals as well. A recent study that added short glycosaminoglycans (GAG) to the luminal portion of APP increased APP sorting to the cell-surface and decreased APP endocytosis [17]. Conversely, APP without the addition of GAG was sorted to an endosomal intermediate before appearing at the cell surface.

In addition to the sorting of APP to the endosomal/lysosomal system, APP can also be recycled back towards the endosomes. The recycling of APP to the Golgi depends upon the retromer complex. The retromer complex has a cargo-recognition complex, which consists of vacuolar protein sorting (VPS) 35, VPS26, and VPS29 [44,45]. An AD mouse model of VPS35 haploinsufficiency causes an increase in A $\beta$  production and plaque accumulation [11]. Furthermore, the brains of AD patients had a decrease in VPS35 and VPS26 protein expression [46]. shRNA silencing of VPS35 in mouse hippocampal cultures increased the amount of APP localized to early endosomes [47]. Phosphorylation of APP at S655 can increase the interaction between APP and VPS35, which decreases sorting of APP to lysosomes in preference for the Golgi [9]. These findings are in agreement with the present work, which demonstrated that phosphorylation of APP can decrease the trafficking of APP to lysosomes. The interaction between APP may depend upon the interaction with the VPS10 family proteins [48]. The VPS10 family protein SorLA has been shown to be genetically associated with AD [49]. Furthermore, APP can interact with SorLA, which mediates its retrograde trafficking from endosomes to lysosomes [9,10].

Similarly, our work also demonstrates that PKC $\epsilon$  activation or mutagenesis of sorting signals can cause an increase in trafficking to early endosomes from the TGN and decrease A $\beta$  production. APP can be phosphorylated on S655 (by APP 695 numbering or S711 by APP 751 numbering) by PKC [50,51]. The work presented here demonstrates that pseudo-phosphorylation of APP can decrease the interaction of APP with AP-3. The loss of this protein interaction decreased the amount of APP delivered to the lysosome from the Golgi and increased the proportion of APP trafficked to the early endosome. Therefore, phosphorylation of APP on S655 may serve as a molecular 'switch', which regulates the final destination of APP. Previous work has

demonstrated that PKC activation, by phorbol ester or receptor activation, causes an increase in non-amyloidogenic  $\alpha$ -secretase cleavage of APP [52-57]. Recent work has shown that  $\alpha$ - and  $\beta$ -secretase are localized in synaptic vesicles and the trafficking of  $\alpha$ - and  $\beta$ -secretase can also be altered by PKC activation [58,59]. ADAM17 enzyme activity can be up regulated by PKC $\epsilon$  activation [60]. In addition to these factors, we suggest that the alteration of the intracellular itinerary of APP may be another aspect in increasing non-amyloidogenic  $\alpha$ -secretase cleavage.

## 5.4 Lysosomal secretion of A $\beta$

The question of A $\beta$  release is lost in the literature of AD. In fact, to our knowledge A $\beta$  has never been imaged in a secretory compartment. Our work here suggests that A $\beta$  stored in lysosomes can be secreted by a Rab27b dependent mechanism. Previous work has demonstrated that neuronal lysosomes are critical in providing the membrane required for neurite extension [61]. Rab27 has been shown to be involved in the delivery and docking of lysosome-related organelles in melanocytes and cytotoxic T lymphocytes [62-64]. Previous work has also suggested that A $\beta$  is secreted in association with exosomes from N2A cells [65]. Exosomes were first suggested to be a mechanism for post-mitotic cells to clear undegraded proteins from the cell. More recent work suggests that exosomes can participate in intercellular signalling. For example, mRNA and microRNAs have been shown to be shuttled between cells and regulate protein expression in the receiving cell [66,67]. Neurons have also been shown to secrete exosomes in response to neuronal activity [68,69]. Furthermore, exosomes secreted from N2A cells can be internalized by rat cortical neurons [69]. Exosomes have also been shown to be responsible for the intercellular transfer of other neurodegenerative proteins, such as  $\alpha$ -synuclein and PrpSc [70-73]. AD pathology appears to have a regimented transneuronal spread between pyramidal neurons from different brain regions [74]. Therefore, it is not surprising that the lysosome is a source of A $\beta$  release, and A $\beta$  released from exosomes may be a mechanism for interneuronal spread of amyloid pathology in AD.

The production and accumulation of amyloid in endosomes and lysosomes bears a striking resemblance to the formation of fibrillar structures in melanosomes. These fibrillar structures are formed by the sequential proteolytic cleavage of the precursor protein Premelanosome protein

(PMEL) [75]. The first cleavage is by proprotein convertase and is followed by a second juxtamembrane cleavage [75]. The second cleavage has been suggested to be carried out by BACE2, ADAM10, or ADAM17 [76,77]. The identity of the enzyme responsible for the cleavage may depend upon the individual cell lines studied. The amyloid fibrils gain pigment by the deposition of melanin and are subsequently secreted and taken up by keratinocytes by a poorly understood mechanism [75]. These observations have led to the suggestion that amyloid may be a naturally occurring product [78]. Indeed, A $\beta$  has been shown to be secreted in non-pathological situations and may perform a normal physiological function [79]. For example, A $\beta$  has been shown to have antimicrobial functions and can bind to *Escherichia Coli* and inhibit its growth [80]. Furthermore, A $\beta$  can also regulate neuronal activity. It is well known that A $\beta$  oligomers can inhibit long-term potentiation [81,82]. However, low (picromolar) levels of A $\beta$  can potentiate long-term potentiation [83]. It has also been previously demonstrated that the production and secretion of A $\beta$  is increased after synaptic activity [84]. These findings have led to the suggestion that A $\beta$  may play a role in maintaining the stability of the synapse (homeostatic plasticity).

## 5.5 Conclusion

The present work follows the intracellular itinerary of nascent APP. Starting at the site of production (the Golgi), we have demonstrated that APP can traffic rapidly to the lysosomal membrane using an AP-3 dependent mechanism. This is reminiscent of the trafficking of other lysosomal membrane proteins, which utilize the intracellular trafficking pathway. We further explored the control of this trafficking, showing that PKC phosphorylation of APP at S655 can regulate the interaction of APP with adaptor proteins responsible for facilitating APP trafficking [9]. Finally, we show the first evidence of a mechanism for A $\beta$  secretion from intracellular lysosomal stores.

These data suggest that the routing of APP to lysosomes can promote the production of A $\beta$ . This lysosomal amyloid can then fibrilize and form aggregates. Such intracellular aggregates have been found in animal models and human patients have evidence of intracellular aggregates of A $\beta$  and can seed the formation of extracellular aggregates [85,86]. This thesis suggests that the

lysosome produces A $\beta$  and is the missing secretory organelle for A $\beta$  (Figure 5.1). This work is critical for understanding the underlying cellular physiology of APP and potentially reveals additional therapeutic targets for the treatment of AD.

Figure 5.1: APP trafficking and A $\beta$  production and secretion.

APP is synthesized in the endoplasmic reticulum and in the Golgi. 1a) After synthesis, APP can be presented at the cell surface or 1b) delivered rapidly and directly to the lysosome. 2a) After presentation at the cell surface, APP can be internalized in a clathrin dependent manner (clathrin depicted as gray shading) into early endosomes. 2b) Alternatively, APP can be internalized rapidly to lysosomes from the cell surface, in a macropinocytosis dependent manner. 3) APP is eventually delivered to lysosomes and processed to form A $\beta$ . 4) Through an interaction with the retromer complex, APP can also be recycled to the Golgi from the endosome. 5) After cleavage of APP by  $\gamma$ -secretase, A $\beta$  remains in the lysosomal lumen. From the lysosome, A $\beta$  can be secreted into the extracellular space in a Rab27b dependent manner. Note: The red boxes represent novel contributions to our understanding of APP trafficking, with the appropriate chapter reference included. The grey numbers indicate previously studied trafficking pathways, which are thoroughly discussed in Chapter 1 of this thesis.



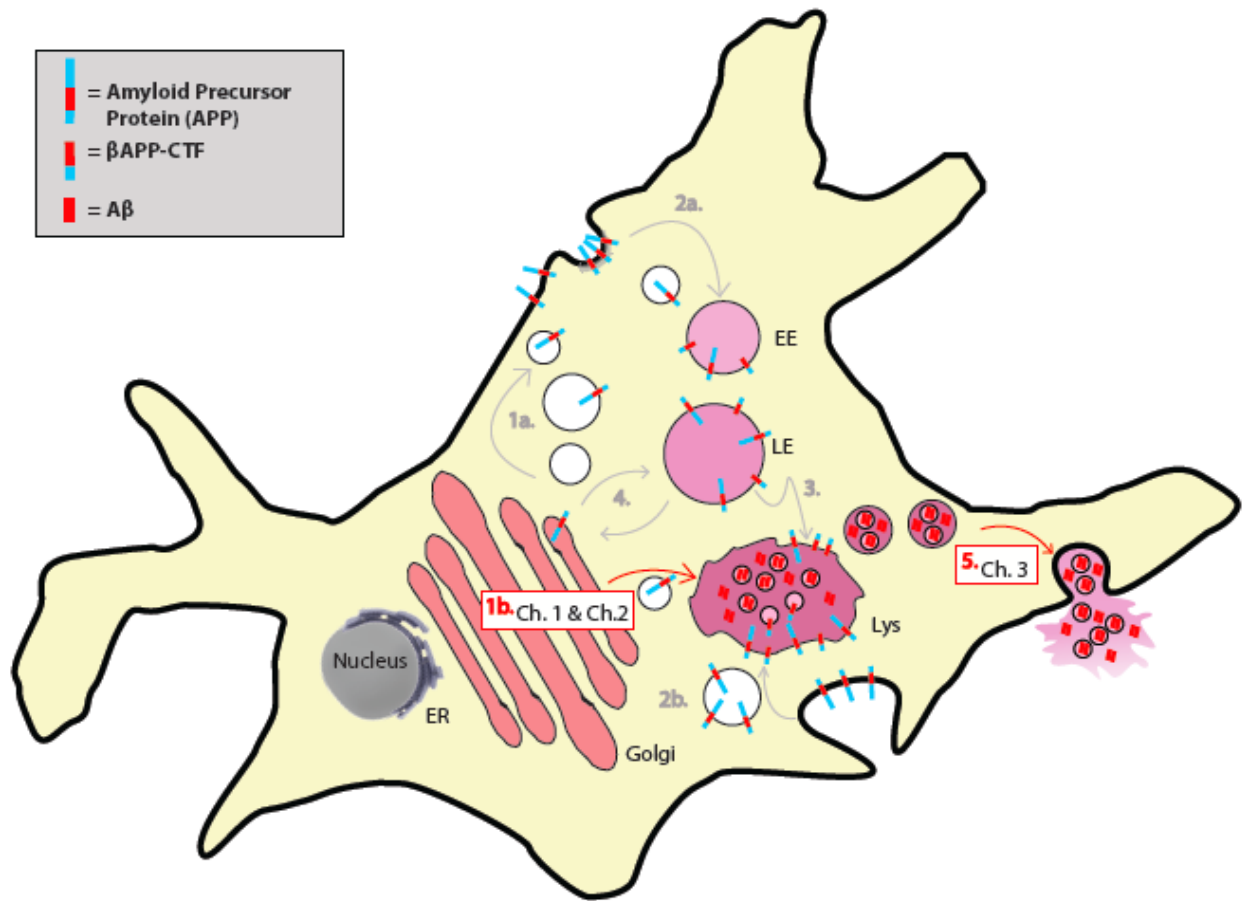


Figure 5.1

## 5.6 References

1. Tang BL. Neuronal protein trafficking associated with Alzheimer disease: from APP and BACE1 to glutamate receptors. *Cell Adh Migr.* 2009;3: 118–128.
2. Brunholz S, Sisodia S, Lorenzo A, Deyts C, Kins S, Morfini G. Axonal transport of APP and the spatial regulation of APP cleavage and function in neuronal cells. *Exp Brain Res.* 2011;217: 353–364. doi:10.1007/s00221-011-2870-1
3. Pasternak SH, Callahan JW, Mahuran DJ. The role of the endosomal/lysosomal system in amyloid-beta production and the pathophysiology of Alzheimer's disease: reexamining the spatial paradox from a lysosomal perspective. *J Alzheimers Dis.* 2004;6: 53–65.
4. Kaether C, Schmitt S, Willem M, Haass C. Amyloid Precursor Protein and Notch Intracellular Domains are Generated after Transport of their Precursors to the Cell Surface. *Traffic.* 2006;7: 408–415. doi:10.1111/j.1600-0854.2006.00396.x
5. Pasternak SH, Bagshaw RD, Guiral M, Zhang S, Ackerley CA, Pak BJ, et al. Presenilin-1, nicastrin, amyloid precursor protein, and gamma-secretase activity are co-localized in the lysosomal membrane. *J Biol Chem.* 2003;278: 26687–26694. doi:10.1074/jbc.M212192200
6. Perez RG, Soriano S, Hayes JD, Ostaszewski B, Xia W, Selkoe DJ, et al. Mutagenesis identifies new signals for beta-amyloid precursor protein endocytosis, turnover, and the generation of secreted fragments, including Abeta42. *J Biol Chem.* 1999;274: 18851–18856.
7. Zhu L, Su M, Lucast L, Liu L, Netzer WJ, Gandy SE, et al. Dynamin 1 regulates amyloid generation through modulation of BACE-1. Xie Z, editor. *PLoS ONE.* 2012;7: e45033. doi:10.1371/journal.pone.0045033
8. Sullivan CP, Jay AG, Stack EC, Pakaluk M, Wadlinger E, Fine RE, et al. Retromer disruption promotes amyloidogenic APP processing. *Neurobiology of Disease.* 2011;43: 338–345. doi:10.1016/j.nbd.2011.04.002
9. Vieira SI, Rebelo S, Esselmann H, Wiltfang J, Lah J, Lane R, et al. Retrieval of the Alzheimer's amyloid precursor protein from the endosome to the TGN is S655 phosphorylation state-dependent and retromer-mediated. *Molecular Neurodegeneration.* 2010;5: 40. doi:10.1186/1750-1326-5-40
10. Fjorback AW, Seaman M, Gustafsen C, Mehmedbasic A, Gokool S, Wu C, et al.

- Retromer binds the FANSHY sorting motif in SorLA to regulate amyloid precursor protein sorting and processing. *Journal of Neuroscience*. 2012;32: 1467–1480. doi:10.1523/JNEUROSCI.2272-11.2012
11. Wen L, Tang F-L, Hong Y, Luo S-W, Wang C-L, He W, et al. VPS35 haploinsufficiency increases Alzheimer's disease neuropathology. *Journal of Cell Biology*. Rockefeller Univ Press; 2011;195: 765–779.
  12. Thinakaran G, Koo EH. Amyloid Precursor Protein Trafficking, Processing, and Function. *Journal of Biological Chemistry*. 2008;283: 29615–29619. doi:10.1074/jbc.R800019200
  13. Patterson GH, Patterson GH, Lippincott-Schwartz J. A photoactivatable GFP for selective photolabeling of proteins and cells. *Science*. American Association for the Advancement of Science; 2002;297: 1873–1877. doi:10.1126/science.1074952
  14. Patterson GH, Lippincott-Schwartz J. Selective photolabeling of proteins using photoactivatable GFP. *Methods*. 2004;32: 445–450. doi:10.1016/j.ymeth.2003.10.006
  15. Kuentzel SL, Ali SM, Altman RA, Greenberg BD, Raub TJ. The Alzheimer beta-amyloid protein precursor/protease nexin-II is cleaved by secretase in a trans-Golgi secretory compartment in human neuroglioma cells. *Biochem J*. 1993;295 ( Pt 2): 367–378.
  16. Caster AH, Kahn RA. Recruitment of the Mint3 adaptor is necessary for export of the amyloid precursor protein (APP) from the Golgi complex. *J Biol Chem*. 2013;288: 28567–28580. doi:10.1074/jbc.M113.481101
  17. Mihov D, Raja E, Spiess M. Chondroitin Sulfate Accelerates Trans-Golgi-to-Surface Transport of Proteoglycan Amyloid Precursor Protein. *Traffic*. 2015;16: 853–870. doi:10.1111/tra.12294
  18. Kang J, Lemaire HG, Unterbeck A, Salbaum JM, Masters CL, Grzeschik KH, et al. The precursor of Alzheimer's disease amyloid A4 protein resembles a cell-surface receptor. *Nature*. 1987;325: 733–736. doi:10.1038/325733a0
  19. Murayama Y, Takeda S, Yonezawa K, Giambarella U, Nishimoto I, Ogata E. Cell surface receptor function of amyloid precursor protein that activates Ser/Thr kinases. *Gerontology*. 1996;42 Suppl 1: 2–11.
  20. Lefort R, Pozueta J, Shelanski M. Cross-Linking of Cell Surface Amyloid Precursor Protein Leads to Increased  $\beta$ -Amyloid Peptide Production in Hippocampal Neurons: Implications for Alzheimer's Disease. *Journal of Neuroscience*. 2012;32: 10674–10685. doi:10.1523/JNEUROSCI.6473-11.2012
  21. Soba P, Eggert S, Wagner K, Zentgraf H, Siehl K, Kreger S, et al. Homo- and heterodimerization of APP family members promotes intercellular adhesion. *The EMBO Journal*. 2005;24: 3624–3634. doi:10.1038/sj.emboj.7600824

22. Groemer TW, Thiel CS, Holt M, Riedel D, Hua Y, Hüve J, et al. Amyloid precursor protein is trafficked and secreted via synaptic vesicles. *PLoS ONE*. 2011;6: e18754. doi:10.1371/journal.pone.0018754
23. Dozynkiewicz MA, Jamieson NB, Macpherson I, Grindlay J, van den Berghe PVE, Thun von A, et al. Rab25 and CLIC3 collaborate to promote integrin recycling from late endosomes/lysosomes and drive cancer progression. *Developmental Cell*. 2012;22: 131–145. doi:10.1016/j.devcel.2011.11.008
24. Macpherson IR, Rainero E, Mitchell LE, van den Berghe PVE, Speirs C, Dozynkiewicz MA, et al. CLIC3 controls recycling of late endosomal MT1-MMP and dictates invasion and metastasis in breast cancer. *Journal of Cell Science*. The Company of Biologists Ltd; 2014;127: 3893–3901. doi:10.1242/jcs.135947
25. Vieira SI, Rebelo S, Domingues SC, Cruz e Silva EF, Cruz e Silva OAB. S655 phosphorylation enhances APP secretory traffic. *Mol Cell Biochem*. 2009;328: 145–154. doi:10.1007/s11010-009-0084-7
26. Shearman MS, Beher D, Clarke EE, Lewis HD, Harrison T, Hunt P, et al. L-685,458, an Aspartyl Protease Transition State Mimic, Is a Potent Inhibitor of Amyloid  $\beta$ -Protein Precursor  $\gamma$ -Secretase Activity. *Biochemistry*. 2000;39: 8698–8704. doi:10.1021/bi0005456
27. Cai D, Zhong M, Wang R, Netzer WJ, Shields D, Zheng H, et al. Phospholipase D1 corrects impaired betaAPP trafficking and neurite outgrowth in familial Alzheimer's disease-linked presenilin-1 mutant neurons. *Proc Natl Acad Sci USA*. 2006;103: 1936–1940. doi:10.1073/pnas.0510710103
28. Cai D, Leem JY, Greenfield JP, Wang P, Kim BS, Wang R, et al. Presenilin-1 regulates intracellular trafficking and cell surface delivery of beta-amyloid precursor protein. *Journal of Biological Chemistry*. 2003;278: 3446–3454. doi:10.1074/jbc.M209065200
29. Cai D, Netzer WJ, Zhong M, Lin Y, Du G, Frohman M, et al. Presenilin-1 uses phospholipase D1 as a negative regulator of beta-amyloid formation. *Proc Natl Acad Sci USA*. 2006;103: 1941–1946. doi:10.1073/pnas.0510708103
30. Kaether C. Presenilin-1 affects trafficking and processing of betaAPP and is targeted in a complex with nicastrin to the plasma membrane. *The Journal of Cell Biology*. 2002;158: 551–561. doi:10.1083/jcb.200201123
31. Barriocanal JG, Bonifacino JS, Yuan L, Sandoval IV. Biosynthesis, glycosylation, movement through the Golgi system, and transport to lysosomes by an N-linked carbohydrate-independent mechanism of three lysosomal integral membrane proteins. *Journal of Biological Chemistry*. 1986;261: 16755–16763.

32. D'Souza MP, August JT. A kinetic analysis of biosynthesis and localization of a lysosome-associated membrane glycoprotein. *Archives of Biochemistry and Biophysics*. 1986;249: 522–532.
33. Dell'Angelica EC, Shotelersuk V, Aguilar RC, Gahl WA, Bonifacino JS. Altered trafficking of lysosomal proteins in Hermansky-Pudlak syndrome due to mutations in the beta 3A subunit of the AP-3 adaptor. *Molecular Cell*. 1999;3: 11–21. doi:10.1016/S1097-2765(00)80170-7
34. Peden AA. Assembly and function of AP-3 complexes in cells expressing mutant subunits. *The Journal of Cell Biology*. 2002;156: 327–336. doi:10.1083/jcb.200107140
35. Ohno H, Aguilar RC, Yeh D, Taura D, Saito T, Bonifacino JS. The medium subunits of adaptor complexes recognize distinct but overlapping sets of tyrosine-based sorting signals. *J Biol Chem*. 1998;273: 25915–25921.
36. Lai A, Sisodia SS, Trowbridge IS. Characterization of sorting signals in the beta-amyloid precursor protein cytoplasmic domain. *J Biol Chem*. 1995;270: 3565–3573.
37. Burgos PV, Mardones GA, Rojas AL, daSilva LLP, Prabhu Y, Hurley JH, et al. Sorting of the Alzheimer's disease amyloid precursor protein mediated by the AP-4 complex. *Developmental Cell*. 2010;18: 425–436. doi:10.1016/j.devcel.2010.01.015
38. Icking A, Amadii M, Ruonala M, Höning S, Tikkanen R. Polarized Transport of Alzheimer Amyloid Precursor Protein Is Mediated by Adaptor Protein Complex AP1-1B. *Traffic*. 2006;8: 285–296. doi:10.1111/j.1600-0854.2006.00526.x
39. Boll W, Rapoport I, Brunner C, Modis Y, Prehn S, Kirchhausen T. The mu2 Subunit of the Clathrin Adaptor AP-2 Binds to FDNPVY and YppO Sorting Signals at Distinct Sites. *Traffic*. 2002;3: 590–600. doi:10.1034/j.1600-0854.2002.30808.x
40. Sullivan SE, Dillon GM, Sullivan JM, Ho A. Mint proteins are required for synaptic activity-dependent amyloid precursor protein (APP) trafficking and amyloid  $\beta$  generation. *J Biol Chem*. 2014;289: 15374–15383. doi:10.1074/jbc.M113.541003
41. Maurer ME, Cooper JA. The adaptor protein Dab2 sorts LDL receptors into coated pits independently of AP-2 and ARH. *Journal of Cell Science*. 2006;119: 4235–4246. doi:10.1242/jcs.03217
42. Pietrzik CU, Yoon I-S, Jaeger S, Busse T, Weggen S, Koo EH. FE65 constitutes the functional link between the low-density lipoprotein receptor-related protein and the amyloid precursor protein. *Journal of Neuroscience*. 2004;24: 4259–4265. doi:10.1523/JNEUROSCI.5451-03.2004
43. Pietrzik CU, Busse T, Merriam DE, Weggen S, Koo EH. The cytoplasmic domain of the LDL receptor-related protein regulates multiple steps in APP processing. *The EMBO*

- Journal. 2002;21: 5691–5700.
44. Seaman MNJ. The retromer complex - endosomal protein recycling and beyond. *Journal of Cell Science*. The Company of Biologists Ltd; 2012;125: 4693–4702. doi:10.1242/jcs.103440
  45. Haft CR, la Luz Sierra de M, Bafford R, Lesniak MA, Barr VA, Taylor SI. Human orthologs of yeast vacuolar protein sorting proteins Vps26, 29, and 35: assembly into multimeric complexes. *Mol Biol Cell*. 2000;11: 4105–4116.
  46. Small SA, Kent K, Pierce A, Leung C, Kang MS, Okada H, et al. Model-guided microarray implicates the retromer complex in Alzheimer's disease. *Ann Neurol*. 2005;58: 909–919. doi:10.1002/ana.20667
  47. Bhalla A, Vetanovetz CP, Morel E, Chamoun Z, Di Paolo G, Small SA. The location and trafficking routes of the neuronal retromer and its role in amyloid precursor protein transport. *Neurobiology of Disease*. 2012;47: 126–134. doi:10.1016/j.nbd.2012.03.030
  48. Lane RF, St George-Hyslop P, Hempstead BL, Small SA, Strittmatter SM, Gandy S. Vps10 family proteins and the retromer complex in aging-related neurodegeneration and diabetes. *Journal of Neuroscience*. 2012;32: 14080–14086. doi:10.1523/JNEUROSCI.3359-12.2012
  49. Rogaeva E, Meng Y, Lee JH, Gu Y, Kawarai T, Zou F, et al. The neuronal sortilin-related receptor SORL1 is genetically associated with Alzheimer disease. *Nat Genet*. 2007;39: 168–177. doi:10.1038/ng1943
  50. Suzuki T, Nairn AC, Gandy SE, Greengard P. Phosphorylation of Alzheimer amyloid precursor protein by protein kinase C. *NSC*. 1992;48: 755–761. doi:10.1016/0306-4522(92)90264-3
  51. Gandy S, Czernik AJ, Greengard P. Phosphorylation of Alzheimer disease amyloid precursor peptide by protein kinase C and Ca<sup>2+</sup>/calmodulin-dependent protein kinase II. *Proc Natl Acad Sci USA*. 1988;85: 6218–6221.
  52. Lanni C, Mazzucchelli M, Porrello E, Govoni S, Racchi M. Differential involvement of protein kinase C alpha and epsilon in the regulated secretion of soluble amyloid precursor protein. *European Journal of Biochemistry*. 2004;271: 3068–3075. doi:10.1111/j.1432-1033.2004.04240.x
  53. Skovronsky DM, Moore DB, Milla ME, Doms RW, Lee VM. Protein kinase C-dependent alpha-secretase competes with beta-secretase for cleavage of amyloid-beta precursor protein in the trans-golgi network. *Journal of Biological Chemistry*. 2000;275: 2568–2575. doi:10.1074/jbc.275.4.2568
  54. Yeon SW, Jung MW, Ha MJ, Kim SU, Huh K, Savage MJ, et al. Blockade of PKC $\epsilon$

- Activation Attenuates Phorbol Ester-Induced Increase of  $\alpha$ -Secretase-Derived Secreted Form of Amyloid Precursor Protein. *Biochemical and Biophysical Research Communications*. 2001;280: 782–787. doi:10.1006/bbrc.2000.4181
55. Benussi L, Govoni S, Gasparini L, Binetti G, Trabucchi M, Bianchetti A, et al. Specific role for protein kinase C alpha in the constitutive and regulated secretion of amyloid precursor protein in human skin fibroblasts. *Neuroscience Letters*. 1998;240: 97–101.
  56. Slack BE, Breu J, Petryniak MA, Srivastava K, Wurtman RJ. Tyrosine phosphorylation-dependent stimulation of amyloid precursor protein secretion by the m3 muscarinic acetylcholine receptor. *J Biol Chem*. 1995;270: 8337–8344.
  57. Nitsch R, Slack B, Wurtman R, Growdon J. Release of Alzheimer amyloid precursor derivatives stimulated by activation of muscarinic acetylcholine receptors. *Science*. 1992;258: 304–307. doi:10.1126/science.1411529
  58. Saraceno C, Marcello E, Di Marino D, Borroni B, Claeysen S, Perroy J, et al. SAP97-mediated ADAM10 trafficking from Golgi outposts depends on PKC phosphorylation. *Cell Death Dis*. 2014;5: e1547. doi:10.1038/cddis.2014.492
  59. Walter J, Fluhrer R, Hartung B, Willem M, Kaether C, Capell A, et al. Phosphorylation regulates intracellular trafficking of beta-secretase. *Journal of Biological Chemistry*. American Society for Biochemistry and Molecular Biology; 2001;276: 14634–14641. doi:10.1074/jbc.M011116200
  60. Lemjabbar-Alaoui H, Sidhu SS, Mengistab A, Gallup M, Basbaum C. TACE/ADAM-17 Phosphorylation by PKC-Epsilon Mediates Premalignant Changes in Tobacco Smoke-Exposed Lung Cells. Rich B, editor. *PLoS ONE*. 2011;6: e17489. doi:10.1371/journal.pone.0017489.g008
  61. Arantes RME. A Role for Synaptotagmin VII-Regulated Exocytosis of Lysosomes in Neurite Outgrowth from Primary Sympathetic Neurons. *Journal of Neuroscience*. 2006;26: 4630–4637. doi:10.1523/JNEUROSCI.0009-06.2006
  62. Ostrowski M, Carmo NB, Krumeich S, Fanget I, Raposo G, Savina A, et al. Rab27a and Rab27b control different steps of the exosome secretion pathway : *Nature Cell Biology*. *Nature Cell Biology*. 2010;12: 19–30– sup pp 1–13. doi:10.1038/ncb2000
  63. Wu XS, Wu XS, Tsan GL, Hammer JA. Melanophilin and myosin Va track the microtubule plus end on EB1. *Journal of Cell Biology*. 2005;171: 201–207. doi:10.1083/jcb.200503028
  64. Elstak ED, Neeft M, Nehme NT, Voortman J, Cheung M, Goodarzifard M, et al. The munc13-4-rab27 complex is specifically required for tethering secretory lysosomes at the plasma membrane. *Blood*. 2011;118: 1570–1578. doi:10.1182/blood-2011-02-339523

65. Rajendran L, Honsho M, Zahn TR, Keller P, Geiger KD, Verkade P, et al. Alzheimer's disease beta-amyloid peptides are released in association with exosomes. *Proc Natl Acad Sci USA*. 2006;103: 11172–11177. doi:10.1073/pnas.0603838103
66. Valadi H, Ekström K, Bossios A, Sjöstrand M, Lee JJ, Lötvall JO. Exosome-mediated transfer of mRNAs and microRNAs is a novel mechanism of genetic exchange between cells. *Nature Cell Biology*. 2007;9: 654–659. doi:10.1038/ncb1596
67. Skog J, Wurdinger T, van Rijn S, Meijer DH, Gainche L, Sena-Estevés M, et al. Glioblastoma microvesicles transport RNA and proteins that promote tumour growth and provide diagnostic biomarkers. *Nature Cell Biology*. 2008;10: 1470–1476. doi:10.1038/ncb1800
68. Lachenal G, Pernet-Gallay K, Chivet M, Hemming FJ, Belly A, Bodon G, et al. Release of exosomes from differentiated neurons and its regulation by synaptic glutamatergic activity. *Mol Cell Neurosci*. 2011;46: 409–418. doi:10.1016/j.mcn.2010.11.004
69. Chivet M, Javalet C, Laulagnier K, Blot B, Hemming FJ, Sadoul R. Exosomes secreted by cortical neurons upon glutamatergic synapse activation specifically interact with neurons. *J Extracell Vesicles*. 2014;3: 24722. doi:10.3402/jev.v3.24722
70. Baron GS, Magalhaes AC, Prado M. Mouse-adapted scrapie infection of SN56 cells: greater efficiency with microsome-associated versus purified PrP-res. *Journal of ...* 2006.
71. Maas E, Geissen M, Groschup MH, Rost R, Onodera T, Schätzl H, et al. Scrapie infection of prion protein-deficient cell line upon ectopic expression of mutant prion proteins. *Journal of Biological Chemistry*. American Society for Biochemistry and Molecular Biology; 2007;282: 18702–18710. doi:10.1074/jbc.M701309200
72. Danzer KM, Kranich LR, Ruf WP, Cagsal-Getkin O, Winslow AR, Zhu L, et al. Exosomal cell-to-cell transmission of alpha synuclein oligomers. *Molecular Neurodegeneration*. 2012;7: 42. doi:10.1186/1750-1326-7-42
73. Alvarez-Erviti L, Seow Y, Schapira AH, Gardiner C, Sargent IL, Wood MJA, et al. Lysosomal dysfunction increases exosome-mediated alpha-synuclein release and transmission. *Neurobiology of Disease*. 2011;42: 360–367. doi:10.1016/j.nbd.2011.01.029
74. Braak H, Braak E. Neuropathological staging of Alzheimer-related changes. *Acta Neuropathol*. 1991;82: 239–259.
75. Watt B, van Niel G, Raposo G, Marks MS. PMEL: a pigment cell-specific model for functional amyloid formation. *Pigment Cell Melanoma Res*. 2013;26: 300–315. doi:10.1111/pcmr.12067
76. Rochin L, Hurbain I, Serneels L, Fort C, Watt B, Leblanc P, et al. BACE2 processes PMEL to form the melanosome amyloid matrix in pigment cells. *Proceedings of the*



- National Academy of Sciences. 2013;110: 10658–10663. doi:10.1073/pnas.1220748110
77. Kummer MP, Maruyama H, Huelsmann C, Baches S, Weggen S, Koo EH. Formation of Pmel17 amyloid is regulated by juxtamembrane metalloproteinase cleavage, and the resulting C-terminal fragment is a substrate for gamma-secretase. *Journal of Biological Chemistry*. American Society for Biochemistry and Molecular Biology; 2009;284: 2296–2306. doi:10.1074/jbc.M808904200
  78. Kelly JW, Balch WE. Amyloid as a natural product. *Journal of Cell Biology*. 2003;161: 461–462. doi:10.1083/jcb.200304074
  79. Parihar MS, Brewer GJ. Amyloid- $\beta$  as a modulator of synaptic plasticity. *J Alzheimers Dis*. 2010;22: 741–763. doi:10.3233/JAD-2010-101020
  80. Soscia SJ, Kirby JE, Washicosky KJ, Tucker SM, Ingelsson M, Hyman B, et al. The Alzheimer's Disease-Associated Amyloid  $\beta$ -Protein Is an Antimicrobial Peptide. Bush AI, editor. *PLoS ONE*. 2010;5: e9505. doi:10.1371/journal.pone.0009505.t001
  81. Walsh DM, Klyubin I, Fadeeva JV, Cullen WK, Anwyl R, Wolfe MS, et al. Naturally secreted oligomers of amyloid beta protein potently inhibit hippocampal long-term potentiation in vivo. *Nature*. 2002;416: 535–539. doi:10.1038/416535a
  82. Ostapchenko VG, Beraldo FH, Mohammad AH, Xie Y-F, Hirata PHF, Magalhaes AC, et al. The prion protein ligand, stress-inducible phosphoprotein 1, regulates amyloid- $\beta$  oligomer toxicity. *Journal of Neuroscience*. Society for Neuroscience; 2013;33: 16552–16564. doi:10.1523/JNEUROSCI.3214-13.2013
  83. Puzzo D, Privitera L, Leznik E, Fà M, Staniszewski A, Palmeri A, et al. Picomolar amyloid-beta positively modulates synaptic plasticity and memory in hippocampus. *Journal of Neuroscience*. 2008;28: 14537–14545. doi:10.1523/JNEUROSCI.2692-08.2008
  84. Wu J, Petralia RS, Kurushima H, Patel H, Jung M-Y, Volk L, et al. Arc/Arg3.1 Regulates an Endosomal Pathway Essential for Activity-Dependent  $\beta$ -Amyloid Generation. *Cell*. Elsevier Inc; 2011;147: 615–628. doi:10.1016/j.cell.2011.09.036
  85. Hu X, Crick SL, Bu G, Frieden C, Pappu RV, Lee J-M. Amyloid seeds formed by cellular uptake, concentration, and aggregation of the amyloid-beta peptide. *Proceedings of the National Academy of Sciences*. 2009;106: 20324–20329. doi:10.1073/pnas.0911281106
  86. Iulita MF, Allard S, Richter L, Munter L-M, Ducatenzeiler A, Weise C, et al. Intracellular A $\beta$  pathology and early cognitive impairments in a transgenic rat overexpressing human amyloid precursor protein: a multidimensional study. *Acta Neuropathol Commun*. 2014;2: 61. doi:10.1186/2051-5960-2-61

## Appendices

All the videos associated with this thesis stored at the School of Graduate and Postdoctoral Studies' Electronic Theses & Dissertation site (<http://ir.lib.uwo.ca/etd/>).

### Appendix A: Figure Legends to Chapter 2 Videos

**Video 2.1:** APP is trafficked rapidly to the lysosome and cleared.

SN56 cells were transiently transfected with GalT-CFP to identify the Golgi apparatus, LAMP1-mRFP to identify lysosomes, and  $\beta$ APP-paGFP. Irradiation targets (circles) were drawn over the Golgi apparatus and the were irradiated with 405 nm laser light, alternating with imaging for 15 minutes (indicated by the green word 'photoactivating' on the images. Cells were then followed in a 'chase period' imaging every 30 seconds for the time indicated.

**Video 2.2:** APP paGFP is accurately photoactivated in the Golgi apparatus.

SN56 cells were transiently transfected with GalT-CFP to identify the Golgi apparatus, LAMP1-mRFP to identify lysosomes, and  $\beta$ APP-paGFP and were treated with Nocodazole to block exit from the Golgi. Irradiation targets (circles) were drawn over the Golgi apparatus and the were irradiated with 405 nm laser light, alternating with imaging for 15 minutes (indicated by the green word 'photoactivating' on the images. Cells were then followed in a 'chase period' imaging every 30 seconds for the time indicated. Photoactivated  $\beta$ APP-paGFP can be seen accumulating in the Golgi.

**Video 2.3:** APP processing in the lysosome is blocked by Chloroquine in the lysosome.

SN56 cells were transiently transfected with GalT-CFP to identify the Golgi apparatus, LAMP1-mRFP to identify lysosomes, and  $\beta$ APP-paGFP. Cells were pretreated with 100  $\mu$ M chloroquine 30 minutes before imaging. Irradiation targets (circles) were drawn over the Golgi apparatus and the were irradiated with 405 nm laser light, alternating with imaging for 15 minutes (indicated by the green word 'photoactivating' on the images. Cells were then followed in a 'chase period' imaging every 30 seconds for the time indicated. Photoactivated  $\beta$ APP-paGFP can be seen accumulating in lysosomes.

**Video 2.4:** APP processing in the lysosome is blocked by L685, 458 in the lysosome.

SN56 cells were transiently transfected with GalT-CFP to identify the Golgi apparatus, LAMP1-mRFP to identify lysosomes, and  $\beta$ APP-paGFP. Cells were pretreated with 0.5  $\mu$ M L685, 458 overnight. Irradiation targets (circles) were drawn over the Golgi apparatus and the were irradiated with 405 nm laser light, alternating with imaging for 15 minutes (indicated by the green word 'photoactivating' on the images. Cells were then followed in a 'chase period' imaging every 30 seconds for the time indicated. Photoactivated  $\beta$ APP-paGFP can be seen accumulating in lysosomes.

**Video 2.5:** APP<sub>sw</sub> trafficking is rapidly processed.

SN56 cells were transiently transfected with GalT-CFP to identify the Golgi apparatus, LAMP1-mRFP to identify lysosomes, and  $\beta$ APP<sub>sw</sub>-paGFP. Irradiation targets (circles) were drawn over the Golgi apparatus and the were irradiated with 405 nm laser light, alternating with imaging for 15 minutes (indicated by the green word 'photoactivating' on the images. Cells were then followed in a 'chase period' imaging every 30 seconds for the time indicated. APP<sub>sw</sub> is cleaved so rapidly that it is unable to accumulate in any compartment.

**Video 2.6:** APP<sub>sw</sub> is not cleared in the Golgi apparatus.

SN56 cells were transiently transfected with GalT-CFP to identify the Golgi apparatus, LAMP1-mRFP to identify lysosomes, and  $\beta$ APP<sub>sw</sub>-paGFP and were treated with 66  $\mu$ M nocodazole and 10  $\mu$ M cytochalasin. Irradiation targets (circles) were drawn over the Golgi apparatus and the were irradiated with 405 nm laser light, alternating with imaging for 15 minutes (indicated by the green word 'photoactivating' on the images. Cells were then followed in a 'chase period' imaging every 30 seconds for the time indicated. Photoactivated  $\beta$ APP<sub>sw</sub>-paGFP can be seen accumulating in the Golgi.

**Video 2.7:** APP<sub>sw</sub> processing in the lysosome is blocked by chloroquine.

SN56 cells were transiently transfected with GalT-CFP to identify the Golgi apparatus, LAMP1-mRFP to identify lysosomes, and  $\beta$ APP<sub>sw</sub>-paGFP and were treated with 100  $\mu$ M chloroquine. Irradiation targets (circles) were drawn over the Golgi apparatus and the were irradiated with 405

nm laser light, alternating with imaging for 15 minutes (indicated by the green word 'photoactivating' on the images. Cells were then followed in a 'chase period' imaging every 30 seconds for the time indicated. Photoactivated  $\beta$ APPsw-paGFP can be seen accumulating in lysosomes.

**Video 2.8:** APPsw processing in the lysosome is blocked by L685, 458;  $\gamma$ -cleavage occurs in the lysosome.

SN56 cells were transiently transfected with GalT-CFP to identify the Golgi apparatus, LAMP1-mRFP to identify lysosomes, and  $\beta$ APPsw-paGFP and were treated with 0.5  $\mu$ M L685, 458 overnight. Irradiation targets (circles) were drawn over the Golgi apparatus and the were irradiated with 405 nm laser light, alternating with imaging for 15 minutes (indicated by the green word 'photoactivating' on the images. Cells were then followed in a 'chase period' imaging every 30 seconds for the time indicated. Photoactivated  $\beta$ APPsw-paGFP can be seen accumulating in lysosomes.

### Appendix B: Figure Legends to Chapter 3 Videos

**Video 3.1:** APP is trafficked rapidly to lysosomes from the Golgi.

SN56 cells were transiently transfected with  $\beta$ APP-paGFP (green), LAMP1-mRFP (lysosome marker, red), and GalT-CFP (Golgi marker, blue). APP was photo-activated in the Golgi (blue) with 405nm light, alternating with imaging for 15 minutes (indicated by green word 'Photo-activating'). The white circles appearing over the Golgi denote the initial ROIs for  $\beta$ APP-paGFP photoactivation. These ROIs are carefully monitored and adjusted to remain on the Golgi during the photoactivation period. Cells were then chased imaging every 30 seconds for the indicated time.

**Video 3.2:** APP bearing the Y709A mutation does not traffic to lysosomes.

SN56 cells were transiently transfected with  $\beta$ APP Y709A-paGFP (green), LAMP1-mRFP (lysosome marker, red), and GalT-CFP (Golgi marker, blue). APP was photo-activated in the Golgi (blue) with 405nm light, alternating with imaging for 15 minutes (indicated by green word

‘Photo-activating’). White circles appearing over the Golgi denote the initial ROIs for  $\beta$ APP-paGFP photoactivation. Cells were then chased by imaging every 30 seconds for the indicated time.

**Video 3.3.** APP bearing the Y738A mutation traffics to lysosomes.

SN56 cells were transiently transfected with  $\beta$ APP Y738A-paGFP (green), LAMP1-mRFP (lysosome marker, red), and GalT-CFP (Golgi marker, blue). APP was photo-activated in the Golgi (blue) with 405nm light, alternating with imaging for 15 minutes (indicated by green word ‘Photo-activating’). Photo-activation ROIs in the Golgi are denoted by white circles in the video. Cells were then chased by imaging every 30 seconds for the indicated time.

**Video 3.4.** APP bearing the Y743A mutation does not traffic to lysosomes.

SN56 cells were transiently transfected with  $\beta$ APP Y743A-paGFP (green), LAMP1-mRFP (lysosome marker, red), and GalT-CFP (Golgi marker, blue). APP was photo-activated in the Golgi (blue) with 405nm light, alternating with imaging for 15 minutes (indicated by green word ‘Photo-activating’). White circles appearing over the Golgi denote the initial ROIs for  $\beta$ APP-paGFP photoactivation. Cells were then chased by imaging every 30 seconds for the indicated time.

**Video 3.5.** APP bearing the dephosphomimetic (S711A) mutation traffics to lysosomes.

SN56 cells were transiently transfected with  $\beta$ APP S711A-paGFP (green), LAMP1-mRFP (lysosome marker, red), and GalT-CFP (Golgi marker, blue). APP was photo-activated in the Golgi (blue) with 405nm light, alternating with imaging for 15 minutes (indicated by green word ‘Photo-activating’). The white circles appearing over the Golgi denote the initial ROIs for  $\beta$ APP-paGFP photoactivation. Cells were then chased by imaging every 30 seconds for the indicated time. This movie has been intentionally cropped to focus on the trafficking around the Golgi.

**Video 3.6.** APP bearing the phosphomimetic (S711E) mutation does not traffic to lysosomes.

SN56 cells were transiently transfected with  $\beta$ APP S711E-paGFP (green), LAMP1-mRFP (lysosome marker, red), and GalT-CFP (Golgi marker, blue). APP was photo-activated in the Golgi (blue) with 405nm light, alternating with imaging for 15 minutes (indicated by green word 'Photo-activating'). Photo-activation ROIs in the Golgi are denoted by white circles in the video. Cells were then chased by imaging every 30 seconds for the indicated time. This movie has been intentionally cropped to focus on the trafficking around the Golgi.

**Video 3.7.** DCP-LA treatment disrupts APP trafficking to the lysosome.

SN56 cells were transiently transfected with  $\beta$ APP-paGFP (green), LAMP1-mRFP (lysosome marker, red), and GalT-CFP (Golgi marker, blue) and treated with 500nM DCP-LA. APP was photo-activated in the Golgi (blue) with 405nm light, alternating with imaging for 15 minutes (indicated by green word 'Photo-activating'). White circles in the video denote photo-activation ROIs in the Golgi. Cells were then chased imaging every 30 seconds for the indicated time.

### **Appendix C: Figure Legends to Chapter 4 Videos**

**Video 4.1.** Lysosomal secretion detected by mApple-LAMP1-pHluorin.

SN56 cells were transfected with mApple-LAMP1-pHluorin and imaged using TIR-FM after treatment with ionomycin. Vesicles positive for mApple (red) and activated pHluorin (green) are circled in white. Scale bar represents 5  $\mu$ M. Images were taken every 112 ms.

## Curriculum Vitae

**Name:** Joshua Hoi Ki Tam

**Post-secondary Education and Degrees:** The University of Western Ontario  
London, Ontario, Canada  
2005-2009 B.Sc.

The University of Western Ontario  
London, Ontario, Canada  
2009-2015 PhD.

**Honours and Awards:** Graduate Student Teaching Award Nominee  
University of Western Ontario, London, ON  
2010

CIHR Graduate Scholarships  
Master's Award  
2010-2011

Following the trafficking of APP using photoactivatable green fluorescent protein."  
2nd Runner –Up, Oral presentation,  
Clinical Neurological Sciences Research Day  
2010

Live cell imaging of APP trafficking: From the Golgi to the Lysosome  
1st Prize, Master's and Undergraduate Category  
Taylor Symposium Poster Competition  
Robarts Research Institute  
2010

Direct trafficking of APP from the Golgi to the lysosomes is mediated by AP-3.  
1st Prize, Oral presentation  
Clinical Neurological Sciences Research Day  
2011

Ontario Graduate Scholarships  
 Doctoral Award  
 2011

A $\beta$  is secreted from lysosomes in neuronal cells  
 1st Runner-up, Oral presentation  
 Clinical Neurological Sciences Research Day  
 2012

Queen Elizabeth II Graduate Scholarships in Science and Technology  
 (QEII-GSST)  
 Doctoral Award  
 2012

International Society for Neurochemistry (ISN) Travel Award  
 ISN-ASN Biennial Meeting  
 2013

Ontario Graduate Scholarships  
 Doctoral Award  
 2013

Alteration in APP trafficking due to C-terminal tyrosine mutations.  
 1st Prize, Oral presentation (Graduate Student Category)  
 Clinical Neurological Sciences Research Day  
 2014

**Related Work Experience**      Teaching Assistant  
    The University of Western Ontario  
    2009-2015

**Publications:**

Ta, R., Suchy, M., **Tam, J. H.**, Li, A. X., Martinez-Santesteban, F. S., Scholl, T. J., et al. (2013).  
 A dual magnetic resonance imaging/fluorescent contrast agent for Cathepsin-D detection.  
*Contrast Media & Molecular Imaging*, 8(2), 127–139. <http://doi.org/10.1002/cmml.1502>

**Tam, J. H.**, & Pasternak, S. H. (2012). Amyloid and Alzheimer's disease: inside and out. *The Canadian Journal of Neurological Sciences. Le Journal Canadien Des Sciences Neurologiques*, 39(3), 286–298.

**Tam, J. H.**, & Pasternak, S. H. (2015). Imaging the Intracellular Trafficking of APP with



Photoactivatable GFP. *Journal of Visualized Experiments : JoVE*, (104), 1–9.  
<http://doi.org/10.3791/53153>

**Tam, J. H.**, Seah, C., & Pasternak, S. H. (2014). The Amyloid Precursor Protein is rapidly transported from the Golgi apparatus to the lysosome and where it is processed into beta-amyloid. *Molecular Brain*, 7(1), 54. <http://doi.org/10.1186/s13041-014-0054-1>

Tang, W., **Tam, J. H.**, Seah, C., Chiu, J., Tyrer, A., Cregan, S. P., et al. (2015). Arf6 controls beta-amyloid production by regulating macropinocytosis of the Amyloid Precursor Protein to lysosomes. *Molecular Brain*, 8(1), 41. <http://doi.org/10.1186/s13041-015-0129-7>

Caetano, F. A., Dirk, B. S., **Tam, J. H.**, Cavanagh, P. C., Goiko, M., Ferguson, S. S. G., et al. (2015). MliSR: Molecular Interactions in Super-Resolution Imaging Enables the Analysis of Protein Interactions, Dynamics and Formation of Multi-protein Structures. *PLoS Computational Biology*, 11(12), e1004634. <http://doi.org/10.1371/journal.pcbi.1004634>

**Tam, J.H.** & Pasternak, S.H. (2016). Alzheimer's Disease. In J. Cechetto, D. & Weishaupt, N. (Eds.), *The Cerebral Cortex in Neurodegenerative and Neuropsychiatric Disorders: Experimental Approaches to Clinical Issues*. San Diego, CA: Elsevier. (Undergoing Editing)

**Tam, J. H.**, Cobb, M.R., Seah, C., & Pasternak, S. H. (2015). Tyrosine Binding Protein sites regulate the intracellular trafficking and processing of Amyloid Precursor Protein. *PLOS ONE*. (Submitted).

## Presentations

**Tam, J.H.**, Cobb, R., Pasternak, S.H., Alteration in APP trafficking due to C-terminal tyrosine mutations. Oral Presentation, Department of Clinical and Neurological Sciences Research Day 2014 (UWO). (Presenting author)

**Tam, J.**, Cobb, R., Pasternak, S.H., Mutagenesis of carboxyl-terminal tyrosines disrupts APP trafficking to lysosomes. Abstract 429.18 Poster presentation, Society for Neuroscience, Abstracts of the Society for Neuroscience, 2013. (Presenting author)

**Tam, J.H.**, Seah, C., Pasternak, S.H., AP-3 mediates the direct and rapid trafficking of APP to lysosomes and is implicated in Alzheimer's Disease. Poster Presentation, ISN-ASN Biennial Meeting Cancun (2013)

**Tam, J.H.**, Seah, C., Pasternak, S.H., AP-3 but not AP-1 mediates the direct and rapid trafficking of APP from Golgi to lysosomes. Poster Presentation, Alzheimer's Association International Conference on Alzheimer's Disease (2012)

- Tam, J.H.**, Seah, C., Pasternak, S.H., A $\beta$  is secreted from lysosomes in neuronal cells. Oral Presentation, Department of Clinical and Neurological Sciences Research Day 2012 (UWO). (Presenting author)
- Tam, J.H.**, Seah, C., Pasternak, S.H., Lysosome mediated exocytosis of A $\beta$ 42 from SN56 cells. Poster Presentation, Department of Physiology and Pharmacology Research Day 2011 (UWO). (Presenting author)
- Tam, J.H.**, Pasternak, S.H., AP-3 interacts with APP and directs its trafficking from the Golgi to lysosomes. Abstract 12.05 Platform/Oral presentation, Society for Neuroscience, Abstracts of the Society for Neuroscience, 2011. (Presenting author)
- Tam, J.H.**, Pasternak, S.H., Direct trafficking of APP from the Golgi to the lysosomes is mediated by AP-3. Poster Presentation, A.C. Camargo Global Meeting of Translational Science. (Presenting author)
- Tam, J.H.**, Pasternak, S.H., Direct trafficking of APP from the Golgi to the lysosomes is mediated by AP-3. Oral Presentation, Department of Clinical and Neurological Sciences Research Day 2011 (UWO). (Presenting author)
- Tam, J.H.**, Pasternak, S.H., Live cell imaging demonstrates that APP is transported rapidly and directly from the Golgi to the lysosome. Abstract 11.5 Platform/Oral presentation, Society for Neuroscience, Abstracts of the Society for Neuroscience, 2010. (Presenting author)
- Tam, J.H.**, Pasternak, S.H., Live cell imaging of APP: From Golgi to Lysosomes. Poster Presentation, Department of Physiology and Pharmacology Research Day 2010 (UWO). (Presenting author)
- Tam, J.H.**, Pasternak, S.H., Live cell imaging of APP: From Golgi to Lysosomes. Poster 29. Poster Presentation, J. Allyn Taylor International Prize in Medicine 2010 (UWO). (Presenting author)
- Tam, J.H.**, Pasternak, S.H., Following the trafficking of APP using photoactivatable green fluorescent protein. Oral Presentation, Department of Clinical and Neurological Sciences Research Day 2010 (UWO). (Presenting author)
- Tam, J.H.**, Pasternak, S.H., Subcellular Localization of Presenilin 1 and its Mutants. Margaret Moffat Research Day 2009 (UWO). (Presenting author)